



HAL
open science

Lanthanides and actinides: Annual survey of their organometallic chemistry covering the year 2019

Joy Farnaby, Tajrian Chowdhury, Samuel Horsewill, Bradley Wilson, Florian Jaroschik

► **To cite this version:**

Joy Farnaby, Tajrian Chowdhury, Samuel Horsewill, Bradley Wilson, Florian Jaroschik. Lanthanides and actinides: Annual survey of their organometallic chemistry covering the year 2019. *Coordination Chemistry Reviews*, 2021, 437, pp.213830. 10.1016/j.ccr.2021.213830 . hal-03264385

HAL Id: hal-03264385

<https://hal.science/hal-03264385>

Submitted on 18 Jun 2021

HAL is a multi-disciplinary open access archive for the deposit and dissemination of scientific research documents, whether they are published or not. The documents may come from teaching and research institutions in France or abroad, or from public or private research centers.

L'archive ouverte pluridisciplinaire **HAL**, est destinée au dépôt et à la diffusion de documents scientifiques de niveau recherche, publiés ou non, émanant des établissements d'enseignement et de recherche français ou étrangers, des laboratoires publics ou privés.

Review

Lanthanides and Actinides: Annual Survey of their Organometallic Chemistry Covering the Year 2019

Joy H. Farnaby^a, Tajrian Chowdhury^a, Samuel J. Horsewill^a,
Bradley Wilson^a, Florian Jaroschik^b

a *Joseph Black Building, University Avenue, Glasgow, G12 8QQ, Scotland*

b *ICGM, Université de Montpellier, CNRS, ENSCM, 34080 Montpellier, France*

Received ; accepted

*Tel. +44 1413304653 (J. Farnaby); +33 4 67 14 43 17 (F. Jaroschik)

E-mail addresses: Joy.Farnaby@glasgow.ac.uk (J. Farnaby), florian.jaroschik@enscm.fr
(F. Jaroschik)

A B S T R A C T

This review summarizes the progress in organo-*f*-element chemistry during the year 2019. Organo-*f*-element chemistry, including Sc, Y, the lanthanides and the actinides, has been a flourishing research area for many years. The mainly ionic and Lewis acid character of the lanthanide metals provides a vast array of intriguing structural features supported by numerous organic ligands. In this year's edition several new types of complexes are presented, including the first scandacyclopentadiene complex $[\text{Cp}^*(\text{BuC}(\text{NiPr})_2)\text{Sc}(\eta^2\text{-PhCCPh})][\text{K}(\text{crypt})]$ displaying an aromatic metallacycle, the first lanthanide-aluminabenzene complexes $[(1\text{-Me-3,5-tBu}_2\text{-C}_5\text{H}_3\text{Al})(\mu\text{-Me})\text{Ln}(2,4\text{-di-tbutylpentadienyl})]$ (Ln = Y, Lu) and the first scandium phosphonioketene complex $[\text{LSc}(\eta^2\text{-COCHPPH}_3)\text{I}]$ (L = $[\text{MeC}(\text{NDIPP})\text{CHC}(\text{NDIPP})\text{Me}^-]$), which all showed interesting reactivities. Furthermore, a wide range of lanthanide alkyl complexes were synthesized and structurally characterized, including the first isolated ScMe_3 derivatives $[\text{Sc}(\text{AlMe}_4)_3(\text{Al}_2\text{Me}_6)_{0.5}]$ and $[(\text{Me}_3\text{TACN})\text{ScMe}_3]$. A very important finding in divalent lanthanide chemistry was the synthesis of the first neutral divalent Dy and Tb sandwich complexes, $\text{Ln}(\text{C}_5\text{iPr}_5)_2$, which were investigated for their magnetic properties. The reactivity of divalent metallocenes towards transition metals precursors or As^0 provided unprecedented multimetallic complexes, for example $[(\text{Cp}^*_2\text{Sm})_4\text{As}_8]$, $[(\text{Cp}^*_2\text{Sm})_3\{(\mu\text{-O}_4\text{C}_4)(\mu\text{-}\eta^2\text{-CO})_2(\mu\text{-}\eta^1\text{-CO})(\text{CO})_5\text{Re}_2\}\text{SmCp}^*_2(\text{thf})]$ and $[\text{Cp}^*_2\text{Yb}(\text{taphen})\text{MMe}_2\text{YbCp}^*_2]$ (M = Ni, Pt; taphen = 4,5,9,10-tetraazaphenanthrene). New reactivity of lanthanide complexes was unveiled, such as the direct dinitrogen to hydrazine conversion using a low-valent Sc complex or the reductive coupling of CS_2 using different divalent Yb complexes affording for the first time a CS_2^{2-} bridging unit as shown in the complex $[\text{Yb}_2(\text{DippForm})_4(\text{CS}_2)]$ or an intriguing acetylendithiolate bridged Yb(III) complex $\text{Yb}_2\text{L}_4(\text{C}_2\text{S}_2)$ (L = $(\text{OtBu})_3\text{SiO}^-$). Numerous new lanthanide catalysed homo- and co-polymerization processes involving polar or non-polar monomers were reported, including efficient and stereoselective polymerization of *o*-methoxystyrene, vinylpyridine or isoprene. The regio-, diastereoselective and stereoregular cyclopolymerization of different ether and thioether substituted 1,6-heptadienes was reported. A wide range of hydrofunctionalization reactions were developed, among them an efficient hydrophosphinylation process of styrenes and alkynes. It was further shown that alkyllanthanide halides could undergo efficient halogen/lanthanide exchange with arylhalides and vinylhalides providing useful organolanthanide transfer reagents, for example in the stereoselective Zweifel olefination.

Organolanthanide complexes have also found new applications in material sciences, for example, $\text{Ce}(\text{C}_5\text{H}_4\text{iPr})_3$ was employed for the formation of an ultrathin CeO_2 overlayer on a Pt electrode via atomic layer deposition to improve low-temperature solid oxide fuel cells. An increasingly studied field is the area of endohedral metallafullerenes (EMF) which gave rise to a large number of unprecedented lanthanide compounds with unusual cages, as well as dimetallafullerenes with interesting single molecular magnet (SMM) properties and new insights on direct Ln-Ln bonds.

Hydrocarbyl complexes of the actinides continued to flourish, in spite of the challenges presented by synthesis and characterization. The first examples of structurally-characterised uranium(IV) homoleptic aryl complexes and transuranic hydrocarbyl Np(III) complex have been reported. An experimental and computational study has demonstrated that f-orbitals have a structure-directing role in overlap-driven covalency in carbene-stabilised metalla-allene complexes and ^{13}C NMR shift has been shown to be a simple and direct probe of the actinide-carbon bond covalency in the acetylides. Small molecule activation chemistry has provided some unusual and important results, including a uranium(V) carbene complex coordinated end-on to dinitrogen and a stable dinuclear U(IV) dihydride complex which reacted with CO_2 and CO/H_2 to form methoxide and ultimately methanol. New ligands and binding modes resulted from actinide main group chemistry, with reports of the first examples of terminal η^1 -cyaarside ligands ($\text{C}\equiv\text{As}^-$), bridging diarsaallene ($\text{As}=\text{C}=\text{As}$) $^{2-}$ and trapped radical dianion of the phosphoethynolate ($\text{OCP}^{2-\bullet}$) ligand. The bis- $\text{Cp}^{\text{tBu}2}$ metallocene stabilised thorium phosphinidene continued to demonstrate a wealth small molecule reactivity, including reductive coupling, heterocycle formation and E-H (E = P, N, C) bond activation. Two examples of U(II) complexes are reported, $[\text{K}(\text{crypt})][(\text{C}_5\text{Me}_4\text{H})_3\text{U}]$ and $[\text{K}(\text{crypt})][\text{U}(\text{NR}_2)_3]$ (R = SiMe₃). The first direct assembly of a uranium tri-rhenium triple inverse sandwich complex was reported, both experimental and computation data are consistent with atypical Cp-bonding, with electron density redistributed from Re(I) to U(III). Isopropyl substituted cyclopentadienyl ligands have enabled the synthesis, reactivity and magnetic properties of U(III) metallocenes, including base-free cationic species. The first example of a monomeric thorium terminal dihyrido compound ($\text{Cp}^{\text{Ar}5}$)(Cp^*)ThH₂(THF) (Ar = 3,5-^tBu₂-C₆H₃) has been synthesized. The full characterisation of the organoamericium(III) compound ($\text{C}_5\text{Me}_4\text{H}$)₃Am provided a unique insight into Am-C bonding. The Th(IV)/Th(III) redox couple has been experimentally determined for a range of Th(IV) and Th(III) organometallics. The first uranium phosphazaallene has been synthesised by reaction of a *bis*-phosphide complex

with *tert*-butyl cyanide. Actinide EMFs continued to be an active area of research; molecular structures, synthetic and purification methodologies are reported. How best to computationally model the distinct properties of actinide EMFs was the subject of some debate. Thorium complexes have found application in catalysis, in the selective dihydroboration of nitriles, the hydroboration of imines and polymerization of isoprene.

Contents

1 INTRODUCTION

2 LANTHANIDES

2.1 LANTHANIDE CARBONYL, NHC AND CDP COMPLEXES

2.2 LANTHANIDE ALKYL, BENZYL, ARYL AND ALKYLIDENE COMPLEXES

2.3. LANTHANIDE (HETERO)ALLYL, ALKYNYL AND PENTADIENYL COMPLEXES

2.4. LANTHANIDE CYCLOPENTADIENYL COMPLEXES

2.4.1. *Cp₂Ln and [Cp₃Ln]⁻ Compounds*

2.4.2. *CpLnX₂, Cp₂LnX and Cp₃Ln Compounds*

2.4.3. *Pentamethylcyclopentadienyl Compounds*

2.6. ORGANOLANTHANIDE COMPLEXES WITH HETEROATOM FIVE-MEMBERED RING LIGANDS

2.7. LANTHANIDE ARENE AND HETEROARENE COMPLEXES

2.8. LANTHANIDE CYCLOOCTATETRAENYL COMPLEXES

2.9. HETEROBIMETALLIC ORGANOLANTHANIDE COMPLEXES

2.10. LANTHANIDE METALLOFULLERENES

2.11. ORGANOLANTHANIDE CATALYSIS

2.11.1. *Organolanthanide-catalyzed Polymerization Reactions*

2.11.2. *Organolanthanide-catalyzed Hydrofunctionalization Reactions*

2.11.3. *Other Organolanthanide-catalyzed Reactions*

2.12. ORGANOLANTHANIDES IN ORGANIC SYNTHESIS

2.13. ORGANOLANTHANIDES IN MATERIALS SCIENCE

3 ACTINIDES

3.1. ACTINIDE CARBONYL COMPLEXES

3.2. ACTINIDE HYDROCARBYLS COMPLEXES

3.3. ACTINIDE CYCLOPENTADIENYL COMPLEXES

3.3.1. *Cp₃An, CpAnX₃, Cp₂AnX₂ and Cp₃AnX Compounds*

3.3.2. *Pentamethylcyclopentadienyl Compounds*

3.4. ACTINIDE ARENE COMPLEXES

3.5. ACTINIDE METALLOFULLERENES

3.6. ORGANOACTINIDES IN CATALYSIS

ACKNOWLEDGEMENTS

REFERENCES

Keywords: Lanthanides; Actinides; Cyclopentadienyl complexes; Cyclooctatetraenyl complexes; Organometallic chemistry

1. INTRODUCTION

Organo-*f*-element chemistry has been a flourishing research field for many years, providing new findings in structural and redox chemistry, unveiling new physical properties and leading to many catalytic processes and applications in organic synthesis and material sciences. Following a long tradition - the first annual review was published by Prof. Frank Edelmann in 1992 - this annual review summarizes the literature reports of the year 2019 involving lanthanide (including Sc, Y, La) and actinide complexes containing at least one metal-carbon bond.

Several research fields concerning the structure, reactivity or physical properties of organo-*f*-element complexes have been reviewed in 2019.

O. Walter provided a mini-review on actinide organometallic complexes with π -ligands (mainly Cp and COT ligands) with a special focus on the comparison of the bonding situation in the recently synthesized transuranium complexes (Np, Pu) with the corresponding Th and U complexes as well as with lanthanide complexes.[1]

Cui and coworkers have summarized the application of rare earth metal catalysts in hydrosilylation reactions. Various Ln alkyl, benzyl or amido complexes carrying Cp ligands, nitrogen or oxygen based anionic or dianionic ligands were presented in the hydrosilylation of mono-olefins and dienes leading often in good selectivity to either the Markovnikov or anti-Markovnikov addition. The majority of examples concerned the addition of primary silanes.[2]

The vast area of ring-opening polymerization of cyclic esters using rare earth metal catalysts was reviewed by A. Trifonov and coworkers. This comprehensive overview

describes the polymerization of lactones and lactides initiated by a range of trivalent lanthanide complexes having Ln-O, Ln-N, Ln-C, Ln-H or Ln-BH₄ bonds as well as by divalent lanthanide complexes. It is shown that depending on the ancillary ligand and the reactive site of the catalyst high molecular weight aliphatic polyesters could be obtained in very good yields under mild conditions. Furthermore, control of the molecular weight distribution and the stereoselectivity of the polymers was achieved with well-designed catalysts.[3]

The investigation of lanthanide complexes as single-molecule magnets (SMM) has seen a huge development in recent years. A large part of a review by R. A. Layfield, is dedicated to lanthanide and actinide complexes having interaction with main group elements, including 2p donor ligands (B, C and N) and heavier p-block donors (P, S, As, Sb).[4]

The field of lanthanide and actinide containing endohedral metallofullerenes (EMF) is increasingly popular and four reviews have been published in this area. The first paper by F. Liu, S. M. Avdochenko, A. A. Popov and coworkers describes recent advances in the study of single-electron lanthanide-lanthanide bonds inside fullerenes, which are interesting targets towards robust redox-active molecular magnets. Depending on the lanthanide metal different metal-metal bonding situations exist in dimetallofullerenes Ln₂@C₈₀, which determine the reactivity, the redox-chemistry and the SMM behavior.[5]

A second review by L. Spree and A. A. Popov, concerns the recent advances in single molecule magnetism of dysprosium-metallofullerenes. Different Dy-containing EMF families, such as nitride, sulfide and carbide clusterfullerenes as well as dimetallofullerenes are described and their SMM behavior is outlined. Furthermore, the influence of 1D, 2D or 3D arrays on their properties is summarized.[6]

The use of EMFs in novel drug design strategy was reviewed by F. Zhao and coworkers. The recently synthesized metallofullerenol Gd@C₈₂(OH)₂₂ has shown promising results in suppressing tumor growth and metastasis without significant toxicity. This paper shows the mechanism of action by engaging the tumor and discusses how the interaction of this metallofullerenol and other derivatives with key biomolecules could open up new avenues in nanomedicine and drug design.[7]

A survey on actinide metallofullerenes was provided by Echevoyen and coworkers, showing recent developments in the synthesis and properties of this class of molecules, thereby highlighting the differences with respect to related lanthanide metallofullerene chemistry.[8]

2. LANTHANIDES

2.1. LANTHANIDE CARBONYL, NHC AND CDP COMPLEXES

The gas-phase synthesis of the late lanthanide metal octacarbonyl anion complexes $\text{Ln}(\text{CO})_8^-$ ($\text{Ln} = \text{Tm}, \text{Yb}, \text{Lu}$) as well as their experimental and theoretical analysis was reported. [9] These complexes were identified by comparison of mass-selected infrared photodissociation spectroscopy and theoretical data, showing that eight carbonyl groups corresponded to the stable, saturated complexes. Each complex exhibited a relatively sharp signal in the infrared spectrum and the observed CO-stretching frequencies were strongly red-shifted ($\text{Tm } 1904 \text{ cm}^{-1}$, $\text{Yb } 1901 \text{ cm}^{-1}$, $\text{Lu } 1899 \text{ cm}^{-1}$) compared to free CO (2143 cm^{-1}). The optimized geometries of the $\text{Ln}(\text{CO})_8^-$ anions with the calculated bond lengths were determined by quantum chemical calculations and are shown in Scheme 1. Analysis of the electronic structures of these complexes provided insights into the orbital interactions involved in the Ln-CO bonds. Whereas the major contribution (77%) to the mainly covalent bonding comes from $[\text{Ln}(d)] \rightarrow (\text{CO})_8 \pi$ backdonation, $[\text{Ln}(d)] \leftarrow (\text{CO})_8 \sigma$ donation provides 16%. In contrast, f-orbitals are only involved with 3-4% to the total orbital interactions. In these complexes, the lanthanide ions possess 32 (Tm), 33 (Yb) or 34 (Lu) electrons, however, they all obey the 32 electron rule as the additional electrons in the Yb and Lu complexes occupy a ligand-based orbital of the carbonyl cage, which has nearly no contributions from the 4f atomic orbitals of the metals.[9]

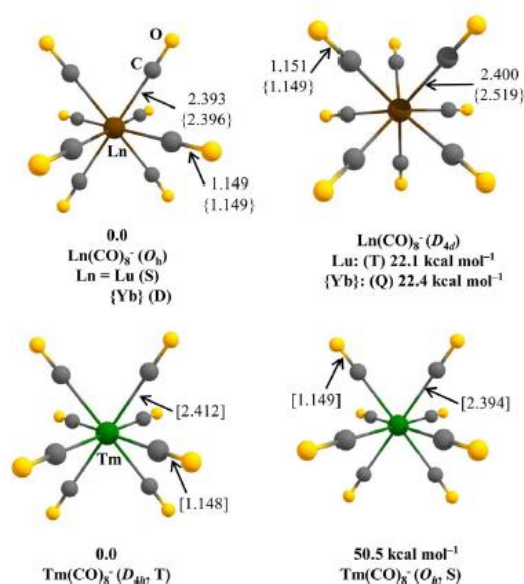
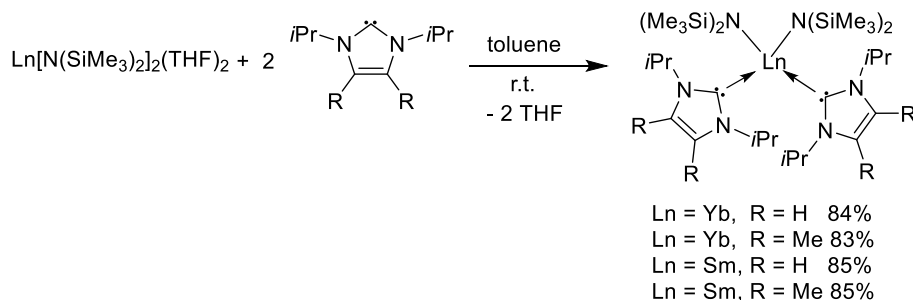


Figure 1. Optimized geometries of the $\text{Ln}(\text{CO})_8^-$ ($\text{Ln} = \text{Tm}, \text{Yb}, \text{Lu}$) complexes at the B3LYP-D3(BJ)/def2-TZVPPD/Stuttgart RSC Segmented/ECP level. Bond lengths are given in Å. Reproduced with permission from Wiley 2019.[9]

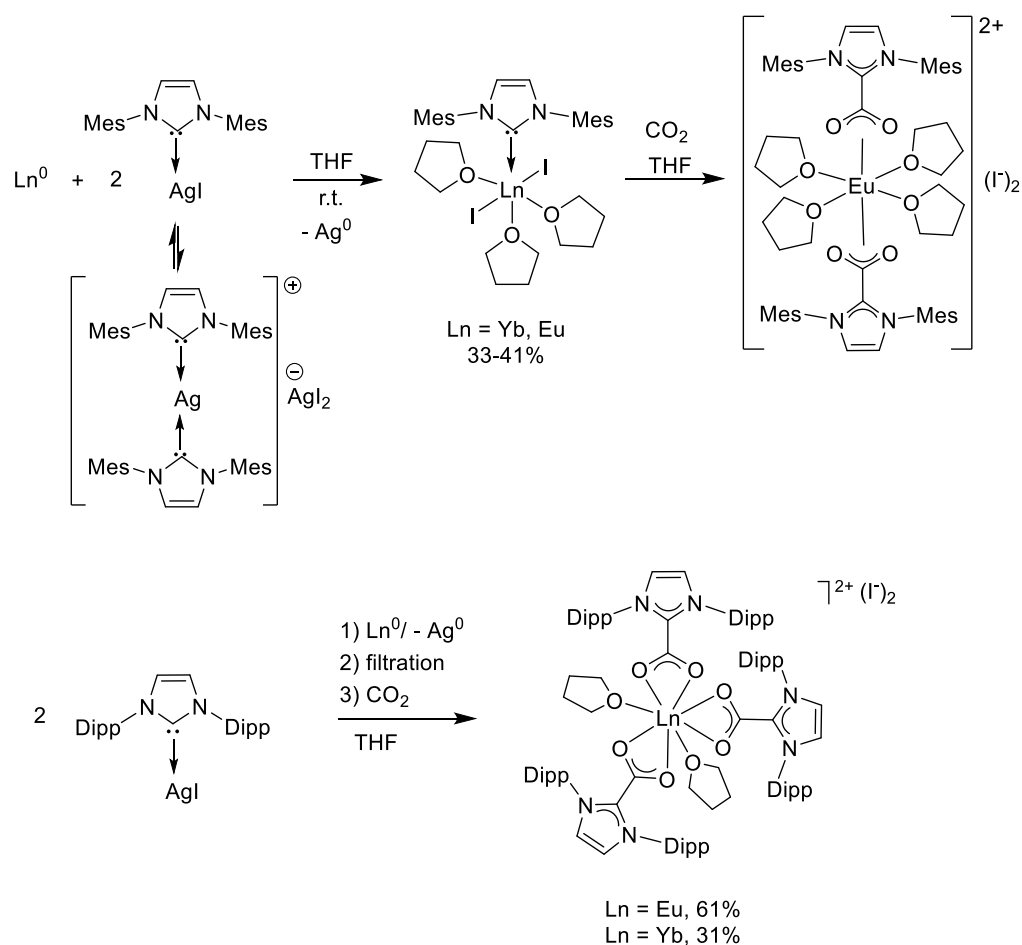
A combined experimental and theoretical study was conducted to synthesize and identify $\text{LnO}(\text{CO})_n^+$ ($\text{Ln} = \text{Sc}, \text{Y}, \text{La}; n = 5-11$) cations in the gas phase using infrared photodissociation spectroscopy. [10] The vibrational spectra showed a blue-shift of the CO stretching frequencies for all complexes with respect to free CO. The ground states of all the LnO^+ cations were singlets due to non-occupied d-orbitals. In the case of Sc, the saturation of the first coordination shell was observed for $\text{ScO}(\text{CO})_6^+$, leading to a 7-coordinate, 18-electron complex cation, as the Sc-O triple bond provided 6 electrons. This complex showed a single band at 2206 cm^{-1} in the ir spectrum in good agreement with C_{5v} symmetry with 5 CO in the equatorial position and one CO in the axial position. In the case of Y, the most abundant complex in the mass spectra was $\text{YO}(\text{CO})_7^+$ exhibiting two bands in the ir spectrum at 2191 and 2203 cm^{-1} . The bonding situation in this saturated, formal 20 electron complex was analyzed, identifying the HOMO-2 orbital as a non-bonding orbital between metal and CO. In the case of La, the availability of 4f atomic orbitals provided the possibility of accommodating more than 18 electrons and complexes $\text{LaO}(\text{CO})_n^+$ with $n = 6-11$ could be identified. It was shown that for $n=9$ a saturated complex was obtained with two bands at 2181 and 2189 cm^{-1} . NBO analysis revealed an unusually high f-orbital contribution in this complex of up to 21%, which accounted for the first three HOMOs. The structural variation between the Sc, Y and La complexes was attributed to effects of steric hindrance caused by the O atoms as well as the differences in ionic radii. In the calculated complexes, increasing Ln-O and Ln-C values were obtained when going from Sc to La to reduce the ligand repulsion.[10]

The new divalent Yb and Sm bis(amide) NHC complexes $[(\text{Me}_3\text{Si})_2\text{N}]_2\text{Ln}(\text{NHC})_2$ ($\text{Ln} = \text{Yb}, \text{Sm}; \text{NHC} = 1,3\text{-di-isopropyl-4,5-dimethylimidazol-2-ylidene}$ or $1,3\text{-di-isopropylimidazol-2-ylidene}$) were synthesized in high yields from the corresponding lanthanide bis(amide) THF precursors in toluene at room temperature (Scheme 1).[11] All complexes were stable in solution and in the solid state. XRD studies showed no significant difference in the Ln-N distances between the THF precursor and the NHC complexes for Sm. The Ln-C distances were in the range $2.637(2)$ to $2.658(7)\text{\AA}$ for Yb and $2.780(2)$ and $2.815(2)\text{\AA}$ for Sm. These complexes were successfully employed in the hydrophosphination reaction of alkenes and alkynes (see section 2.11.2).[11]



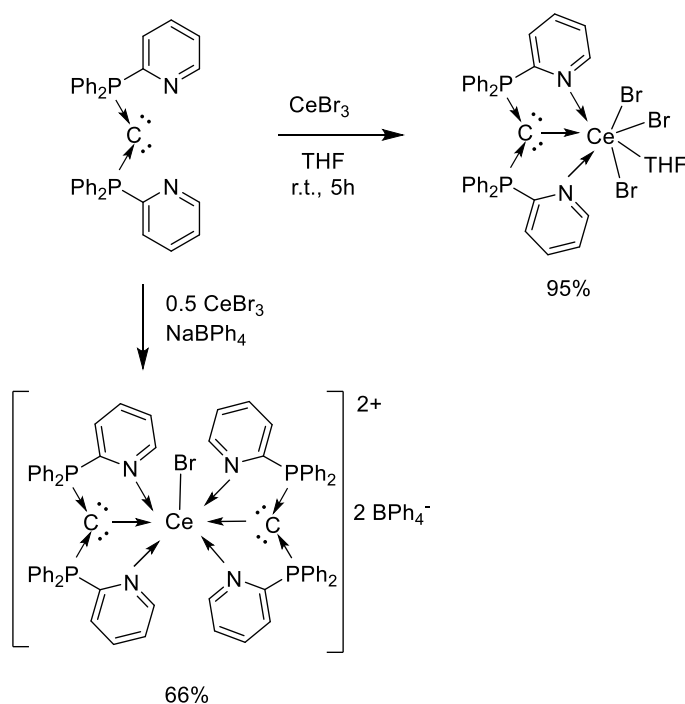
Scheme 1. Synthesis of divalent Yb and Sm bis(amide) NHC complexes $[(\text{Me}_3\text{Si})_2\text{N}]_2\text{Ln}(\text{NHC})_2$.^[11]

The redox-transmetallation reaction of a silver NHC complex $\text{Ag}(\text{IMes})\text{I}$ (IMes = 1,3-dimesitylimidazol-2-ylidene) with elemental lanthanide metals was developed to access the new divalent NHC lanthanide complexes $\text{LnI}_2(\text{IMes})(\text{THF})_3$ ($\text{Ln} = \text{Eu}, \text{Yb}$) in 33-41% isolated yield (Scheme 2).^[12] XRD studies on these complexes showed Yb-C and Eu-C bond lengths of 2.650(3) Å and 2.749(6) Å, respectively. Excitation of the Eu complex under UV light provided bright yellow-green luminescence in a C_6D_6 solution and in the solid state, whereas in THF the luminescence changed to purple. Reaction of the divalent Eu complex with CO_2 in THF led to the formation of the zwitterionic IMes-CO_2 ligand, containing a carboxylate and an imidazolium moiety, without oxidation of the metal center and the isolation of $[\text{Eu}(\text{IMes-CO}_2)_2(\text{THF})_4]\text{I}_2$. When the bulkier NHC ligand-based silver complex $\text{Ag}(\text{IDipp})\text{I}$ (IDipp = di-isopropylphenyl imidazol-2-ylidene) was employed in the redox-transmetallation reaction, no coordination of the NHC ligand to the lanthanide metal was observed and only $\text{EuI}_2(\text{THF})_5$ and non-coordinated IDipp ligand was obtained. A one pot procedure without isolating the intermediate Ln-NHC complex was then developed to access directly the CO_2 insertion products for both IMes and IDipp ligands.^[12]



Scheme 2. Synthesis of divalent NHC-Ln complexes via direct metal reaction with silver-NHC carbenes and reactivity towards CO₂.^[12]

The synthesis of the first carbodiphosphorane cerium adducts was reported. Reaction of CeBr₃ and the pyridyl-containing carbodiphosphorane C(PPh₂py)₂ (CDP) in THF at room temperature afforded (CDP)CeBr₃(THF), which was characterized by ¹H and ³¹P NMR spectroscopy and XRD analysis (Scheme 3).^[13] The measured Ce-C bond length of 2.597(6) Å has a formal Ce=C double bond character. The reaction of CeBr₃ with two equivalents of CDP ligand and NaBPh₄ provided the dicationic complex [(CDP)₂CeBr][BPh₄]₂ with two dative Ce-C(0) bonds. XRD analysis of this complex revealed a C-Ce-C bond angle of 162.7(2)° and Ce-C bond lengths of 2.597(6) and 2.573(6) Å. Both complexes were analysed by DFT calculations showing rather strong interaction between Ce and CDP as the Ce-C bond dissociation energies are fairly high (82.1 kcal mol⁻¹ for (CDP)CeBr₃(THF) and 420.0 kcal mol⁻¹ for [(CDP)₂CeBr]²⁺). Further theoretical analysis on the nature of the Ce-C bond revealed strong σ-donation from CDP to Ce with only weak π-donation and bond orders indicating Ce-C single bonds in both complexes.^[13]

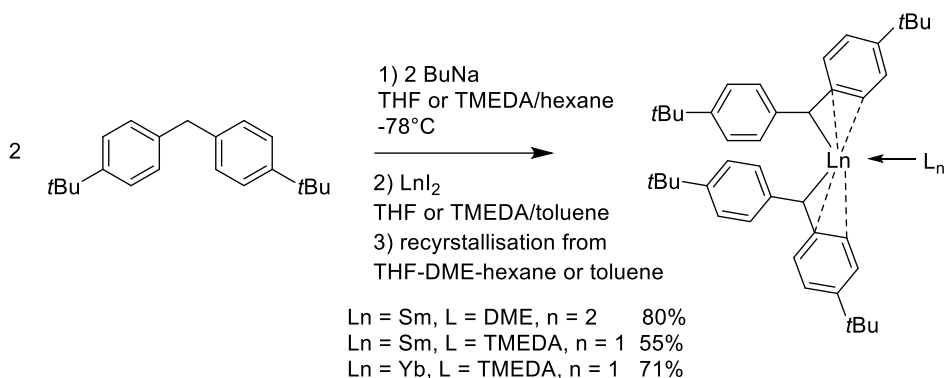


Scheme 3. Synthesis of cerium carbodiphosphorane complexes with one or two dative Ce-C(0) bonds. [13]

2.2 LANTHANIDE ALKYL, BENZYL, ARYL AND ALKYLIDENE COMPLEXES

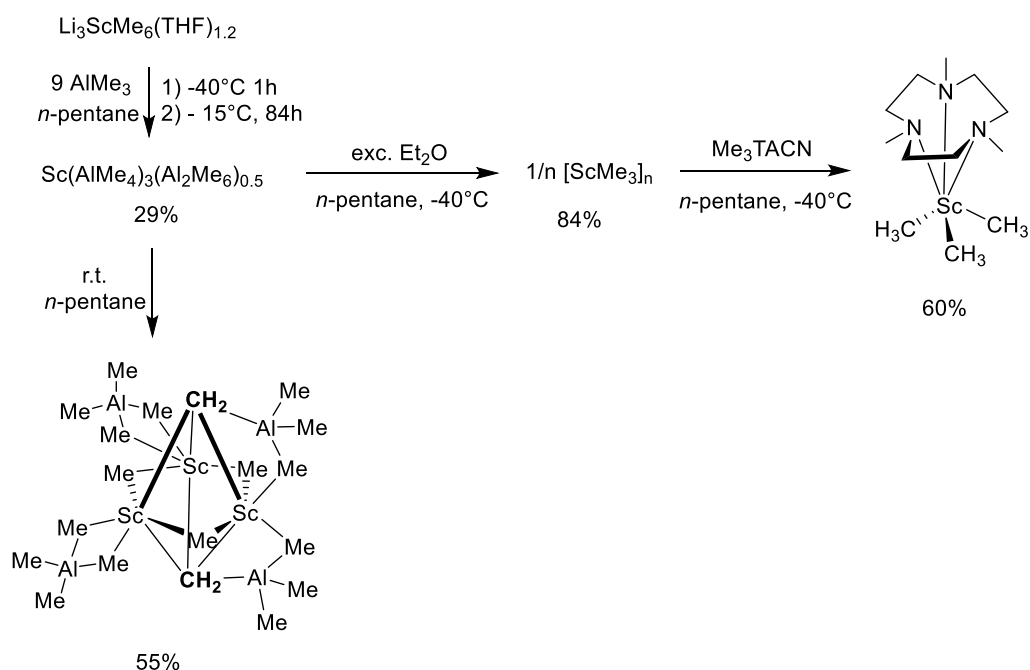
The homoleptic divalent benzhydryl complexes $[(p\text{-}t\text{Bu-C}_6\text{H}_4)_2\text{CH}]_2\text{Ln}(\text{L})_n$ ($\text{Ln} = \text{Sm}$, $\text{L} = \text{DME}$, $n = 2$; $\text{Ln} = \text{Sm}$, Yb , $\text{L} = \text{TMEDA}$, $n = 1$) were synthesized via salt metathesis from LnI_2 and Na-benzhydryl (Scheme 4).[14] These complexes showed high thermal stability due to the absence of β -hydrogens on the ligand. The new complexes were analyzed by XRD analysis and multinuclear NMR spectroscopy. Interestingly, the chemical shift observed in the ^{171}Yb NMR of 507 ppm was significantly upfield shifted compared to other Yb(II) alkyl complexes (between 700 and 1200 ppm). The coordination mode of the benzhydryl ligands varied from η^2 to η^4 , depending on the metal size and the coordination number. In the six-coordinated $[(p\text{-}t\text{Bu-C}_6\text{H}_4)_2\text{CH}]_2\text{Sm}(\text{DME})_2$, the $\text{Sm-C}_{\text{benzhydryl}}$ bond lengths are 2.760(3) Å and short contacts between the Sm(II) ion and the ipso-carbon atom of one of the Ph rings on each ligand (3.085(3) and 3.065(3) Å) was observed, indicating η^2 -coordination of the ligands. In the formally four-coordinate complexes $[(p\text{-}t\text{Bu-C}_6\text{H}_4)_2\text{CH}]_2\text{Ln}(\text{TMEDA})$ ($\text{Ln} = \text{Yb}$, Sm) the covalent $\text{M-C}_{\text{benzhydryl}}$ bonds (2.863(2) Å (Sm), 2.668(2) Å (Yb)) were found to be longer than one ipso short contact, M-C_{ipso} (2.701(2) Å (Sm), 2.617(2) Å (Yb)). Furthermore, short contacts with one ortho-phenyl carbon were also measured. In the case of Sm, short contacts between metal and both ipso-carbons of one benzhydryl ligand (2.999(2), 3.060(2) Å) were observed, so in this case an η^4

coordination mode can be assumed. The hapticity was further confirmed by DFT calculations. The new complexes were studied in hydrophosphination reactions (see section 2.11.2).[14]



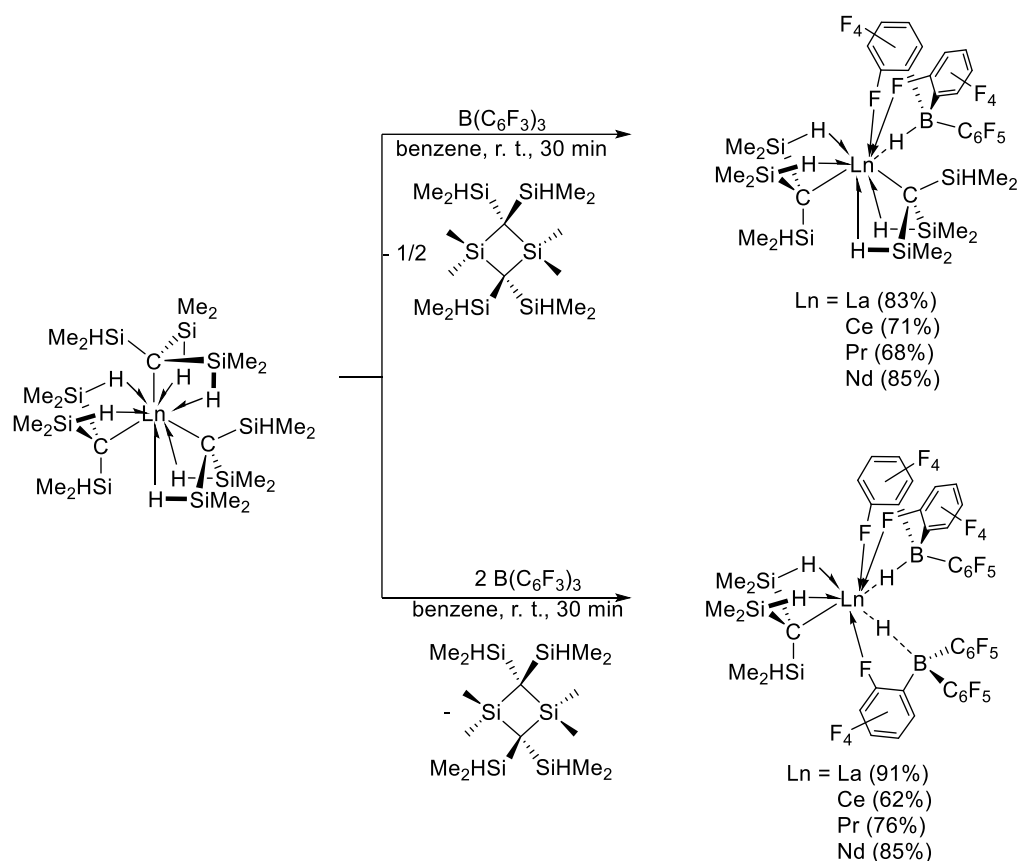
Scheme 4. Synthesis of homoleptic divalent lanthanide benzhydryl complexes.[14]

A breakthrough in the synthesis of trimethylscandium derivatives was achieved. The highly temperature sensitive homoleptic tetramethylaluminate complex [Sc(AlMe₄)₃] was synthesized from the reaction of the ate complex [Li₃ScMe₆(thf)_{1.2}] with AlMe₃ at -40°C (Scheme 5).[15] Characterization by ¹H NMR spectroscopy showed slow methyl exchange and ⁴⁵Sc NMR spectroscopy revealed the presence of only one Sc species at 290.8 ppm. XRD analysis of [Sc(AlMe₄)₃(Al₂Me₆)_{0.5}], the cocrystallisation product with AlMe₃, showed a nearly perfect octahedral arrangement around the Sc center, with Sc-C bond lengths in the range of 2.385(1) and 2.402(2) Å. [Sc(AlMe₄)₃] decomposed at room temperature in *n*-pentane to yield a mixed methyl/methylidene complex [Sc₃(μ₃-CH₂)₂(μ₂-CH₃)₃(AlMe₄)₂(AlMe₃)₂] via multiple C-H bond activations, as shown by NMR and XRD studies. ⁴⁵Sc NMR spectroscopy showed two signals in a 2:1 ratio at 338.3 and 331.1 ppm. Addition of a donor solvent, such as diethyl ether, at low temperature produced cleavage of [Sc(AlMe₄)₃(Al₂Me₆)_{0.5}] to afford THF-soluble [ScMe₃]_n in good yield, which was characterized by ⁴⁵Sc NMR (601.7 ppm), ¹H, ¹³C NMR and IR spectroscopy. Further derivatization with trimethyltriazacyclononane (Me₃TACN) led to the formation of structurally characterized [(Me₃TACN)ScMe₃], exhibiting a signal at +624.6 ppm in the ⁴⁵Sc NMR spectrum and Sc-C bond lengths of 2.278(9) and 2.285(10) Å according to XRD analysis. [Sc(AlMe₄)₃(Al₂Me₆)_{0.5}] was employed in isoprene polymerization (see section 2.11.1).[15]



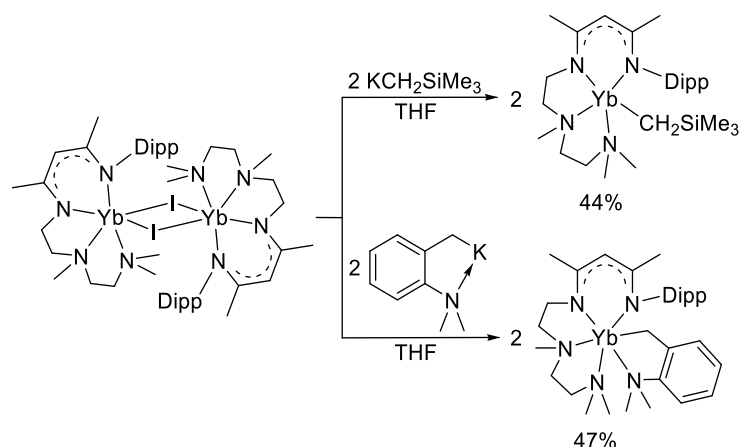
Scheme 5. Synthesis of new trimethylscandium derivatives and a decomposition product of $[\text{Sc}(\text{AlMe}_4)_3(\text{Al}_2\text{Me}_6)_{0.5}]$. [15]

From the reaction of the homoleptic tris(alkyl)lanthanide complexes $\text{Ln}\{\text{C}(\text{SiHMe}_2)_3\}_3$ ($\text{Ln} = \text{La}, \text{Ce}, \text{Pr}, \text{Nd}$) with 1 or 2 equiv of $\text{B}(\text{C}_6\text{F}_5)_3$ was isolated a series of well-defined zwitterionic species $\text{Ln}\{\text{C}(\text{SiHMe}_2)_3\}_2\text{HB}(\text{C}_6\text{F}_5)_3$ ($\text{Ln} = \text{La}, \text{Ce}, \text{Pr}, \text{Nd}$) or $\text{LnC}(\text{SiHMe}_2)_3\{\text{HB}(\text{C}_6\text{F}_5)_3\}_2$ ($\text{Ln} = \text{La}, \text{Ce}, \text{Pr}, \text{Nd}$), respectively (Scheme 6). [16] These mono- and dicationic alkyl hydridoborate lanthanide complexes resulted from hydride abstraction of a β -SiH leading to the new B-H bond and formation of the disilacyclobutane byproduct $\{\text{Me}_2\text{Si}-\text{C}(\text{SiHMe}_2)_2\}_2$ via head-to-tail dimerisation of two $\text{Me}_2\text{Si}=\text{C}(\text{SiHMe}_2)_2$ molecules. The presence of labile, bridging $\text{Si}-\text{H} \rightarrow \text{Ln}$ and $\text{o}-\text{F} \rightarrow \text{Ln}$ interactions in these new complexes was ascertained via ^1H and ^{19}F NMR, IR spectroscopy and XRD analysis. Paramagnetic ^{11}B NMR shifts showed close B-Ln interactions. In contrast, the reaction with the weaker Lewis acid AlMe_3 , instead of $\text{B}(\text{C}_6\text{F}_5)_3$, did not afford hydride abstraction but simple adduct formation was observed by ^1H and ^{29}Si NMR spectroscopy. The new compounds were studied as precatalysts in butadiene polymerisation (see section 2.11.1). [16]



Scheme 6. Synthesis of zwitterionic trivalent mono and bis(alkyl)lanthanide complexes.[16]

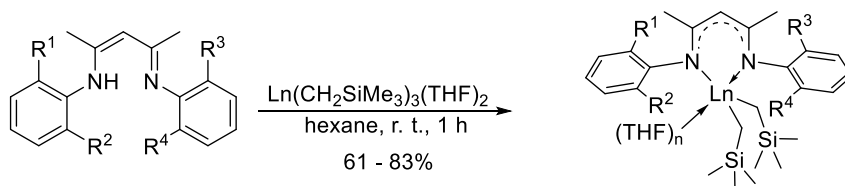
Among anionic non-Cp ligands, β -diketiminato ligands have been applied for the synthesis of lanthanide (alkyl) complexes for a long time. Two examples of divalent alkyl and benzyl Yb complexes containing a tetradentate β -diketiminato ligand with a tethered diamino chain, $(\text{L})\text{YbCH}_2\text{SiMe}_3$ and $(\text{L})\text{Yb}(\text{o-CH}_2\text{C}_6\text{H}_4\text{NMe}_2)$ ($\text{L} = [\text{MeC}(\text{NDipp})\text{CHC}(\text{Me})\text{NCH}_2\text{CH}_2\text{N}(\text{Me})\text{CH}_2\text{CH}_2\text{NMe}_2]^-$), were synthesized by salt metathesis starting from the (β -diketiminato)Yb-iodide precursor $[(\text{L})\text{Yb}(\mu\text{-I})_2]$ and $\text{KCH}_2\text{SiMe}_3$ or $\text{K}(\text{o-CH}_2\text{C}_6\text{H}_4\text{NMe}_2)$ (Scheme 7).[17] The alkyl complex could be analyzed by XRD studies revealing an Yb-C bond length of 2.499(5) Å. These complexes were applied to the homo and heterocoupling of primary arylsilanes (see section 2.11.3).[17]



Scheme 7. Synthesis of divalent (β -diketiminato)Yb alkyl and benzyl complexes.[17]

A series of trivalent β -diketiminato lanthanide bis(alkyl) complexes $(L)Ln(CH_2SiMe_3)_2(THF)_n$ ($Ln = Gd, Tb, Dy, Ho, Er, Tm, Lu, Y, Sc; n = 0, 1; L = ArNC(Me)CHC(Me)NAr$) was synthesized using the protonolysis pathway (Scheme 8). The complexes with mostly dissymmetrical, bulky ligands were characterized by NMR spectroscopy for Y and XRD analysis for Gd, Ho, Er and Tm. These five-coordinate complexes show a distorted trigonal-bipyramidal geometry around the Ln center. They were further investigated in the polymerization of *ortho*-methoxystyrene (see section 2.11.1).[18] A sterically less demanding Sc bis(alkyl) complex, carrying one phenyl group and one 2,6-diisopropylphenyl group on the β -diketiminato ligand, was obtained by the same synthetic pathway, characterized by XRD and studied in the hydroaminoalkylation of alkenes (see section 2.11.2).[19]

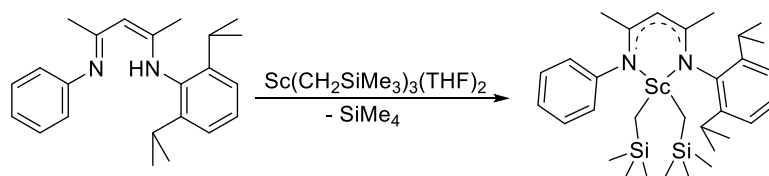
for *ortho*-methoxystyrene polymerisation :



HL¹: R¹ = R² = R³ = R⁴ = Me;
 HL²: R¹ = R² = Me; R³ = R⁴ = Et;
 HL³: R¹ = R² = R³ = R⁴ = Et;
 HL⁴: R¹ = H, R² = MeO, R³ = R⁴ = *i*Pr;
 HL⁵: R¹ = R³ = H, R² = R⁴ = MeO

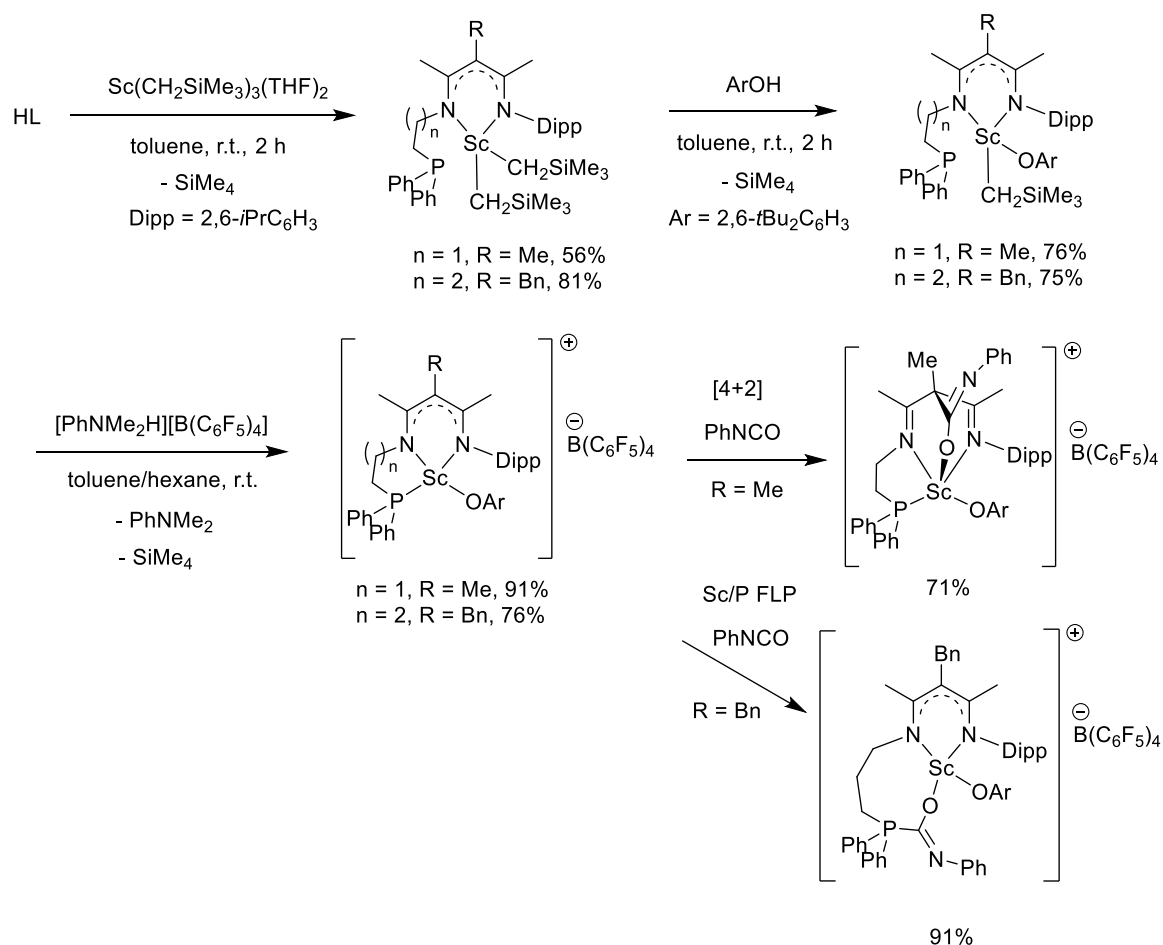
L¹⁻³-Y, n = 1
 L⁴⁻⁵-Y, n = 0
 L¹-Ln, n = 1
 (Ln = Gd, Tb, Dy, Ho, Er, Tm, Lu)
 L¹-Sc, n = 0

for hydroaminoalkylation of alkenes :



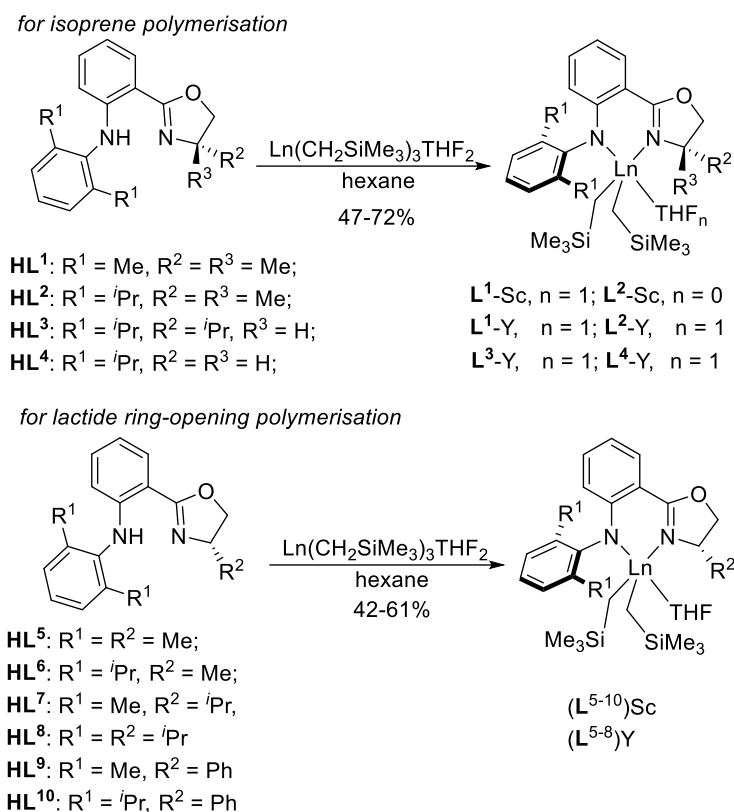
Scheme 8. Synthesis of β -diketiminato lanthanide bis(alkyl) complexes.[18][19]

Bulky β -diketiminato ligands with a tethered diphenylphosphine group were applied to the synthesis of new Sc alkyl and aryloxy complexes (Scheme 9).[20] Initial protolysis of the proligand HL with $\text{Sc}(\text{CH}_2\text{SiMe}_3)_3(\text{THF})_2$ provided the intermediate Sc dialkyl complexes $(\text{L})\text{Sc}(\text{CH}_2\text{SiMe}_3)_2$ ($\text{L} = \text{CH}_3\text{C}(2,6\text{-}i\text{Pr}_2\text{C}_6\text{H}_3\text{N})\text{C}(\text{R})\text{C}(\text{CH}_3)(\text{N}(\text{CH}_2)_n\text{CH}_2\text{PPh}_2)$ with $n = 1$ or 2 , $\text{R} = \text{Me}$, Bn), which reacted selectively with 2,6-diisopropylphenol (HOAr) to the mixed ligand complexes $(\text{L})\text{Sc}(\text{CH}_2\text{SiMe}_3)(\text{OAr})$. XRD analysis and ^{31}P NMR spectroscopy (-18.5 (Me) and -17.5 ppm (Bn)) revealed no Sc-P interactions in these complexes. In the final step, selective protonation with the Brønsted acid $[\text{PhNMe}_2\text{H}][\text{B}(\text{C}_6\text{F}_5)_4]$ provided the cationic Sc-aryloxy complexes $[(\text{L})\text{Sc}(\text{OAr})][\text{B}(\text{C}_6\text{F}_5)_4]$, for which a significant down-field shift in the ^{31}P NMR spectra was observed with large peaks at -2.2 and -11.9 ppm, for Me and Bn ligands respectively, indicating Sc-P interactions in these complexes. The reactivity of these complexes towards several electrophiles, such as benzaldehyde, isocyanates and isothiocyanates, was investigated. Whereas C-C bond formation was obtained on the backbone of the β -diketiminato ligand ($\text{R} = \text{Me}$) via $[4+2]$ cycloaddition reactions, the larger Bn-substituted ligand led to Sc/P Frustrated Lewis Pair (FLP) behaviour and the phenyl isocyanate addition product was isolated in high yield.[20]



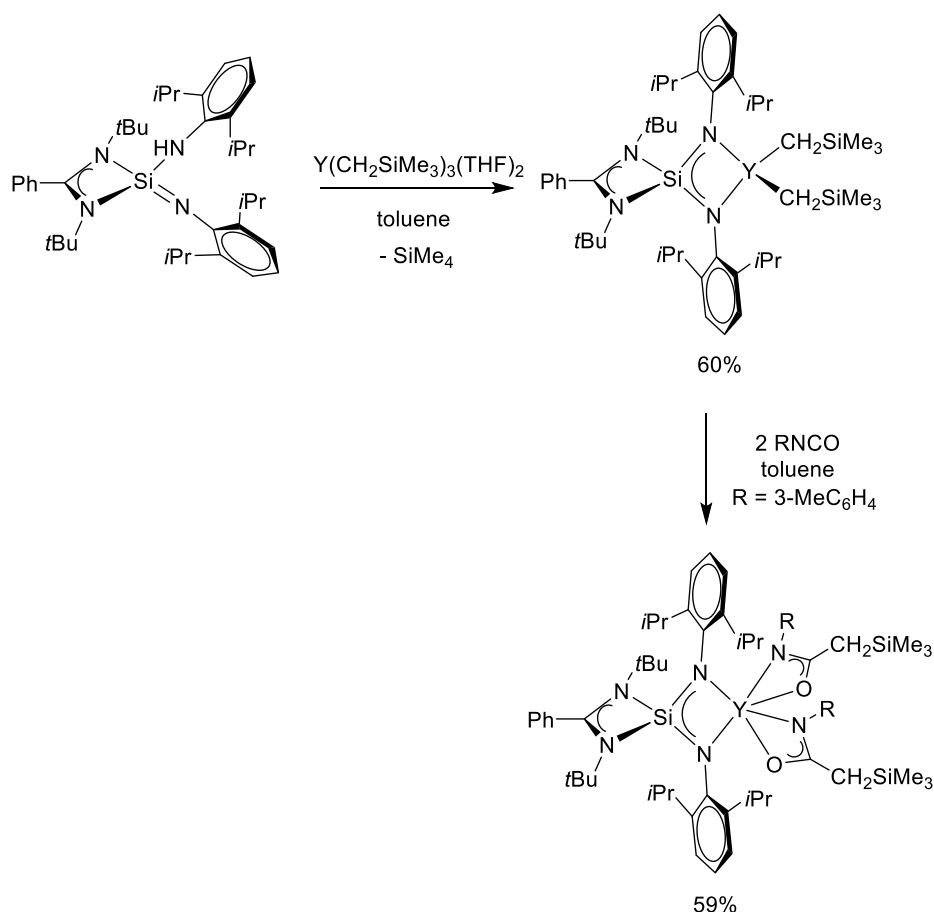
Scheme 9. Synthesis and reactivity of phosphine-stabilised cationic β -diketiminato-Sc aryloxy complexes.[20]

The anilido-oxazoline-ligated lanthanide dialkyl complexes (\mathbf{L}^{1-4}) $\text{Ln}(\text{CH}_2\text{SiMe}_3)_2(\text{THF})_n$ ($\text{Ln} = \text{Sc}, \text{Y}, n = 0, 1$) were obtained in good yields from the reaction of equimolar amounts of pro-ligands $\mathbf{HL}^1\text{-HL}^4$ and $\text{Ln}(\text{CH}_2\text{SiMe}_3)_3(\text{THF})_2$ in hexane (Scheme 10).[21] The THF solvates $\mathbf{L}^1\text{-Sc}$, $\mathbf{L}^1\text{-Y}$ and $\mathbf{L}^2\text{-Y}$ crystallised in a distorted trigonal bipyramidal configuration, whereas the solvent-free Sc complex $\mathbf{L}^2\text{-Sc}$ showed pseudo-tetrahedral configuration according to XRD studies. The Ln-N bond distances are shorter for the Ln-anilido bond than the Ln-oxazoline bond by around 0.1 Å. IR and NMR studies confirmed the coordination of the oxazolidine ring onto the lanthanide metal. The complexes showed blue-green fluorescence upon excitation at 400nm and were analysed by DFT and TD-DFT calculations. Their performance in isoprene polymerization is shown in section 2.11.1.[21] In a subsequent study, the complexes (\mathbf{L}^{5-10})Sc and (\mathbf{L}^{5-8})Y bearing chiral anilido-oxazoline ligands were synthesized and characterized in a similar way (scheme 10). These complexes were tested in lactide ring-opening polymerization (see section 2.11.1).[22]



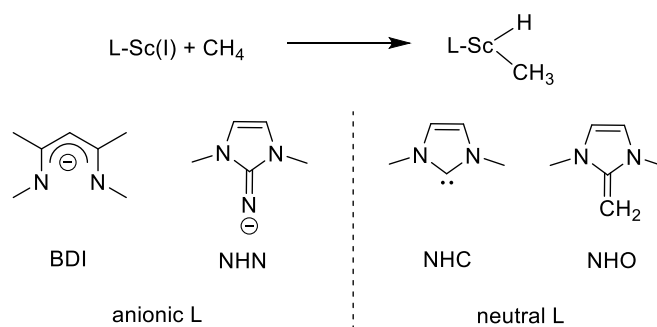
Scheme 10. Synthesis of anilido-oxazoline ligated lanthanide complexes.[21][22]

A low-coordinate yttrium dialkyl complex $[\text{PhC}(\text{N}t\text{Bu})_2\text{Si}(\text{NAr})_2]\text{Y}(\text{CH}_2\text{SiMe}_3)_2$ (Ar = 2,6-*i*Pr-C₆H₃) stabilised by a bulky silaamidinate ligand was synthesized via an alkane elimination reaction using $\text{Y}(\text{CH}_2\text{SiMe}_3)_3(\text{THF})_2$ (Scheme 11).[23] This solvent-free, four-coordinate complex showed C₂ symmetry in solution according to ¹H and ¹³C NMR spectroscopy and in the solid state as demonstrated by XRD studies. The Y metal is η²-bound to the silaamidinate ligand and together with the two alkyl groups forms a distorted tetrahedron. As this complex showed good activity for the cyclotrimerization of arylisocyanates (see section 2.11.3), a stoichiometric reaction with 3-methylphenylisocyanate was carried out to gain insights into the mechanism (Scheme 11). From this reaction, the new complex $[\text{PhC}(\text{N}t\text{Bu})_2\text{Si}(\text{NAr})_2]\text{Y}[\text{OC}(\text{CH}_2\text{SiMe}_3)\text{N}(3\text{-MeC}_6\text{H}_4)]_2$ was isolated, resulting from the insertion of two isocyanate molecules into the Y-C bonds. This complex was fully characterized by XRD analysis and NMR studies and it also showed very high efficiency as catalyst for the trimerization reaction, indicating its key role in the catalytic cycle.[23]



Scheme 11. Synthesis and reactivity of an yttrium dialkyl complex supported by a silaamidinate ligand.[23]

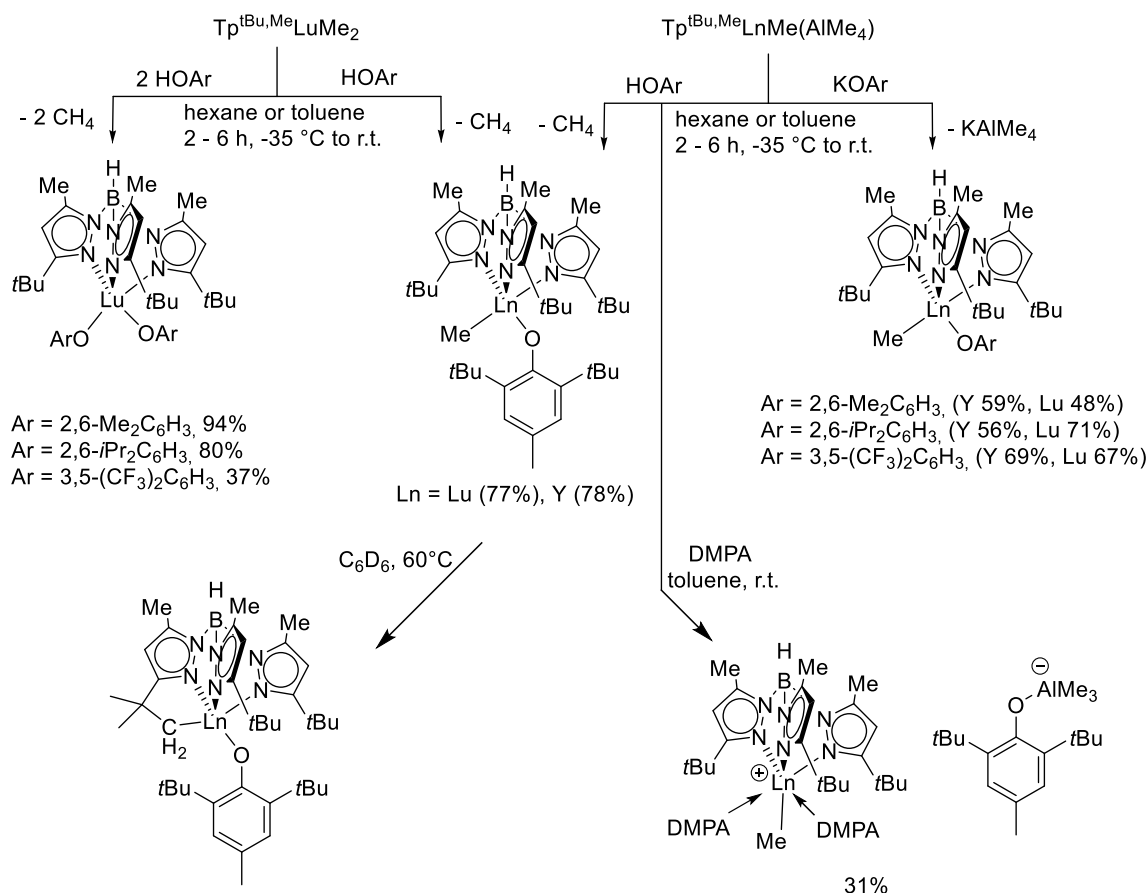
The formation of scandium methyl complexes via C-H activation of methane by Sc(I) complexes carrying neutral or anionic ligands was investigated by DFT calculations (Scheme 12).[24] Initially, the electronic properties of Sc(I) complexes bearing anionic β -diketiminato (BDI) or imidazoline-2-iminato ligands (NHN) as well as neutral N-heterocyclic carbene (NHC) or N-heterocyclic olefin (NHO) ligands were determined providing insights into the stabilization of the Sc(I) metal via mainly σ (BDI, NHC) or π (NHO) interactions or a combination of both (NHN). The first step in the CH₄ activation, the coordination of CH₄ to the Sc center is much more favored for the cationic complexes, with -15.3 and -13.0 kcal mol⁻¹ for NHC and NHO ligands, respectively, vs. -1.8 and -0.8 kcal mol⁻¹ for BDI and NHN ligands, respectively. The transition state for the C-H activation has the highest value for the NHN ligand with 18.7 kcal mol⁻¹, whereas it is relatively low (between 0.4 and 4.3 kcal mol⁻¹) for the other ligands. In all cases, the reaction is highly exergonic. In the final complexes, the Sc-C and Sc-H bonds of the inserted CH₄ molecule are significantly longer for the anionic ligands than with the neutral ligands.[24]



Scheme 12. DFT investigation on C-H activation of methane by Sc(I) complexes.[24]

The formation of mixed methyl/aryloxy lanthanide complexes stabilized by a highly encumbered tris(pyrazolyl)borato ($\text{Tp}^{\text{tBu,Me}}$) ligand was achieved using selective protonolysis or salt metathesis approaches (Scheme 13).[25] The reaction of $(\text{Tp}^{\text{tBu,Me}})\text{LuMe}_2$ with small phenols (1 or 2 equiv.) having methyl or isopropyl groups in the 2,6 positions or CF_3 groups in the 3,5 positions only led to the formation of the bis(phenolato) products $(\text{Tp}^{\text{tBu,Me}})\text{Lu}(\text{OAr})_2$. With the sterically most hindered 2,6-(tBu)₂-4-methylphenol single protonolysis was achieved, even with 2 equivalents of phenol, and the mixed ligand complex $(\text{Tp}^{\text{tBu,Me}})\text{LuMe}(\text{OAr})$ was isolated in good yield. This five-coordinate complex was characterized by ¹H and ¹³C NMR spectroscopy and its structure confirmed by XRD analysis, revealing a distorted trigonal bipyramidal coordination geometry. The corresponding Y complex was obtained from the reaction of $(\text{Tp}^{\text{tBu,Me}})\text{YMe}(\text{AlMe}_4)$ with 2,6-(tBu)₂-4-methylphenol and characterized by NMR spectroscopy. For the smaller phenols, the salt-metathesis approach starting from $(\text{Tp}^{\text{tBu,Me}})\text{LnMe}(\text{AlMe}_4)$ (Ln = Lu, Y) and KOAr proved successful to obtain the mixed methyl/aryloxy complexes in moderate to good yields, the formation of insoluble KAlMe_4 being the driving force in this reaction. These complexes were characterized by NMR spectroscopy and XRD analysis, the latter showing the influence of the metal size on the Ln-C(Me) and Ln-O bond lengths. The complexes based on the 3,5-(CF)₃-phenolate ligand were the least stable compounds in the series. The thermal stability of the mixed methyl/phenolate Lu complex $(\text{Tp}^{\text{tBu,Me}})\text{LuMe}(\text{OAr})$ (OAr = 2,6-(tBu)₂-4-methylphenolate) was investigated leading to C-H bond activation after heating at 60°C in benzene. The resulting complex showed a nearly linear Lu-O-C arrangement (175.9(2)°) in XRD studies whereas this angle was 168.2(2)° for the initial complex. Furthermore, the addition of DMAP to the reaction mixture of $(\text{Tp}^{\text{tBu,Me}})\text{LnMe}(\text{AlMe}_4)$ (Ln = Y, Lu) and 2,6-(tBu)₂-4-methylphenol allowed the isolation and structural characterization of the ion pairs $[(\text{Tp}^{\text{tBu,Me}})\text{LnMe}(\text{DMAP})_2][\text{Me}_3\text{Al}(\text{OAr})]$. XRD studies on the Y complex showed a

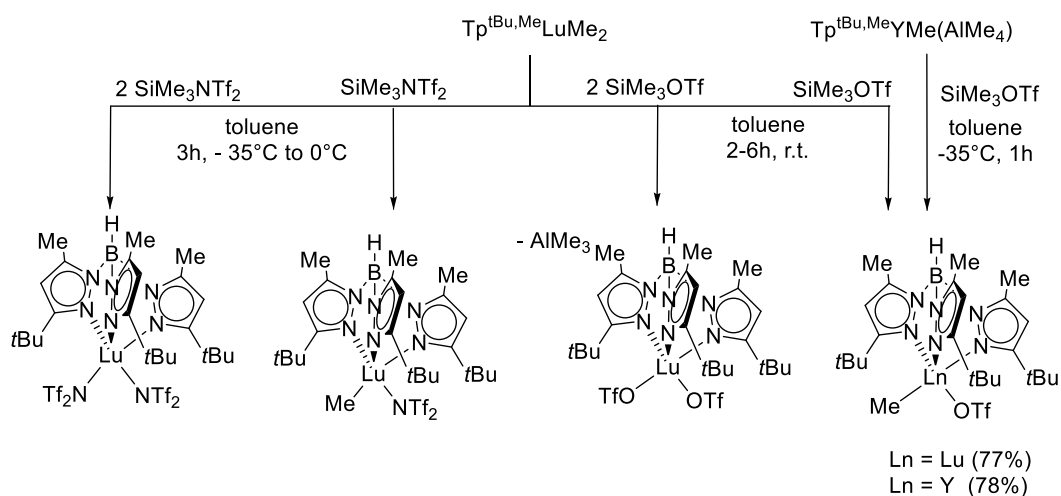
considerably shortened Y-C(Me) bond length and elongated Y-N distances compared to the mixed methyl/aryloxy complexes.[25]



Scheme 13. Synthesis and reactivity of mixed alkyl/aryloxy lanthanide complexes stabilised by the bulky $\text{Tp}^{\text{tBu,Me}}$ ligand.[25]

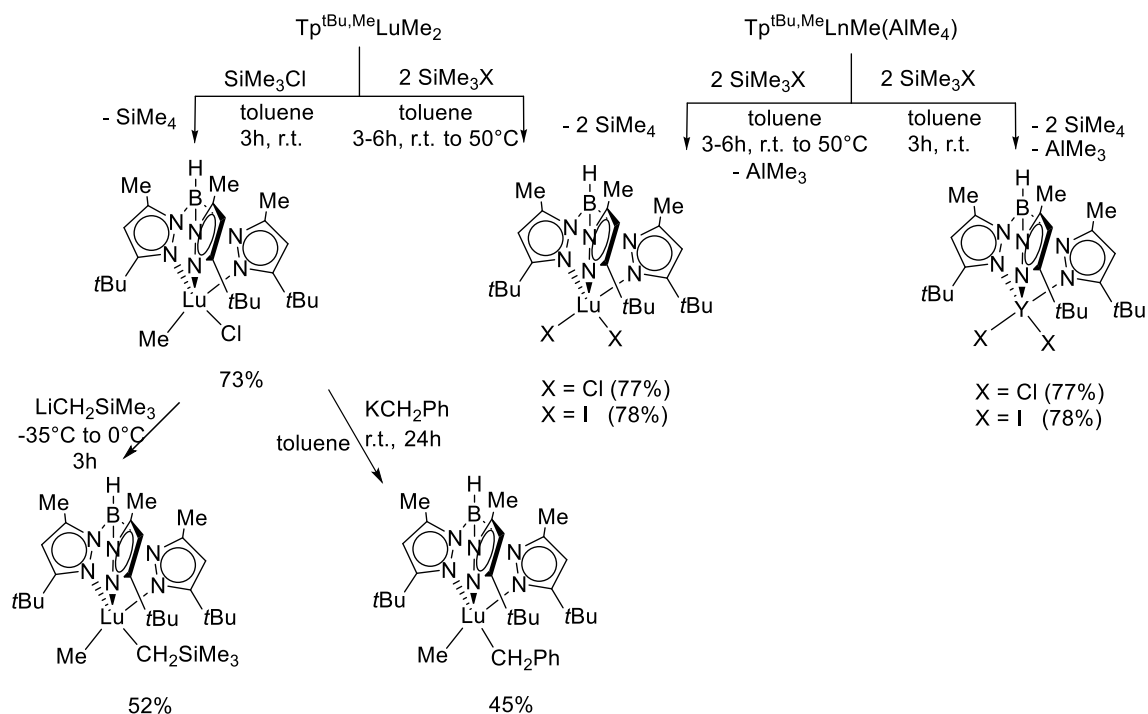
In a related study, the bulky $\text{Tp}^{\text{tBu,Me}}$ ligand was employed to stabilize heteroleptic solvent free terminal lanthanide bisalkyl complexes and mixed alkyl/triflate or alkyl/triflimide complexes as potential precursor for terminal methylidene complexes.[26] Initially, the $(\text{Tp}^{\text{tBu,Me}})\text{LuMe}_2$ and $(\text{Tp}^{\text{tBu,Me}})\text{YMe}(\text{AlMe}_4)$ complexes were reacted with the mild trimethylsilyl based transfer reagents SiMe_3X ($\text{X} = \text{OTf}$, NTf_2) to afford the methyl complexes with the weakly coordinated anions $(\text{Tp}^{\text{tBu,Me}})\text{LnMe}(\text{X})$ or the $(\text{Tp}^{\text{tBu,Me}})\text{LuX}_2$ complexes depending on the stoichiometry (Scheme 14). The complexes showed highly fluxional behaviour by NMR spectroscopy and XRD studies on the $(\text{Tp}^{\text{tBu,Me}})\text{LuMe}(\text{X})$ complexes revealed monodentate coordination of the OTf and NTf_2 groups via one of the oxygen atoms. In addition, shorter Lu-N and Lu-C(Me) bond distances were observed compared to the starting complex, which was related to the electron-withdrawing character of the OTf and NTf_2 groups. Attempted transformation of these complexes to terminal methylidene complexes using the Wittig reagent $\text{H}_2\text{C}=\text{P}(\text{Ph})_3$ was not successful at room

temperature and led to C-H bond activation involving one tBu group of the Tp ligand at higher temperature (in analogy to reaction shown in Scheme 13).[26]



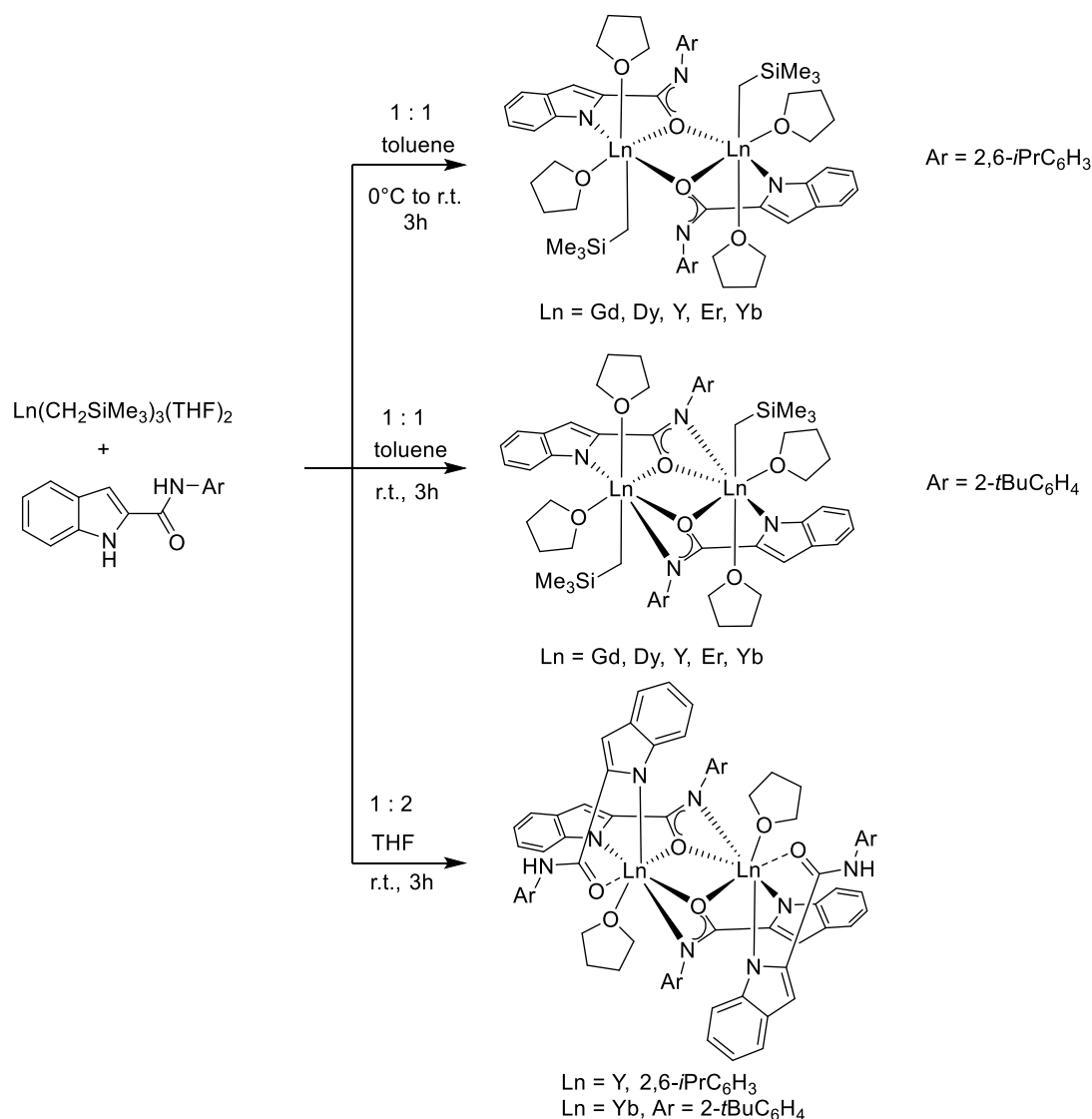
Scheme 14. Synthesis of Ln triflate and triflimide complexes stabilised by the bulky $\text{Tp}^{\text{tBu,Me}}$ ligand.[26]

Subsequently, the preparation of mixed bis(alkyl) complexes was envisaged starting from mixed methyl halide complexes. It turned out that the reaction of $(\text{Tp}^{\text{tBu,Me}})\text{LuMe}_2$ or $(\text{Tp}^{\text{tBu,Me}})\text{YMe}(\text{AlMe}_4)$ with SiMe_3Cl or SiMe_3I reagents provided in most cases the dihalide complexes $(\text{Tp}^{\text{tBu,Me}})\text{LuX}_2$ ($\text{X} = \text{Cl}, \text{I}$) due to ligand rearrangement, independent on the stoichiometry (Scheme 15). Only for the reaction between $(\text{Tp}^{\text{tBu,Me}})\text{LuMe}_2$ and one equivalent of SiMe_3Cl could the mixed methyl chloride complex $(\text{Tp}^{\text{tBu,Me}})\text{LuMeCl}$ be isolated in 73% yield and fully characterized by NMR spectroscopy and XRD analysis. Salt metathesis of this complex with $\text{LiCH}_2\text{SiMe}_3$ at low temperature or with KCH_2Ph at room temperature, provided the expected mixed methyl/alkyl complexes $(\text{Tp}^{\text{tBu,Me}})\text{LuMeR}$ ($\text{R} = \text{CH}_2\text{SiMe}_3, \text{CH}_2\text{Ph}$). Both complexes were analysed by NMR spectroscopy and XRD studies. The intramolecular deprotonation of these complexes which should lead to the terminal alkylidene complexes was studied by NMR spectroscopy. However, neither heating nor addition of N or O donor molecules (DMAP or THF) were successful and only decomposition of the starting complexes was observed.[26]



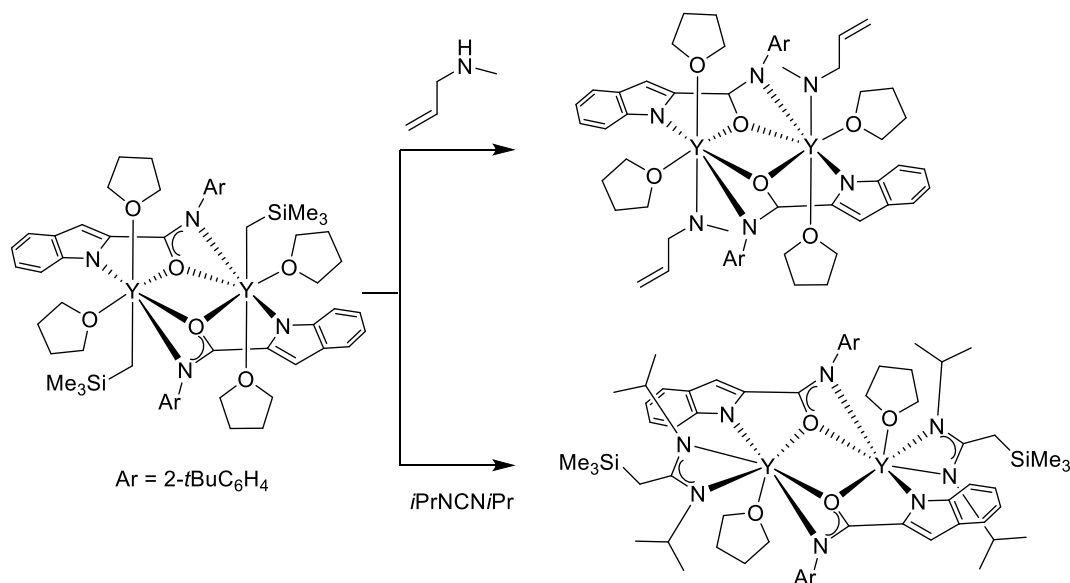
Scheme 15. Synthesis of Ln dihalide and mixed alkyl complexes stabilised by the bulky $\text{Tp}^{\text{tBu,Me}}$ ligand.[26]

The synthesis of dinuclear lanthanide metal alkyl complexes bearing two different 2-amidate-functionalised indolyl ligands using an alkane elimination pathway was reported.[27] Depending on the steric bulk on the amidate group two different binding modes were observed (Scheme 16). For the bulkier ligand carrying a 2,6-diisopropylphenyl group, the $\{[\eta^1:(\mu_2-\eta^1:\eta^1)-(L^1)]\text{Ln}(\text{CH}_2\text{SiMe}_3)(\text{THF})_2\}_2$ ($L^1 = 2-(2,6-i\text{Pr}_2\text{C}_6\text{H}_3\text{NC}=\text{O})\text{C}_8\text{H}_5\text{N}$, Ln = Gd, Dy, Y, Er and Yb) complexes were isolated in good yields. XRD analysis revealed two bridging amidate units involving only the oxygen atoms. On the other hand, the 2-*t*-butylphenyl group on the amidate ligand led to the synthesis of the complexes $\{[\eta^1:(\mu_2-\eta^1:\eta^1):\eta^1-(L^2)]\text{Ln}(\text{CH}_2\text{SiMe}_3)(\text{THF})_2\}_2$ ($L^2 = 2-(2-t\text{BuC}_6\text{H}_4\text{NC}=\text{O})\text{C}_8\text{H}_5\text{N}$, Ln = Gd, Dy, Y, Er and Yb), showing coordination of the bridging amidate groups via the O and N atoms to the lanthanide centers. Changing the metal precursor to ligand ratio to 1:2 afforded the dinuclear complexes $\{(\eta^1:\eta^1\text{-HL})[\eta^1:(\mu_2-\eta^1:\eta^1):\eta^1\text{-L}]\text{Ln}(\text{THF})\}_2$ (Ln = Y, L = L^1 ; Ln = Yb, L = L^2), with O and N bridging mode, independent of the size of the aryl group. The new complexes were characterized by XRD analysis and by NMR in the case of Y.[27]



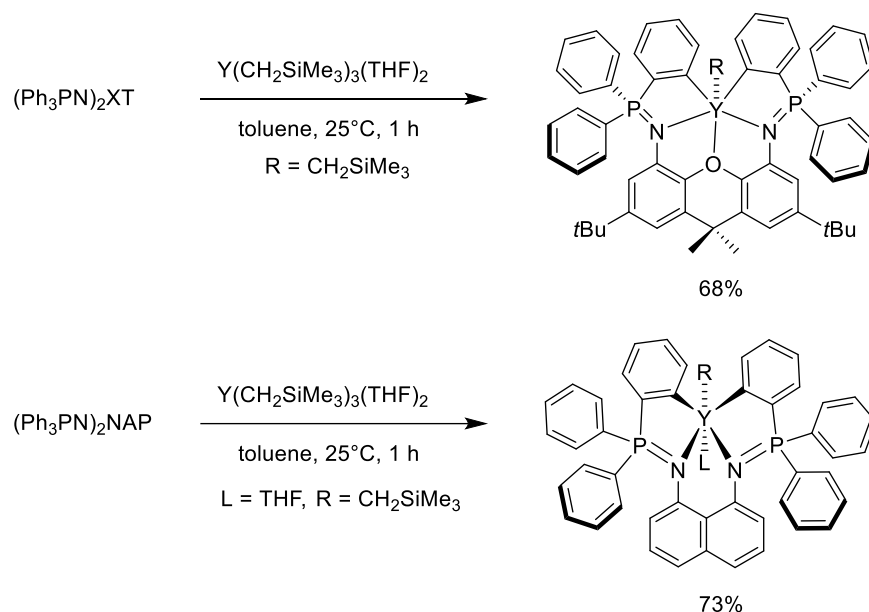
Scheme 16. Synthesis of 2-amidate indolyl lanthanide complexes.[27]

Reactivity studies with a range of small organic products provided access to new complexes derived from C-H activation, insertion or substitution reactions. Reaction with pyridine, DMAP or N-phenylimidazole did not lead to C-H activation reactions but only THF exchange reactions at the metal center were observed. Addition of N-methylallyl amine provided the corresponding amide complex via N-H activation, however, due to steric bulk, no further reaction with the C=C double bond was observed (Scheme 17). With diisopropylcarbodiimide and phenylisocyanate insertion of the alkyl group onto the central carbon atom was observed (Scheme 17). Both series of complexes were also investigated in the polymerization of isoprene (see section 2.11.1).[27]



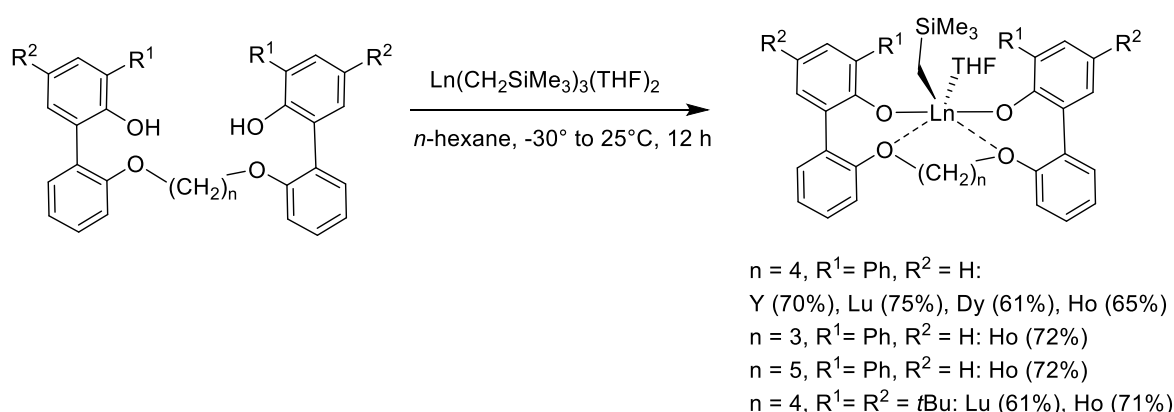
Scheme 17. Reactivity of 2-amidate indolyl lanthanide alkyl complexes.[27]

The first examples of monometallic lanthanide alkyl diaryl complexes were reported making use of the rigid xanthene and naphthalene based bis(phosphinimine) ligands, (Ph₃PN)₂XT and (Ph₃PN)₂NAP, respectively (Scheme 18).[28] Reaction of these ligands with Y(CH₂SiMe₃)₃(THF)₂ led to double cyclometallation in the ortho position of one of the phenyl groups on each of the two phosphinimine donors, providing the base-free, stable complex ((Ph₃PN)₂XT)Y(CH₂SiMe₃) and the much less stable THF solvate ((Ph₃PN)₂NAP)Y(CH₂SiMe₃)(THF). Both complexes showed C_s symmetry according to ¹H, ¹³C and ³¹P NMR spectrometry. XRD analysis of the THF adduct (Ph₃PN)₂XT)Y(CH₂SiMe₃)(THF) and the DME adduct ((Ph₃PN)₂NAP)Y(CH₂SiMe₃)(DME) revealed rather long Y-C(alkyl) bond lengths (2.465(3) and 2.520(2) Å, respectively) due to the high coordination number (CN = 7). Furthermore, both complexes have distorted pentagonal bipyramidal coordination geometries. However, whereas the Y is in the plane of the meridionally bound pentadentate dianionic XT-based ligand, the metal is out of the ligand plane (0.27 Å) in the case of the NAP-based complex with the tetradentate dianionic NAP ligand adopting a facial coordination mode.[28]



Scheme 18. Synthesis of yttrium alkyl complexes derived from xanthene and naphthalene-based bis(phosphinimide) pincer ligands via double cyclometallation.[28]

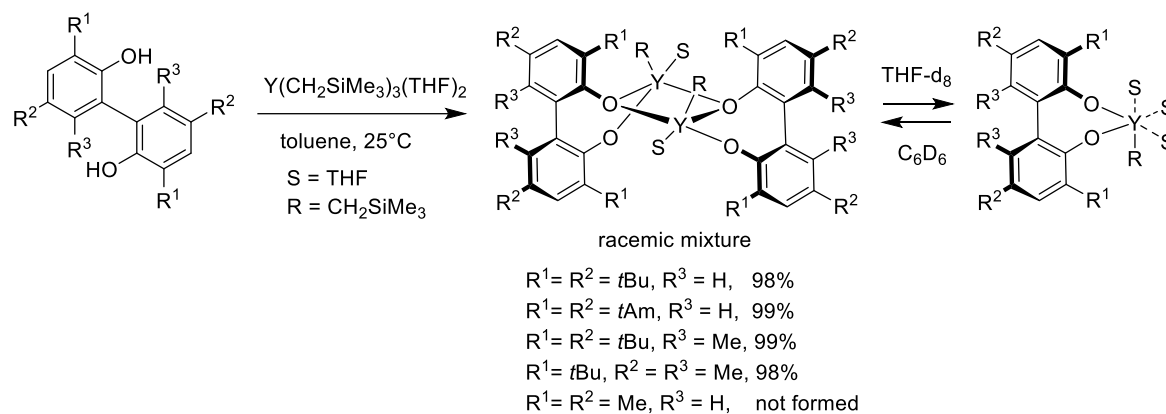
Tetradentate phenol ether proligands were employed in the synthesis of lanthanide alkyl complexes $[\text{L}]\text{Ln}(\text{CH}_2\text{SiMe}_3)(\text{THF})$ ($\text{Ln} = \text{Dy, Ho, Lu, Y, Sc}$; $\text{L} = ^-\text{OAr-ArO}-(\text{CH}_2)_n-\text{OAr-ArO}^-$ with $n = 3, 4, 5$) via deprotonation with $\text{Ln}(\text{CH}_2\text{SiMe}_3)_3(\text{THF})_2$ (Scheme 19).[29] The Lu complex with two *t*Bu groups on the aryl rings could be analysed by DRX showing a six-coordinate, distorted octahedral geometry around the metal center with the phenolate oxygen atoms in the axial positions. These complexes were studied as catalysts for 2-vinylpyridine polymerization (see section 2.11.1).[29]



Scheme 19. Synthesis of phenolato lanthanide(alkyl) complexes.[29]

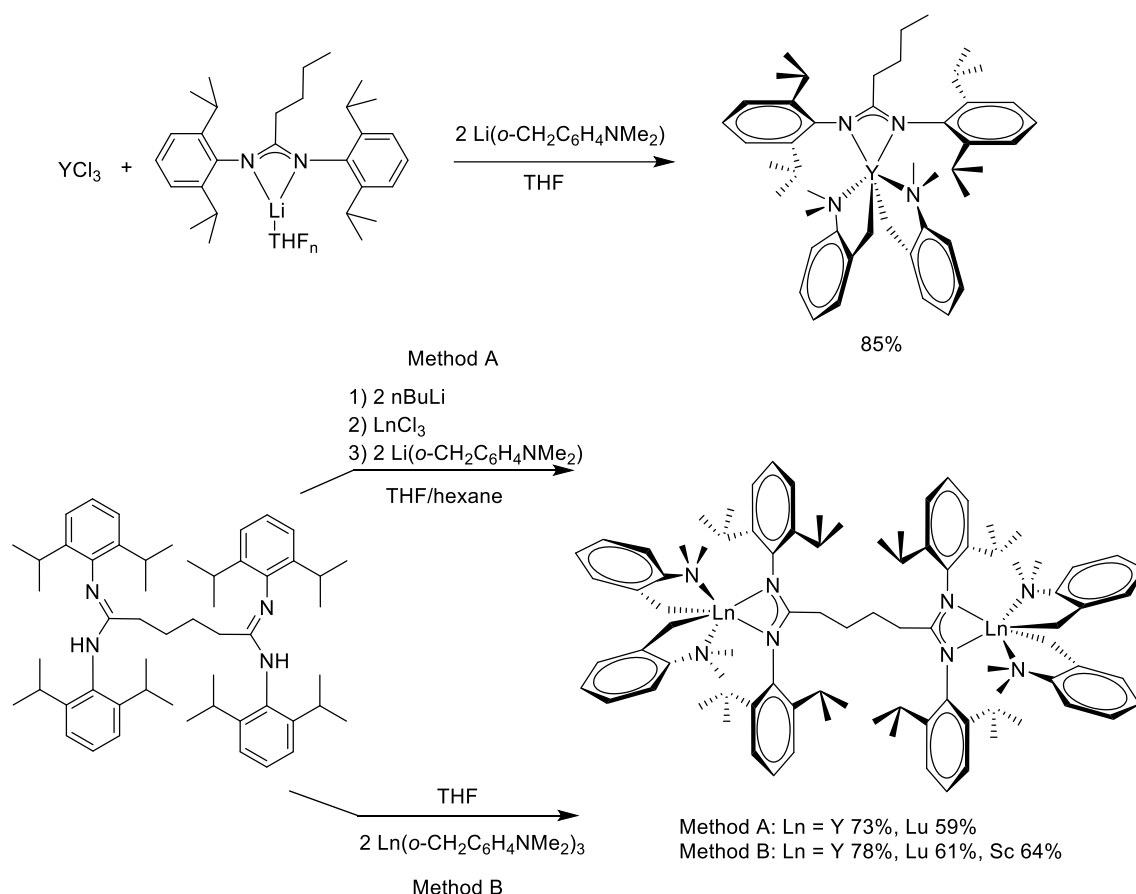
The use of biphenols with bulky substituents in the 3,3'-positions in the reaction with $\text{Y}(\text{CH}_2\text{SiMe}_3)_3(\text{THF})_2$ led to the isolation of dinuclear yttrium biphenolate alkyl complexes $[\text{L}]\text{Y}(\text{CH}_2\text{SiMe}_3)(\text{THF})_2$ ($\text{L} = ^-\text{OAr-ArO}^-$) (Scheme 20).[30] DRX studies showed the

formation of homochiral dimers, despite the use of racemic biphenols, which was further corroborated by DFT calculations. Addition of THF to the dimeric complex, led slowly to the formation of a monomeric complex, a process that could be reversed upon addition of C_6D_6 . Both monomeric and dimeric complexes were investigated as pre-catalysts for 2-vinylpyridine polymerization (see section 2.11.1).[30]



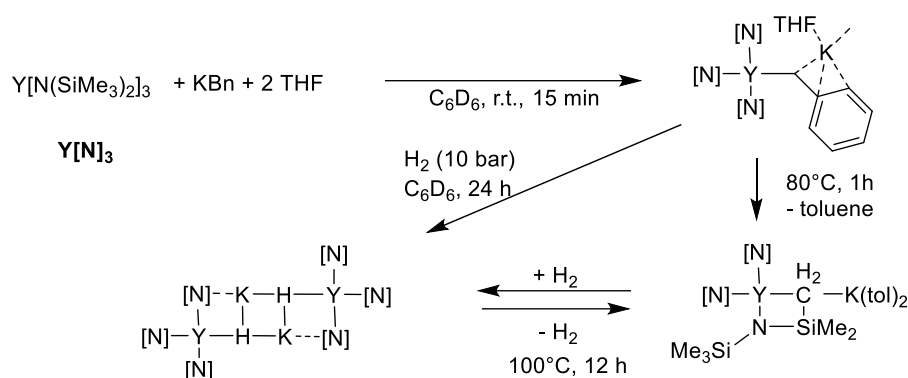
Scheme 20. Synthesis of biphenolate alkyl lanthanide complexes.[30]

The synthesis of mono and binuclear bis(aminobenzyl) lanthanide complexes $[C_4H_9C(NR)_2]Y(o-CH_2C_6H_4NMe_2)_2$ and $[(RN)_2C(CH_2)_4C(NR)_2][Ln\{CH_2C_6H_4(o-NMe_2)\}_2]_2$ ($R=2,6-iPr_2C_6H_3$, $Ln = Y, Lu, Sc$) carrying bulky formamidinato ligands was achieved via salt metathesis (for Y, Lu) or protonolysis (for Y, Lu, Sc) pathways (Scheme 21).[31] The THF-free and thermally stable complexes were fully characterized by NMR and XRD analysis, showing in the case of Y that the Y-C bond lengths were longer in the mononuclear complex compared to the binuclear complex. The new complexes were investigated in the copolymerization of isoprene and myrcene (see section 2.11.1).[31]



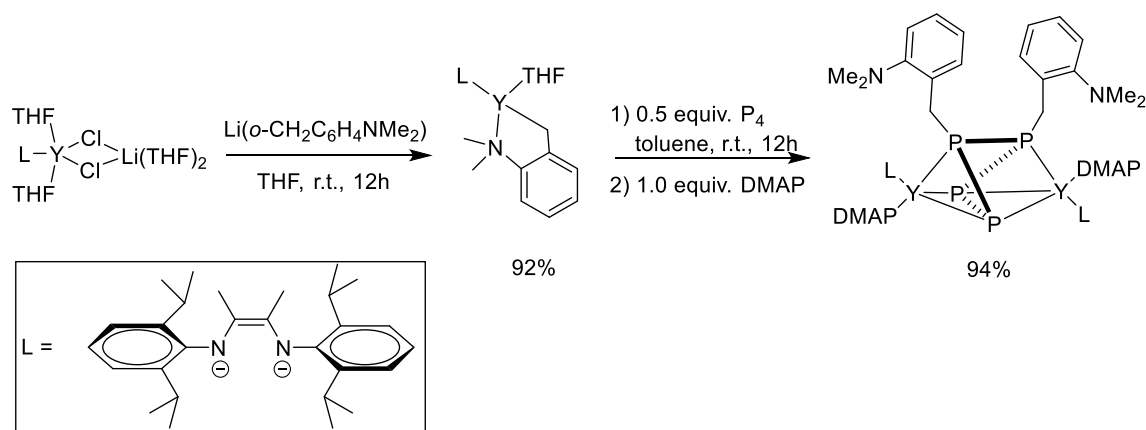
Scheme 21. Synthetic pathways to mono and binuclear bis(aminobenzyl) lanthanide formamidinato complexes.[31]

A potassium yttrium benzyl ate complex $\{YBn[N(SiMe_3)_2]_3\}[K(THF)]$ was synthesized from the reaction of $Y[N(SiMe_3)_2]_3$ with KBn in benzene (Scheme 22).[32] This complex was stable at low temperatures but gradually underwent peripheral deprotonation of one of the methyl groups at higher temperature to form the four-membered metallacycle $Y[N(SiMe_3)_2]_2[\mu-CH_2SiMe_2N(SiMe_3)]K(tol)_2$. Both complexes were crystallographically characterized, showing a contact ion pair for the initially formed benzyl ate complex in which the potassium ion is not only bound to the benzyl moiety but also to another molecular unit providing a supramolecular structure. Hydrogenation of either of these complexes led to the formation of the dimeric hydride complex $\{KHY[N(SiMe_3)_2]_3\}_2$. XRD analysis of this compound revealed a solvent-free $(KH)_2$ core supported by two Y amide complexes via Y-H and K-N interactions. Heating this hydride ate complex reversed the hydrogenation process and provided again the four-membered metallacycle. These properties were applied to the catalytic hydrogenation of unsaturated organic substrates as shown in section 2.11.2.[32]



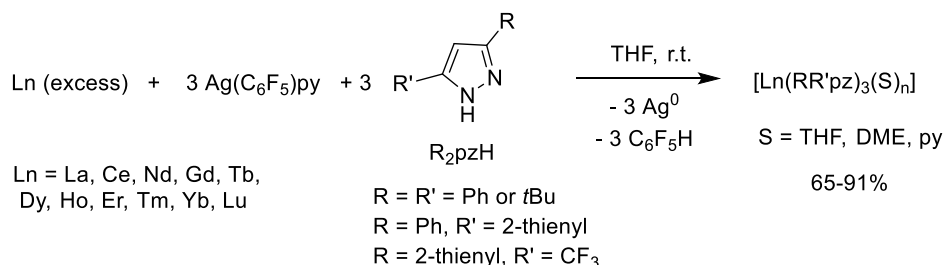
Scheme 22. Synthesis and further transformation of a potassium yttrium benzyl ate complex.[32]

The synthesis of an yttrium benzyl complex bearing the dianionic *N,N'*-2,6-diisopropylphenyl diazabutadiene ligand (L) was performed using the salt-metathesis approach between $(L)Y(THF)_2(\mu-Cl)_2Li(THF)_2$ and $Li(CH_2(o-NMe_2C_6H_4))$ (Scheme 23).[33] The monomeric THF-solvated complex $(L)Y(CH_2(o-NMe_2C_6H_4))(THF)$ was characterized by NMR spectroscopy and XRD analysis. The direct functionalization of P_4 was achieved in toluene using this benzyl complex. Addition of DMAP at the end of the reaction afforded crystals of the new complex $((L)Y-DMAP)_2[1,2-(CH_2(o-NMe_2C_6H_4)-cyclo-P_4)]$, which were analyzed by ^{31}P NMR spectroscopy (2 peaks at +2.8 and -186.9 ppm) and XRD studies. The structure consists of a binuclear Y complex coordinated to a nonplanar dibenzyl-substituted *cyclo-P*₄ unit $[R_2P_4]^{2-}$, with each Y center being coordinated to one alkylated P atom and two non-substituted P atoms. This complex could be further transformed to *cyclo-P*₃ and Zintl-type *P*₇ complexes.[33]



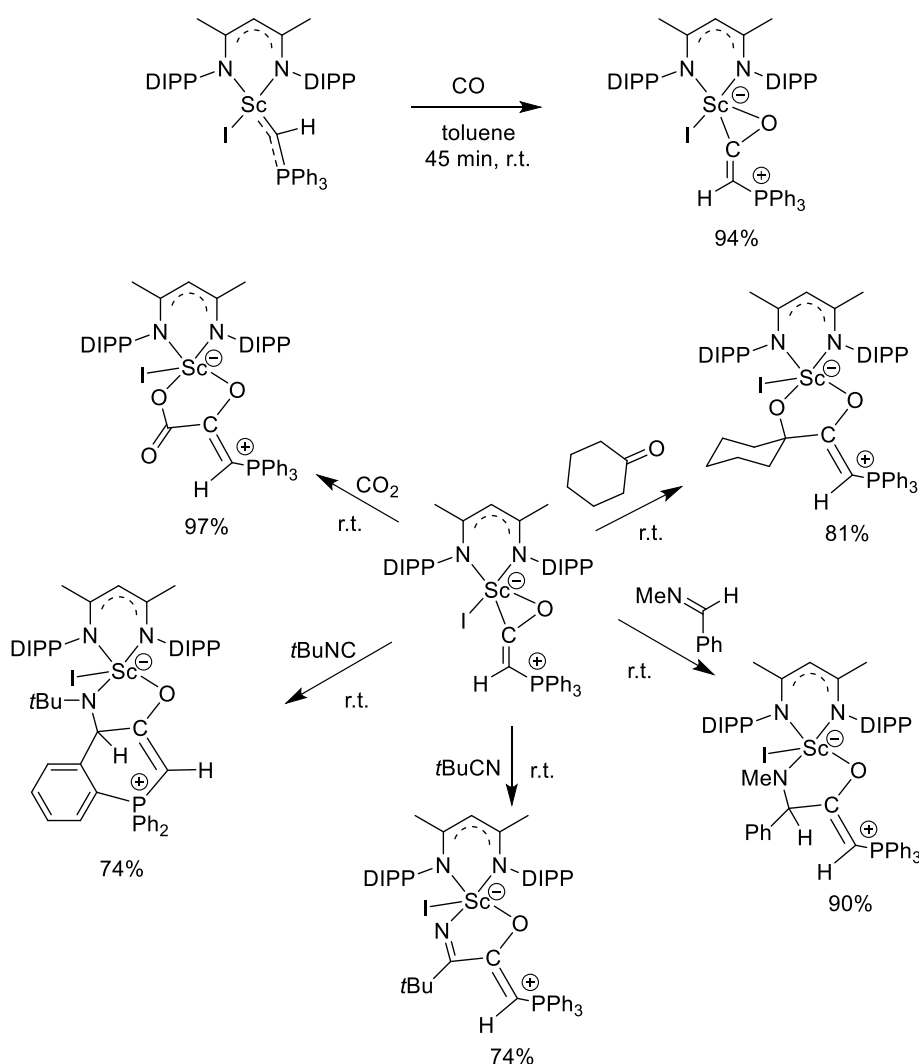
Scheme 23. Synthesis of a diazabutadiene-diyl yttrium benzyl complex and its reactivity towards P_4 .[33]

Redox-transmetallation ligand exchange reactions provide access to a variety of lanthanide complexes via the intermediate formation of highly reactive lanthanide-aryl complexes. It was shown that a series of lanthanide metals reacted with $[\text{AgC}_6\text{F}_5(\text{py})]$ and differently substituted pyrazole ligands $\text{RR}'\text{pzH}$ in THF to afford a range of tris(pyrazolato)lanthanide complexes $[\text{Ln}(\text{RR}'\text{pz})_3(\text{S})_n]$ in good yields (Scheme 24).[34]



Scheme 24. Redox-transmetallation ligand exchange reaction employing $[\text{AgC}_6\text{F}_5(\text{py})]$ with lanthanide metals and pyrazole ligands.[34]

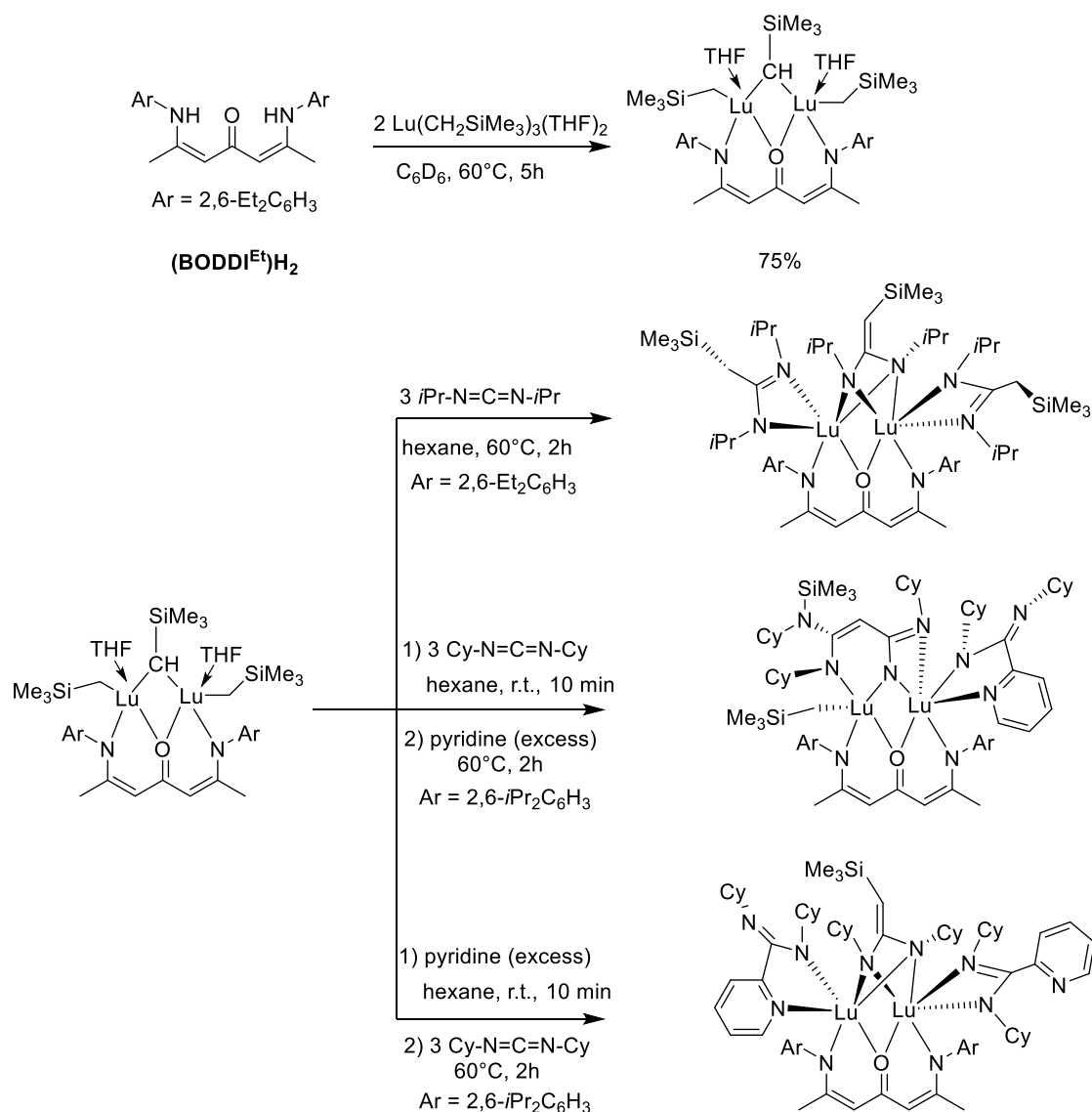
The first scandium phosphonioketene complex was synthesized in a very high yield from the reaction of the scandium phosphoniomethylidene precursor $[\text{LSc}(\text{CHPPH}_3)\text{I}]$ ($\text{L} = [\text{MeC}(\text{NDIPP})\text{CHC}(\text{NDIPP})\text{Me}^-]$) with CO (Scheme 25).[35] The thermally stable complex was characterized by NMR spectroscopy, showing the ¹³C signal for the C-O unit at $\delta = 259.5$ ppm. XRD studies revealed an η^2 coordination of the C-O unit to the Sc center, with a very short Sc-C bond (2.138(2) Å) and the C-O bond length close to a single bond (1.333(3) Å). DFT studies indicated strong Sc-C and Sc-O bonding interactions in the HOMO. Ionic coulomb interactions between Sc and C in addition to the η^2 coordination mode could contribute significantly to the short Sc-C bond. A range of unsaturated organic molecules, such as CO₂, cyclohexanone, imine or nitrile reacted with the phosphonioketene complex under mild conditions via insertion into the nucleophilic Sc-C bond (Scheme 25). In the case of *t*butyl-isocyanide, the initial insertion product was unstable and reacted further via deprotonation of one of the phenyl groups on the phosphorus atom.[35]



Scheme 25. Synthesis and reactivity of a scandium phosphonioketene complex.[35]

The reactivity of four-coordinate lutetium-methanediide-alkyl complexes stabilized by β -oxo- δ -diimine (BODDI^R) ligands with variable steric bulk ($R = \text{Et}, \text{iPr}$) was investigated (Scheme 26).[36] The new complex (BODDI^{Et})Lu₂-(CH₂SiMe₃)₂(μ_2 -CHSiMe₃)(THF)₂ was obtained in good yields via protonolysis of (BODDI^{Et})H₂ and characterized by NMR spectroscopy. Its reactions towards electrophilic N,N-diisopropylcarbodiimide (iPrN=C=NiPr) afforded insertion of three molecules of iPrN=C=NiPr into the Lu- μ_2 -CHSiMe₃ or Lu-CH₂SiMe₃ bonds as confirmed by XRD analysis. Reaction of the bulkier complex (BODDI^{iPr})Lu₂-(CH₂SiMe₃)₂(μ_2 -CHSiMe₃)(THF)₂ with N,N-dicyclohexylcarbodiimide (CyN=C=NCy) and pyridine, provided access to new products, depending on the order of addition. In the case of initial addition of three equivalents of CyN=C=NCy followed by reaction with pyridine afforded the crystallographically characterized complex (BODDI^{iPr})Lu₂(CH₂SiMe₃)[CyNC(NCy)CHC(NCy)NCy(SiMe₃)] [CyNC(C₆H₄N)NCy] resulting from the insertion of two CyN=C=NCy molecules into the Lu- μ_2 -CHSiMe₃ bond

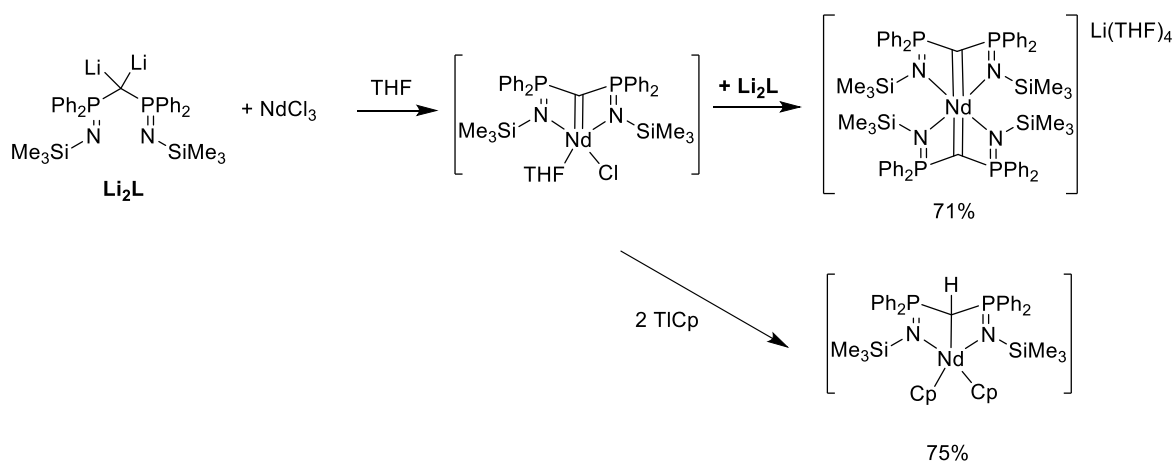
and ortho-C-H activation on pyridine. Upon inverting the addition of reagents, i.e. first reaction with pyridine followed by $\text{CyN}=\text{C}=\text{NCy}$, provided the new complex $(\text{BODDI}^{\text{iPr}})\text{Lu}_2[\text{CyNC}(\text{NCy})\text{-C}_6\text{H}_4\text{N}][\text{CyNC}(\text{=CHSiMe}_3)\text{NCy}][\text{CyNC}(\text{C}_6\text{H}_4\text{N})\text{NCy}]$, as shown by XRD analysis, with double ortho C-H activation on pyridine and insertion of only one molecule of $\text{CyN}=\text{C}=\text{NCy}$ into the $\text{Lu}-\mu_2\text{-CHSiMe}_3$ bond. Possible mechanistic pathways were proposed based on DFT calculations.[36]



Scheme 26. Synthesis of Lu-methanediide alkyl complexes stabilized by BODDI pincer ligands and reactivity towards pyridine and carbodiimides.[36]

A new Nd bis-carbene complex $\text{Nd}\{\text{C}(\text{Ph}_2\text{P}=\text{NSiMe}_3)_2\}_2[\text{Li}(\text{THF})_4]$ was obtained and structurally characterized from the reaction of NdCl_3 with two equivalents of the dianionic precursor $\text{Li}_2\text{C}(\text{Ph}_2\text{P}=\text{NSiMe}_3)_2$ (Li_2L) in THF (Scheme 27).[37] The $\text{C}=\text{Nd}=\text{C}$ bond angle is quasi-linear ($178.21(10)^\circ$) and the very short $\text{Nd}=\text{C}$ bond lengths are identical ($2.583(3)$

Å), the latter indicating some multiple bonding interactions. The two metallacycles defined by the two Nd-NPCPN frameworks and joined by the Nd ion are nearly perpendicular to each other ($84.62(4)^\circ$). According to DFT calculations and NBO analysis, the C=Nd bond contains 21.19 % carbon and 14.43 % Nd component. When the proposed mono-carbene Nd intermediate complex, resulting from the equimolar reaction of Li_2L with NdCl_3 , was reacted with 2 equiv. of TICp , the metallocene complex $\text{Cp}_2\text{Nd}\{\text{CH}(\text{Ph}_2\text{P}=\text{NSiMe}_3)_2\}$ was isolated and characterized by XRD, showing an unexpected protonation of the methandiide carbon (Scheme 27).[37]



Scheme 27. Synthesis of a new Nd bis(carbene) complex $[\text{Nd}\{\text{C}(\text{Ph}_2\text{P}=\text{NSiMe}_3)_2\}_2][\text{Li}(\text{THF})_4]$. [37]

2.3. LANTHANIDE (HETERO)ALLYL, ALKYNYL AND PENTADIENYL COMPLEXES

The reactions of 1,4-pentadiene and 1-pentyne with lanthanum metal under laser-vaporization molecular beam source conditions were reported.[38] One major lanthanum complex of the general formula $\text{La}(\text{C}_5\text{H}_6)$, resulting from dehydrogenation in the gas phase, was observed in both reactions by TOF mass spectrometry. A minor species $\text{La}(\text{C}_3\text{H}_4)$, also detected by TOF MS, could result from C-C bond cleavage and ethylene elimination. Figure 2 shows the proposed structure of the major isomer of $\text{La}(\text{C}_5\text{H}_6)$, a six-membered lanthanacycle, and the two possible isomers of $\text{La}(\text{C}_3\text{H}_4)$ as three or four-membered rings. These structures were deduced from mass-analyzed threshold ionization (MATI) spectroscopy and quantum chemical calculations. In the case of 1,4-pentadiene, La addition to a C=C double bond followed by metal insertion into two C(sp³)-H bonds and concerted hydrogen elimination would lead to $\text{La}(\text{C}_5\text{H}_6)$. For 1-pentyne, after an initial

formation of a pi-complex by coordination of La to the triple bond an isomerization through hydrogen migration would be required before the same steps as for 1,4-pentadiene could occur.[38]

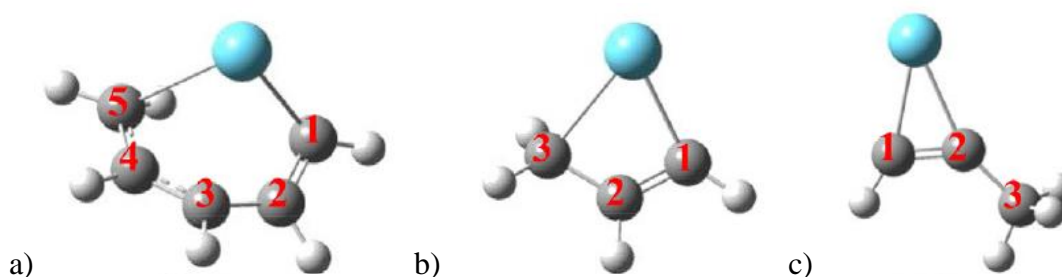
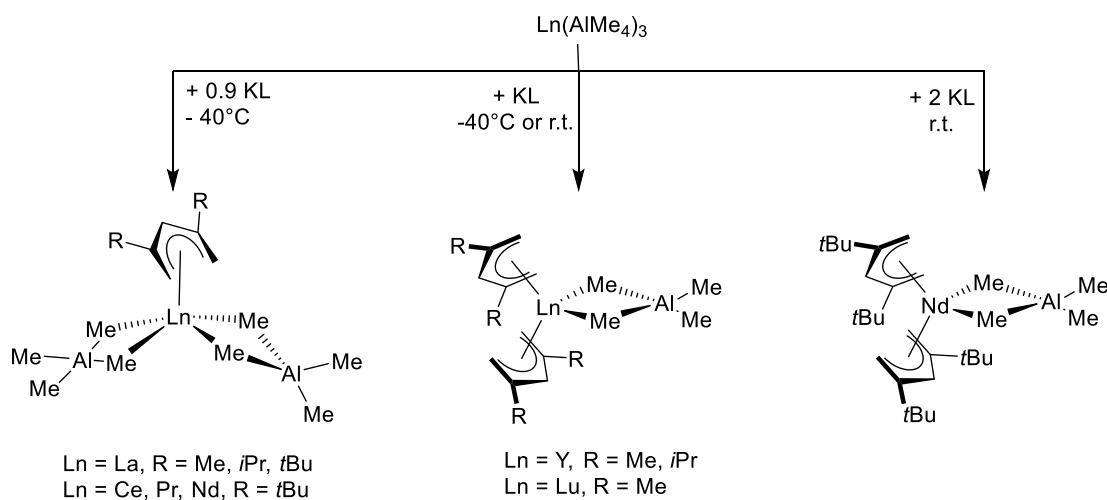


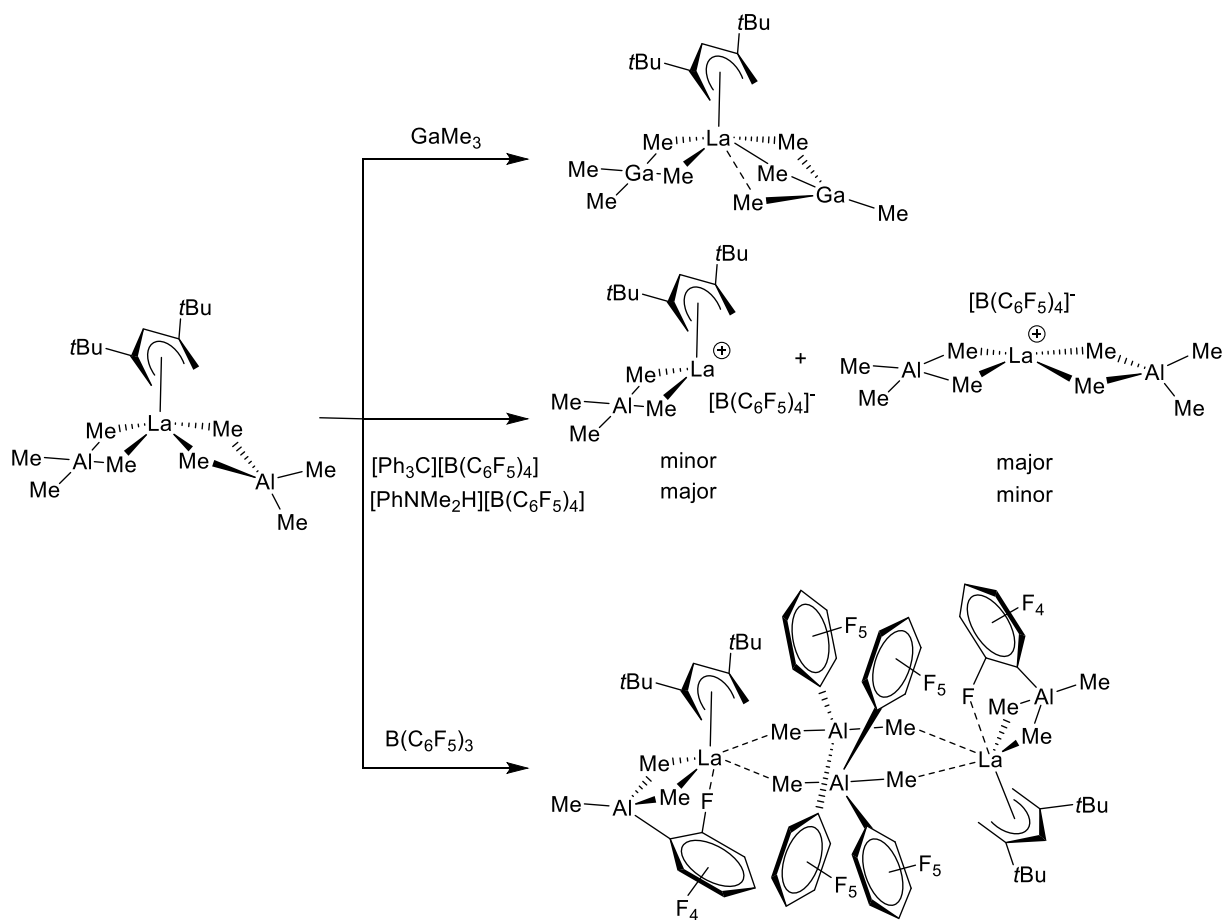
Figure 2. Structures of isomers of $\text{La}(\text{C}_5\text{H}_6)$ (a) and $\text{La}(\text{C}_3\text{H}_4)$ [(b),(c)]. Adapted with permission from ref. [38]. Copyright 2019 Elsevier

The synthesis of new trivalent lanthanide half-sandwich and sandwich complexes supported by various pentadienyl ligands (pdl = 2,4-di-methylpentadienyl (2,4-dmp), 2,4-di-isopropylpentadienyl (2,4-dip), 2,4-di-*t*-butylpentadienyl (2,4-dtbp)) was achieved by the salt metathesis reaction of $\text{Ln}(\text{AlMe}_4)_3$ with one or two equivalents of $\text{K}(\text{pdl})$ (Scheme 28).[39] The half-sandwich complexes $[(2,4\text{-dtbp})\text{Ln}(\text{AlMe}_4)_2]$ ($\text{Ln}=\text{La}$, Ce, Pr, Nd), $[(2,4\text{-dipp})\text{La}(\text{AlMe}_4)_2]$, and $[(2,4\text{-dmp})\text{La}(\text{AlMe}_4)_2]$, were obtained selectively at low temperature and characterized by NMR spectroscopy, revealing a rigid coordination of the pdl, except for La. XRD analysis showed a η^5 -type U-shaped coordination of the ligand to the metal. Interestingly, for Y and Lu, only the sandwich complexes $[(2,4\text{-dipp})_2\text{Y}(\text{AlMe}_4)]$ and $[(2,4\text{-dmp})_2\text{Ln}(\text{AlMe}_4)]$ ($\text{Ln}=\text{Y}$, Lu) could be obtained, independent on stoichiometry and temperature.



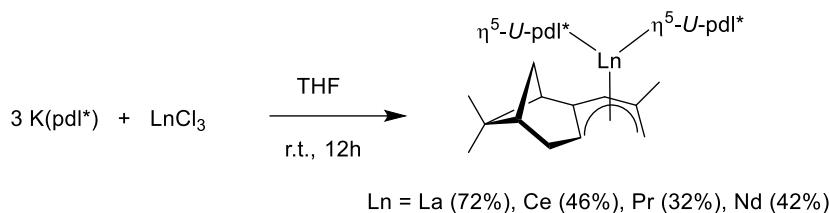
Scheme 28. Synthesis of pentadienyl lanthanide sandwich and half-sandwich complexes.[39]

The reactivity of the bulky (2,4-dtbp)La(AlMe₄)₂ complex was further examined (Scheme 29). Reaction with GaMe₃ led to a replacement of the trimethylaluminium groups and formation of the alkylgallate complex (2,4-dtbp)La(GaMe₄)₂ as shown by XRD studies. The lower Lewis acidity of Ga vs. Al led to a bent η²-coordination of one of the [GaMe₄]⁻ units. Activation of the (2,4-dtbp)La(AlMe₄)₂ complex with [Ph₃C][B(C₆F₅)₄] afforded mainly pentadienyl abstraction and formation of the cationic species La(AlMe₄)₂[B(C₆F₅)₄]⁺, whereas protonation with [PhNMe₂H][B(C₆F₅)₄] provided the cationic monopentadienyl (2,4-dtbp)La(AlMe₄)[B(C₆F₅)₄]⁺ as major product, according to NMR studies. Finally, reaction with B(C₆F₅)₃ led to the isolation and structural characterization of the multimetallic La-Al complex {(2,4-dtbp)La[(μ-Me)₂AlMe(C₆F₅)]}₂[Me₂Al(C₆F₅)₂]₂ having two bridging Me₂Al(C₆F₅)₂ units between the La centers. The different complexes were also investigated in isoprene polymerization (see section 2.11.1).[39]



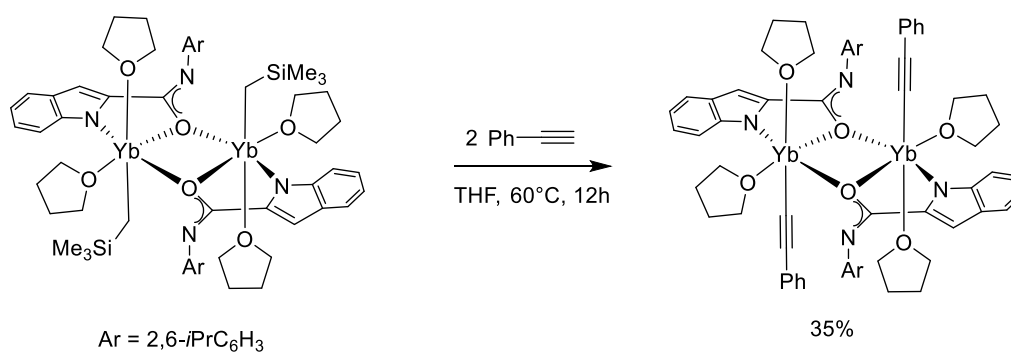
Scheme 29. Reactivity of a pentadienyl-based lanthanum half-sandwich complex.[39]

A chiral pentadienyl ligand (pdl*), derived from (1R)-(-)-myrtenal, was employed in the synthesis of the first series of enantiomerically pure tris(pentadienyl)lanthanide Ln(pdl*)₃ complexes by salt metathesis (Scheme 30).[40] The new complexes, which showed high thermal stability, were characterized in solution by NMR spectroscopy showing idealised C₃-symmetry. XRD analysis revealed exclusive coordination of the metal to the less sterically hindered face of the ligand with the typical η⁵-U coordination.[40]



Scheme 30. Synthesis of enantiomerically pure tris(pentadienyl)lanthanide Ln(pdl*)₃ complexes.[40]

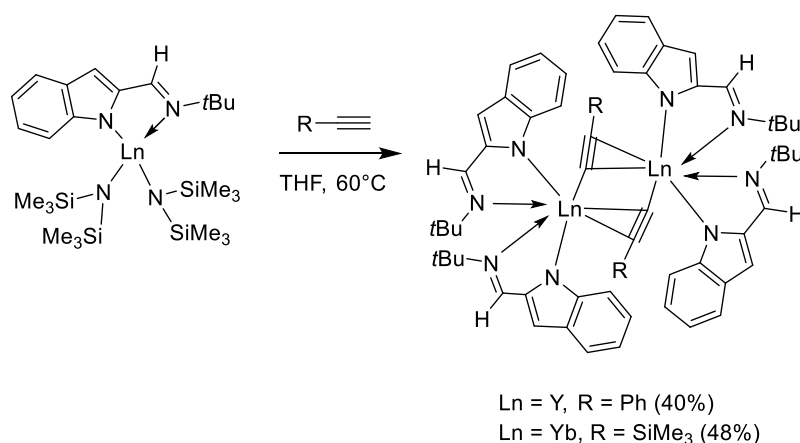
Reaction of the dinuclear 2-amidate-indolyl ytterbium alkyl complex (synthesis see Scheme 16) with two equivalents of phenylacetylene in warm THF provided access to a rare example of a terminal lanthanide alkynyl complex (Scheme 31).[27] This compound was characterized by XRD analysis showing no changes in the coordination of the amidate functionality towards the Yb center. In the Yb-alkynyl fragment, a short Yb-C bond of 2.314(12) Å and a normal C≡C triple bond of 1.192(14) Å were measured, with the M-C≡C unit exhibiting an angle of 162.4°.[27]



Scheme 31. Synthesis of a terminal alkynyl lanthanide complex stabilized by 2-amidate indolyl ligand.[27]

In the course of the study on the reaction mechanism of alkyne addition onto carbodiimides, the reaction of terminal alkynes with bis(amido)lanthanide complexes stabilized by bulky imino-functionalized indolyl ligands was carried out (Scheme 32).[41]

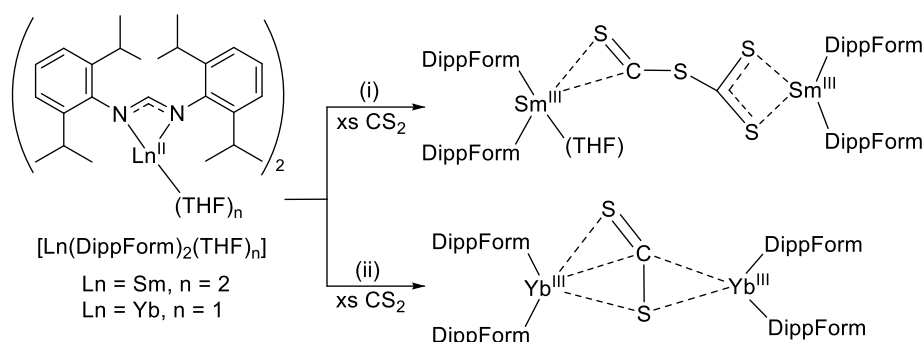
Performing the reaction at 60°C in THF led to the isolation of a dinuclear lanthanide alkynide species $\{(\mu\text{-}\eta^1\text{:}\eta^2\text{-RC}\equiv\text{C})\text{Ln}[2\text{-}(\text{tBuN}=\text{CH})\text{C}_8\text{H}_5\text{N}]_2\}_2$ (Ln = Y, R = Ph; Ln = Yb, R = SiMe₃), obtained after protonolysis and ligand rearrangement. Characterization by XRD revealed a bridging alkynyl group between two metal centers in a $\mu\text{:}\eta^1\text{:}\eta^2$ binding mode. The C≡C triple bond lengths are in the expected range (1.176-1.216 Å) and the Y-C≡C bonds are longer (2.513 Å av.) than the corresponding Yb-C≡C bonds (2.485 Å av.). However, the angle of the M-C≡C moiety deviates from linearity (161.9°). Further analysis in solution by NMR and IR spectroscopy were in agreement with the XRD structure.[41]



Scheme 32. Synthesis of dinuclear lanthanide metal alkynide complex.[41]

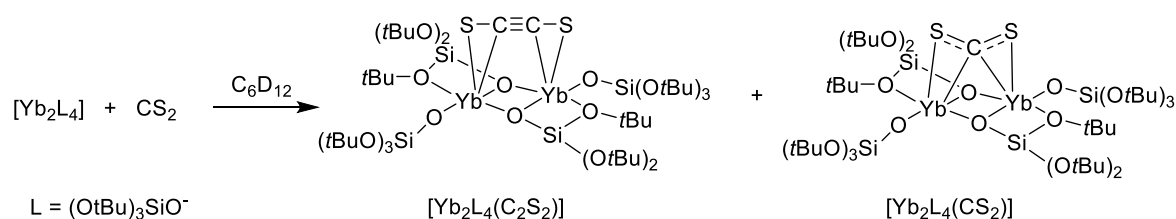
The linear first-row metal acetylene complexes, HC≡C-TM-H (TM = Sc-Ni) were studied by DFT and ab-initio calculations to explore their capacity of adsorbing multiple hydrogen molecules.[42] The ground state of the Sc complex was determined to be 2 and a maximum of six H₂ molecules could be adsorbed onto this complex, corresponding to a gravimetric hydrogen storage capacity of 14.56 %. It should be noted, that no dissociation of the first adsorbed hydrogen molecule was observed. However, the adsorption is a reversible process depending on the temperature. At 300 K, only two H₂ molecules could be adsorbed (5.37% gravimetric H₂ storage capacity).[42]

The reaction between an excess of CS₂ and the divalent Yb formamidinate complex [Yb(DippForm)₂(THF)] allowed the isolation of the CS₂²⁻ bridged dimeric Yb(III) complex [Yb₂(DippForm)₄(CS₂)] (Scheme 33). [43] XRD analysis revealed an unprecedented $\mu\text{-}1\eta^3(\text{S,C,S}'):2\eta^2(\text{S,C})$ binding motif in the Yb₂CS₂ unit. It should be noted, that in a previous study, the analogous Sm complex led to a dimerisation of two CS₂ units due to the larger Sm²⁺ ion.[43]



Scheme 33. Synthesis of CS_2^{2-} bridged Yb-formamidinate complex.[43]

Multimetallic cooperativity was observed in the reduction of CS_2 by the dinuclear divalent ytterbium siloxide complex Yb_2L_4 ($\text{L} = (\text{OtBu})_3\text{SiO}^-$) (Scheme 34).[44] Reacting CS_2 with this complex at room temperature in cyclohexane, followed by crystallization in hexane at -40°C led to the co-crystallisation of two complexes. The acetylenedithiolate bridged Yb(III) complex $\text{Yb}_2\text{L}_4(\text{C}_2\text{S}_2)$ was characterized by XRD analysis, showing a near-linear acetylenedithiolate unit which is bound to two Yb centers in a $\mu\text{-}1\eta^3(\text{S},\text{C},\text{S}'):2\eta^2(\text{S},\text{C})$ fashion with mean Yb-C distances of 2.62(2) Å. The second complex is an intermediate CS_2 -bridged complex, $\text{Yb}_2\text{L}_4(\text{CS}_2)$, revealing an unprecedented double side-on binding mode of the CS_2^{2-} bridge with the Yb centers. The formation of both complexes was investigated by DFT calculations. Initial double reduction of CS_2 by the two divalent Yb centers led to the formation of the unusual end-on bound intermediate. This binding mode then favors a [2+2] cycloaddition with another CS_2 molecule and after release of S_2 the final acetylenedithiolate complex is formed.[44]



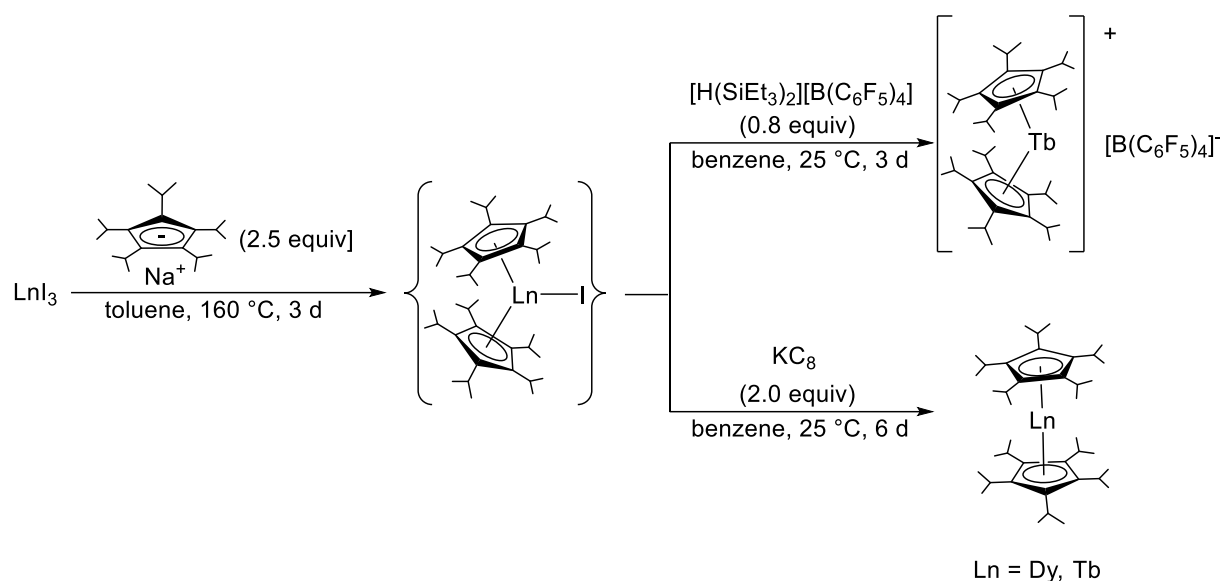
Scheme 34. Reduction of CS_2 by divalent Yb complex leading to a new acetylenedithiolate complex and an intermediate end-on bound CS_2^{2-} complex.[44]

2.4. LANTHANIDE CYCLOPENTADIENYL COMPLEXES

2.4.1. Cp_2Ln and $[\text{Cp}_3\text{Ln}]^-$ Compounds

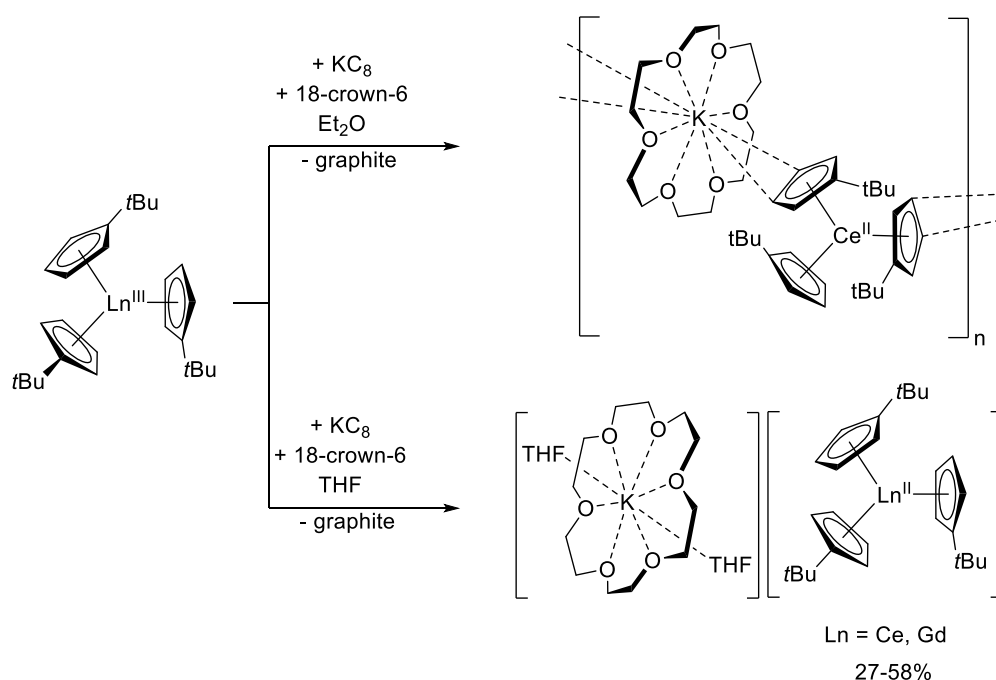
The search for non-classical divalent lanthanide complexes, i.e. other than Eu, Yb, Sm, based on Cp ligands was continued in 2019.

A break-through report was the synthesis of the first neutral divalent metallocene complexes of Tb and Dy using the sterically very hindered penta-isopropylCp ligand ($\text{Cp}^{5i\text{Pr}}$).^[45] Reduction of the trivalent precursors $(\text{Cp}^{5i\text{Pr}})_2\text{LnI}$ with KC_8 in benzene for several days afforded the linear sandwich complexes $\text{Ln}(\text{Cp}^{5i\text{Pr}})_2$ ($\text{Ln} = \text{Tb, Dy}$) which exhibited high stability at room temperature (Scheme 35). XRD studies showed a high symmetry core structure (D_{5d}), with only slightly increased metal-carbon distances compared to the trivalent precursor, in agreement with a $4f^n5d^1$ electron configuration for Dy and Tb. The latter was further supported by DFT calculations. Magnetic susceptibility was measured for the divalent complexes, showing room temperature χ_{MT} values of 12.72 and 15.15 emu K/mol for Tb and Dy, respectively, which are different from the calculated values for Tb ($4f^9$, 14.13) and Dy ($4f^{10}$, 14.07) but also lower than previously reported complexes with $4f^n5d^1$ electron configuration (Tb 14.42, Dy 17.01). This could be explained by a strong $5d_{z^2}$ -6s orbital mixing. In order to compare the SMM behaviour of the divalent complexes with the corresponding cationic trivalent complexes, the iodide abstraction reaction of the $(\text{Cp}^{5i\text{Pr}})_2\text{TbI}$ precursor with $[\text{H}(\text{SiEt}_3)_2][\text{B}(\text{C}_6\text{F}_5)_4]$ was performed to yield the cationic $(\text{Cp}^{5i\text{Pr}})_2\text{Tb}[\text{B}(\text{C}_6\text{F}_5)]$ complex, which showed no interaction between the anion and the metal center (Scheme 35). The divalent Tb complex (Kramer ion) showed interesting magnetic properties with a large effective barrier to magnetic relaxation $U_{\text{eff}} = 1205 \text{ cm}^{-1}$ and a 100-s magnetic blocking temperature of 52 K. For the cationic Tb(III) complex, the magnetic properties are considerably different from the divalent Dy complex, even though both complexes contain a non-Kramer ion. Magnetic relaxation is much faster for Tb(III) and hysteresis is largely absent at 2 K, whereas for Dy(II) butterfly magnetic hysteresis was observed between 2 K and 75 K. This could be explained by the more axial symmetry structure of the neutral Dy(II) complex compared to the cationic Tb(III) complex.^[45]



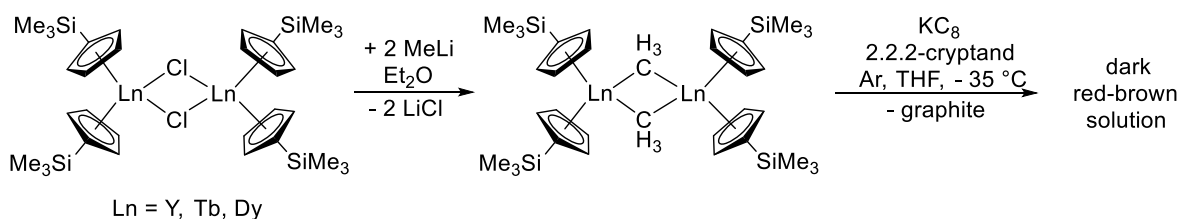
Scheme 35. Synthesis of first neutral divalent metallocenes of Tb and Dy and the cationic Tb complex.[45]

In order to study the electronic influence on the synthesis and stability of divalent complexes of the $[\text{Ln}(\text{Cp})_3]^-$ type, based on sterically similar Cp^* ($\text{C}_5\text{H}_4\text{SiMe}_3$) and Cp^t ($\text{C}_5\text{H}_4t\text{Bu}$) ligands, the reduction of $\text{Ln}(\text{Cp}^t)_3$ ($\text{Ln} = \text{La}, \text{Ce}, \text{Nd}, \text{Gd}, \text{Ho}, \text{Dy}, \text{Y}$) with KC_8 in the presence of crown ether or cryptand in different solvents was investigated (Scheme 36).[46] In the case of Ce and Gd, reduction in THF with 18-crown-6/ KC_8 at -35°C yielded the monomeric complexes $[\text{K}(18\text{-crown-6})(\text{THF})_2][\text{LnCp}^t_3]$ ($\text{Ln} = \text{Ce}, \text{Gd}$), which were characterized by XRD, UV-visible and EPR spectroscopy and provided data similar to previously synthesized divalent complexes. The dark colour of both complexes disappeared after 24 h at room temperature. In the case of cerium the reduction was also carried out in Et_2O and afforded a polymeric divalent Ce complex $\{[\text{K}(18\text{-crown-6})][(\mu\text{-Cp}^t)\text{CeCp}^t_2]\}_n$ with one terminal Cp^t and two bridging Cp^t ligands. In addition, after several months, a small amount of crystals of a bimetallic mixed valent complex $[\text{K}(18\text{-crown-6})][(\mu\text{-Cp}^t)\text{CeCp}^t_2]_2$ was obtained in which each Ce has two terminal Cp^t and one bridging Cp^t ligand. The Ce centers cannot be distinguished as the molecule is located on an inversion center with the potassium ion in the center. Reduction reactions with LaCp^t_3 and YCp^t_3 provided EPR spectra consistent with divalent complexes as reported previously, i.e. an isotropic eight line pattern for La and a two-line pattern for Y, but no crystalline material could be isolated. In the case of DyCp^t_3 , reduction with 2.2.2-cryptand/ KC_8 in Et_2O provided again a crystallographically characterized mixed valent complex $[\text{K}(2.2.2\text{-cryptand})][\text{DyCp}^t_3]_2$, in analogy to the Ce complex.[46]



Scheme 36. Synthesis of new monomeric and polymeric divalent Ce complexes based on Cp^{*} ligand.[46]

The dimeric methyl-bridged trivalent complexes $[\text{Cp}'_2\text{Ln}(\mu\text{-Me})_2]$ (Ln = Y, Tb, Dy; Cp' = C₅H₄SiMe₃) were obtained by reaction of the corresponding chloride bridged precursors with two equivalents of MeLi (Scheme 37).[47] Reduction of these complexes with KC₈ in the presence of cryptand in THF at - 35°C afforded dark solutions, showing broad absorption bands in the UV-vis spectrum at around 400 nm, indicative of possible Ln²⁺ complexes based on previous literature results. Furthermore, the EPR spectrum of the Y complex displayed an axial signal at 77 K and an isotropic signal at room temperature, in agreement with previously described Y(II) complexes. None of the complexes provided crystals suitable for XRD analysis.[47]



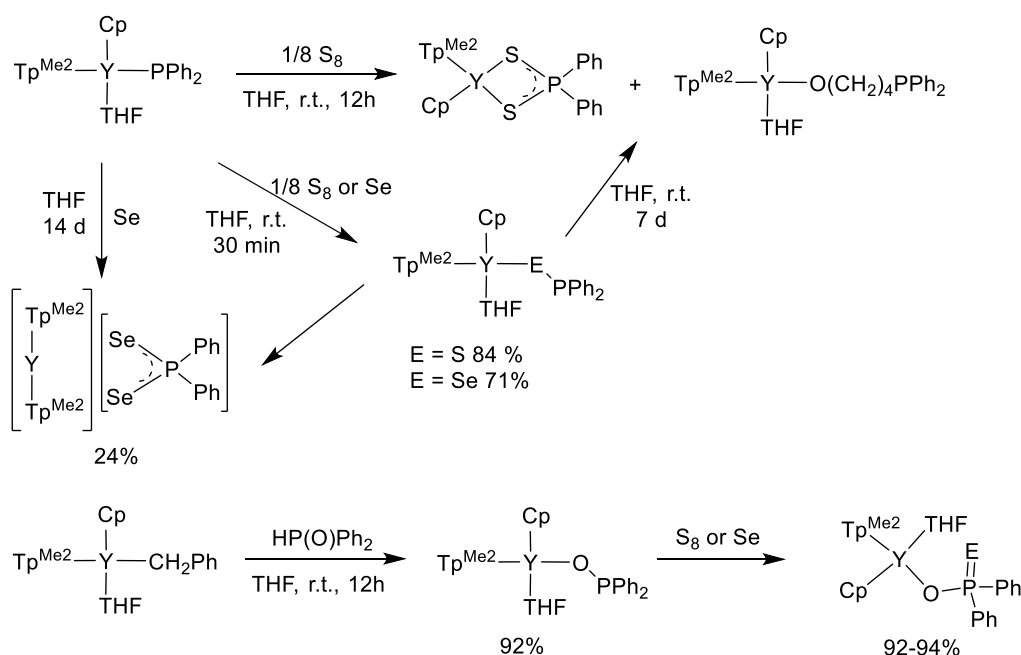
Scheme 37. Synthesis and reduction of $[\text{Cp}'_2\text{Ln}(\mu\text{-Me})_2]$ (Ln = Y, Tb, Dy).[47]

The electronic configuration of a series of [K(2.2.2-cryptand)][LnCp₃]⁻ complexes (Ln = Y, La, Pr, Eu, Gd; Cp' = C₅H₄SiMe₃) was studied by magnetic circular dichroism spectroscopy (MCD).[48] Experiments using NIR MCD allowed the first observation of low energy f–f transitions, however, only in the case of [PrCp₃]⁻, in agreement with the previously assigned 4f²5d¹ electronic ground-state configuration. The signals exhibited unusual broadening (fwhm 600 cm⁻¹) for typically narrow f–f transitions (fwhm 50 cm⁻¹), suggesting some 5d orbital character of the f-orbitals. For Y and La complexes, no f-f transitions were observed, in agreement with the absence of f-electrons (Y) and the 5d¹ configuration (La). Furthermore, in the case of Eu and Gd, the half-filled f orbital configuration (4f⁷ and 4f⁷5d¹) in which all f-f transitions are spin-forbidden, was also confirmed by the absence of NIR transitions. UV-vis MCD studies were combined with theoretical studies for the three complexes [YCp₃]⁻, [PrCp₃]⁻, and [GdCp₃]⁻, showing that the lowest energy transitions in the UV–vis region are nd to (n + 1)p transitions.[48] The divalent complexes [K(2.2.2-cryptand)][LnCp₃] (Ln = Y, Lu, La) have been investigated by EPR spectroscopy and DFT/CASSCF calculations for their properties as molecular qubits.[49] Despite their non-rigid character and the presence of many hydrogen atoms and methyl groups these complexes show long memory times (*T_m*) and spin-lattice relaxation times (*T₁*) in frozen THF solution and in single crystals up to 300 K, e.g. *T₁* = 2μs and *T_m* = 0.5μs for the divalent Y complex at room temperature. The robust relaxation behaviour was related to the highly isotropic electronic structure which arises from quenching of orbital angular momentum in the ground state (*S* = ½).[49]

2.4.2. CpLnX₂, Cp₂LnX and Cp₃Ln Compounds

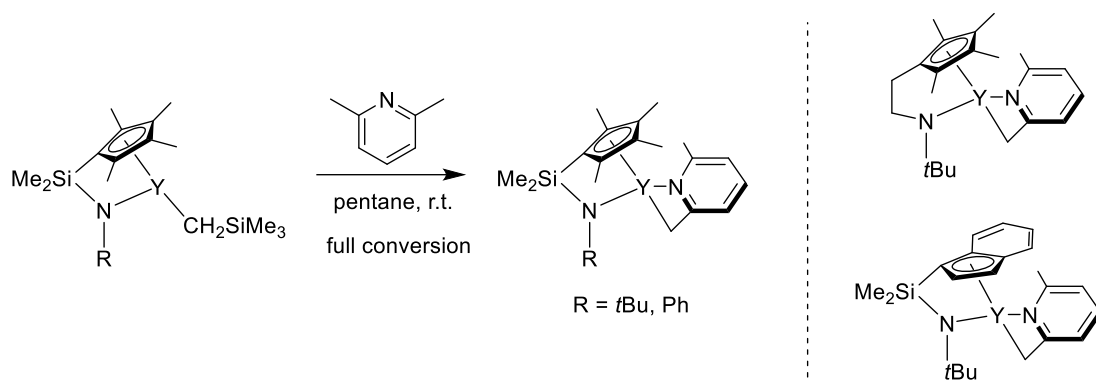
The reactivity of the mixed-ligand Cp/scorpionate yttrium phosphide complex (Tp^{Me2})CpY(PPh₂)(THF) towards chalcogens was studied (Scheme 38).[50] Reaction with elemental sulphur rapidly provided insertion of sulphur into the Y-P bond to yield the new complex (Tp^{Me2})CpY(SPPPh₂)(THF) in high yield, which was characterized by NMR spectroscopy. Leaving the reaction for 12 h, provided a mixture of dithiophosphate bound complex (Tp^{Me2})CpY(SP(S)Ph₂) and complex (Tp^{Me2})CpY(O(CH₂)₄PPh₂), the latter being derived from THF ring opening. Both complexes were characterized by XRD analysis. In the case of the reaction between (Tp^{Me2})CpY(PPh₂)(THF) and selenium, the initial insertion occurred as in the case of sulphur, but the ligand rearrangement was slower (14 days) and finally the separated ion pair complex [Y(Tp^{Me2})₂][SeP(Se)Ph₂] was isolated,

as shown by XRD analysis. Concerning the mechanism, it was proposed that oxidation of the PPh₂ group occurred followed by a tautomerization process. This was based on the observation that a mixed ligand benzyl complex (Tp^{Me2})CpY(CH₂Ph) reacted with HP(O)Ph₂ to afford the corresponding phosphinate complex (Tp^{Me2})CpY(OPPh₂) in high yields. The latter was more stable than the S and Se analogues and could further react with S or Se to the P-oxygenated products.[50]



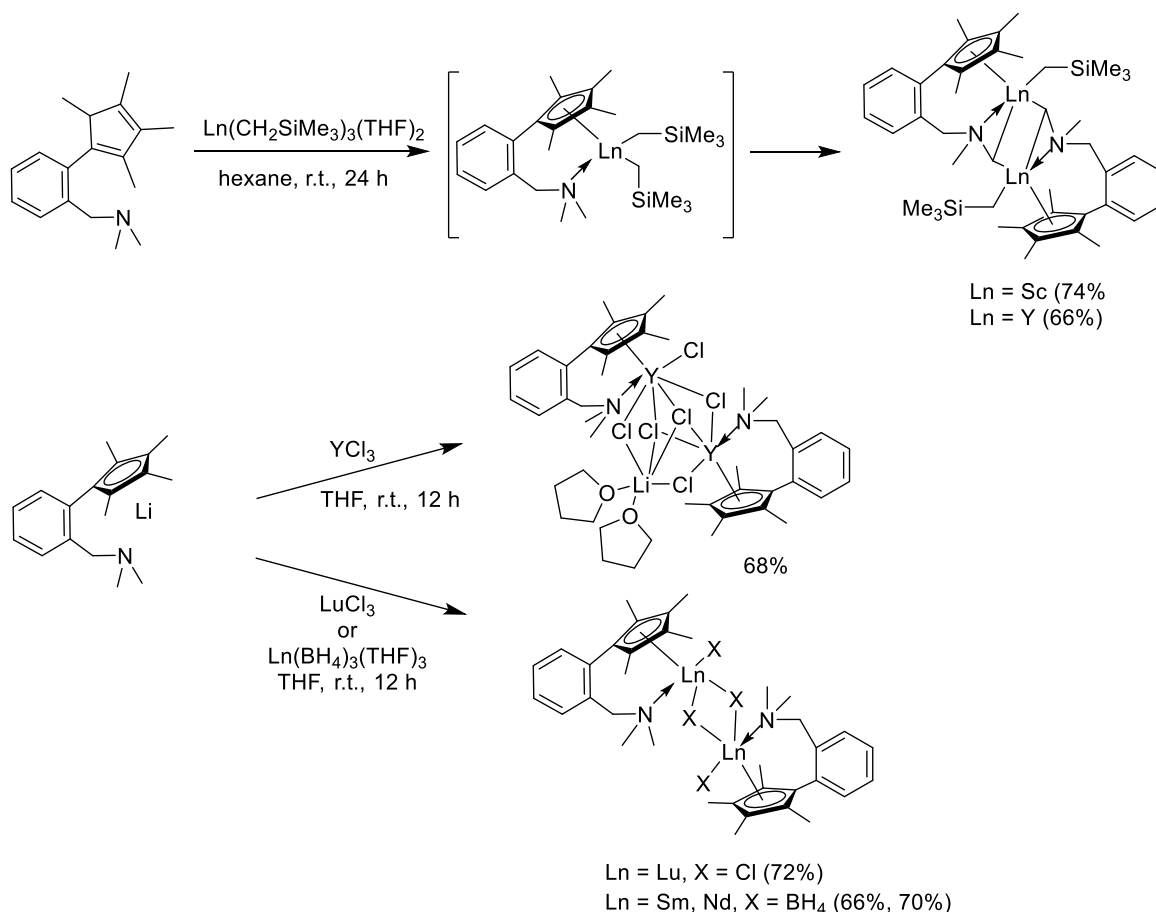
Scheme 38. Reactivity of (Tp^{Me2})CpYPPH₂(THF) towards chalcogens.[50]

The preparation of constrained-geometry (CG) yttrium complexes containing a lutidynyl (lut = CH₂(C₅H₃NMe-o)) moiety was achieved by alkane elimination reaction of the corresponding CG yttrium alkyl complexes [Me₂Si(Cp/Ind)NR]Y(CH₂SiMe₃) (Cp = C₅Me₄, Ind = C₉H₆, R = tBu, Ph) or [C₅Me₄(CH₂CH₂N*t*Bu)]Y(CH₂SiMe₃) with 2,6-lutidine (Scheme 39).[51] The resulting C-H bond activation reaction provided quantitatively the new lutidynyl complexes, which were characterized by NMR spectroscopy and XRD analysis. The THF adduct of complex [Me₂Si(C₅Me₄)N*t*Bu]Y(lut) crystallised as monomer, whereas the solvent-free indenyl analogue crystallised as dimer with two Y-CH₂-Y bridges. These new complexes were employed in the polymerization of diethylvinylphosphonate (see section 2.11.1).[51]



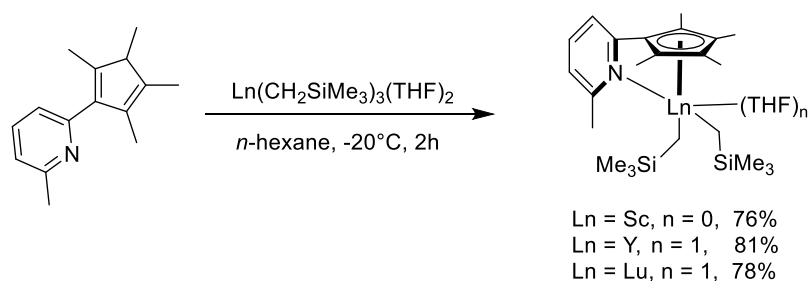
Scheme 39. Synthesis of lutidinyl containing CG Y complexes.[51]

The synthesis of new Cp half-sandwich bis(alkyl) lanthanide complexes containing a Cp tethered N,N-dimethylbenzylamine ligand was achieved using protonolysis of the proligand (Cp^N-H) with Ln(CH₂SiMe₃)₃(THF)₂ precursors. After formation of the initial bis(alkyl) complex further C-H activation on the N-CH₃ group occurred to yield the dimeric CH₂-bridged complexes [(C₅Me₄-C₆H₄-o-CH₂N(Me)CH₂-μ)Ln(CH₂SiMe₃)₂] (Ln = Sc, Y) in good yields (Scheme 40).[52] XRD analysis and NMR spectroscopic characterization confirmed the dimeric structure of the complexes. The bond lengths for the Ln-CH₂ bridges are considerably longer (by 0.22 Å) than the Ln-CH₂SiMe₃ bond lengths. An alternative salt metathesis approach was then investigated with the same amine tethered ligand. Starting from the LiCp^N precursor and LnCl₃ (Ln = Y, Lu) or Ln(BH₄)₃(THF)₃ (Ln = Sm, Nd), the dimeric chloride (C₅Me₄-C₆H₄-o-CH₂NMe₂)₂Y₂Cl₄[LiCl(THF)₂], [(C₅Me₄-C₆H₄-o-CH₂NMe₂)LuCl(μ-Cl)]₂ or borohydride [(C₅Me₄-C₆H₄-o-CH₂NMe₂)Ln(μ-BH₄)BH₄]₂ complexes were obtained in good yields. In the case of Y, a heterotrimetallic complex resulting from LiCl incorporation was identified by XRD analysis. The borohydride complexes showed μ₂ and μ₃ coordination to the metal centers as revealed by IR spectroscopy and in agreement with XRD analysis. The new complexes were investigated as precatalysts for isoprene, 1-hexene and MMA polymerization (see section 2.11.1).[52]



Scheme 40. Synthesis of half-sandwich lanthanide bis(alkyl), dichloride and di(borohydride) complexes with a dimethylamino-tethered Cp ligand.[52]

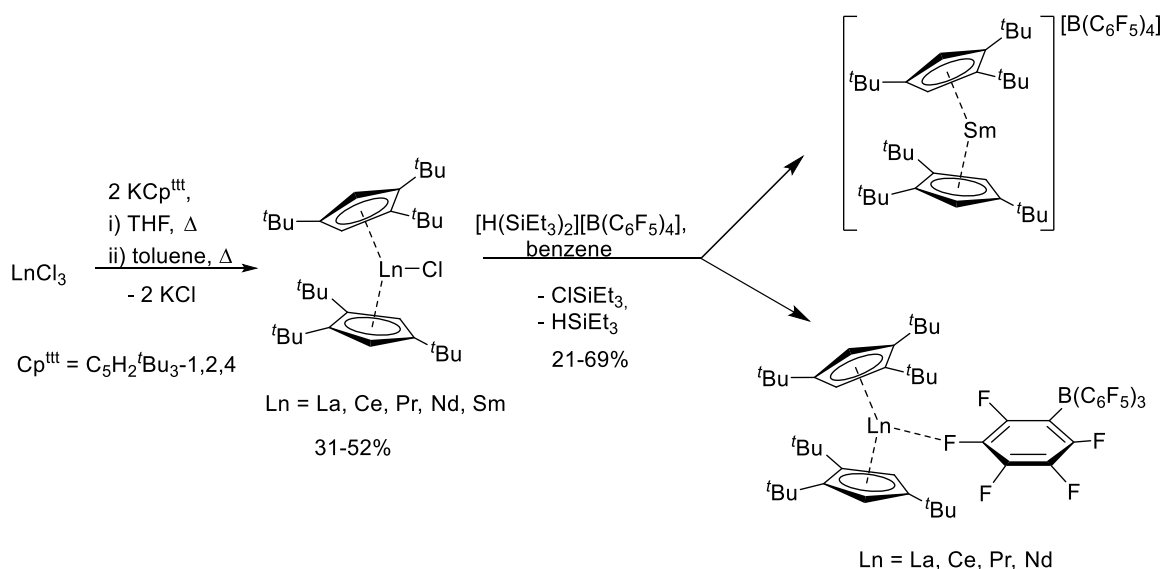
The new 2-picoline-tethered Cp lanthanide bis(alkyl) complexes ($\eta^5\text{-}\kappa\text{-C}_5\text{Me}_4\text{-C}_5\text{H}_3\text{NMe-o}$) $\text{Ln}(\text{CH}_2\text{SiMe}_3)_2(\text{THF})_n$ (Ln = Sc, n = 0; Ln = Y, Lu, n = 1) were synthesized in high yields from the neutral pro-ligand and $\text{Ln}(\text{CH}_2\text{SiMe}_3)_3$ (Scheme 41).[53] All complexes were characterized by NMR spectroscopy and the Sc complex was structurally analysed by an XRD study. The Sc complex showed high activity in the tandem cyclisation/hydroarylation of α,ω -dienes (see section 2.11.2) [53]



Scheme 41. Synthesis of 2-picoline-tethered Cp lanthanide bis(alkyl) complexes.[53]

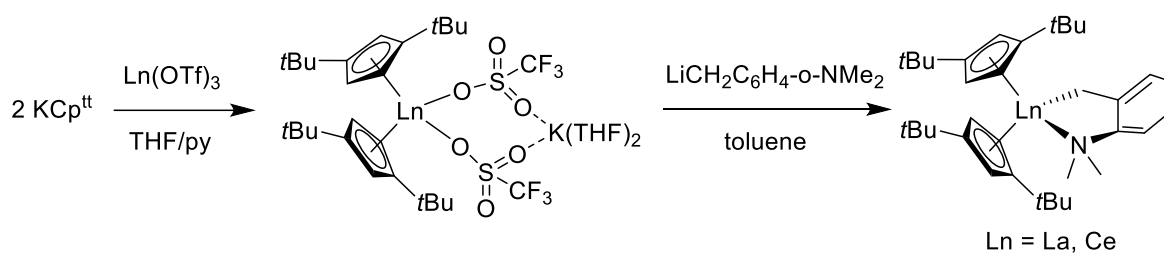
Following previous reports on the synthesis of heavy lanthanide complexes $\text{Cp}^{\text{III}}_2\text{LnCl}$ and their cationic analogues $[\text{Cp}^{\text{III}}_2\text{Ln}][\text{B}(\text{C}_6\text{F}_5)_4]$ (Ln = Gd - Lu) with the very bulky tris-t-

butylcyclopentadienyl ligand (Cp^{ttt}), the series was completed with the lighter analogues La, Ce, Pr, Nd and Sm (Scheme 42).[54] The cationic complexes were obtained in moderate yields via chloride abstraction using $[\text{H}(\text{SiEt}_3)_2][\text{B}(\text{C}_6\text{F}_5)_4]$. Only Eu was not accessible due to auto-reduction of the trivalent $\text{Cp}^{\text{ttt}}_2\text{EuCl}$ complex to the divalent sandwich complex. Whereas all cationic complexes starting from Sm^{3+} showed no equatorial interaction between the cationic $[\text{Cp}^{\text{ttt}}_2\text{Ln}]$ moiety and the counteranion, the larger lanthanide ions (La-Nd) showed Ln-F_{meta} interactions according to XRD analysis. This led to smaller Cp-Ln-Cp angles, hence less linearity, for the lighter lanthanides, for example Nd $148.10(13)^\circ$ vs Sm $153.23(6)^\circ$. The Ln-F distances were in the range 2.679(9) to 2.632(4) Å. However, the borate anion is only weakly bound as no Ln-F interactions could be observed in solution by ^{19}F NMR spectroscopy. The electronic structures of all new complexes were studied theoretically and experimentally. It was found that along the $[\text{Cp}^{\text{ttt}}_2\text{Ln}]^+$ series, the relaxation dynamics were consistent and lower Raman exponents were observed compared to the $\text{Cp}^{\text{ttt}}_2\text{LnCl}$ complexes. [54]



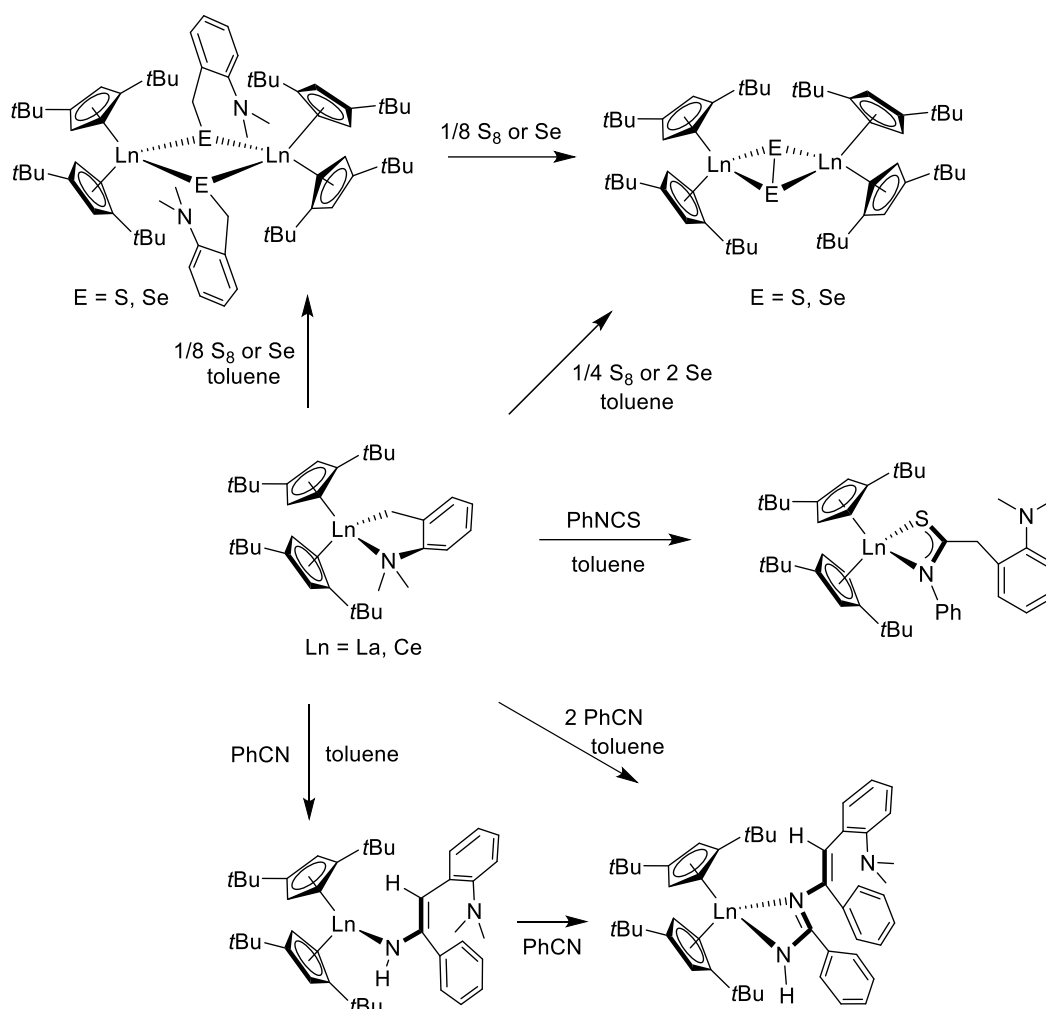
Scheme 42. Synthesis of a series of $[\text{Cp}^{\text{ttt}}_2\text{Ln}][\text{B}(\text{C}_6\text{F}_5)_4]$ complexes.[54]

The bulky metallocene benzyl complexes of the early lanthanides, $\text{Cp}^{\text{tt}}_2\text{Ln}(\text{CH}_2\text{C}_6\text{H}_4\text{NMe}_2\text{-o})$ ($\text{Ln} = \text{La, Ce}$), were synthesized in two steps from the $\text{Ln}(\text{OTf})_3$ precursors (Scheme 43).[55]. The first salt metathesis reaction with KCp^{tt} in THF/py afforded the $[\text{Cp}^{\text{tt}}_2\text{Ln}(\text{OTf})_2\text{K}(\text{THF})_2]_n$ complexes, which crystallised as centrosymmetric dimers according to DRX analysis. Further reaction with Li-benzyl reagent in toluene gave the $\text{Cp}^{\text{tt}}_2\text{Ln}(\text{CH}_2\text{C}_6\text{H}_4\text{NMe}_2\text{-o})$ complexes. These monomeric complexes were characterized by NMR spectroscopy and XRD analysis showing a monomeric metallocene structure with coordination of the benzyl-NMe₂ group onto the lanthanide center.[55]



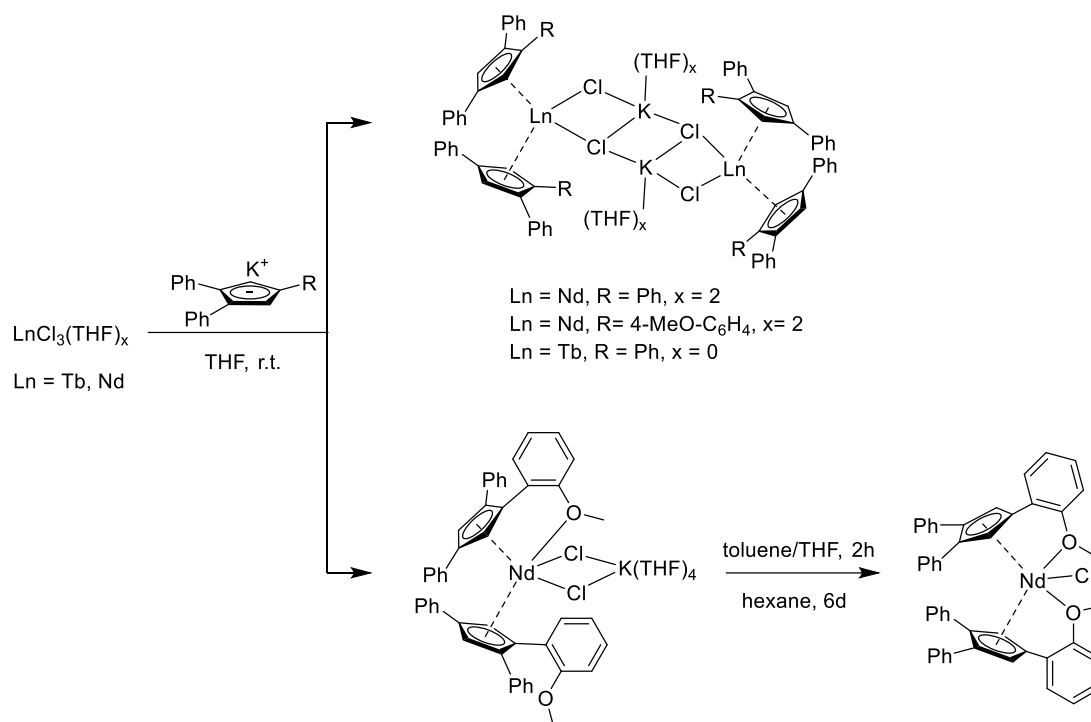
Scheme 43. Synthesis of $\text{Cp}^{\text{t}}_2\text{Ln}(\text{CH}_2\text{C}_6\text{H}_4\text{NMe}_2\text{-o})$ from triflate precursors.[55]

Reaction of these complexes with sulfur or selenium in toluene led to the isolation and structural characterization of thiolates/selenolates (1 equiv. chalcogen) or disulfides/diselenides (2 equiv. chalcogen) (Scheme 44). Further insertion reactions into the Ln-C(benzyl) bond were studied using various electrophiles. Addition of benzonitrile (1 equiv.) afforded the unexpected lanthanide-1-aza-allyl complex, as confirmed by ^1H NMR spectroscopy and XRD analysis. This compound may result from initial C-N insertion into the Ln-C bond followed by 1,3-hydrogen migration. Addition of another equivalent of benzonitrile led to the amidinato-complex from insertion into the Ln-N bond and hydrogen migration. The structure showed a charge delocalization on the N-C-N unit. Finally, reaction of $\text{Cp}^{\text{t}}_2\text{Ln}(\text{CH}_2\text{C}_6\text{H}_4\text{NMe}_2\text{-o})$ with DCC or PhNCS, yielded the expected aminobenzyl transfer from the Ln center to the electrophilic carbon centers, as shown by XRD analysis. [55]



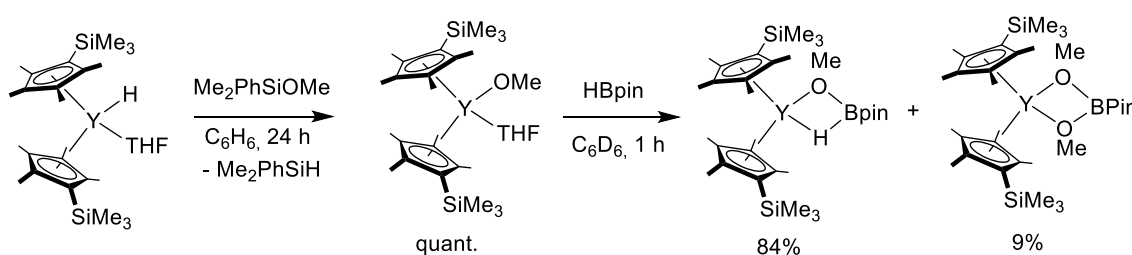
Scheme 44. Reactivity of $\text{Cp}^{\text{tBu}}_2\text{Ln}(\text{CH}_2\text{C}_6\text{H}_4\text{NMe}_2\text{-o})$ complexes with electrophiles.[55]

The synthesis of new trisarylcyclopentadienyl neodymium complexes was achieved using the salt metathesis approach (Scheme 45).[56] Reaction of two equivalents KCp^{Ar} with LnCl_3 in THF provided the dimeric ate complexes $[\text{Cp}^{\text{Ar}}_2\text{NdCl}_2\text{K}(\text{THF})_2]_2$ ($\text{Cp}^{\text{Ar}} = \text{C}_5\text{Ph}_3\text{H}_2$, $\text{C}_5\text{Ph}_2(4\text{-MeOC}_6\text{H}_4)\text{H}_2$) due to KCl incorporation. The structure of these complexes was confirmed by XRD analysis and NMR spectroscopy. An ortho-methoxy substituent on one of the aryl groups of the Cp ligand, afforded the corresponding monomeric ate complex $\text{Cp}^{\text{Ar}}_2\text{NdCl}_2\text{K}(\text{THF})_4$ ($\text{Ar} = \text{C}_5\text{Ph}_2(2\text{-MeOC}_6\text{H}_4)\text{H}_2$), which was transformed to the neutral complex $\text{Cp}^{\text{Ar}}_2\text{NdCl}$ after stirring for 6d in hexane. XRD analysis showed that in this case, the two MeO groups were coordinated to the Nd center, whereas in the ate-complex only one MeO group was coordinated. The new metallocenes were studied in ethylene polymerization (see section 2.12.1).[56]



Scheme 45. Synthesis of trisarylcyclopentadienyl lanthanide complexes.[56]

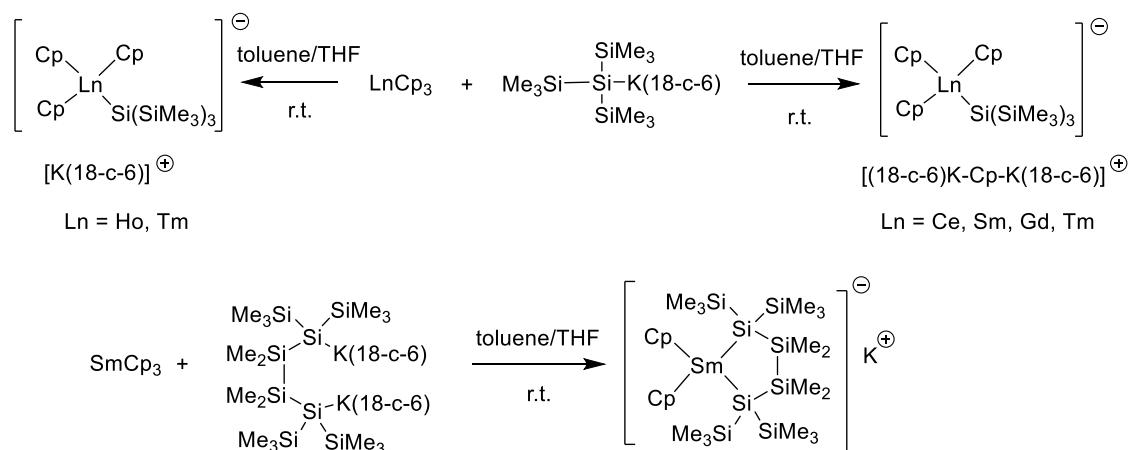
In the course of mechanistic studies concerning the reduction of alkoxy silanes with yttrium metallocene hydrides (see section 2.12.3), the reaction of $\text{Cp}'_2\text{YH}(\text{THF})$ with $\text{Me}_2\text{PhSiOMe}$ was performed, affording the alkoxy complex $\text{Cp}'_2\text{Y}(\text{OMe})(\text{THF})$ in quantitative yield (Scheme 46).[57] Further reaction with an equimolar amount of HBpin yielded a mixture of the two metallocene complexes $\text{Cp}'_2\text{Y}(\mu\text{-OMe})_2\text{Bpin}$ and $\text{Cp}'_2\text{Y}(\mu\text{-H})(\mu\text{-OMe})\text{Bpin}$ in 9 and 84% yield, respectively. All new complexes were characterized by NMR spectroscopy and XRD analysis.[57]



Scheme 46. Transformation of $\text{Cp}'_2\text{YH}(\text{THF})$ with alkoxy silane followed by HBpin.[57]

The reaction of various LnCp_3 complexes with potassium tris(trimethylsilyl)silanide, $\text{K}(\text{18-crown-6})\text{Si}(\text{SiMe}_3)_3$, afforded the hypersilylated lanthanidocenes $[\text{Cp}_3\text{LnSi}(\text{SiMe}_3)_3]^+$ which displayed different cationic counterions depending on the lanthanide metal (Scheme 47).[58] For Ce, Sm, Gd, a sandwich counter-cation was obtained, $[(\text{18-crown-6})\text{KCp}$

K(18-crown-6)], whereas for Ho a simple $K(18\text{-crown-6})^+$ was observed, according to XRD studies. In the case of Tm, two types of crystals were identified showing the two types of cations. The observation of the sandwich counterion implies a more complex reaction process, with abstraction of Cp ligands from the initial Cp_3Ln complexes. Reaction of Cp_3Sm with an oligosilanyl-dianion yielded the samaracyclopentasilanate complex $Cp_2Sm[(SiMe_3)_2Si(SiMe_2)_2Si(SiMe_3)_2]^-$ involving one Cp^- displacement. The Sm-Si bonds are considerably shorter than in the $[Cp_3SmSi(SiMe_3)_3]^-$ complex (3.063(3) and 3.049(3) vs. 3.103(2) Å).[58]



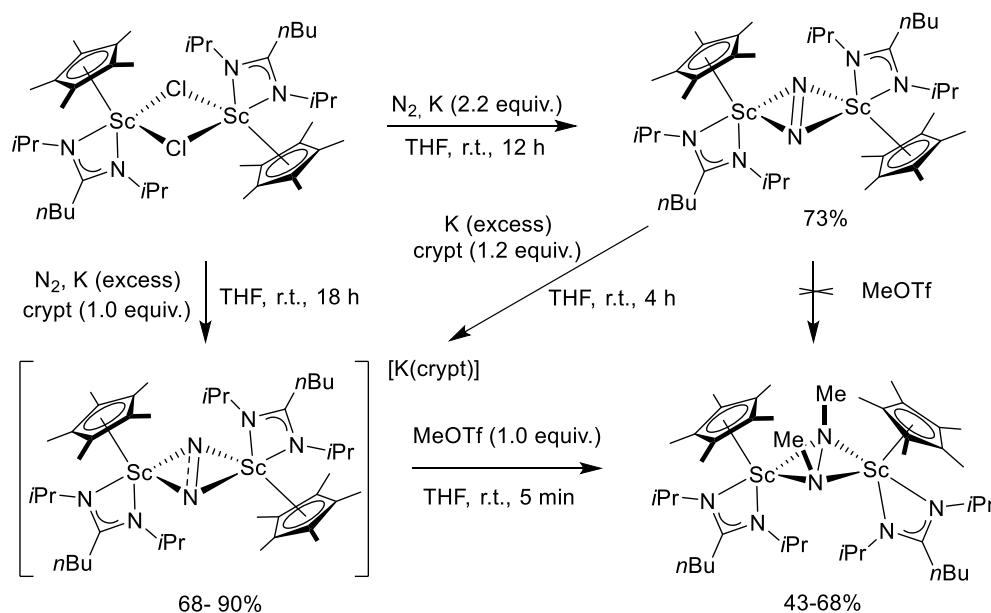
Scheme 47. Reaction of $LnCp_3$ complexes with silanyl anion and oligosilanyl dianion reagents.[58]

Reaction of the highly soluble $LnCp''_3$ ($Ln = La, Ce, Tb, Dy$; $Cp'' = 1,3-SiMe_3-C_5H_3$) complexes with lithium metal in the presence of bipyridine (bipy) provided a new synthetic pathway to the THF-insoluble complexes $Ln(\kappa^2\text{-bipy})_4$ ($Ln = La, Ce$) and $[Li(THF)_4][Ln(\kappa^2\text{-bipy})_4]$ ($Ln = Tb, Dy$).[59] The formed $LiCp''$ byproduct was soluble in THF and could be readily removed after the reaction. For La and Ce, the THF solvates $M(\kappa^2\text{-bipy})_4(THF)_x$ ($x = 1,2$) were obtained in moderate yields (36-55%) when the reaction was conducted in THF. In diethyl ether, a solvent-free complex was obtained for La in low yield. The Tb and Dy anions were obtained in 9% and 60%, respectively.[59]

2.4.3. Pentamethylcyclopentadienyl Compounds

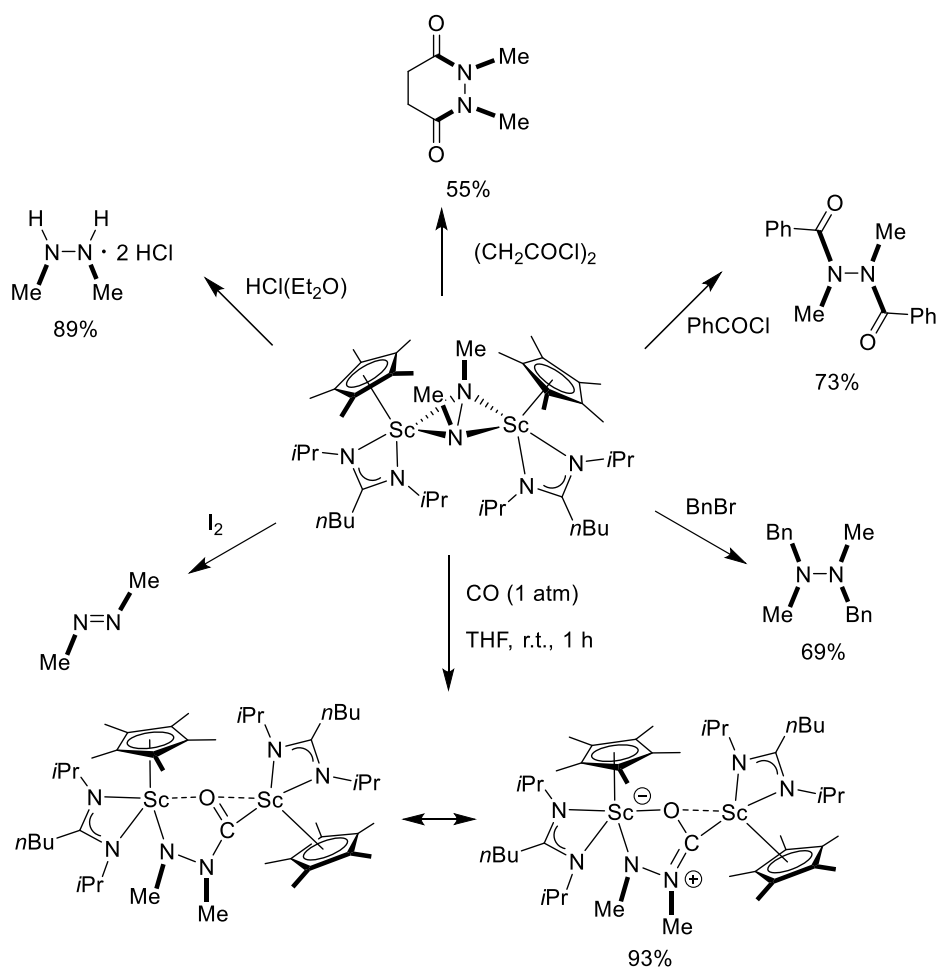
Direct conversion of dinitrogen to hydrazine derivatives was achieved using a low-valent Sc complex.[60] Reduction of the mixed-ligand trivalent precursor $[Cp^*(NCN)ScCl]_2$ ($NCN = BuC(NiPr)_2$), readily synthesized from $ScCl_3$, Cp^*Li and $Li(NCN)$, with K under nitrogen atmosphere yielded the dimeric $(N_2)^{2-}$ -bridged complex $[Cp^*(NCN)Sc]_2(N_2)$ in 73% yield (Scheme 48). This complex was characterized by XRD analysis, Raman

spectroscopy and NMR spectroscopy with a ^{15}N NMR signal at 455.9 ppm. Further reduction with K in the presence of cryptand led to the paramagnetic $(\text{N}_2)^{3-}$ radical bridged Sc dimer $\{[\text{Cp}^*(\text{NCN})\text{Sc}]_2(\text{N}_2)\}[\text{K}(\text{crypt})]$ in 90% yield. The structure of this separated ion-pair complex was confirmed by XRD analysis showing a planar Sc_2N_2 moiety with an N-N bond length of 1.3693(16) Å, as well as by Raman and EPR spectroscopy. Addition of MeOTf to this complex in THF afforded the dimeric Sc hydrazide complex, $[\text{Cp}^*(\text{NCN})\text{Sc}]_2(\text{N}_2\text{Me}_2)$, with a non-planar Sc_2N_2 unit according to XRD analysis and a ^{15}N NMR signal at -231 ppm. It is important to note that the $\text{Sc}_2(\text{N}_2)^{2-}$ complex did not react with MeOTf (Scheme 48).[60]



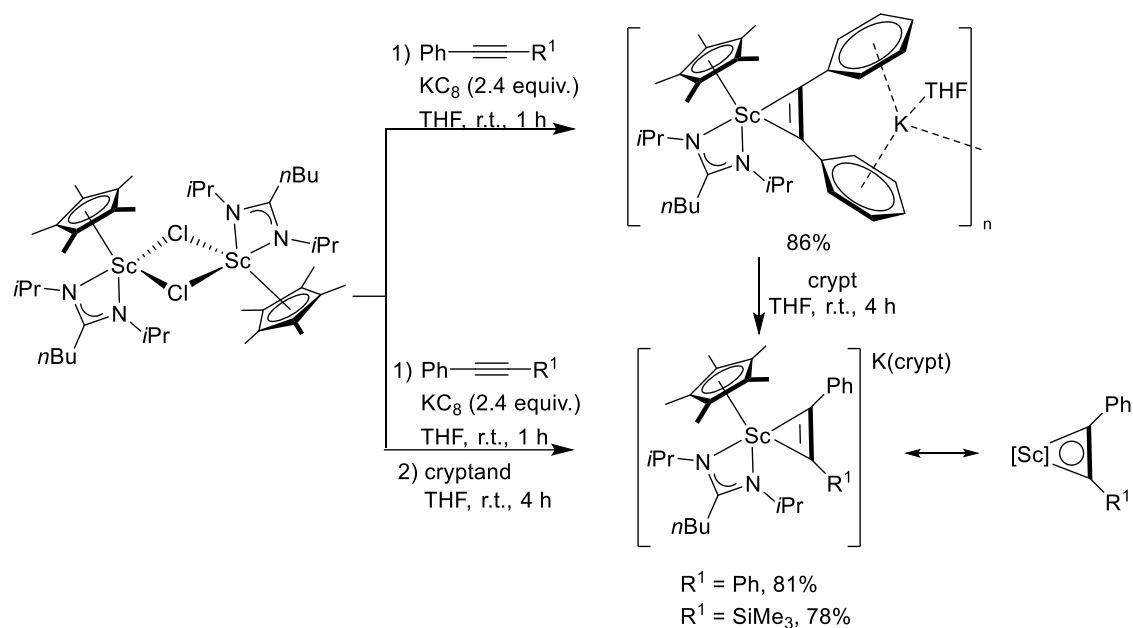
Scheme 48. Synthesis of Sc-hydrazide $[\text{Cp}^*(\text{NCN})\text{Sc}]_2(\text{N}_2\text{Me}_2)$ complex via N_2 activation.[60]

The $[\text{Cp}^*(\text{NCN})\text{Sc}]_2(\text{N}_2\text{Me}_2)$ complex could be quenched with a large range of electrophiles (Scheme 49).[60] Protonolysis with HCl in ether afforded dimethylhydrazine, whereas oxidation with I_2 gave azomethane. Tetra-substituted hydrazines were obtained from the reactions with acylchlorides or benzylbromide. All reactions afforded the organic products in good to high yields and allowed the recovery of the halide bridged trivalent Sc complexes $[\text{Cp}^*(\text{NCN})\text{ScX}]_2$ ($\text{X} = \text{Cl}, \text{Br}, \text{I}$). The use of carbon monoxide as electrophile led to the formation of a dimeric complex resulting from the 1,1-insertion of CO into one Sc-N bond. XRD analysis and DFT studies indicated that this complex should be described by the two mesomeric structures shown in Scheme 49, with the greater contribution coming from the zwitterionic species.[60]



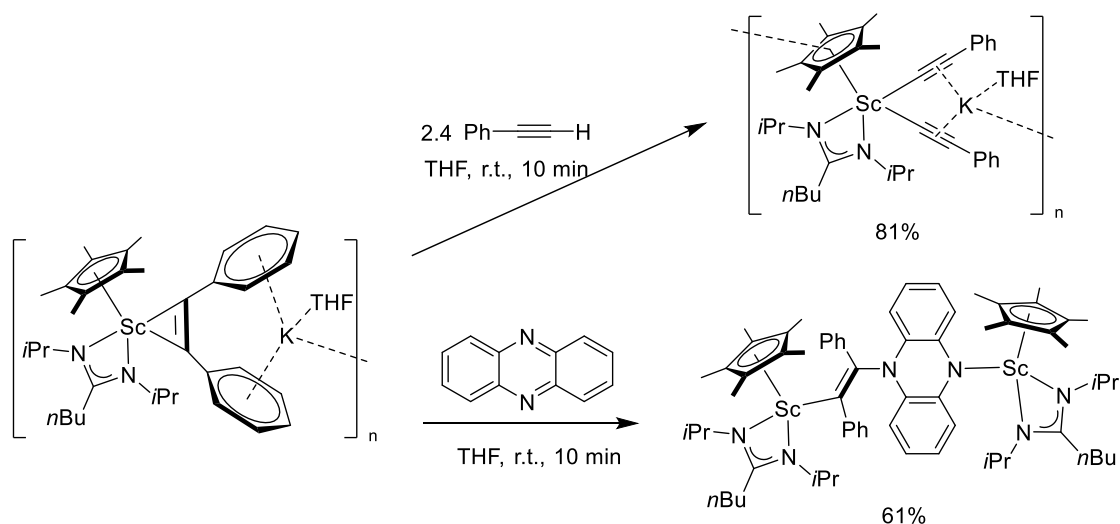
Scheme 49. Reactivity of Sc-hydrazide complex $[\text{Cp}^*(\text{NCN})\text{Sc}]_2(\text{N}_2\text{Me}_2)$ with electrophiles.[60]

Following this work, the same Sc precursor complex $[\text{Cp}^*(\text{NCN})\text{ScCl}]_2$ was reduced with KC_8 in the presence of internal alkynes, providing access to the first lanthanide metallacyclopropene complexes (Scheme 50).[61] Reduction with KC_8 in THF provided a polymeric structure, whereas addition of cryptand yielded the monomeric compounds $[\text{Cp}^*(\text{NCN})\text{Sc}(\eta^2\text{-RCCR}')][\text{K}(\text{crypt})]$ ($\text{R} = \text{R}' = \text{Ph}$; $\text{R} = \text{Ph}$, $\text{R}' = \text{SiMe}_3$) in good yields. ^{13}C NMR spectroscopy showed broad peaks above 214 ppm for the coordinated carbon atoms of the $(\text{RCCR}')^{2-}$ moieties. XRD analysis of the separated ion pair complex $[\text{Cp}^*(\text{NCN})\text{Sc}(\eta^2\text{-PhCCPh})][\text{K}(\text{crypt})]$ indicated short Sc-C distances and a C-C bond length of 1.350(2) Å with C-C-C(Ph) angles of 127.94(16) and 130.19(15)° for the reduced alkyne moiety in agreement with sp^2 hybridisation. According to DFT calculations, the bonding in this complex could be described with two Sc-C σ -bonds and one Sc-(C=C) dative π -bond. The aromaticity of this three-center-two-electron scandacyclopropene unit was determined to be -10.0 ppm (NICS(1) $_{zz}$ value), which makes it the first aromatic system of lanthanide metallacycles.[61]



Scheme 50. Synthesis of scandium metallacyclopropene complexes.[61]

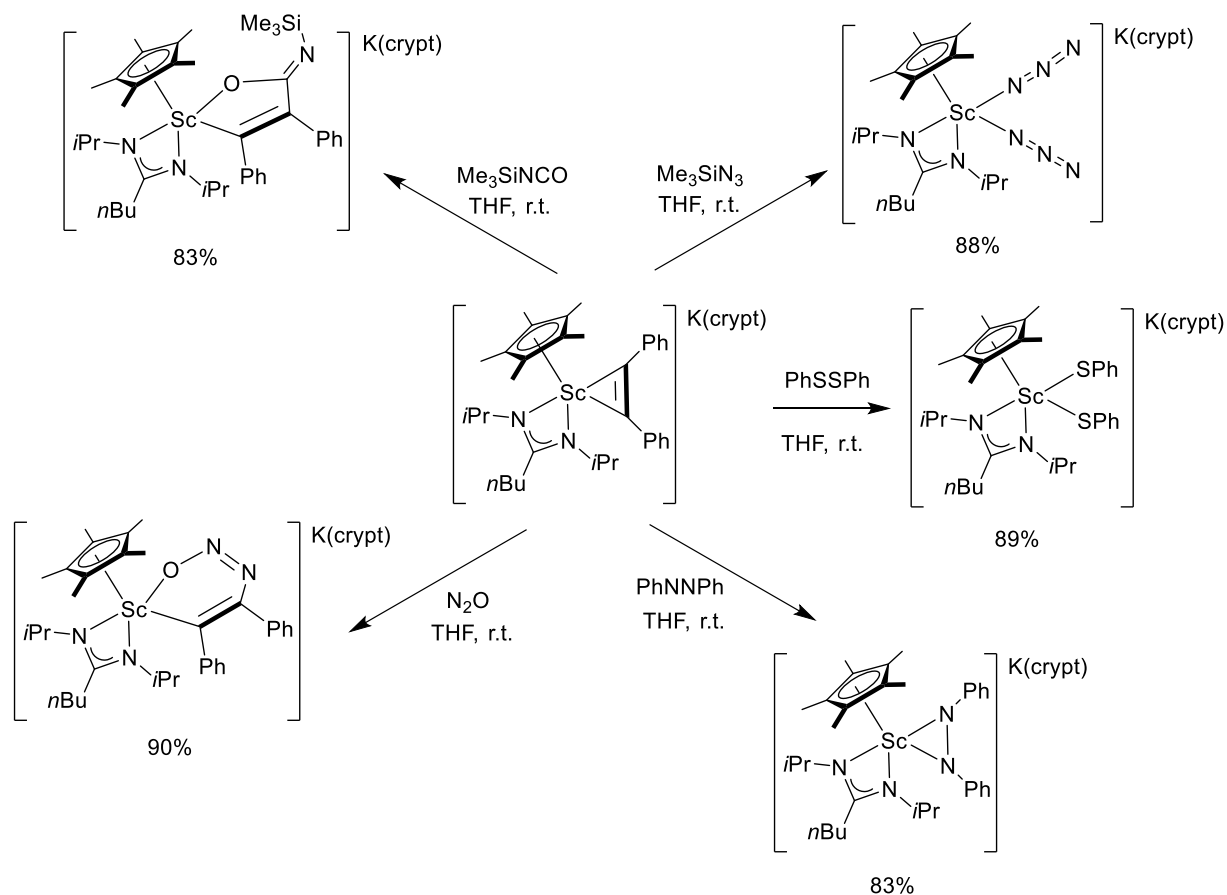
Reaction of the polymeric scandacyclopropene with phenylacetylene liberated *cis*-stilbene and afforded the structurally characterized one-dimensional chain polymer Sc bis(phenylacetylide) complex in good yield (Scheme 51).[61] In contrast, reaction with phenazine resulted in a dimeric Sc complex with one phenazine inserted into the Sc(PhC=CPh)²⁻ unit.



Scheme 51. Reactivity studies of polymeric metallacyclopropene complex.[61]

Insertion of electrophiles into the Sc-C bond of the alkene moiety was studied with the separated ion pair complex, [Cp*(NCN)Sc(η²-PhCCPh)][K(crypt)], and all new complexes were characterized by XRD analysis (Scheme 52). Reaction with TMSNCO afforded

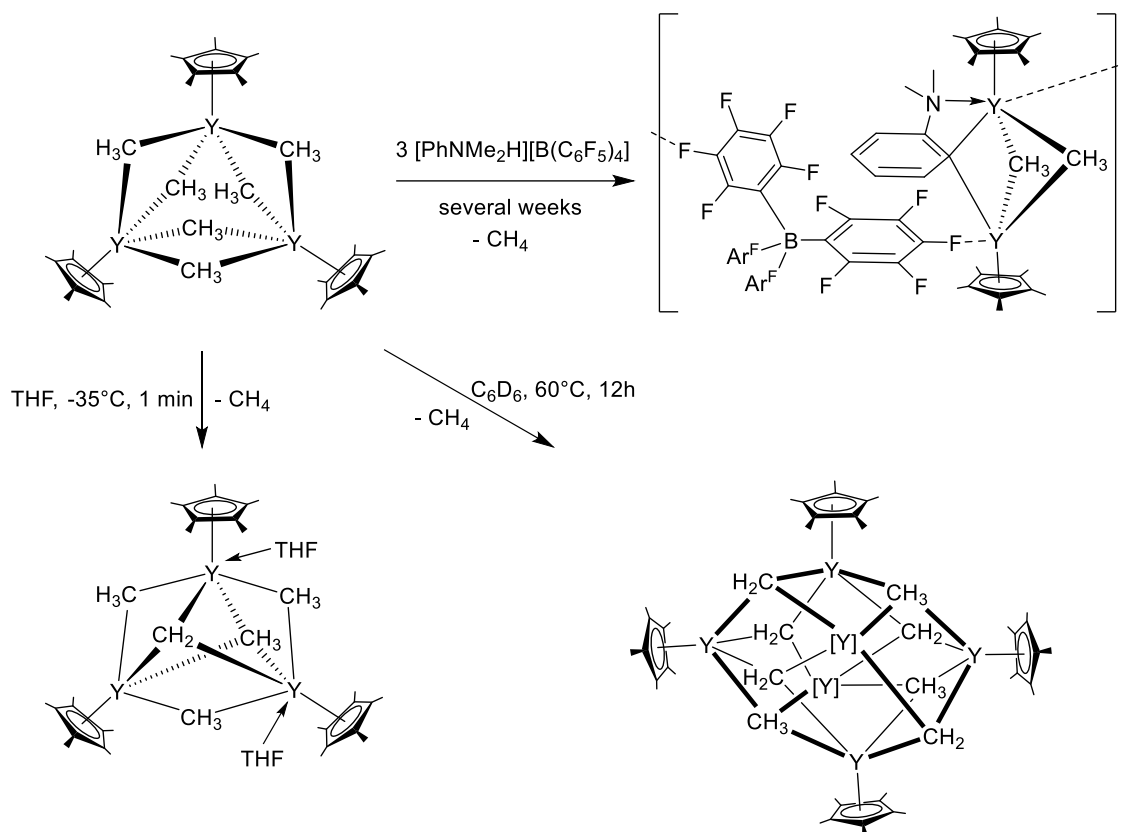
insertion of the C=O double bond into the Sc-C bond to give a five-membered scandacycle. From the addition of nitrous oxide (N_2O) a six-membered scandacycle was obtained resulting from the insertion of the whole N_2O molecule into the Sc-C bond. With the organic azide $TMSN_3$, Si-N bond cleavage was observed to yield the bis(azide) complex in 88% yield. Furthermore redox-reactions, using for example $PhSSPh$ or azobenzene, were also successful, showing the capability of the scandacyclopentene to act as two-electron reducing agent.[61]



Scheme 52. Reactivity studies of separated ion-pair metallacyclopentene complex.[61]

The multimetallic $[Cp^*YMe_2]_3$ complex was investigated for its stability towards heat or a donor solvent like THF and for its reactivity with ammonium borate $[PhNMe_2H][B(C_6F_5)_4]$, the latter being employed as cocatalyst in polymerization reactions (Scheme 53).[62] Addition of THF to $[Cp^*YMe_2]_3$ at low temperature led to C-H activation and formation of methane gas. The new multimetallic complex $[(Cp^*_3Y)_3Me_4(CH_2)(THF)]$ was isolated and characterized by XRD analysis. A similar observation of C-H activation and methane liberation was made upon heating the complex $[Cp^*YMe_2]_3$ in benzene at $60^\circ C$, leading to the mixed methyl/methylene cluster complex $[Cp^*_6Y_6Me_4(CH_2)_4]$ as shown by XRD analysis. From the reaction of $[Cp^*YMe_2]_3$ with

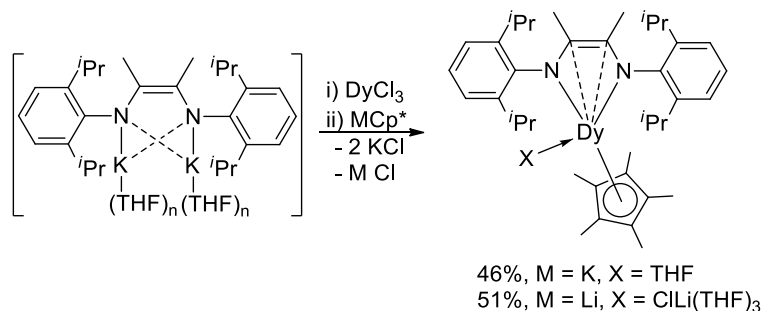
[PhNMe₂H][B(C₆F₅)₄], several products were observed by NMR spectroscopy. One principal product, the polymeric complex [(Cp*Y)₂Me₂(N(Me)₂C₆H₄)]_n[B(C₆F₅)₄]_n could be isolated and characterized by XRD analysis. The use of [Cp*YMe₂]₃ and [(Cp*₃Y)₃Me₄(CH₂)(THF)] in butadiene and isoprene polymerization will be discussed in section 2.11.1).[62]



Scheme 53. Reactivity of multimetallic [Cp*YMe₂]₃ complex.[62]

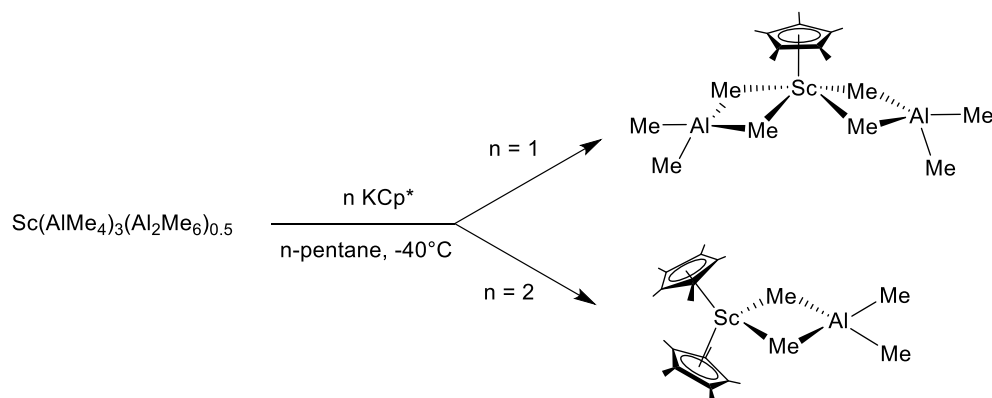
The association of the doubly reduced, bulky diazabutadiene ligand [2,6-*i*Pr₂C₆H₃N=C=NC₆H₃*i*Pr₂-2,6]²⁻ (DAD)²⁻ with the rigid anionic Cp* moiety was exploited in the synthesis of heteroleptic dysprosium complexes showing SMM behavior.[63] The two half-sandwich complexes, the neutral [Dy(DAD)Cp*(THF)] and the Li-ate complex [Li(THF)₃(μ-Cl)Dy(DAD)Cp*], were synthesized by a cascade reaction of anhydrous DyCl₃ with [DADK₂(THF)_n], followed by reaction with MCp* (M = Li, K) as shown in Scheme 54. Single XRD of these complexes indicated η²-coordination of the C-C double bond of the DAD ligand to Dy³⁺ by the short Dy-C distances, 2.837(2) and 2.845(2) Å for the neutral complex and 2.764(2) and 2.769(2) Å for the Li-ate complex. The angles Ct(NCCN)-Dy-Ct(Cp*) are 142.0(2)° and 139.6(2)° and the shortest intermolecular Dy³⁺-Dy³⁺ distances are 9.543(2) and 11.413(2) Å for the neutral and the Li-ate complex, respectively. The two new complexes showed slow relaxation of magnetization under zero DC-field. The slight

differences in Dy-N distances and Cp*-Dy-DAD angles, caused by the additional ligands (THF vs Cl⁻) coordinated to the metal, led to distinct relaxation dynamics.[63]



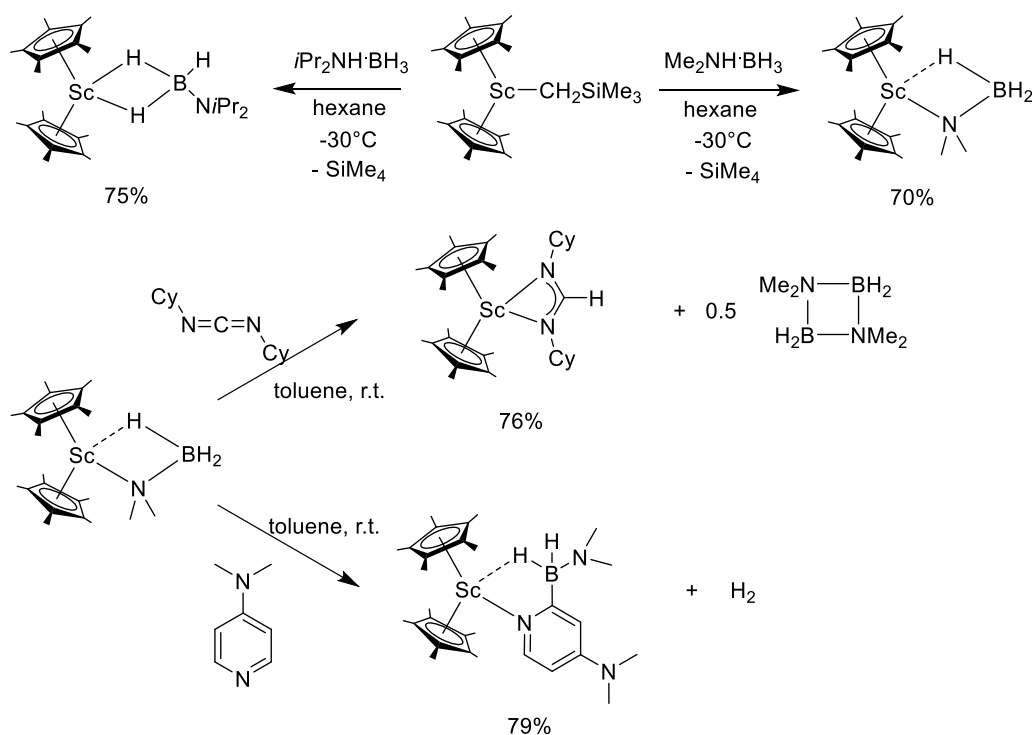
Scheme 54. Synthesis of neutral [Dy(DAD)Cp*(THF)] and the Li-ate complex [Li(THF)₃(μ-Cl)Dy(DAD)Cp*].[63]

Starting from the newly synthesized [Sc(AlMe₄)₃(Al₂Me₆)_{0.5}] complex (see Scheme 5), the half-sandwich complex [Cp*Sc(AlMe₄)₂] and the sandwich complex [Cp*₂Sc(AlMe₄)] were accessible by salt metathesis reactions with KCp* in pentane at low temperatures (Scheme 55).[15] Despite its temperature sensitivity, crystals of the mono-Cp complex could be grown, showing a short average Sc-C(Cp) distance of 2.486(13) Å compared to the Y analogue (2.584(8) Å). In contrast, the metallocene complex [Cp*₂Sc(AlMe₄)] was stable at room temperature. In the ¹H NMR spectrum, only the monomeric complex was present at room temperature, whereas at lower temperatures signals for a dimeric species appeared. For Y, Sm, Yb and Lu analogues such a monomer-dimer equilibrium was already present at room temperature. Crystals for both the monomeric and the dimeric Sc metallocene could be obtained. The monomeric sandwich complex displayed longer Sc-C(Cp) bonds (av. 2.530(3) and 2.532(7)) than the half-sandwich complex. In both cases, the AlMe₄ unit was η²-bound to the Sc center with similar Sc-C(Me) bond lengths.[15]



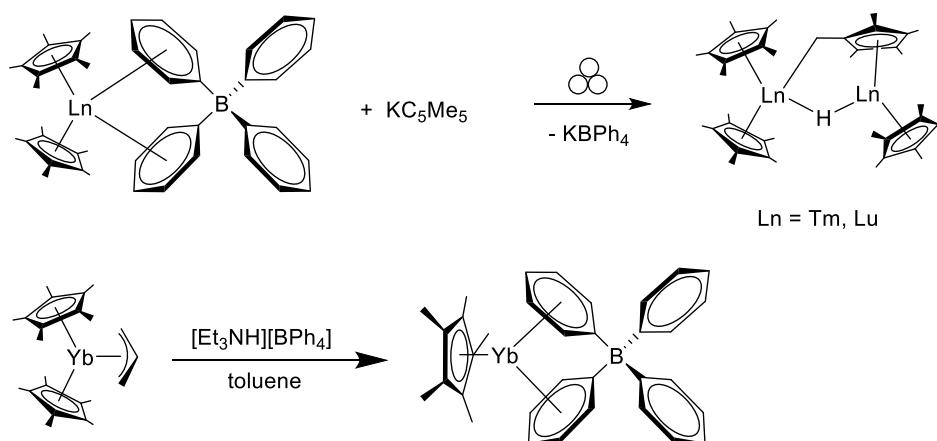
Scheme 55. Synthesis of [Cp*Sc(AlMe₄)₂] and the sandwich complex [Cp*₂Sc(AlMe₄)].[15]

In order to obtain information on the mechanism of the Sc-catalyzed dehydrogenation of amino-boranes (see section 2.11.3), the reaction of the scandium metallocene alkyl complex $\text{Cp}^*_2\text{Sc}(\text{CH}_2\text{SiMe}_3)$ with two sterically different amino-boranes was investigated (Scheme 58). [64] The smaller dimethylaminoborane afforded a rare example of a β -B-agostic scandium amidoborane complex $[\text{Cp}^*_2\text{Sc}(\text{NMe}_2\text{BH}_3)]$ at low temperature, which displayed a relatively long Sc-N bond and a Sc-H-B interaction in the crystal structure. Furthermore, IR spectroscopy showed signals corresponding to terminal and bridging B-H bonds. In solution, ^{11}B NMR spectroscopy indicated the presence of two species, with broad signals at 5.2 and -8.7 ppm, the latter being attributed to the scandium amidoborane complex. Reaction of the scandocene alkyl complex with diisopropylaminoborane yielded the Sc hydride complex $\text{Cp}^*_2\text{Sc}(\mu\text{-}\eta^2\text{-BH}_3\text{N}(\text{iPr})_2)$, displaying a peak at 23.3 ppm in ^{11}B NMR spectrum. This complex may result from an irreversible β -H elimination reaction of a plausible β -B-agostic intermediate. Consequently, in order to provide evidence that such a β -H elimination process could also occur in the Sc amidoborane complex $[\text{Cp}^*_2\text{Sc}(\text{NMe}_2\text{BH}_3)]$, the reaction with DCC was conducted. The formed complex, resulting from the insertion of the electrophile into an intermediate Sc-H bond, was isolated in good yield (76%) together with the formation of the cyclic borazane. In addition, reaction of the scandocene complex with DMAP yielded H_2 evolution and the isolation of a Sc-DMAP adduct bearing a dimethylaminoboryl group in the ortho position, providing further evidence for a possible β -H elimination process.[64]



Scheme 56. Reactivity of $\text{Cp}^*_2\text{Sc}(\text{CH}_2\text{SiMe}_3)$ towards aminoboranes and consecutive transformations.[64]

The reaction of the cationic complexes $\text{Cp}^*_2\text{Ln}(\text{BPh}_4)$ ($\text{Ln} = \text{Tm}, \text{Lu}$) with KCp^* under solvent-free ball-milling conditions did not lead to the formation of LnCp^*_3 complexes, as previously observed for larger lanthanides, but to the tuck-over complexes $\text{Cp}^*_2\text{Ln}(\mu\text{-H})(\mu\text{-}\eta^1:\eta^5\text{-CH}_2\text{C}_5\text{Me}_4)\text{LnCp}^*$ ($\text{Ln} = \text{Tm}, \text{Lu}$) in low isolated yields (Scheme 57).[65] The structure was confirmed in the case of Tm by XRD analysis. Attempted preparation of the trivalent Yb precursor $\text{Cp}^*_2\text{Yb}(\text{BPh}_4)$ from the reaction of the allyl precursor $\text{Cp}^*_2\text{Yb}(\text{C}_3\text{H}_5)$ and $[\text{HNEt}_3][\text{BPh}_4]$ yielded the divalent Yb complex $\text{Cp}^*\text{Yb}(\text{BPh}_4)$ instead. [65]



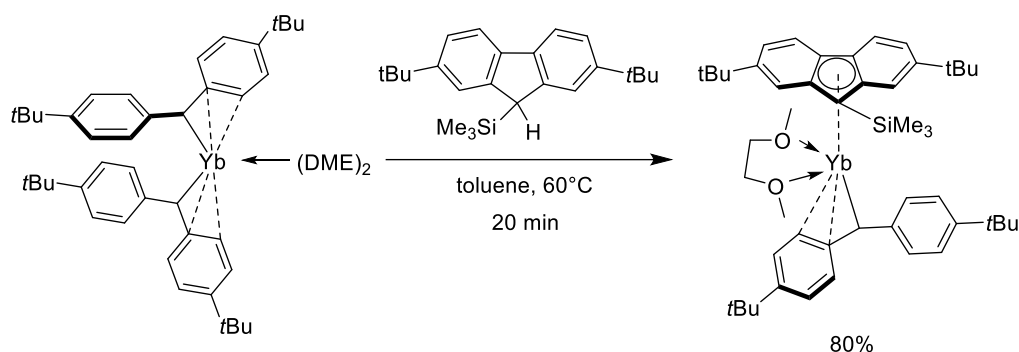
Scheme 57. Solvent-free ball-milling conditions for the synthesis of tuck-over complexes $\text{Cp}^*_2\text{Ln}(\mu\text{-H})(\mu\text{-}\eta^1:\eta^5\text{-CH}_2\text{C}_5\text{Me}_4)\text{LnCp}^*$ ($\text{Ln} = \text{Tm}, \text{Lu}$).[65]

A theoretical study on the understanding of the factors governing σ -bond metathesis, olefin insertion and olefin metathesis in $\text{Cp}^*_2\text{Ln}(\text{CH}_3)$ ($\text{Ln} = \text{Sc}, \text{Y}, \text{Lu}$) complexes was conducted and compared to the cationic $\text{Cp}^*_2\text{Ti}(\text{CH}_3)^+$ derivative.[66] The ^{13}C NMR chemical shift tensors (CST) of the methyl group in all complexes were calculated, showing good agreement with the experimental value for the Sc complex ($\delta_{\text{iso}} = 28$ ppm). For Sc, Y, Lu the isotropic chemical shift values were only moderately deshielded ($\delta_{\text{iso}} = 21\text{-}28$ ppm) compared to the Ti analogue ($\delta_{\text{iso}} = 94$ ppm). For all four complexes, the CST revealed significant anisotropy. It was found that the π -character of the M-C bond was required not only for the olefin insertion and olefin metathesis but also for the σ -bond metathesis reaction. For these three isolobal processes, two low-lying empty orbitals on

the metal fragment are necessary, one engaging in the σ -bond to the alkyl or alkylidene group and serving as the coordination site for the incoming substrate, and another one forming a π -interaction with the alkyl or alkylidene fragment, resulting in a polarization perpendicular to the M-C axis. Consequently, the coordination and reaction of the substrate is enabled and a π (M-C) character is present throughout the whole reaction, in the ground and the transition state.[66]

2.5. LANTHANIDE INDENYL AND FLUORENYL COMPLEXES

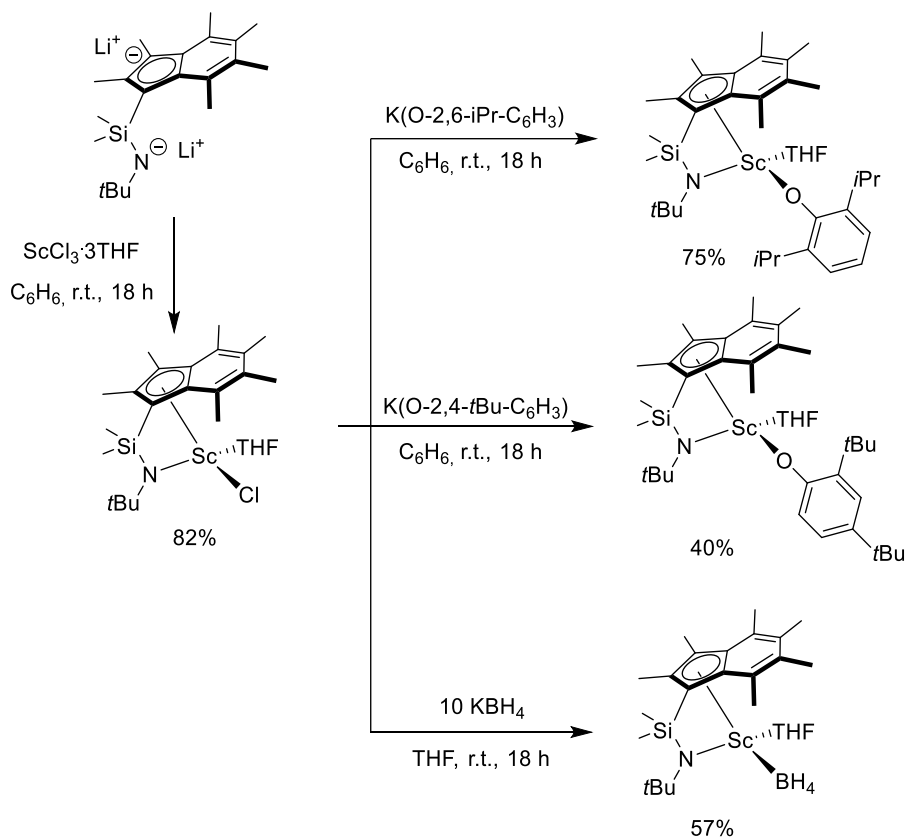
The divalent fluorenyl Yb benzhydryl complex $[(p\text{-}t\text{Bu-C}_6\text{H}_4)_2\text{CH}]Yb(2,7\text{-}t\text{Bu}_2\text{-}9\text{-SiMe}_3\text{-C}_{13}\text{H}_6)(\text{DME})$ was synthesized in high yield from the reaction of the homoleptic benzhydryl precursor $[(p\text{-}t\text{Bu-C}_6\text{H}_4)_2\text{CH}]_2Yb(\text{DME})_2$ with 2,7-di-tert-butyl-9-trimethylsilyl-fluorene in toluene at 60°C (Scheme 58).[67] The complex showed high thermal stability even at 100°C and was fully characterized by NMR spectroscopy and XRD analysis. In the ^{171}Yb NMR spectrum a peak at 280 ppm was observed. The benzhydryl ligand is η^3 -coordinated and the fluorenyl ligand is η^5 -coordinated to the metal center, with the Yb-C bonds being considerably longer for the Yb-C(ipso) and Yb-C(o-Ph) bonds than for the Yb-C(benzhydryl) bond, 2.721(2) Å and 2.737(2) Å vs 2.589(2) Å, respectively.[67]



Scheme 58. Synthesis of mixed fluorenyl/benzhydryl ytterbium(II) complex.[67]

A series of constrained geometry scandium complexes based on a permethylated indenyl ligand containing a dimethylsilylamide-tether was synthesized by a salt-metathesis approach starting from ScCl_3 (Scheme 59).[68] The initially obtained Sc chloride complex $[\text{C}_9\text{Me}_6(\text{SiMe}_2\text{N}t\text{Bu})]\text{ScCl}(\text{THF})$ was characterized by NMR spectroscopy and further converted to the aryloxide and borohydride complexes $[\text{C}_9\text{Me}_6(\text{SiMe}_2\text{N}t\text{Bu})]\text{Sc}(\text{R})(\text{THF})$ ($\text{R} = \text{O-}2,6\text{-}i\text{Pr-C}_6\text{H}_3$, $\text{O-}2,4\text{-}t\text{Bu-C}_6\text{H}_3$, BH_4). XRD analysis of the aryloxide complexes showed slightly shorter Sc-N, Sc-O bond lengths and a longer Sc-Cp(Ct) distance for the less bulky $\text{O-}2,4\text{-}t\text{Bu-C}_6\text{H}_3$ substituted complex. Especially the Sc-O-C is significantly

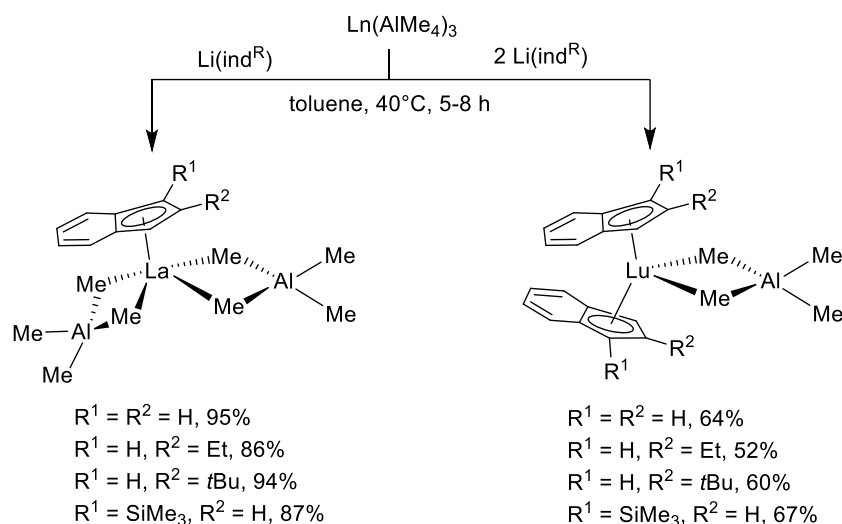
influenced by the steric bulk with 175.6 vs 152.9° for the di-*isopropyl* vs di-*tert*-butyl aryloxy substituents, respectively. XRD studies on the borohydride complex revealed a κ^3 -coordination mode of the BH₄ group to scandium with a Sc–B distance of 2.3572(16) Å. The application of these compounds as initiators in ROP of lactides was studied (see section 2.11.1).[68]



Scheme 59. Synthesis of CG scandium complexes bearing permethylated indenyl ligands.[68]

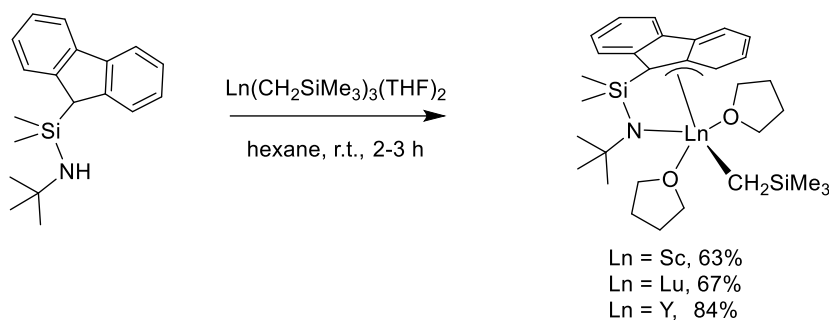
The salt-metathesis reaction of Ln(AlMe₄)₃ with differently substituted Li-indenyl precursors afforded a series of half-sandwich and sandwich indenyl lanthanide complexes (Scheme 60).[69] For La, the half-sandwich complexes (Ind)La(AlMe₄)₂ were obtained in high yields, which did not undergo ligand scrambling at room temperature. For Lu, the sandwich complexes (Ind)₂Lu(AlMe₄) were always the major products, independent of the stoichiometry. The new complexes were studied by NMR spectroscopy showing high fluxionality of the AlMe₄ groups in the La complexes (only a single signal in ¹H NMR for both AlMe₄ groups). The prochirality of the C1 trimethylsilyl-substituted indenyl ligand led to the formation of a 9:1 mixture of meso:rac isomers of the corresponding Lu-sandwich complex according to ¹H NMR. XRD analysis revealed that the C2 *t*-butyl

substituted indenyl La complex crystallized as monomer. In contrast, the other La complexes showed dimeric structural motifs, either with linear $\text{La}(\mu\text{-CH}_3)\text{Al}$ bridging units *cis* (for parent and ethyl substituted indenyl ligand) or *trans* to the indenyl ligand (silyl substituted indenyl). The substituents on the indenyl ligands also influenced the conformation of the Lu sandwich complexes, i.e. the overlap of the arene rings of the indenyl ligands. Whereas the least substituted parent indenyl ligand led to a near eclipsed conformation (torsion angle between two indenyl ligands 33°), the ethyl and trimethylsilyl substituted indenyl ligands favored a staggered conformation (178° and 172°). The *t*Bu groups on the indenyl ligand led to an intermediate conformation (129°). The influence of the steric bulk of the indenyl ligands in these new complexes was investigated in isoprene polymerization (see section 2.11.1).[69]



Scheme 60. Synthesis of mono and bis(indenyl)lanthanide complexes.[69]

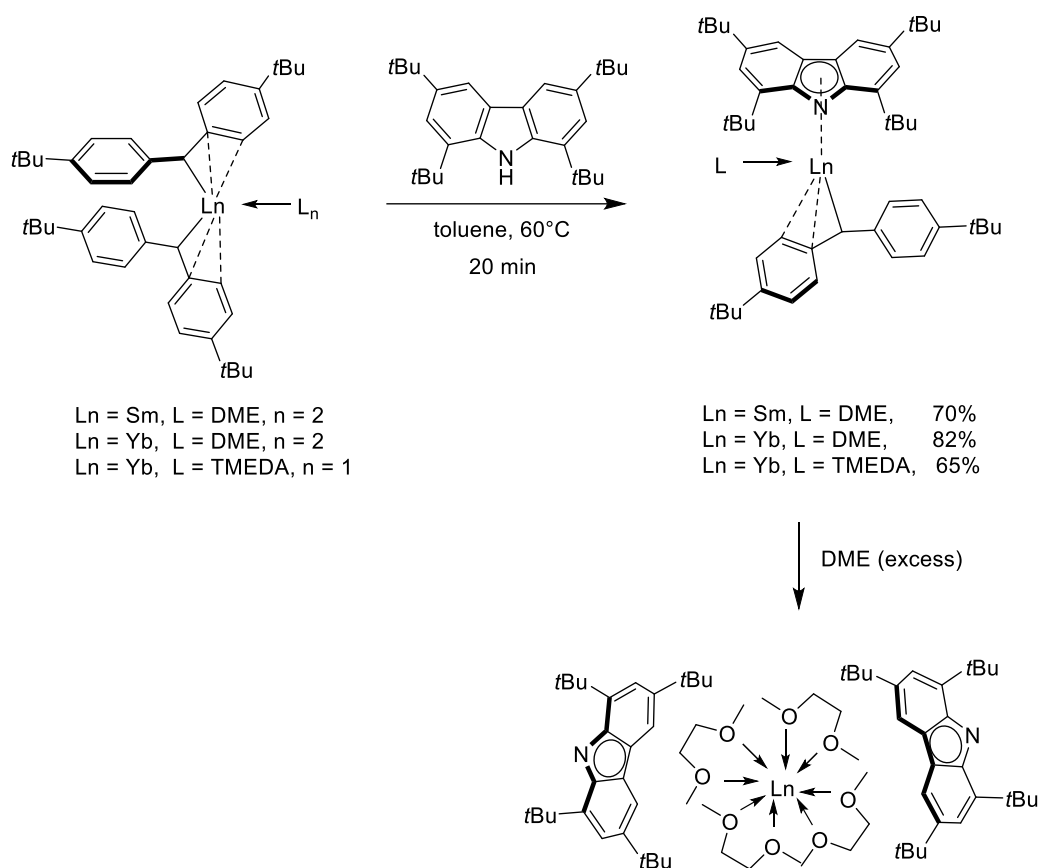
New fluorenyl-amide based constrained geometry lanthanide alkyl complexes ($\eta^3:\eta^1$ - $\text{FluSiMe}_2\text{N}i\text{Bu}$) $\text{Ln}(\text{CH}_2\text{SiMe}_3)(\text{THF})_2$ ($\text{Ln} = \text{Sc}$, Y , Lu) were synthesized in good yields using the protonolysis pathway (Scheme 61).[70] The coordination of the fluorenyl ligand to the metal centers can be described as an asymmetric η^3 -allyl mode as seen from XRD analysis and ^1H NMR spectroscopy (four signals for the eight fluorenyl protons). These complexes were studied as initiators in the polymerization of isoprene, myrcene and styrene (see section 2.12.1).[70]



Scheme 61. Synthesis of amide-tethered fluorenyl lanthanide alkyl complexes.[70]

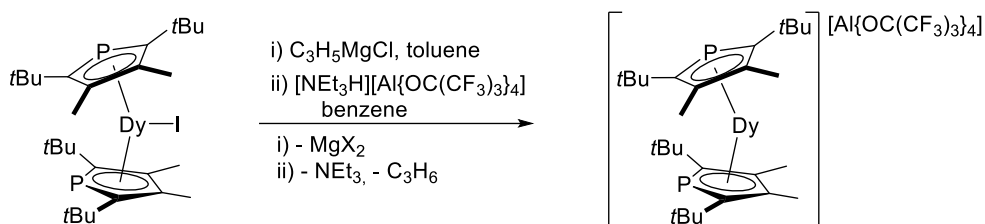
2.6. ORGANOLANTHANIDE COMPLEXES WITH HETEROATOM FIVE-MEMBERED RING LIGANDS

The divalent carbazolyl lanthanide benzhydryl complexes $[\text{tBu}_4\text{Carb}]\text{Ln}[(p\text{-}t\text{Bu-C}_6\text{H}_4)_2\text{CH}](\text{L})$ ($\text{Ln} = \text{Yb}, \text{Sm}, \text{L} = \text{DME}$; $\text{Ln} = \text{Yb}, \text{L} = \text{TMEDA}$) were obtained in good yields after reacting the corresponding homoleptic bis(benzhydryl) lanthanide complexes and 1,3,6,8-tetra-*t*butylcarbazole in toluene at 60°C (Scheme 62).[67] In these complexes the carbazolyl ligand is η^5 -coordinated as shown by XRD. For the benzhydryl ligand, η^3 coordination was observed for the DME adducts, whereas in the case of the Yb-TMEDA complex the ligand is only η^1 bound via the central benzhydryl carbon atom with a Ln-C bond length of 2.597(3) Å (2.540(4) Å for Yb-DME complex). Interestingly, the solvent adducts also influenced the ^{171}Yb NMR shifts, going from 259 ppm for the DME adduct to 178 ppm for the TMEDA adduct. Finally, addition of an excess of DME to the carbazolyl lanthanide benzhydryl complexes led to ligand rearrangement and the formation of solvent-separated ion-pairs $[\text{Ln}(\text{DME})_4][\text{carbazolyl}]_2$ ($\text{Ln} = \text{Yb}, \text{Sm}$) as confirmed by XRD analysis.[67]



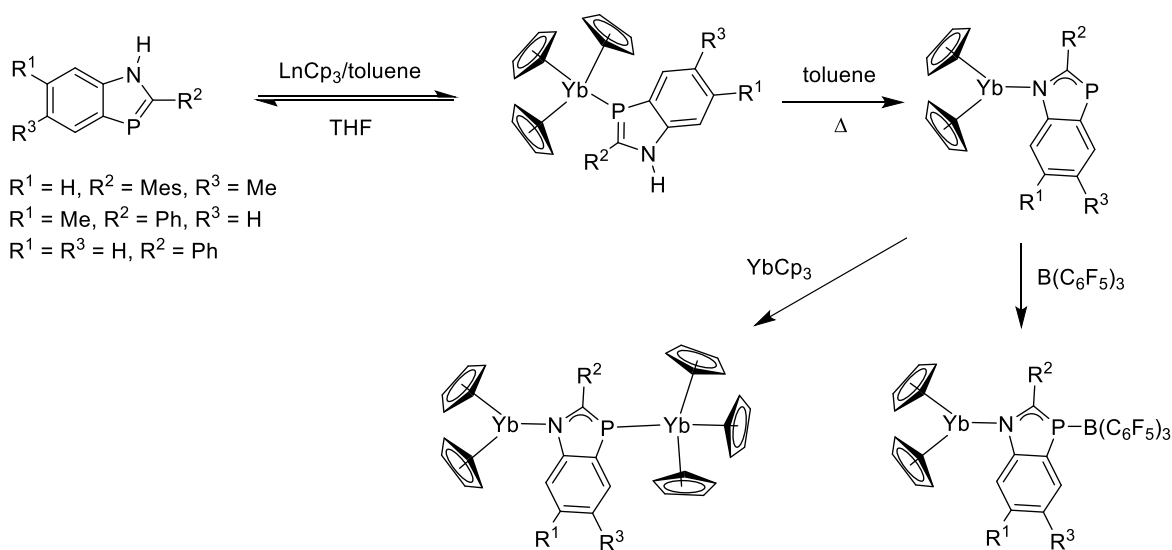
Scheme 62. Synthesis of mixed-ligand carbazolyl/benzhydryl complexes and formation of solvent-separated ion pair.[67]

The cationic bis(phospholyl)dysprosium sandwich complex $[\text{Dy}(\text{Dtp})_2][\text{Al}(\text{OC}(\text{CF}_3)_3)_4]$ ($\text{Dtp} = 2,5\text{-tBu}_2\text{-3,4-Me}_2\text{-phospholyl}$) was synthesized according to Scheme 63 and its SMM properties were investigated.[71] In a first step, reaction of $\text{Dy}(\text{Dtp})_2$ with allylmagnesium bromide led to the formation of the corresponding Dy-allyl complex which could not be isolated. Further reaction with $[\text{Et}_3\text{NH}][\text{Al}(\text{OC}(\text{CF}_3)_3)_4]$ afforded the dysprosocenium complex which could be characterized by single XRD and ^{19}F NMR. In the crystal structure, no interaction between the anion and the dysprosium center was observed, however, electrostatic contacts between Dy^{3+} and the t-butyl groups were observed as indicated by short Dy-C and Dy-H distances. The cation has a bent geometry with a $\text{Ct}(\text{Dtp})\text{-Dy-Ct}(\text{Dtp})$ angle of $157.94(4)^\circ$ and Dy-Ct(Dtp) distances of $2.354(3)$ Å. The new complex showed SMM behaviour with an effective barrier to magnetization reversal $U_{\text{eff}} = 1760$ K and magnetic hysteresis up to $T_{\text{H}} = 48$ K. The relaxation is therefore more efficient in this complex than in the corresponding $[\text{Dy}(\text{Cp}^{\text{ttt}})_2][\text{B}(\text{C}_6\text{F}_5)_4]$ (same U_{eff} , $T_{\text{H}} = 60$ K) complex, which could be explained by smaller energy gaps between excited states which become on-resonance with a series of vibrational modes. [71]



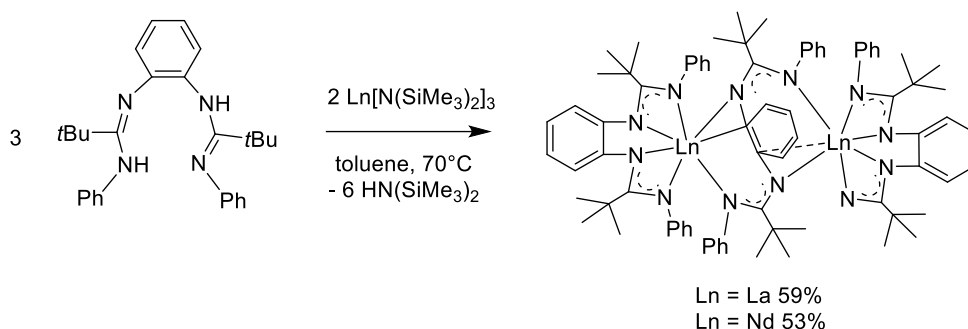
Scheme 63. Synthesis of bis(phospholyl)dysprosocenium complex
 $[\text{Dy}(\text{Dtp})_2][\text{Al}(\text{OC}(\text{CF}_3)_3)_4] \cdot [\text{71}]$

Differently substituted 1H-1,3-benzazaphospholes (HBp) were reacted with LnCp_3 precursors in toluene at room temperature to afford the Lewis-base adducts $[(\eta^1(\text{P})\text{-HBp})\text{LnCp}_3]$ ($\text{Ln} = \text{Y}, \text{Yb}$) in good yields (Scheme 64).[72] The adducts were characterized by IR and NMR spectroscopy. XRD analysis of $[(5\text{-Me-2-mesityl-1,3-benzazaphosphole})\text{YbCp}_3]$ showed a long Yb-P bond of 2.903(4) Å and the mesityl group being perpendicular to the HBp plane. It should be noted that the adduct formation could be reversed in THF. On the other hand, refluxing the adducts in toluene for 2 h led to deprotonation of the N-H group with liberation of Cp-H. The resulting $[(\text{Bp})\text{YbCp}_2]$ complexes were highly air and moisture sensitive and showed the disappearance of the N-H stretching frequency in the IR spectra. The coordination of another Cp_3Ln moiety or the Lewis acid $\text{B}(\text{C}_6\text{F}_5)_3$ to the phosphorus lone pair was achieved in toluene. The new complexes $[\text{Cp}_2\text{Yb}(\mu\text{-}\eta^1(\text{N})\text{:}\eta^2(\text{C,C})\text{:}\eta^1(\text{P})\text{-Bp})\text{YbCp}_3]$ and $[\text{Cp}_2\text{Yb}(\mu\text{-}\eta^1(\text{N})\text{:}\eta^2(\text{C,C})\text{:}\eta^1(\text{P})\text{-Bp})\text{B}(\text{C}_6\text{F}_5)_3]$ were characterized by IR spectroscopy and XRD studies. In both cases, the phenyl group (R^2) coordinated onto the Yb metal in an η^2 fashion. [72]



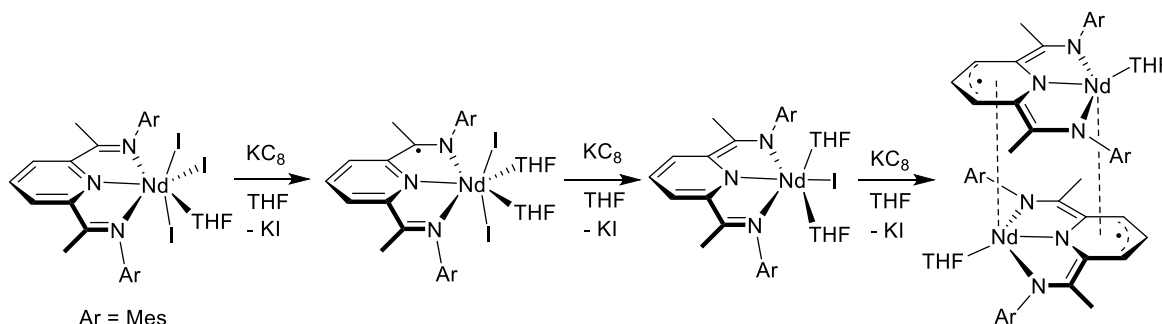
Scheme 64. Interaction and reactivity of Cp_3Ln complexes with 1H-1,3-benzazaphospholes.[72]

moderate yields (Scheme 66).[74] XRD analysis of the La complex revealed that one bis(amidinato) ligand was bound in a classical mode and one in a $\mu\text{-}\eta^2\text{:}\eta^1\text{:}\eta^2\text{:}\eta^1$ -bridging mode, with La-C distances of 2.967(6) and 2.986(5) Å. It should be noted that the same reaction with smaller lanthanides (Y, Er) resulted in the formation of monomeric bis(amidinato) amide complexes, $[\text{C}_6\text{H}_4\text{-1,2-}\{\text{NC}(\text{tBu})\text{NPh}\}_2]\text{LnN}(\text{SiMe}_3)_2$. All new complexes were investigated as initiators for the polymerization of ϵ -caprolactone and L-lactide (see section 2.11.1).[74]



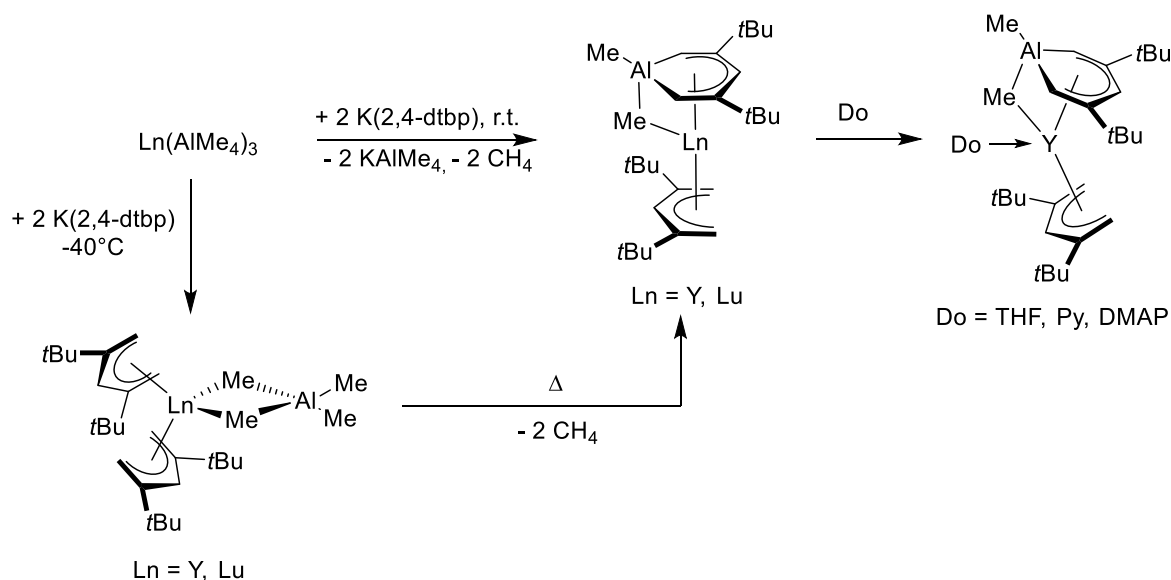
Scheme 66. Synthesis of arene-bridged bis(amidinato) lanthanide complexes.[74]

Coordination of the bulky redox active pyridine-diimine ligand $^{\text{Mes}}\text{PDI}^{\text{Mes}}$ to $\text{NdI}_3(\text{THF})_{3.5}$ afforded initially the simple adduct which could be reduced stepwise with KC_8 in THF to provide eventually the dimeric Nd-pyridyl complex, $[\text{MesPDI}^{\text{Mes}}\text{Nd}(\text{THF})]_2$ (Scheme 67).[75] UV/vis and magnetic measurements conducted on this series of complexes were in agreement with the presence of Nd^{3+} centers in all complexes, hence the reduction occurring on the ligand. XRD analysis of the dimeric complex indicated loss of the planarity of the pyridine moiety, with the nitrogen atom sitting 0.468 Å below the plane and coordinating to the opposite Nd center. The pyridyl moiety is η^6 coordinated to the Nd metal with Nd-C distances in the range from 2.781 to 3.157 Å. In the ligand, the initial C–N_{imine} bond distances were elongated to 1.371(8) and 1.395(9) Å and the C–C distances contracted to 1.396(10) and 1.365(11) Å.[75]



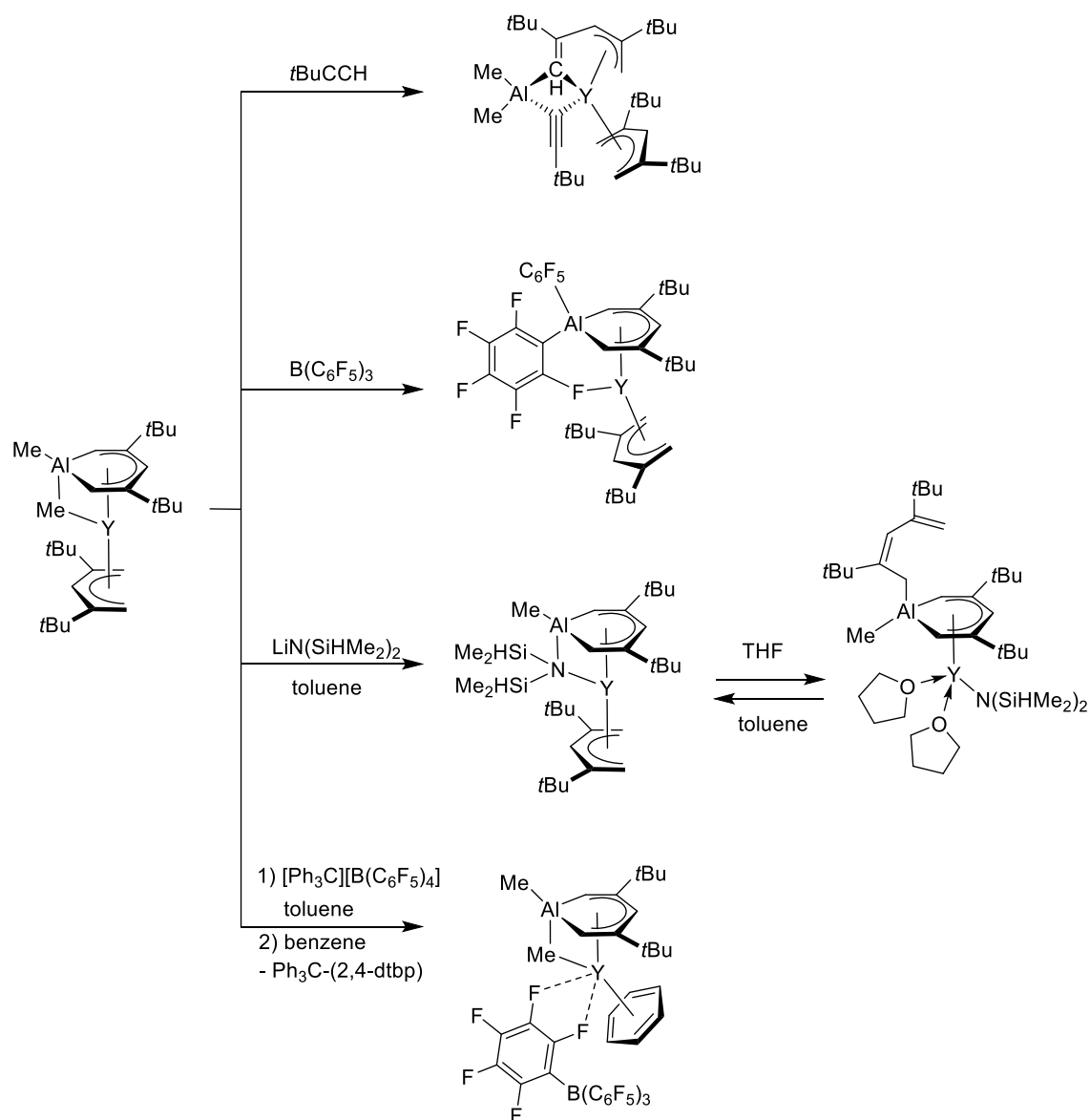
Scheme 67. Stepwise reduction of $^{\text{Mes}}\text{PDI}^{\text{Mes}}\text{NdI}_3(\text{THF})$ to the dimeric Nd-pyridyl complex $[\text{MesPDI}^{\text{Mes}}\text{Nd}(\text{THF})]_2$.[75]

The coordination of a dianionic aluminabenzene ligand to trivalent lanthanide metals was achieved via the reaction of 2,4-di-*t*-butylpentadienyl potassium K(2,4-dtbp) with Ln(AlMe₄)₃ (Ln = Y, Lu) at room temperature (Scheme 68).[76] The resulting complexes [(1-Me-3,5-*t*Bu₂-C₅H₃Al)(μ-Me)Ln(2,4-dtbp)] (Ln = Y, Lu) containing one pentadienyl and one methyl-bridged aluminabenzene ligand were isolated in high yields and fully characterized by XRD analysis and solution NMR spectroscopy. The structure revealed η⁵ coordination of the almost planar aluminabenzene ligand to the lanthanide metal with very short Ln-Al distances (2.769(9) Å for Y, 2.718(6) for Lu), whereas the pentadienyl ligand was slightly twisted in a U-shape. Following the reaction course by ¹H NMR spectroscopy revealed the initial formation of the sandwich complexes [(2,4-dtbp)₂Ln(AlMe₄)] by salt metathesis, which could be isolated at low temperatures. In a second step, ring closure occurred via double deprotonation of one of the metal-bound pentadienyl ligand by the basic AlMe₄ and concomitant methane elimination. Addition of various donor molecules, such as THF, pyridine, 4-DMAP or 4,4'-bipyridine, to the yttrium complex [(1-Me-3,5-*t*Bu₂-C₅H₃Al)(μ-Me)Y(2,4-dtbp)] led exclusively to the coordination at the yttrium center without changing the overall coordination mode of the ligands as shown by XRD analysis and NMR spectroscopy. This result is in agreement with a strong Al-CH₃-Y linkage and a reduced Lewis acidity of the four-coordinate aluminum center.[76]



Scheme 68. Synthesis of lanthanide-pentadienyl complexes bearing an aluminabenzene ligand.[76]

Reaction with $B(C_6F_5)_3$ afforded complete Me/C₆F₅ exchange at the aluminum center to yield the new complex $[\{1-(C_6F_5)-3,5-tBu_2-C_5H_3Al\} \{\mu-C_6F_5\} Y \{2,4-dtbp\}]$ and release of $Me_2B(C_6F_5)$ (Scheme 69).[76] XRD analysis showed that in this case the Al is bent out of the ring plane due to the steric bulk of the C₆F₅ ligand and the Y-Al distance is more elongated (3.071(2) Å). The structure also features a Y-F interaction of 2.413(9) Å, in between bridging and weakly coordinating Y-F distances. Finally, reaction with tBuCCH provided the vinyl acetylide complex $[\{2,4-dtbp\} Y \{(\mu-\eta^1:\eta^3-2,4-tBu_2-C_5H_4)(\mu-CctBu)AlMe_2\}]$, via protonation of the aluminabenzene ligand and coordination of the resulting alkynyl moiety between yttrium and aluminum. In this complex, the Y is bound η^5 to the U-shaped pentadienyl ligand and $\eta^3:\eta^1$ to a pentadienediyl ligand in its S-form. In a subsequent study it was shown that reaction of the Y aluminabenzene complex with $LiN(SiHMe_2)_2$ led to methyl/silylamido exchange and formation of $(1-Me-3,5-tBu_2-C_5H_3Al)[\mu-N(SiHMe_2)_2]Y(2,4-dtbp)$ (Scheme 69).[77] The characteristic features of this complex, obtained from DRX analysis, are a nearly planar aluminabenzene moiety and a distortion of the silylamido group towards the metal center due to agostic interactions. In the ¹H NMR spectrum, the Si-H signal appears strongly upfield shifted at 3.73 ppm probably due to the shielding ring current of the aluminabenzene ligand. Addition of THF to this complex led to coordinative rearrangement, with two THF molecules replacing the pentadienyl moiety on the Y metal, leading to a silylamido/pentadienyl exchange between the Al and Y centers. Structural analysis indicated significant bending in the previously planar aluminabenzene ligand, with Al 0.934 Å out of the ring plane, and a U-shaped coordination of the pentadienyl ligand to Al. In aliphatic or aromatic solvents or under vacuum this complex rearranged back to the initial complex. Finally, the reactivity of the Y aluminabenzene complex with an equimolar amount of $[Ph_3C][B(C_6F_5)_4]$ in toluene was tested. The resulting pentadienyl abstraction afforded the cationic complex $(1-Me-3,5-tBu_2-C_5H_3Al)(\mu-Me)Y(benzene)[B(C_6F_5)_4]$ as the sole metal-containing product according to NMR spectroscopy. No considerable change in the Y-aluminabenzene moiety was observed in the XRD studies. The Y center was stabilized by an η^6 -bound benzene molecule and by Y-F interactions with the ortho and meta F atoms of one ring of $[B(C_6F_5)_4]$. The new Y-aluminabenzene complexes were further studied in isoprene polymerization (see section 2.11.1).[77]

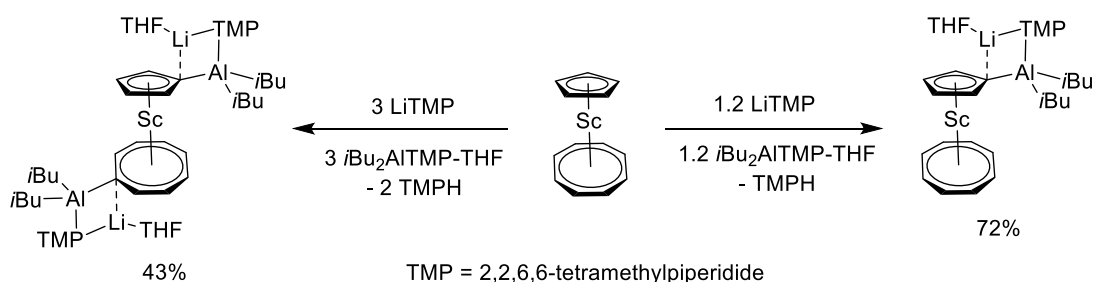


Scheme 69. Reactivity studies of yttrium aluminabenzene complex.[76][77]

2.8. LANTHANIDE CYCLOOCTATETRAENYL COMPLEXES

The mixed-ligand scandium complex $(\eta^5\text{-C}_5\text{H}_4)\text{Sc}(\eta^8\text{-C}_8\text{H}_8)$ (CpScCOT) was selectively mono- and dimetallated using a trans-metal trapping protocol.[78] Reaction with 1.2 equiv. of $\text{LiTMP}/i\text{Bu}_2\text{AlTMP}/\text{THF}$ ($\text{TMP} = 2,2,6,6\text{-tetramethylpiperidide}$) in refluxing hexane afforded selective deprotonation at the Cp ligand to form the monometallated complex $[\text{THF-Li}-(\mu\text{-TMP})\{\mu\text{-}\{(\eta^5\text{-C}_5\text{H}_4)\text{Sc}(\eta^8\text{-C}_8\text{H}_8)\}\}\text{Al}(i\text{Bu})_2]$ in near quantitative NMR yield and good 72% isolated yield (Scheme 70).[78] Whereas reaction with only LiTMP provided very low conversion, the presence of the more carbophilic $i\text{Bu}_2\text{AlTMP}$, which trapped and stabilized the initially formed lithiated species, shifted the

equilibrium towards the desired metallated complex. This complex was characterized by XRD and multinuclear NMR spectroscopy, including ^1H DOSY NMR experiments suggesting that the complex remained intact in THF solution. Addition of 2 equiv of $\text{LiTMP}/i\text{Bu}_2\text{AlTMP}/\text{THF}$ provided a mixture of reaction products, however, addition of 3 equiv. of reagent in refluxing methylcyclohexane, yielded the dimetallated complex $[\{\text{THF-Li}(\mu\text{-TMP})\text{Al}(i\text{Bu})_2\}_2\{\mu\text{-}\{(\eta^5\text{-C}_5\text{H}_4)\text{Sc}(\eta^8\text{-C}_8\text{H}_7)\}\}]$ in excellent NMR yield (Scheme 70). This new complex resulted from selective deprotonation at the Cp and the COT ligand and was fully characterized by XRD and NMR spectroscopy. Interestingly, both mono- and dimetallated complexes reacted sluggishly with electrophiles, such as I_2 , D_2O , TMSCl or MeOTf , and afforded complex reaction mixtures. DFT calculations on the new metallated complexes as well as on the parent CpScCOT complex revealed a similar electronic structure for all three compounds. For the metallated complexes, electron-density on ring carbons was only found in low-lying molecular orbitals (HOMO-4 for the monometallated and HOMO-7 for the dimetallated complex), in agreement with the observed low nucleophilic reactivity.[78]



Scheme 70. Synthesis of selectively mono and dimetallated complexes using $\text{LiTMP}/i\text{Bu}_2\text{AlTMP}/\text{THF}$ as trans-metal-trap reagent with CpScCOT . [78]

The reaction of LnI_3 with $\text{K}_2(\text{COT})$ in THF at room temperature provided the first solution-based synthesis of $\text{M}_2(\text{COT})_3(\text{THF})_2$ ($\text{Ln} = \text{Y}, \text{La}$) complexes,[79] which were previously only accessible via metal-atom evaporation methods. The compounds were isolated in good yields and characterized by ^1H NMR and XRD analysis. The structure shows one $[\text{Ln}(\text{COT})_2]^-$ unit coordinated via one COT ligand in an η^2 fashion to one $[\text{Ln}(\text{COT})(\text{THF})_2]^+$ unit (Figure 3). In the $[\text{La}(\text{COT})_2]^-$ fragment, the La-centroid distances are not equal (2.045(4) Å and 2.154(5)) and the Ct-La-Ct angle deviates from linearity (172.9°) due to a slight bending of the doubly coordinated COT-2 ligand. In the ^1H NMR spectrum, the COT ligands show only 1 signal at room temperature but two signals in a 2:1 ratio at -80°C . [79]

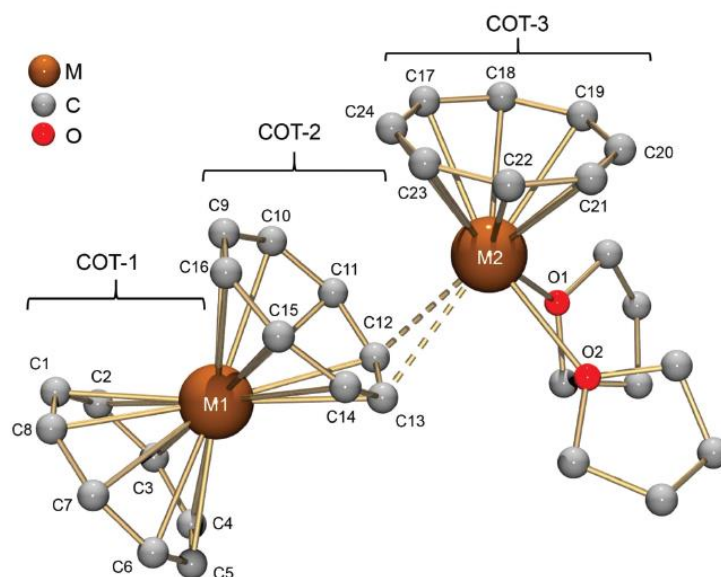


Figure 3. Ball-and-stick model of $[M_2(COT)_3(THF)_2]$ (hydrogen atoms are omitted for clarity). Reproduced with permission from.[79] Copyright 2019 Royal Society of Chemistry.

A theoretical study was conducted on neutral and anionic $Ln_n(COT)_m$ ($Ln = Ce, Nd, Eu, Ho, Yb$; $n, m = 1, 2$) complexes to explore their structural and electronic properties.[80] In the case of $Ln(COT)_2$, $[Ln(COT)_2]^-$, $Ln_2(COT)_2$ and $[Ln_2(COT)_2]^-$ complexes, sandwich structures with alternating metal and COT ligands were determined, with the exception of $Nd_2(COT)_2$ and $[Nd_2(COT)_2]^-$, which have two Nd metals sandwiched between two COT ligands (Figure 4). For Ce, in the case of $Ln_2(COT)$ and $[Ln_2(COT)]^-$ complexes, a COT ligand is bound between to Ce centers, whereas for all other lanthanides, two Ln metals bind in an associative manner on the surface of the COT molecule. A systematic increase of Ln-COT distances was observed when going from the neutral to the anionic complexes. Frontier molecular orbital analysis and Hirshfeld charge population analysis indicate a weak bond between the Ln 4f electrons and the π cloud of the COT ligand as well as limited electron transfer from Ln to COT.[80]

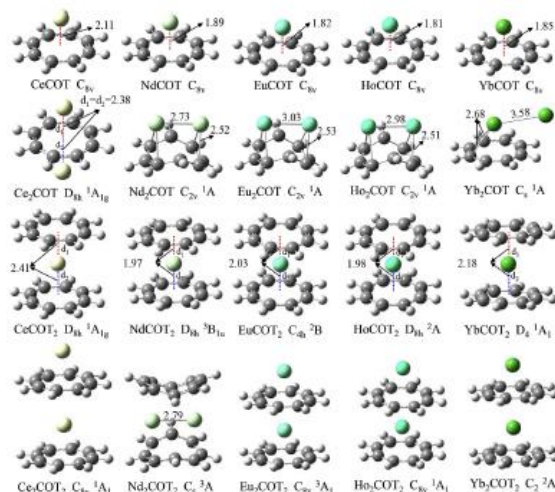


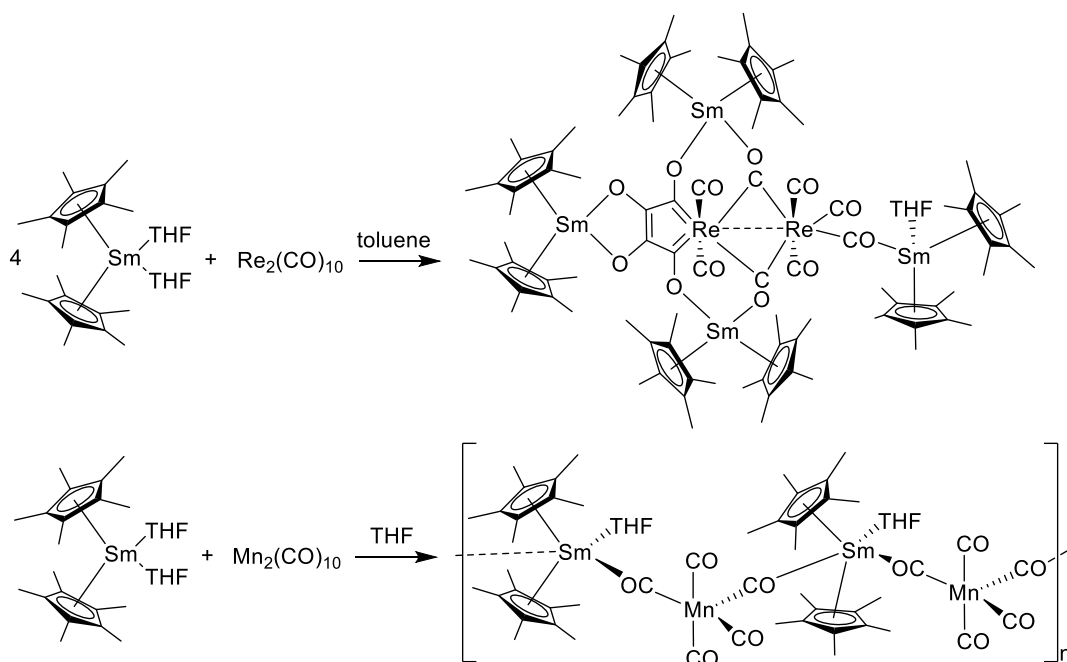
Figure 4. The ground state structures of neutral $\text{Ln}_n(\text{COT})_m$ ($\text{Ln} = \text{Ce}, \text{Nd}, \text{Eu}, \text{Ho}, \text{Yb}$; $n, m = 1, 2$) complexes. Their symmetries, electron states, bond lengths, as well as the distance between the Ln and the mass center of COT ring are also shown in the figure. The bond lengths are in Å. Reproduced with permission from [80]. Copyright 2019 Elsevier.

Quantum chemical calculations were performed on the monomer $[\text{Ce}(\text{COT})_2]^-$ and the dimer $[\text{Ce}_2(\text{COT})_3]$, with a special focus on the magnetic coupling of the dimer, which had experimentally shown an isotropic and a small anisotropic coupling.[81] In this study, the magnetic coupling of the dimer was rationalized by a model based on crystal field theory. The calculations indicate that the main contribution to the isotropic coupling is kinetic and arises from the f_σ - f_σ interaction due to the large transfer integral between these orbitals, while f_π - f_π interaction have a non-negligible role. The origin for the anisotropic coupling resides in the difference of exchange energy of states due to the $f_\sigma f_\pi$ configuration.[81]

2.9. HETEROBIMETALLIC ORGANOLANTHANIDE COMPLEXES

The reaction of the divalent samarocene complex $\text{Cp}^*_2\text{Sm}(\text{THF})_2$ with group 8 metal carbonyls $\text{M}_2(\text{CO})_{10}$ ($\text{M} = \text{Re}, \text{Mn}$) provided access to the new heterobimetallic complexes $[\{(\text{Cp}^*)_2\text{Sm}\}_3\{(\mu\text{-O}_4\text{C}_4)(\mu\text{-}\eta^2\text{-CO})_2(\mu\text{-}\eta^1\text{-CO})(\text{CO})_5\text{Re}_2\}\text{SmCp}^*_2(\text{thf})]$ and $[\{\text{Cp}^*_2\text{Sm}(\text{thf})\}(\mu\text{-CO})_2\{\text{Mn}(\text{CO})_3\}]_n$ as shown in Scheme 71.[82] In the case of $\text{Re}_2(\text{CO})_{10}$, the unprecedented tetramerization of CO occurred to afford a Fischer-type rhenacycle, a representation which was supported by XRD studies and theoretical calculations. This complex consists of four $[\text{SmCp}^*_2]^+$ units bound to the central $[(\mu\text{-O}_4\text{C}_4)(\mu\text{-}\eta^2\text{-CO})_2(\mu\text{-}\eta^1\text{-CO})(\text{CO})_5\text{Re}_2]^{4-}$ core via bridging isocarbonyls or the $\mu\text{-O}_4\text{C}_4$ entity. The corresponding reaction with $\text{Mn}_2(\text{CO})_{10}$ yielded a 1D coordination polymer as shown by

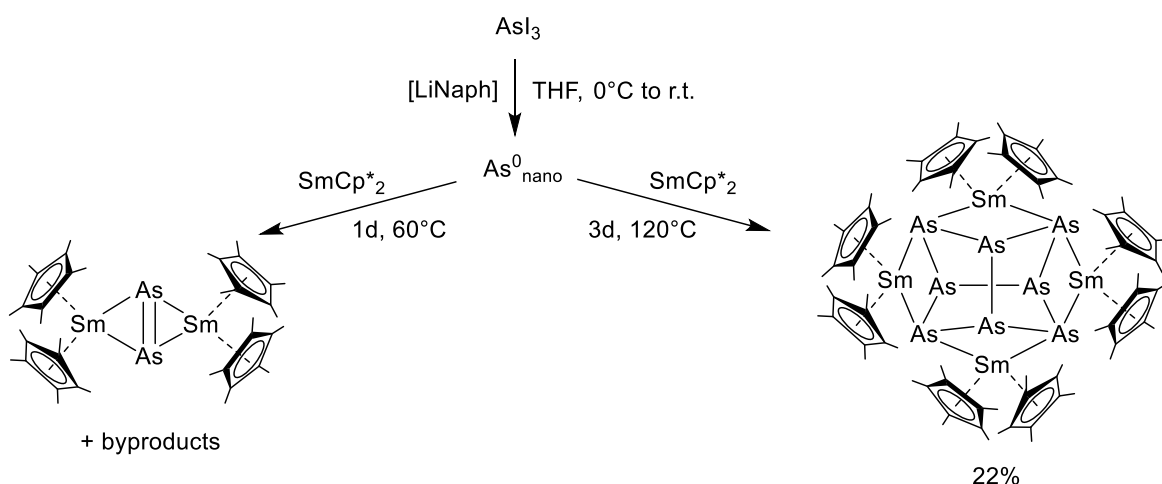
XRD studies, resulting from the expected cleavage of the Mn-Mn bond upon reduction with divalent samarocene. The trivalent $[\text{SmCp}^*_2]^+$ cations are connected to the $[\text{Mn}(\text{CO})_5]^-$ anions via bridging isocarbonyl groups. In order to study the influence of steric bulk of the ligand on the lanthanide metal on these reduction reactions, the analogous reactions of $\text{M}_2(\text{CO})_{10}$ ($\text{M} = \text{Re}, \text{Mn}$) with a bulky formamidinate lanthanide complex, $(\text{DippForm})_2\text{Sm}(\text{THF})_2$, ($\text{DippForm} = N,N\text{-bis}(2,6\text{-diisopropylphenyl})\text{formamidinate}$) was investigated. With Re, the first $[\text{Re}_2(\text{CO})_8]^{2-}$ dianion, complexed between two $[(\text{DippForm})_2\text{Sm}]^+$ units, could be isolated and structurally characterized, whereas with Mn the monomeric complex $[(\text{DippForm})_2\text{Sm}(\text{THF})]\{\text{Mn}(\text{CO})_5\}$ formed after Mn-Mn bond cleavage.[82]



Scheme 71. Synthesis of heterobimetallic Sm-Re and Sm-Mn complexes by reduction of carbonyl precursors $\text{M}_2(\text{CO})_{10}$ ($\text{M} = \text{Re}, \text{Mn}$) with divalent samarocene $\text{SmCp}^*_2(\text{THF})_2$. [82]

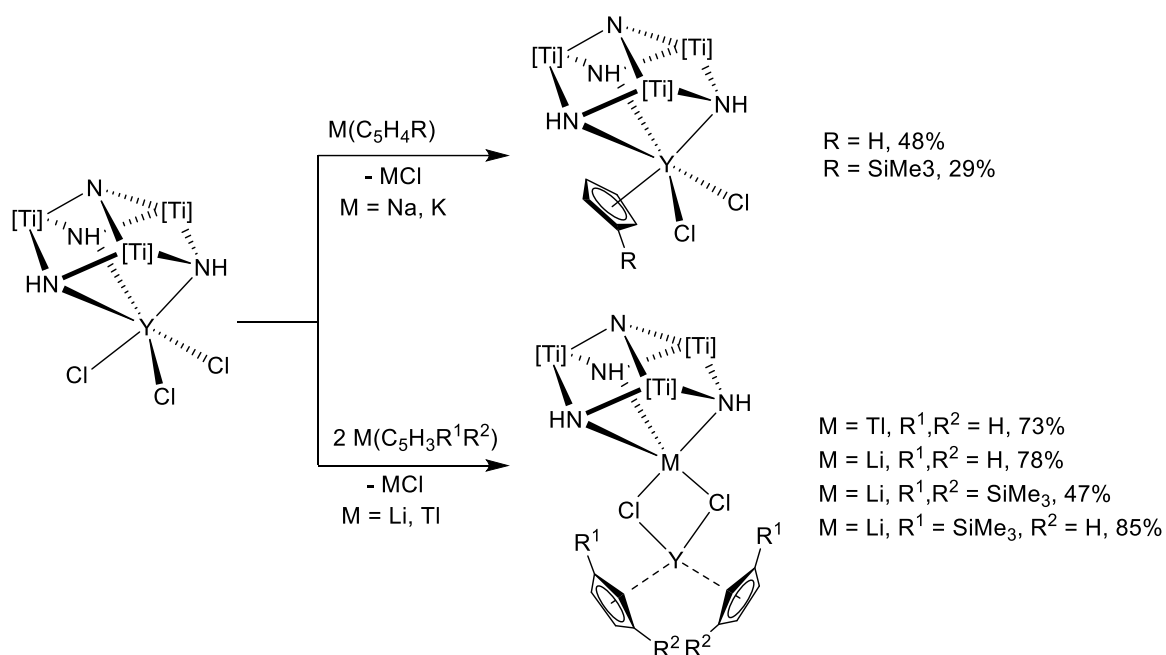
The preparation of salt- and surfactant-free nanoscale arsenic $\text{As}^0_{\text{nano}}$, via reduction of AsI_3 with a freshly prepared lithium naphthalenide solution, provided a reactive As^0 source for the successful oxidation of the divalent solvent-free samarocene complex Cp^*_2Sm . [83] Depending on the reaction conditions, two principal products could be isolated and structurally characterized. The reaction at 60°C furnished the dimeric product $[(\text{Cp}^*_2\text{Sm})_2(\mu\text{-}\eta^2\text{:}\eta^2\text{-As}_2)]$ after 24h in low yields (Scheme 72). This complex contains a formal $[\text{As}_2]^{2-}$ bridge with an As-As bond length of $2.278(2) \text{ \AA}$, consistent with an As=As double bond. Heating the reaction at higher temperature for three days provided the

thermodynamically more favorable product $[(\text{Cp}^*\text{Sm})_4\text{As}_8]$, displaying the realgar-type tetraanion $[\text{As}_8]^{4-}$, which was previously reported for other polypnictides. XRD studies showed that all As-As bonds were single bonds and that the Sm-As bonds were only slightly longer than in the dimeric complex. The complex was further analyzed by ^1H NMR and IR spectroscopy, showing good agreement with the phosphorus and antimony analogues.[83]



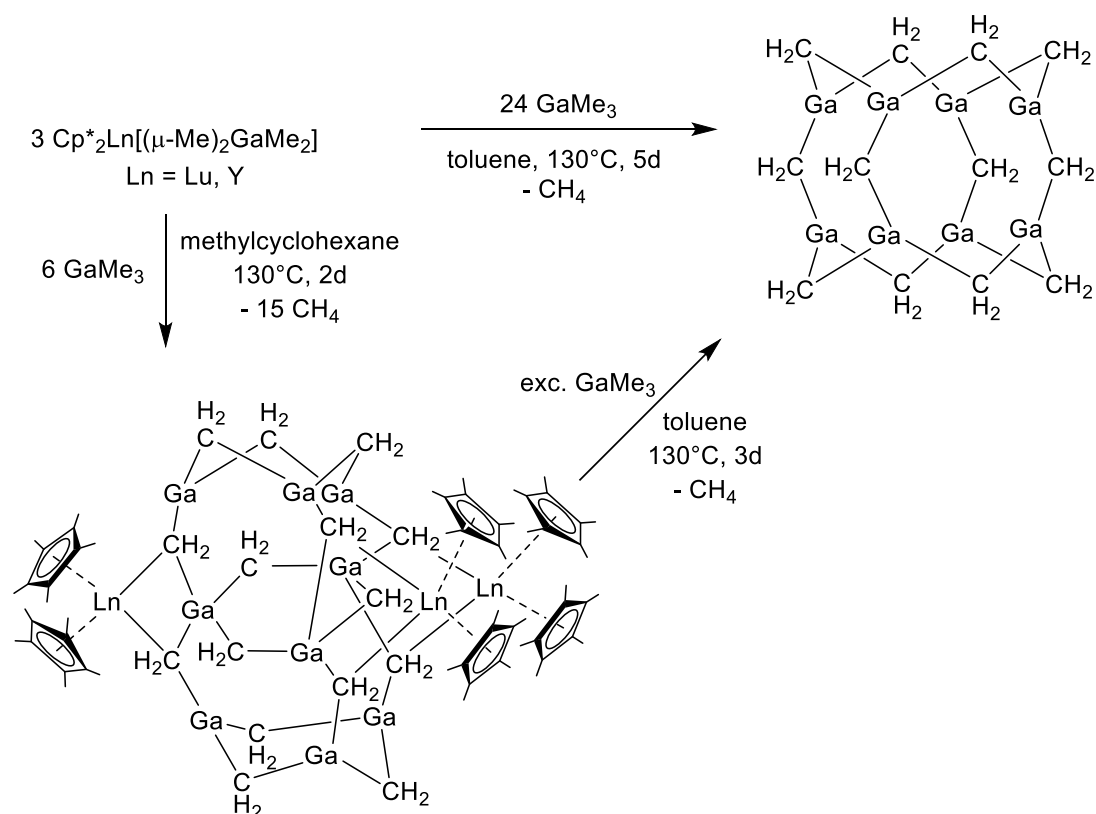
Scheme 72. Synthesis of $[(\text{Cp}^*\text{Sm})_2(\mu\text{-}\eta^2\text{:}\eta^2\text{-As}_2)]$ and $[(\text{Cp}^*\text{Sm})_4\text{As}_8]$ from nanoscale As^0 . [83]

The substitution of one or two chloride ligands at the YCl_3 center in the heterobimetallic complex $[\text{Cl}_3\text{Y}\{(\mu^3\text{-NH})_3\text{Ti}_3(\eta^5\text{-C}_5\text{Me}_5)_3(\mu^3\text{-N})\}]$, bearing the neutral trimetallic imido-nitrido titanium(IV) ligand, with different cyclopentadienyl reagents was explored.[84] The reaction with one equivalent of sodium or potassium reagents $\text{M}(\text{C}_5\text{H}_4\text{R})$ ($\text{M}=\text{Na}, \text{K}$; $\text{R}=\text{H}, \text{SiMe}_3$) provided the expected mono-Cp yttrium complexes $[(\text{C}_5\text{H}_4\text{R})\text{Cl}_2\text{Y}\{(\mu^3\text{-NH})_3\text{Ti}_3(\eta^5\text{-C}_5\text{Me}_5)_3(\mu^3\text{-N})\}]$, in moderate yields (Scheme 73). The reaction with two equivalents of MCp did not provide the expected double substitution but a mixture of compounds. In contrast, reaction with two equivalents of different lithiated Cp reagents or TiCp led to the complexation of two Cp ligands at the yttrium center. However, the *in situ* formed LiCl or TlCl were incorporated into the final compound $[(\text{C}_5\text{H}_3\text{R}_1\text{R}_2)_2\text{Y}(\mu\text{-Cl})_2\text{M}\{(\mu^3\text{-NH})_3\text{Ti}_3(\eta^5\text{-C}_5\text{Me}_5)_3(\mu^3\text{-N})\}]$ ($\text{M}=\text{Li}, \text{Tl}$) via displacement of Y from the titanium metalloligand, probably for steric reasons.[84]



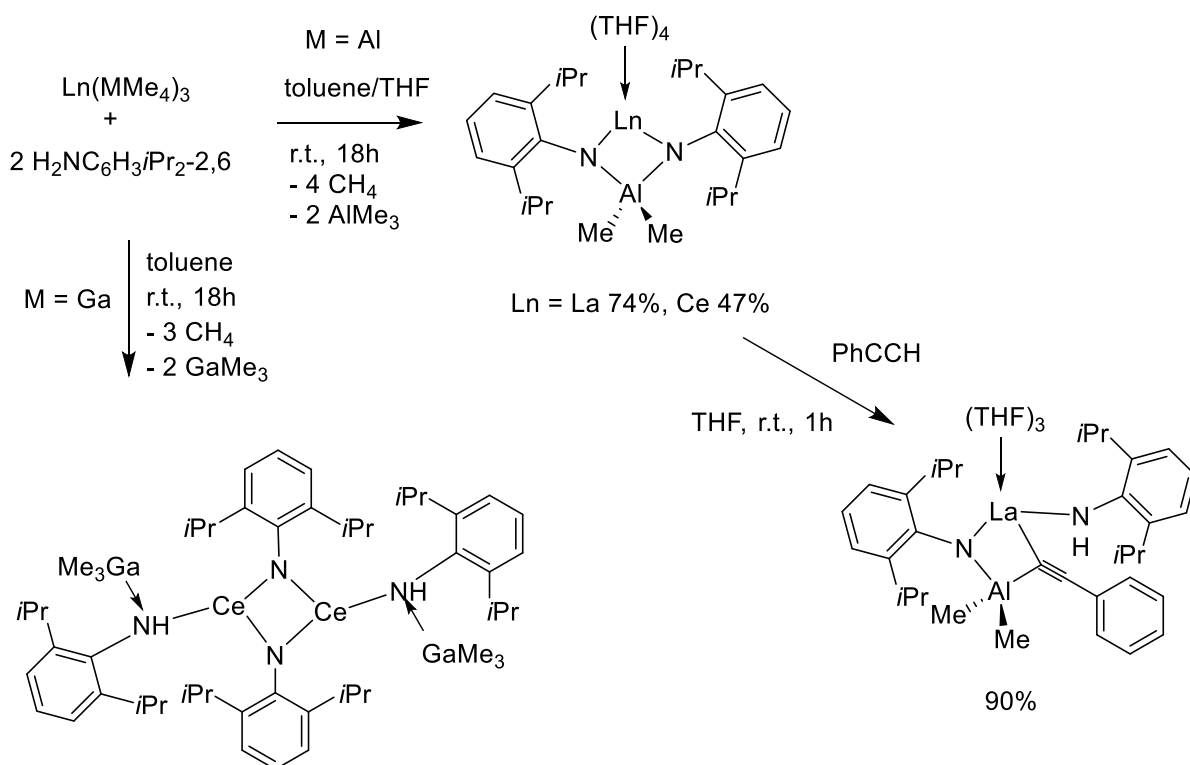
Scheme 73. Reaction of bimetallic Y-Ti complexes with different metal cyclopentadienyl reagents.[84]

The preparation of oligomeric gallium methylene $Ga_8(\mu-CH_2)_{12}$ was achieved in high yields by reaction of the heterobimetallic complexes $Cp^*_2Ln[(\mu-Me)_2GaMe_2]$ ($Ln=Lu, Y$) with an excess of $GaMe_3$ in toluene at elevated temperatures (Scheme 74).[85] This process was shown to involve multiple C-H bond activation steps. An important intermediate of this transformation, the dodecametallic complex $Cp^*_6Ln_3[(\mu_3-CH_2)_6Ga_9(\mu-CH_2)_9]$ ($Ln = Lu, Y$) could be isolated and characterized by XRD studies, solution 1H NMR and solid state ^{13}C CP/MAS NMR spectroscopy. The crystal structure showed significantly shorter Lu-C(methylene) distances than the Lu-C(Me) bond lengths of the starting material (2.510 Å vs 2.614 Å), indicating an increased negative charge at the methylene groups. In order to establish that this complex was indeed a reaction intermediate, the isolated complex was reacted with $GaMe_3$ at 130°C for 3 days resulting again in the formation of gallium methylene.[85]



Scheme 74. Synthesis of gallium methylene via C-H activation of GaMe_3 with $\text{Cp}^*_2\text{Ln}[(\mu\text{-Me})_2\text{GaMe}_2]$ ($\text{Ln}=\text{Lu, Y}$) involving the multimetallic intermediate $\text{Cp}^*_6\text{Ln}_3[(\mu_3\text{-CH}_2)_6\text{Ga}_9(\mu\text{-CH}_2)_9]$. [85]

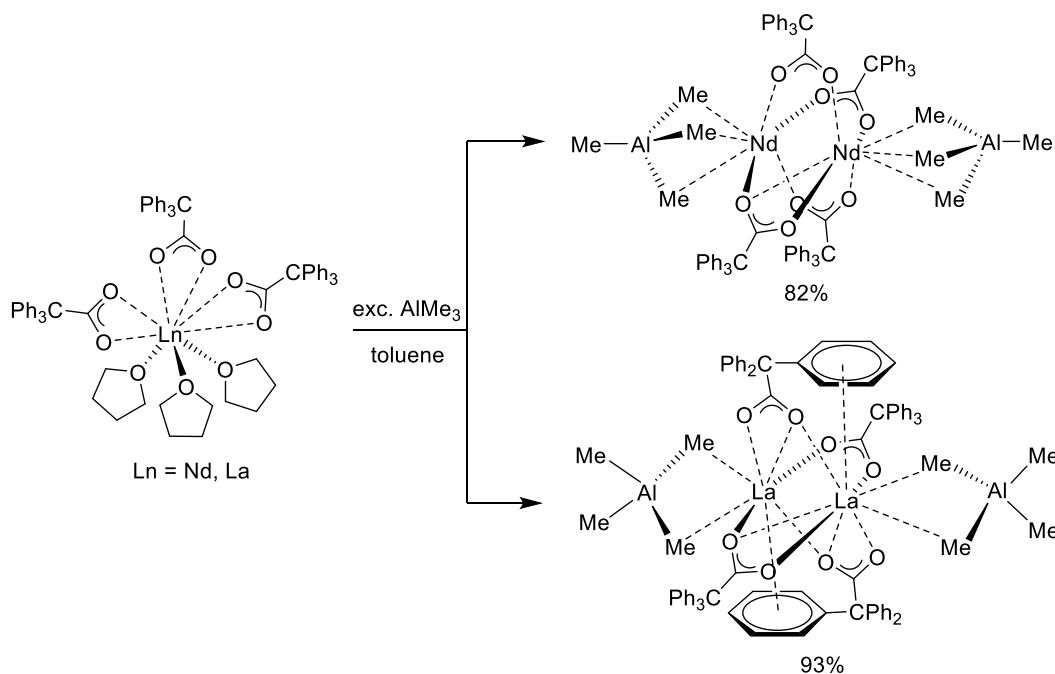
The new lanthanide diimide complexes $\text{Ln}[(\mu\text{-NC}_6\text{H}_3\text{iPr}_{2-2,6})_2\text{AlMe}_2](\text{thf})_4$ ($\text{Ln} = \text{La, Ce}$), bearing a bidentate AlMe_2 -linked diimido ligand, were synthesized in moderate to good yields by protonolysis of the corresponding tetramethylaluminate complexes with two equivalents of 2,6-diisopropylaniline (Scheme 75). [86] The use of cerium tetramethylgallate as starting material did not provide the diimido complexes but a tetrametallic mixed amide-imide complex due to the lower reactivity of the more covalent Ga-Me bonds compared to the Al-Me bonds. The lanthanum diimide complex reacted with phenylacetylene to the bimetallic alkynyl complex $(\text{HNC}_6\text{H}_3\text{iPr}_{2-2,6})\text{La}[(\mu\text{-NC}_6\text{H}_3\text{iPr}_{2-2,6})\text{AlMe}_2(\text{CCPh})](\text{thf})_2$ in high yield. Even though this complex readily decomposed in THF solution within one day, it could be analysed by ^1H NMR spectroscopy, revealing a NH proton resonance at 5.09 ppm and three sets of signals for the aryl rings, in agreement with protonation at one imido site and not at the AlMe_2 moiety. Further structural insights were obtained by XRD analysis, showing the phenylacetylide unit accommodated in the bridging position between La and Al. [86]



Scheme 75. Reaction of $\text{Ln}(\text{Mme}_4)_3$ ($\text{M} = \text{Al}$, Ga) complexes with 2,6-diisopropylaniline and reactivity of a bimetallic Ln/Al diimide complex.[86]

The interaction of trimethylaluminum with lanthanide carboxylates was studied in order to gain further insights on parameters influencing their activity and selectivity in polymerization reactions. Addition of an excess of AlMe_3 to the tris(triphenylacetate)lanthanide complexes $\text{Ln}(\text{Ph}_3\text{CCOO})_3(\text{THF})_3$ ($\text{Ln} = \text{La}$, Nd) in toluene afforded the heterometallic complexes $[\text{Ln}(\text{Ph}_3\text{CCOO})_3(\text{THF})_3]_2[\text{AlMe}_4]_2$ in high yields (Scheme 76).[87] Both complexes were characterized by XRD analysis revealing significant differences due to the size of the lanthanide ions. In the case of the Nd complex, two structural isomers were observed, differing in the coordination mode of the carboxylate anions. One isomer contained four equivalent Ph_3CCOO groups in $\mu_2\text{-}\kappa^1:\kappa^1$ coordination, whereas another centrosymmetric isomer possessed two Ph_3CCOO groups in $\mu_2\text{-}\kappa^1:\kappa^1$ coordination and two in the semi-bridging $\mu_2\text{-}\kappa^1:\kappa^2$ coordination. In both isomers, the $[\text{AlMe}_4]^-$ groups were η^3 -coordinated to the neodymium center. In contrast, in the corresponding centrosymmetric La complex, the $[\text{AlMe}_4]^-$ anion was bound in a planar η^2 fashion and each lanthanum ion was additionally η^6 -coordinated to one of the phenyl rings of the semi-bridging triphenylacetate ligand. Addition of THF to these complexes led to

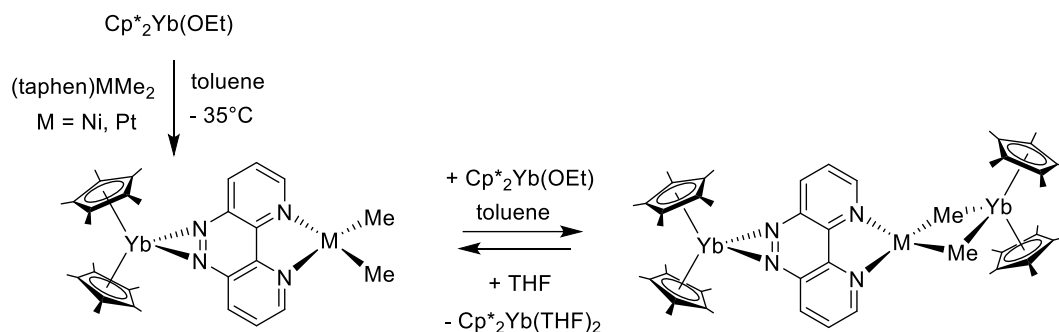
the cleavage of the dimeric structure and the ion-separated complexes $[(\text{Ph}_3\text{CCOO})_2\text{Ln}(\text{THF})_5]^+[\text{AlMe}_4]^-$ were isolated and structurally characterized. These heterometallic complexes are not active catalysts for butadiene or isoprene polymerization without addition of a co-catalyst such as $\text{Al}i\text{Bu}_3$.^[87]



Scheme 76. Synthesis of heterobimetallic triphenylacetate-tetramethylaluminate lanthanide complexes.^[87]

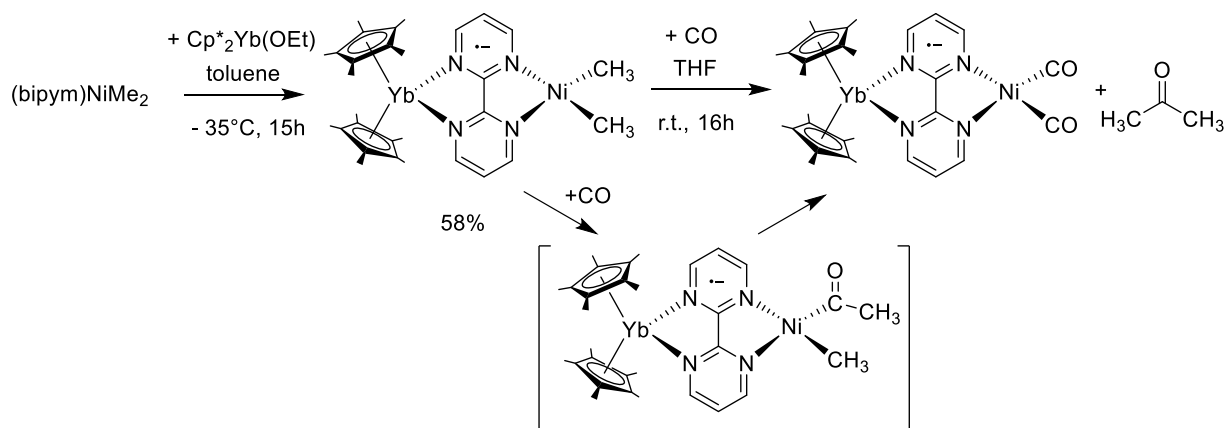
The redox non-innocent ligand 4,5,9,10-tetraazaphenanthrene (taphen) was employed for the synthesis of the new bimetallic Yb-Pt complex $\text{Cp}^*_2\text{Yb}(\text{taphen})\text{PtMe}_2$ and the heterotrimetallic Yb-M-Yb complexes, $\text{Cp}^*_2\text{Yb}(\text{taphen})\text{MMe}_2\text{YbCp}^*_2$ ($\text{M} = \text{Ni}, \text{Pt}$) (Scheme 77).^[88] In the bimetallic Yb-Pt complex, the initially divalent Yb fragment transfers an electron onto the taphen ligand leading to a paramagnetic Yb(III) center, as shown by NMR and solid-state magnetic measurements. Reaction of the bimetallic taphen-bridged Yb-Pd or Yb-Pt complexes with another equivalent of divalent $\text{Cp}^*_2\text{Yb}(\text{OEt})$ in toluene at room temperature provided access to the structurally characterized heterotrimetallic complexes, in which the second Yb fragment is coordinated via the methyl groups on the Pd/Pt center. XRD analysis confirmed a further one-electron reduction of the taphen ligand in these complexes, leading to a taphen^{2-} dianion, and the presence of two trivalent Yb centers. Whereas the solution ^1H NMR spectrum indicated a symmetric structure for these complexes, the solid-state structure revealed a non-linear arrangement with a significant bending of the second Yb moiety over the MMe_2 fragment. In-depth theoretical studies found that this bending originates from weak and mainly

electrostatic interactions in the solid state. Importantly, addition of THF to the isolated trimetallic complexes led to a reverse electron transfer, and the recovery of the bimetallic complexes and divalent $\text{Cp}^*_2\text{Yb}(\text{THF})_2$ complex.[88]



Scheme 77. Synthesis of hetero-bimetallic and heterotrimetallic Yb-Pd and Yb-Pt complexes.[88]

A heterobimetallic bipyrimidine (bipym)-bridged Yb-Ni complex was synthesized from the $(\text{bipym})\text{NiMe}_2$ and $\text{Cp}^*_2\text{Yb}(\text{OEt})$ precursors in toluene (Scheme 78).[89] Crystals of the bimetallic complex $\text{Cp}^*_2\text{Yb}(\text{bipym})\text{NiMe}_2$ were obtained at low temperature in good yield. XRD analysis revealed a significantly shorter C-C bridge of the two pyrimide fragments when compared to the structure of the $(\text{bipym})\text{NiMe}_2$ complex, indicating an electron transfer from the divalent Yb center onto the bipym moiety. This was further confirmed by the Cp(centroid)-Yb distance of $2.31(1) \text{ \AA}$, a value typically found in trivalent Yb complexes. The paramagnetic shifts of the ^1H NMR signals were in agreement with the presence of an Yb(III) fragment and a bipym radical anion. Solid-state magnetic measurements indicated a singlet ground state and a low-lying triplet state. Furthermore, exchange coupling between the Cp^*_2Yb fragment and the bipym ligand was rather strong. The reactivity of this complex towards CO was investigated, leading to the formation of acetone and new organometallic species as shown by ^1H NMR. The final reduced Ni(0) complex dissociated from the Yb fragment leading to the formation of small amounts of $\text{Cp}^*_2\text{Yb}(\text{bipym})\text{YbCp}^*_2$. Determining the reaction kinetics by NMR led to the conclusion that the reaction rate was influenced by the presence of the Yb fragment, leading to a more stable CO migratory insertion intermediate than for the $(\text{bipym})\text{NiMe}_2$ complex alone.[89]



Scheme 78. Synthesis of a heterobimetallic Yb-Ni complex and its reactivity towards CO.[89]

2.10. LANTHANIDE METALLOFULLERENES

The field of lanthanide-containing endohedral metallofullerenes (EMF) has witnessed a spectacular growth in recent years. The contributions reported in 2019 will be roughly divided into three main topics : a) the synthesis of new EMFs, b) chemical modifications of EMFs and c) supramolecular modification of EMFs.

a) Synthesis of new EMFs

Two isomers of $\text{Er}@\text{C}_{82}$ were synthesized and structurally characterized by XRD after co-crystallization with $\text{Ni}(\text{OEP})$ (OEP is the dianion of octaethylporphyrin).[90] Interestingly, whereas the $\text{Er}@\text{C}_{2v}(9)\text{-C}_{82}$ isomer crystallized as a monomer, the $\text{Er}@\text{Cs}(6)\text{-C}_{82}$ isomer was obtained as a dimer displaying a C-C single bond of 1.604 \AA , distant from the internal Er atom (Figure 5). DFT calculations confirmed the higher stability of the dimer by $42.27 \text{ kcal mol}^{-1}$ compared to the two monomers and the dimerization may be due to a significant difference in the spin-density distribution on the cage carbon atoms. Vis-NIR absorption spectra for both Er isomers indicate close similarity to the Y analogues, hence a three electron transfer from Er to the C_{82} cage was proposed with the delocalization of an unpaired electron on the fullerene cage.[90]

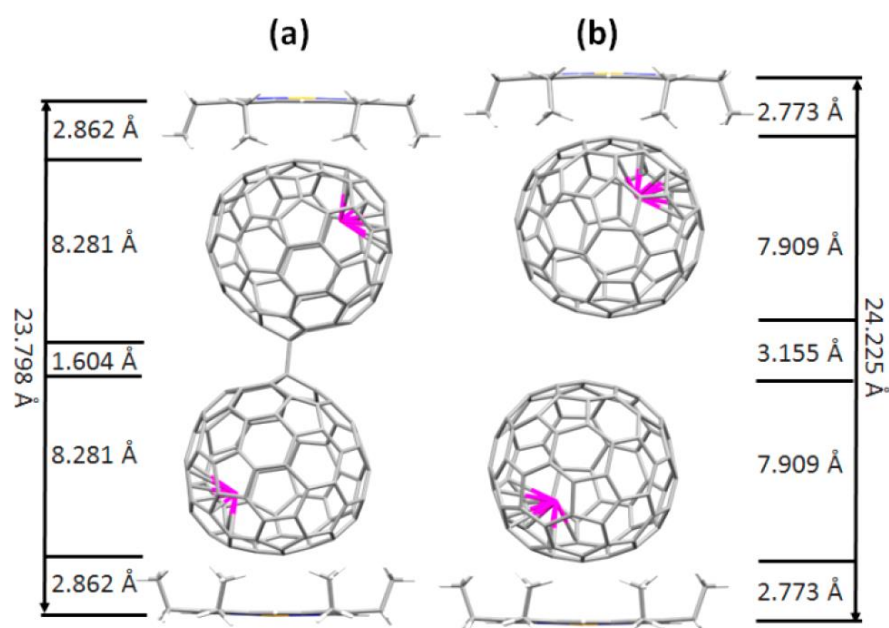


Figure 5. Structures of (a) $[\text{Er}@C_s(6)\text{-C}_{82}]_2 \cdot 2[\text{Ni}(\text{OEP})]$ and (b) $2[\text{Er}@C_{2v}(9)\text{-C}_{82}] \cdot 2[\text{Ni}(\text{OEP})]$. Only one cage orientation is shown for each system. Minor metal sites and solvent molecules are omitted for clarity. Reprinted with permission from [90]. Copyright 2019 American Chemical Society.

A series of dimetallofullerenes of the formula $\text{Er}_2@C_{2n}$ were synthesized and structurally characterized.[91] The Er-Er distances were found to be 3.59, 3.24, 3.76, and 3.70 Å for $\text{Er}_2@C_s(6)\text{-C}_{82}$, $\text{Er}_2@C_{3v}(8)\text{-C}_{82}$, $\text{Er}_2@C_1(12)\text{-C}_{84}$ and $\text{Er}_2@C_{2v}(9)\text{-C}_{86}$, respectively, which was in good agreement with theoretical calculations. Interestingly, for the $\text{Er}_2@C_{82}$ and $\text{Er}_2@C_{86}$ isomers, the electron occupancy was determined to be 1.97 e, whereas in $\text{Er}_2@C_{84}$ a value of only 0.98 e was calculated. This may suggest a weak single-electron Er-Er bond in the latter case, which may be due to the perfectly spherical shape of the C_{84} host, leading to the largest effective inner space and hence the largest Er-Er bond. Electrochemical studies showed an electrochemical band gap of 1.00V for $\text{Er}_2@C_s(6)\text{-C}_{82}$. Further, all dierbium-EMFs could be readily oxidized (-0.12 to +0.21 V) and the first oxidation potentials were metal-dependant in agreement with the description that the M-M bonding MO is the redox-active HOMO whereas the LUMO is based on the cage.[91]

The air-stable dimetallofullerenes $\text{Ln}_2@C_{80}(\text{CH}_2\text{Ph})$ ($\text{Ln}_2 = \text{Y}_2, \text{Gd}_2, \text{Tb}_2, \text{Dy}_2, \text{Ho}_2, \text{Er}_2, \text{TbY}, \text{TbGd}$) were synthesized and investigated for their magnetic and redox properties (Figure 6).[92] The initially formed fullerene anions were reacted with benzylbromide to yield the neutral air-stable benzyl monoadducts, which were all isostructural as shown by UV-vis, IR and Raman spectroscopy. XRD analysis at variable temperatures for Dy_2

showed temperature dependent mobility of the metals within the cage. ^1H NMR spectroscopy showed paramagnetic shifts for the benzyl protons due to dipolar magnetic field created by the Ln_2 dimers. Strong ferromagnetic coupling between the Ln centers was observed due to the delocalization of the unpaired electron spin in the $[\text{Ln}^{3+}-\text{e}-\text{Ln}^{3+}]$ system, which glues their magnetic moments together. The Tb_2 and Dy_2 compounds showed the best SMM behavior, with 100-s blocking temperatures of 25.2 K and 18.2 K, respectively, and a gigantic coercivity of 8.2 Tesla at 5 K was obtained for Tb_2 . In contrast, Ho_2 was only a modest SMM and Er_2 nearly no SMM. Electrochemical reduction of the Ln_2 EMFs led to a change of the valence state from $\text{Ln}^{2.5+}$ to Ln^{2+} and reduced exchange interactions between Ln spins, as shown by a smaller paramagnetic shift in ^1H NMR spectroscopy. These reduction potentials varied from -0.86 V (Gd_2) to -0.42 V (Er_2) whereas the first oxidation potentials were nearly identical in all cases (0.50-0.52 V).[92]

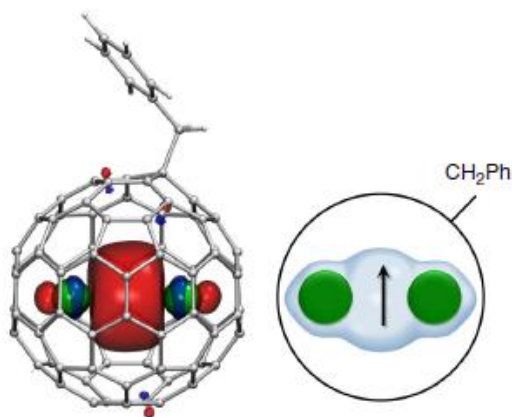


Figure 6. Molecular structure of $\text{Ln}_2@C_{80}(\text{CH}_2\text{Ph})$. Single-occupied Ln–Ln bonding molecular orbital (left; carbons are gray, hydrogens are white, lanthanides are green), and schematic depiction of the molecule (right; the arrow indicates an unpaired electron residing on the Ln–Ln bonding orbital). Reprinted from [92].

The azafullerene $\text{Tb}_2@C_{79}\text{N}$, containing a Tb_2 dimer with a single-electron Tb–Tb bond, was found to show SMM behavior with a high 100-s blocking temperature of magnetization of 24 K and large coercivity of 3.8 Tesla between 1.8 and 10 K.[93] Two mechanisms for the relaxation of magnetization were determined: a quantum tunneling process occurred below 15 K, whereas the Orbach mechanism was followed at higher temperature, with a barrier of $U_{\text{eff}} = 757.4$ K. A comparison between the azafullerene and the analogous $\text{Tb}_2@C_{80}(\text{CH}_2\text{Ph})$, which have the same spin system within a comparable cage only varying by different defects (the nitrogen atom in the azafullerene and the C- sp^3 atom in the benzyl adduct), shows slightly better SMM behaviour for $\text{Tb}_2@C_{80}(\text{CH}_2\text{Ph})$

(T_{B100} value of 29 K, broader hysteresis, longer QTM relaxation time of 18 h and $U_{\text{eff}} = 799$ K). Whereas strong tilting of the magnetic moments from the Tb-Tb axis was observed in the azafullerene, no tilting occurred in the benzylfullerene. This finding was related to the electrostatic potential (ESP) distribution, which is isotropic for benzylfullerene and strongly asymmetric for the azafullerene. The absence of an exohedral substituents on the fullerene provides higher thermal stability to the azafullerene.[93]

A direct Y-Y single bond was confirmed by XRD for the first time in the dimetallofullerenes $Y_2@C_s(6)-C_{82}$ and $Y_2@C_{3v}(8)-C_{82}$, with Y-Y bond lengths of 3.635 Å and 3.596 Å, respectively, in good agreement with theoretical calculations.[94] These compounds were obtained by an efficient separation/purification process, involving Lewis-acid treatment and separation by HPLC. Several other compounds with larger cages were also isolated, showing the formation of carbide cluster metallofullerenes, such as $Y_2C_2@C_s(15)-C_{86}$, $Y_2C_2@C_1(26)-C_{88}$, $Y_2C_2@C_2(41)-C_{90}$ and $Y_2C_2@C_2(61)-C_{92}$. In these compounds the Y-Y distances are in the range 4.024 Å and 4.349 Å as shown by XRD analysis. The formation of the Y_2 -dimer in the small C_{82} cage was proposed to occur in the arc-discharge process because of the presence of the highly reductive carbon plasma in the chamber. The increase in cage size changed the configuration to Y_2C_2 as the valence electrons forming the Y-Y bond were donated to the inserted C_2 -unit. According to calculations, the high thermodynamic stability observed in these EMFs resulted from a four-electron transfer and also the bonding interactions between the internal metallic species and the cage.[94]

The important effect of the cage size on the composition of the encapsulated cluster was also shown in a series of Lu-containing EMFs Lu_2C_{2n} ($2n = 76, 78, 80, 84, 86, 88, 90$), which were characterized by XRD analysis.[95] For small cages, $Lu_2@C_{2n}$ ($2n = 76-86$), dimetallofullerenes were formed with Lu-Lu single bonds in the range of 3.22-3.84 Å. Upon expansion to larger cages, a C_2 -unit was inserted into the Lu-Lu bond, providing Lu-carbide EMFs $Lu_2C_2@C_{2n}$ ($2n = 86, 88$), in which the Lu-Lu distance range from 3.94 to 4.66 Å. These observations were confirmed by theoretical studies.[95]

In a further study it was shown that not only the cage size but also the cage shape could influence the metal-cluster configuration in EMFs. A series of $Er_2C_2@C_{90}$ compounds were synthesized and characterized by mass spectrometry, XRD, spectroscopic and electrochemical studies.[96] An increasing trend in the Er-Er distances of $Er_2C_2@C_2(43)-C_{90}$, $Er_2C_2@C_2(40)-C_{90}$, $Er_2C_2@C_2(44)-C_{90}$ and $Er_2C_2@C_1(21)-C_{90}$ was observed, with values of 3.927, 4.058, 4.172 and 4.651 Å, respectively. This increase corresponded to a

lengthening of the major axis of the cage. In parallel, the C-C bond lengths of the C₂ unit decreased (1.044, 1.036, 0.984, and 0.944 Å, respectively) with the increasing Er-Er distances. Strong metal-cage interactions were also observed with Er-C cage distances in the range 2.026–2.318 Å. Therefore, the C₂ unit was considered like a spring holding together the cluster by supporting the metal-cage interactions.[96]

A rare example of a C₈₄-based oxide clusterfullerene, the Ho₂O@C₈₄ was synthesized and investigated for its structural and electrochemical properties.[97] XRD analysis found an IPR cage of D_{2d}(51591)-C₈₄, which according to DFT calculations is the kinetically and thermodynamically most stable isomer. The cage contains a near-linear endohedral Ho–O–Ho cluster (176°) in which each holmium site has short contacts (2.165(9) to 2.361(9) Å) with the central 6,6-bond of a pyracylene unit. This proximity results in considerable electron back-donation between cluster and cage. Further studies revealed the effects of cluster encapsulation on the EC gap (1.23 V vs. 1.85 V) and the HOMO–LUMO gap (3.0 eV vs. 3.78 eV) in Ho₂O@C₈₄ and the empty species, respectively.[97]

The synthesis and structural characterization of the first Dy-oxide clusterfullerenes, Dy₂O@C₈₂ was reported. For each of the three isolated isomers, having C_s(6), C_{3v}(8), and C_{2v}(9) cage symmetries, XRD studies revealed bent endohedral Dy–(μ₂-O)–Dy clusters with very short Dy–O bonds, close to 2.0 Å. The fullerene cage influenced strongly the SMM behavior of the three compounds, which all showed broad magnetic hysteresis, but variations on the temperature and magnetization relaxation. For example, the C_s isomer, which according to DFT calculations is the most stable isomer and in which the cluster is at a fixed position, led to the shortest magnetization relaxation times. In contrast, for the C_{3v} isomer, in which the cluster is moving almost freely, the strongest SMM behaviour was observed. Very strong antiferromagnetic exchange coupling between the Dy ions was observed, which was related to the compact geometry of the cluster.[98]

The synthesis and purification methods leading to the isolation of the Ln₃N@C₇₈ (Ln = Ho, Tb) cluster fullerenes with a chiral, non-IPR cage C₂(22010)-C₇₈ were reported. XRD analysis of cocrystals with Ni(OEP), revealed a planar Ln₃N cluster, with two metals close to the two unique pentalene regions. These interactions also led to longer Ln–N bonds (ca. 0.1 to 0.2 Å) compared to the one for the third Ln metal, which has an η⁶ half-metallocene like arrangement with a hexagon of the cage (Figure 7).[99]

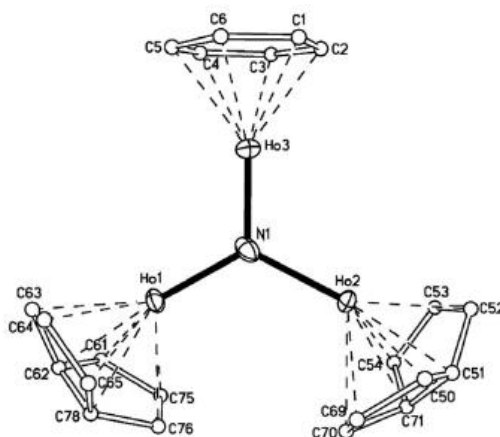


Figure 7. Primary locations of the Ho_3N cluster inside one enantiomer of the C_2 -symmetric C_{78} cage. Reprinted with permission from [99]. Copyright 2019 Wiley VCH.

The synthesis and characterization of a series of Er-nitride clusterfullerenes $\text{Er}_3\text{N}@C_{80-88}$ was achieved. The structure of several compounds was obtained for the first time by XRD analysis, including $\text{Er}_3\text{N}@I_h(7)-C_{80}$, $\text{Er}_3\text{N}@D_{5h}(6)-C_{80}$, $\text{Er}_3\text{N}@C_{2v}(9)-C_{82}$, $\text{Er}_3\text{N}@C_s(51365)-C_{84}$, $\text{Er}_3\text{N}@D_2(35)-C_{88}$. In all the structures, the inserted Er_3N cluster had a planar configuration with increasing Er-N distances (2.019 – 2.312 Å) as a function of the cage expansion in order to maintain strong metal–cage interactions (Er-C distances 2.062 – 2.450 Å). Electrochemical studies showed roughly similar first reduction potentials for the whole series $\text{Er}_3\text{N}@C_{2n}$ ($2n = 80, 84, 86, 88$). On the other hand, the cage size influenced the oxidation potentials, which were cathodically shifted, and consequently, the EC gap decreased along the series. An exception to these findings was the compound $\text{Er}_3\text{N}@C_{2v}(9)-C_{82}$, which exhibited a relatively small first oxidation potential, hence good electron donating properties and also low kinetic stability.[100]

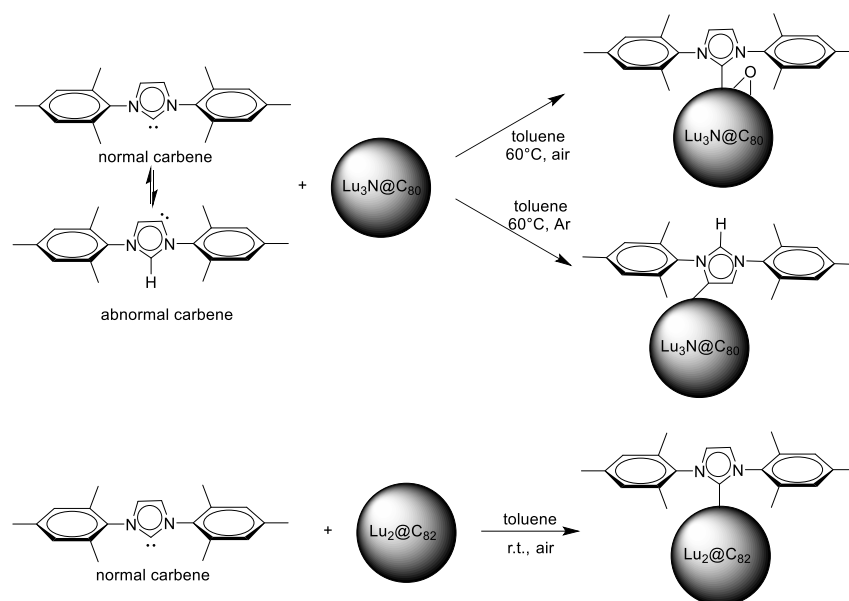
X-ray magnetic circular dichroism was employed to study the magnetic properties of a monolayer of the endohedral single-molecule magnet $\text{Dy}_2\text{ScN}@C_{80}$ on an h-BN/Rh(111) nanomesh, showing large coercive fields, close to the value of bulk samples. A comparison with the SMM on a bare Rh(111) substrate indicated that the additional h-BN spacer layer led to larger hysteresis loops. However, angular deviation in X-ray absorption spectra revealed that less ordering of the endohedral units was obtained with the additional spacer layer compared to the bare Rh(111) substrate.[101]

The synthesis of a series of mixed-metal Dy-Ln nitride clusterfullerenes ($\text{Ln} = \text{Gd}, \text{Er}, \text{Tm}, \text{Lu}$) revealed the impact of the size and nature of the second metal on the yield. The highest relative yields for $\text{Dy}_2\text{LnN}@C_{80}$, $\text{DyLn}_2\text{N}@C_{80}$ and $\text{Ln}_3\text{N}@C_{80}$ species was obtained for Sc (0.75 Å), followed by Lu (0.86 Å) and Er (0.89 Å) in agreement with their ionic radii

given in parenthesis. Much lower yields were obtained for Gd which has a size comparable to Dy and is less prone to NCF formation. An exception was the reaction with Tm which despite its small size provided very low yields of mixed-metal species. An explanation could be the high third ionization potential of Tm, which does not allow to readily access the trivalent state, important for the NCF formation. XRD structure analysis of $\text{DyGd}_2\text{N@C}_{80}$ and $\text{DyEr}_2\text{N@C}_{80}$ showed a remarkable ordering of mixed-metal nitride clusters despite similar size and electronic properties of the metals. The DyGd_2N cluster displayed pronounced pyramidalization, whereas a nearly planar shape was observed for DyEr_2N . A critical analysis of this structure using DFT calculations and reconstruction of the nitrogen inversion barrier in $\text{M}_3\text{N@C}_{80}$ molecules was carried out. Most pyramidal cluster structures present a double-well potential, however, the small size of the inversion barrier can lead to an apparent planar structure, as in $\text{M}_3\text{N@C}_{80}$ molecules, including $\text{Dy}_3\text{N@C}_{80}$ and $\text{DyEr}_2\text{N@C}_{80}$, for which inversion barrier is slightly exceeded by the energy of the lowest vibrational level. On the other hand, the genuine pyramidal structure is observed by XRD only when the inversion barrier is above the lowest vibrational level, as it was found in $\text{Gd}_3\text{N@C}_{80}$ and $\text{DyGd}_2\text{N@C}_{80}$. [102]

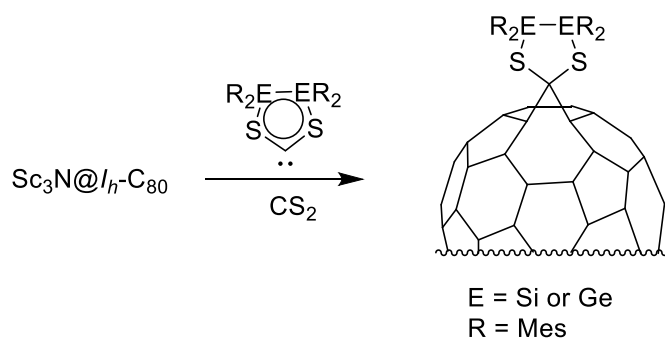
b) Chemical cage modifications

The highly regioselective formation of monoadducts from the Lewis acid-base reaction of different lutetium-containing EMFs with the bis-mesityl NHC was reported. [103] Reaction of $\text{Lu}_3\text{N@I}_h(7)\text{-C}_{80}$, $\text{Lu}_2\text{@C}_{3v}(8)\text{-C}_{82}$ or $\text{Lu}_2\text{@C}_{2v}(9)\text{-C}_{82}$ with a large excess of NHC in toluene at 60°C afforded the products with full conversion, which were characterized by Maldi-TOF MS, XRD analysis and DFT calculations (Scheme 79). For the di-lutetium fullerenes, the carbene moiety reacts as a normal carbene with the formation of a C-C single bond of 1.53 \AA . In the case of the Lu_3N fullerene, two distinct reaction outcomes were observed depending on the absence or presence of oxygen. In air, normal carbene coordination was observed, however, with the concomitant formation of an epoxide group. Under argon, the C-C bond was established with the C5 atom of the abnormal NHC. These results were corroborated by theoretical calculations, showing that the low LUMO energy levels of the EMFs should provide high reactivity with the HOMO of the NHC. Molecular electrostatic potential distributions further agreed with the observed high regioselectivity. Formation of multi-adducts was prevented by the steric bulk of the NHC. [103]



Scheme 79. Reaction of NHC with Lu-EMFs.[103]

Reaction of $\text{Sc}_3\text{N}@I_h\text{-C}_{80}$ with S-heterocyclic carbenes as shown in Scheme 80 yielded the methano-bridged fullerenes which were characterized by Maldi-TOF MS, Vis-NIR spectroscopy and ^{13}C NMR spectroscopy.[104] Theoretical studies were performed on the [6,6] and [5,6] open adducts indicating the higher stability of the [6,6] adducts. Electrochemical studies on the SHC addend indicated a relatively low oxidation potential, in agreement with FMO calculations.[104]



Scheme 80. Reaction of Sc-EMF with SHCs.[104]

A photochemical process for the synthesis of the first stable η^1 -coordinated organometallic complex of an yttrium-containing EMF was reported.[105] Reaction of $\text{Y}@C_{2v}(9)\text{-C}_{82}$ with $\text{Re}_2(\text{CO})_{10}$ in toluene under photoirradiation led to the regioselective formation of a single adduct in quantitative yield (Figure 8). XRD analysis revealed the coordination of a $\text{Re}(\text{CO})_5$ unit to a [5,6,6] carbon atom via a Re-C σ -bond of 2.39(2) Å. The involvement of a radical process, i.e. a one-electron transfer from $\text{Re}(\text{CO})_5$ to the paramagnetic EMF, was deduced from Vis-NIR and ESR measurements on the new complex, which displayed a

closed-shell electronic configuration similar to the anionic $Y@C_{2v}(9)-C_{82}^-$. Interestingly, the electrochemical properties of the new complex are close to the pristine $Y@C_{2v}(9)-C_{82}$. [105]

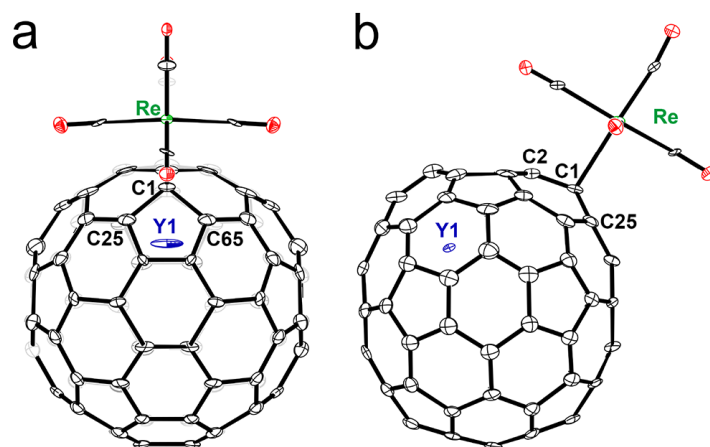


Figure 8. Ortep drawings of $Re(CO)_5 \eta^1$ -coordinated to $Y@C_{2v}(9)-C_{82}$. (a) front view and (b) side view. Thermal ellipsoids are set at the 30% probability level. The solvent molecule (CS_2) and minor metal sites are omitted for clarity. Reproduced with permission from [105]. Copyright 2019 American Chemical Society.

A theoretical study on the Diels-Alder reaction between cyclopentadiene and the non-IPR $C_{2v}(19138)-C_{76}$ and the EMF $YNC@C_{2v}(19138)-C_{76}$ was conducted to evaluate the parameters influencing the reaction outcome. [106] It was found that in the metal free fullerene the most reactive bond was the [5,5] bond of two fused pentagons from both a kinetic and thermodynamic point of view. Upon encapsulation of the YNC cluster this bond becomes less reactive due to coordination between the cluster and the adjacent pentagon pair. Consequently, the Diels-Alder reaction becomes for the first time more favorable on two remote sites of the fullerene cage, a [5,6]- corannulene-type bond and a [6,6] pyracylene-type bond. [106]

The Prato reaction of $Gd_3N@C_{80}$ with an excess of N-ethylglycine and paraformaldehyde at 120 °C allowed the isolation and XRD characterization of a Prato minor bis-adduct $Gd_3N@C_{80}[C_4H_9N]_2$ (Figure 9). [107] In the C_2 -symmetric [6,6][6,6]-structure, the Gd_3N cluster is completely planar and has a less strained geometry since two Gd atoms are coordinated to the C_{80} cage from inside at the two sp^3 addition sites. The minor bis-adduct, which is the kinetic product, could be partially transformed to the major bis-adduct upon heating at 120°C for 5 min, in agreement with similar thermodynamic stability of both bis-adducts. The asymmetric [6,6][6,6]- structure of the major bis-adduct was deduced from

vis-NIR spectra and DFT calculations and the isomerization pathway was determined by linear transit calculations.[107]

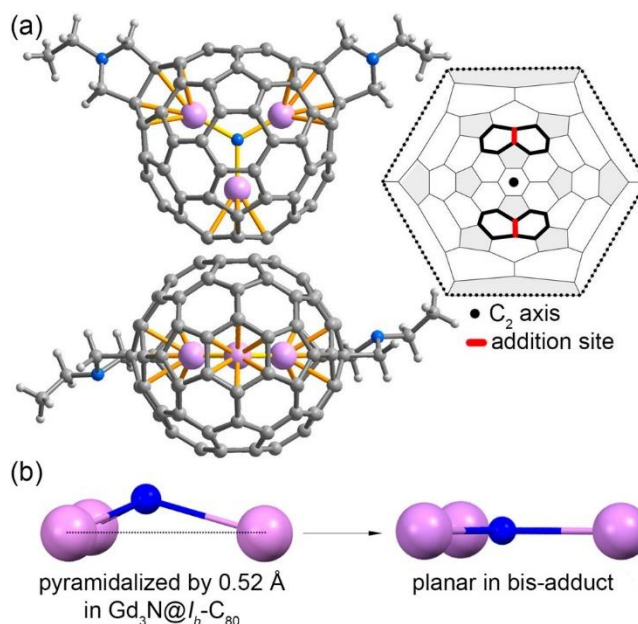
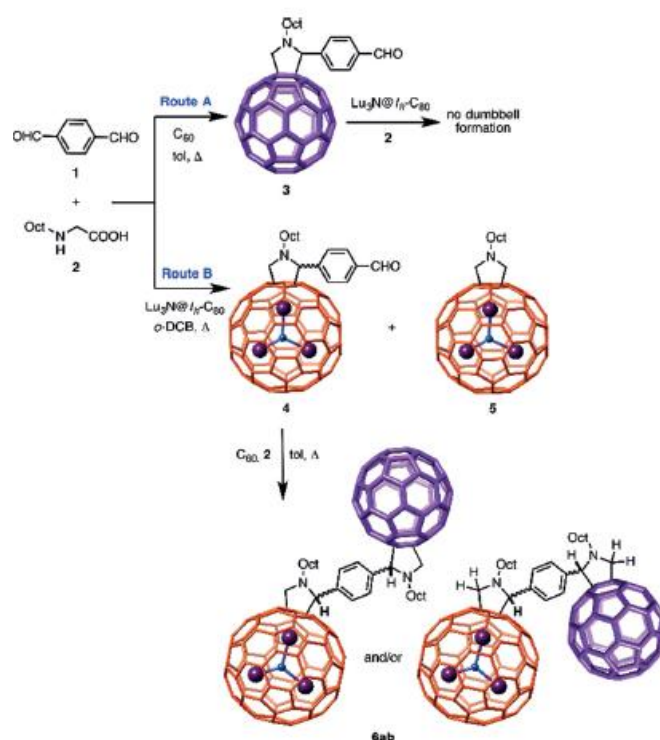


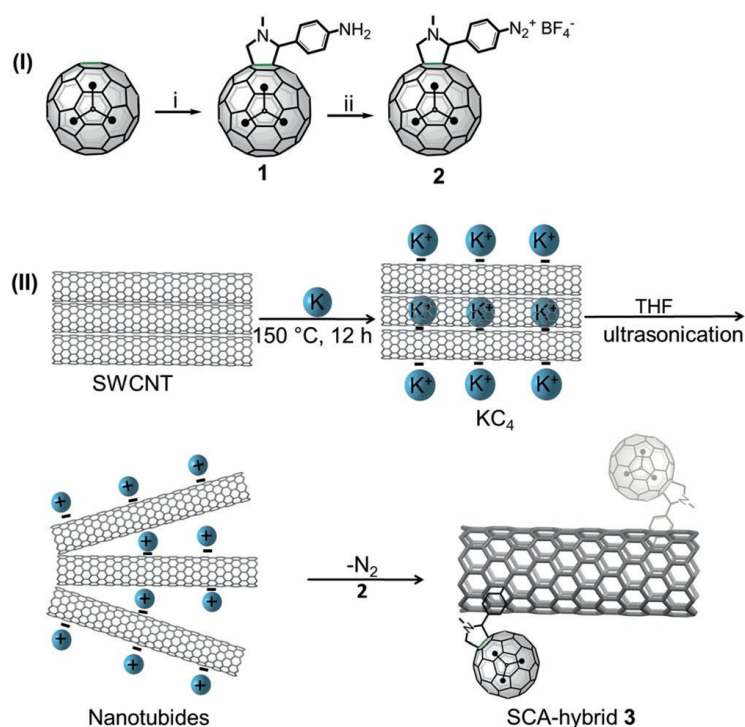
Figure 9. X-ray crystal structure of minor-bis adduct $\text{Gd}_3\text{N}@C_{80}[\text{C}_4\text{H}_9\text{N}]_2$ (side and top views) and the Schlegel diagram showing the addition sites (red thick bonds). The black dot in the center represents C_2 axis. The hexagons coordinated to the endohedral Gd atoms are highlighted with solid or dotted black lines. (b) The geometry of the endohedral Gd_3N cluster with out-of-plane displacement (0.52 Å) of the nitrogen atom inside the pristine $\text{Gd}_3\text{N}@C_{80}$ and the planar configuration inside the minor-bis-adduct. Reprinted with permission from [107]. Copyright 2019 American Chemical Society.

A covalent all-fullerene electron donor-acceptor conjugate $C_{60}\text{-Lu}_3\text{N}@I_h\text{-C}_{80}$ was synthesized and electron transfer reactions were studied (Scheme 81).[108] A 1,3-dipolar cycloaddition reaction of $\text{Lu}_3\text{N}@I_h\text{-C}_{80}$ with terephthalaldehyde and N-octylglycine provided the aldehyde functionalized Lu-EMF. Further transformation of this compound with C_{60} and N-octylglycine in refluxing toluene afforded the dumbbell formation. The inverse route starting from C_{60} was not successful. The new compound could form 16 stereoisomers (8 anti and 8 syn orientation), which all lie in an energetic range of 14 kcal mol⁻¹ according to DFT calculations. The *anti*-RSSS isomer was determined to be the most stable isomer. The formation of $C_{60}^{\cdot-}\text{-Lu}_3\text{N}@I_h\text{-C}_{80}^{\cdot+}$ charge-separated state was supported by spectroelectrochemical absorption and femtosecond transient absorption experiments. The Lu_3N cluster contributes to the spin conversion from the charge-separated singlet state $C_{60}^{\cdot-}\text{-Lu}_3\text{N}@I_h\text{-C}_{80}^{\cdot+}$ into the corresponding triplet state by a heavy-atom effect. This spin conversion considerably slows down the charge recombination.[108]



Scheme 81. Synthesis of covalent all-fullerene electron donor-acceptor conjugate C_{60} - $Lu_3N@I_h-C_{80}$. Reprinted with permission from Ref [108]. Copyright 2019 Wiley-VCH.

A synthetic approach to a covalent inter-carbon-allotrope hybrid structure containing a Sc-EMF, $Sc_3N@C_{80}$, and single-walled carbon nanotubes (SWCNT) was developed (Scheme 82).[109] For grafting the fullerene moiety as an electrophile onto a negatively charged SWCNT, a diazonium salt was introduced on the fullerene cage in a two-step sequence. An initial Prato reaction provided the aniline derivative, which underwent diazotisation upon treatment with isoamyl nitrite and HBF_4 (step (I) in Scheme 82). Coupling this EMF derivative with KC_4 nanotubides, obtained by reduction of pristine SWCNT with potassium, provided the new hybrid compound (step (II) in Scheme 82), which was characterized by Raman spectroscopy and mass spectrometry and visualized by HRTEM, confirming the covalent binding of the two entities.[109]



Scheme 82. Synthesis of covalent inter-carbon-allotrope hybrid structure of $\text{Sc}_3\text{N}@C_{80}$, and single-walled carbon nanotubes by (I) introduction of a diazonium salt on $\text{Sc}_3\text{N}@C_{80}$ and (II) preparation of KC_4 nanotubides and coupling with fullerene. Reprinted with permission from Ref [109]. Copyright 2019 Wiley-VCH.

Covalent modification of several Er-containing EMFs was applied as strategy to turn on the near-infrared photoluminescence of Er^{3+} , which is often quenched by the fullerene cage. $\text{Er}@C_{2n}$ metallofullerenes were reacted with boiling 1,2,4-trichlorobenzene or iodobenzene, yielding after purification, $\text{Er}@C_{72}(\text{C}_6\text{H}_3\text{Cl}_2)$ and $\text{Er}@C_{76}(\text{C}_6\text{H}_5)$, respectively. [110] From the reaction of $\text{Er}@C_{2n}$ with AgCOOCF_3 at 400°C , the products $\text{Er}@C_{76}(\text{CF}_3)_5$, $\text{Er}@C_{82}(\text{CF}_3)_3$ and $\text{Er}@C_{82}(\text{CF}_3)_5$ could be isolated. In the case of C_{82} , the chemical modification changes the open-shell electronic structure to a closed shell-state and the presence of the CF_3 groups enlarges the HOMO-LUMO gap, two factors leading to an enhancement of the photoluminescence by facilitating the energy transfer from the fullerene cage to Er^{3+} . The highest emission intensity was observed for the $\text{Er}@C_{72}(\text{C}_6\text{H}_3\text{Cl}_2)$ derivative. Further insights were gained by DFT calculations, showing that the triplet-energy of the modified EMFs matches the first excited level of Er^{3+} ion.[110]

The influence of coating $\text{La}@C_{82}$ fullerene with a varying number of hydroxyl groups (from 1 to 32) was studied by DFT calculations, providing new insights on the structural arrangement of the hydroxyl groups and their influence on the electron-accepting and

donating properties of the corresponding EMFs. For example the best electron-donor behavior was found for $\text{La@C}_{82}(\text{OH})_{32}$, whereas $\text{La@C}_{82}\text{OH}$ gave the lowest results.[111] The neutral Sc-nitride clusterfullerene $\text{Sc}_3\text{N@I}_h\text{-C}_{80}$ was crystallised from ortho-dichlorobenzene (o-DCB) in the presence or absence of triptycene (TPC) leading to the compounds $\text{Sc}_3\text{N@I}_h\text{-C}_{80}\cdot 3\text{C}_6\text{H}_4\text{Cl}_2$, with the cages highly ordered in a network of o-DCB molecules, and $(\text{Sc}_3\text{N@I}_h\text{-C}_{80})_3(\text{TPC})_2\cdot 5\text{C}_6\text{H}_4\text{Cl}_2$, with the cages ordered in the triptycene layer and not ordered in the o-DCB layer.[112] Both compounds crystallized in a high-symmetry trigonal structure for the Sc_3N cluster with Sc-N bond lengths of 1.95–2.02 Å and Sc-C(C_{80}) distances in the range 2.15–2.40 Å. Reduction of $\text{Sc}_3\text{N@I}_h\text{-C}_{80}$ with Na, K or Cs in the presence of [2.2.2]-cryptand afforded the corresponding radical anions, which dimerized to the diamagnetic singly bonded $\{[2.2.2]\text{cryptand}(\text{M}^+)\}_2(\text{Sc}_3\text{N@I}_h\text{-C}_{80}^-)_2\cdot 2.5\text{C}_6\text{H}_4\text{Cl}_2$ ($\text{M}^+ = \text{Na, K, Cs}$). Whereas the Na compound showed strongly disordered components, the K and Cs phases showed only one major dimer orientation. The Sc_3N triangles were no longer equilateral in the dimers, having two longer Sc-N bonds (2.039(5) and 2.088(6) Å) and one shorter bond of 1.972(7) Å (values for the K compound). The two longer Sc-N bonds are found closer to the intercage C-C bond, which measures 1.635(13) Å and 1.655(17) Å for the K and Cs compounds, respectively (Figure 10). The diamagnetic dimers were EPR-silent, however, in the range 400-460 K dissociation into the monomeric radical anions occurred, as revealed by a strong, broad EPR signal with a hyperfine splitting at 5.8 mT. From these results, the energy of the intercage C-C bond was deduced to be 234.7 kJ mol⁻¹. IR and UV/Vis/NIR spectroscopy for both the monomeric and dimeric $\text{Sc}_3\text{N@I}_h\text{-C}_{80}^-$ anions showed intrinsic shifts (IR) and new bands (NIR) making them readily distinguishable from the neutral species.[112]

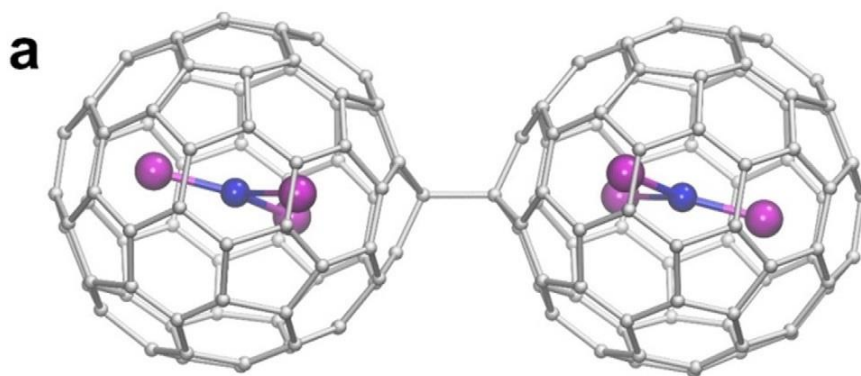


Figure 10. Molecular structure of diamagnetic dimers $(\text{Sc}_3\text{N@I}_h\text{-C}_{80})_2$ in $\{[2.2.2]\text{cryptand}(\text{Cs}^+)\}_2(\text{Sc}_3\text{N@I}_h\text{-C}_{80}^-)_2\cdot 2.5\text{C}_6\text{H}_4\text{Cl}_2$. Reprinted with permission from [112]. Copyright 2019 Wiley VCH.

c) Supramolecular modifications

The encapsulation of the paramagnetic EMF $\text{Sc}_3\text{C}_2@\text{C}_{80}$ in the toluene-filled pores of two different metal-organic frameworks (MOF-177 and MOF-180) and the resulting influence on the electron spin was investigated.[113] Variable EPR signals were observed, depending on the pore size, due to different host-guest interactions between the EMF and the MOF. The toluene solvent also served as lubricating agent for the motion of the EMF inside the MOF and consequently steer its spin relaxation.[113]

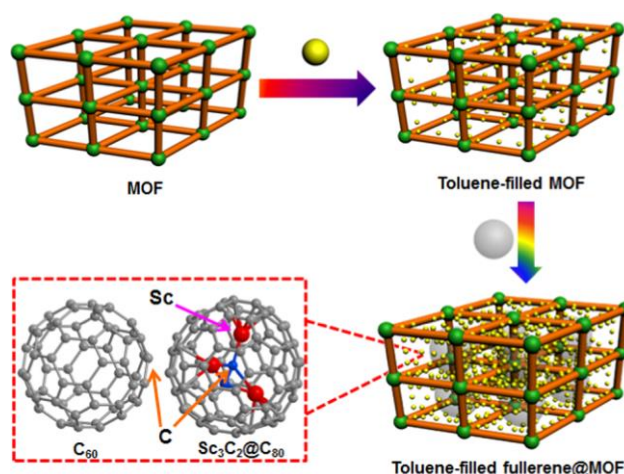


Figure 11. Preparation of toluene filled fullerene@MOF as spin probes. Reprinted with permission from [Ln113]. Copyright 2019 American chemical society.

A theoretical study on the noncovalent interactions of the EMF $\text{Sc}_3\text{N}@I_h\text{-C}_{80}$ with the free-base phthalocyanine H_2Pc and its 3d transition metal(II) complexes MPc (MnPc , singlet and triplet FePc , CoPc , NiPc , CuPc and ZnPc) was conducted.[114] It was shown that the non-covalent binding is rather strong with the following trend: $\text{Ni} (-24.33 \text{ kcal/mol}) < 2\text{H} < \text{Mn} < \text{Cu} < \text{Zn} < \text{t-Fe} < \text{Co} \ll \text{s-Fe} (-42.89 \text{ kcal/mol})$. In certain cases, these binding interactions also impact the geometries of the EMF, for example in the case of MnPc and s-FePc , one of the $\text{Sc-C}(\text{C}_{80})$ bond distances is significantly shortened from 2.720 \AA to 2.309 \AA and 2.314 \AA , respectively, due to a repelling effect. The strongest distortion of the macrocyclic Pc ring was also observed for Mn and s-FePc . In general, for the HOMO-LUMO gap, spin density distribution, electrostatic potential and frontier orbitals, the $\text{MPc} + \text{Sc}_3\text{N}@I_h\text{-C}_{80}$ conjugates are more similar to the $\text{MPc} + \text{C}_{60}$ dyads than the $\text{MPc} + \text{C}_{80}$ dyads.[114]

The effect of intermolecular packing on charge transfer processes in two $\text{Y}@C_{82}/\text{Ni}(\text{OEP})$ cocrystals, obtained from two different solvent systems, was explored.[115] In the case of cocrystallisation from $\text{CS}_2/\text{benzene}$, a one-dimensional structure with EMF and $\text{Ni}(\text{OEP})$

pairs aligned linearly was observed (Figure 12a). In contrast, crystallization from benzene/ CHCl_3 afforded zigzag chains of EMFs aligned diagonally between the Ni(OEP) bilayers (Figure 12b). The photophysical properties of both compounds were studied showing two different deactivation pathways for the CS_2 /benzene cocrystals, involving two species, and only one deactivation pathway for the benzene/ CHCl_3 cocrystals, involving four species.[115]

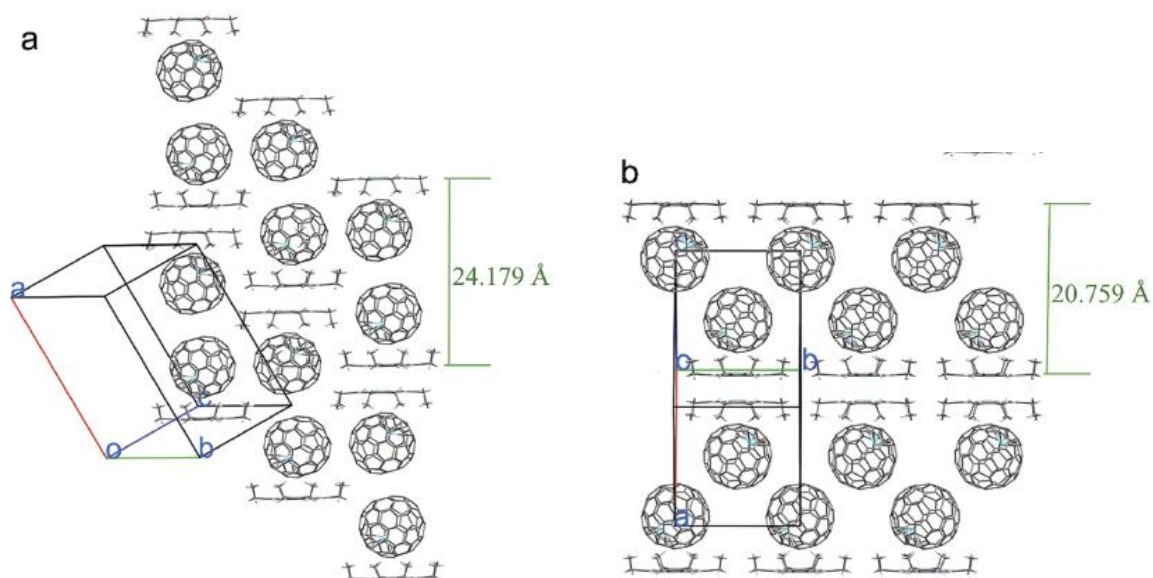


Figure 12. Packing structures of (a) $\text{Y@C}_{82}/\text{Ni(OEP)}$ crystallised from CS_2 /benzene and (b) $\text{Y@C}_{82}/\text{Ni(OEP)}$ crystallised from benzene/ CHCl_3 . Only one cage orientation and the major yttrium site are illustrated with solvent molecules omitted for clarity. Reprinted with permission from [115]. Copyright 2019 Royal Society of Chemistry.

Supramolecular host-guest complexes between EMFs and nanoring-type molecules were synthesized and studied for their electronic and magnetic properties.

The large π -extended nanoring of [4]CHBC (cyclo-2,11-para-hexa-peri-hexabenzocoronene) was applied to the wrapping of $\text{Y}_2@\text{C}_{79}\text{N}$ to form a short metallofullerene-peapod $\text{Y}_2@\text{C}_{79}\text{N} \subset [4]\text{CHBC}$. [116] Reaction of both compounds at 80°C in toluene under N_2 atmosphere provided the highly stable host-guest complex (Figure 13), which, according to DFT calculations, provided a host-guest surface distance of 3.8 \AA , suitable for concave-convex π - π interactions. The unpaired electron of the EMF was found on the internal Y_2 cluster (SOMO). The level of this SOMO significantly increased from -3.9 to -3.2 eV upon wrapping with [4]CHBC, indicative of the induction of electron spin by the host guest interaction. EPR spectroscopy showed anisotropic signals due to the insufficient rotational averaging of the electron spin due to the strong host-guest interactions. As the molecular orientation of the EMF changed at lower temperatures, new

signals were observed in the EPR spectrum, hence the EMF could serve as a spin probe for the orientation process. The spin phase memory time for the supramolecular complex did not vary much between 5K (11 μ s) and 30 K (9 μ s) (confinement effect), whereas for pristine $Y_2@C_{79}N$ a change from 23 to 16 μ s was observed.[116]

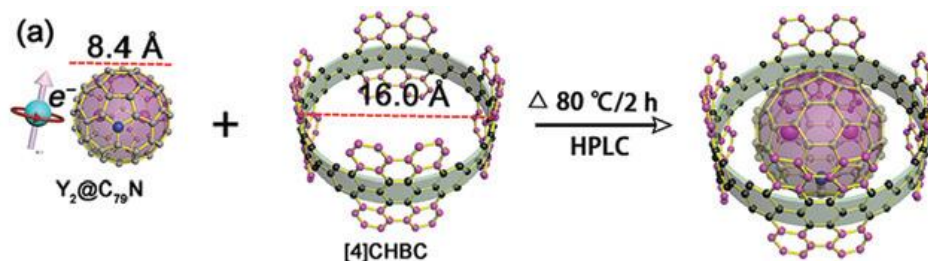


Figure 13. Preparation of metallofullerene-peapod $Y_2@C_{79}N@[4]CHBC$. Reprinted with permission from [116]. Copyright 2019 Royal Society of Chemistry.

In a related study, the electronic and magnetic properties of the EMFs $Y_3N@C_{80}$ and $Y_2@C_{79}N$ were modulated by hooping with [12]cycloparaphenylene ([12]CPP) (Figure 14).[117] These stable host-guest complexes could be synthesized in various solvents (CS_2 , $CDCl_3$, 1,2-dichloroethane, toluene) at room temperature and their formation was confirmed Maldi-TOF spectrometry. In the Raman spectrum a shift from 1201 to 1220 cm^{-1} was observed indicating the influence of the Y_3N cluster on the symmetric C-H vibration in [12]CPP. ^{13}C NMR spectroscopy showed an upfield shift for the C_{80} cage carbons and a downfield shift for [12]CPP carbons. Electrochemical studies revealed an enhanced electron-accepting ability of $Y_3N@C_{80}$ in the supramolecular framework due to the π -extended structure of the host. In accordance, the LUMO which is mainly situated on the fullerene cage decreased from -2.98 eV to -3.13 eV upon complexation. DFT calculations on the optimized structure showed that the metal-clusters Y_3N and Y_2 were situated in the quasi- C_{12} axis plane of [12]CPP. For STM measurements, $Y_3N@C_{80}$ and $Y_3N@C_{80}@[12]CPP$ were transferred onto Au(111) layers using the dip-coating method. Interestingly, whereas the EMF alone produced monolayers, the supramolecular complex led to random absorption on the surface. EPR studies on the paramagnetic $Y_2@C_{79}N@[12]CPP$ showed anisotropic signals in contrast to the EMF alone, which could be related to the reduced rotation of the Y_2 cluster induced by the [12]CPP.[117]

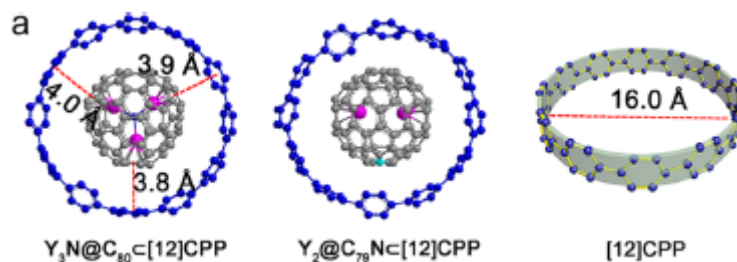


Figure 14. DFT-optimized structures of $Y_3N@C_{80}/Y_2@C_{79}N@[12]CPP$ at the B3LYP/6-31G* level. The interfacial distances between the centroid of the paraphenylene unit of [12]CPP and the nearest centroid of the hexagon of C_{80} are labeled. Reprinted with permission from [117]. Copyright 2019 American Chemical Society.

2.11. ORGANOLANTHANIDE CATALYSIS

2.11.1. Organolanthanide-catalyzed Polymerization Reactions

As most organolanthanide complexes require pre-activation to perform in polymerization reactions, the abbreviation for the most often employed co-catalysts are shown in Figure 15, which will be used throughout this section.

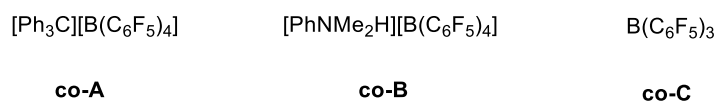


Figure 15. Abbreviation of co-catalysts employed in this polymerization section.

a) Monoolefins (ethylene, propene, styrene, etc.)

In order to gain insights on the difference in performance of early transition metals (Sc, Y, La, Zr, Hf) and main group metals (Al, Ga, In) in ethylene polymerization, a DFT study was conducted focusing on the insertion of ethylene into metal-methyl (M-Me) and metal-allyl (M-allyl) bonds with different ancillary ligands on the metal (Figure 16).[118] It was found that the insertion into M-Me bonds proceeded via a four-membered metalacyclic transition state, the energy of which depended on the nature of the metal leading to different strain in the structure. For the transition metals, the presence of d-orbitals reduced the strain and the energy was lower than for the main group metals. Also, lighter metals had lower energy than their heavier congeners. In contrast, for M-allyl bonds the insertion reaction proceeded via a six-membered transition structure, the strain of which was only dependent on the metal size and not the nature of the metal. The same result was found for the β -hydrogen transfer termination step, which also involved a six-membered transition structure.[118]

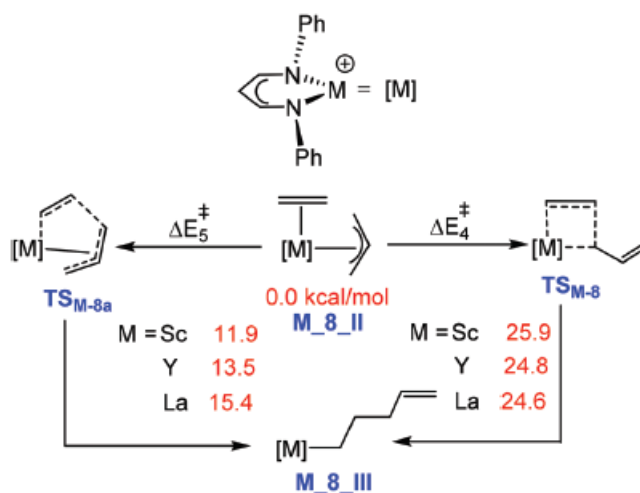


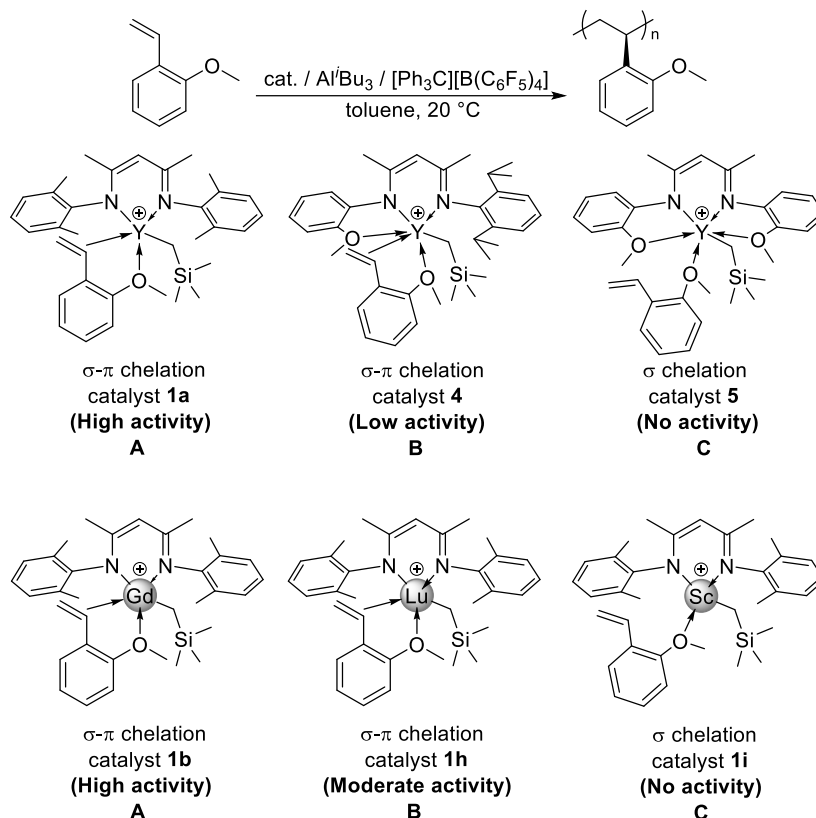
Figure 16. Ethylene insertion into M-allyl bonds: 4 vs 6-membered ring transition structures. Reprinted with permission from [118]. Copyright 2019 Royal Society of Chemistry.

The (trisaryl)cyclopentadienyl-based metallocenes $[\text{Cp}^{\text{Ar}}_2\text{LnCl}_2\text{K}(\text{THF})_n]_2$ ($\text{Ln} = \text{Nd}, \text{Tb}$) (shown in Scheme 45) were employed in the Coordinative Chain Transfer Polymerisation (CCTP) of ethylene using two different magnesium chain transfer agents, MgEt_2 and $(\text{BHT})(n\text{Bu})\text{Mg}(\text{THF})_2$ ($\text{BHT} = 2,6\text{-di-tert-butyl-4-methylphenoxide}$).^[56] Significantly higher polymerization degrees were obtained with the heteroleptic $(\text{BHT})(n\text{Bu})\text{Mg}$ complex (P_n 26-55) compared to the use of the dialkyl Mg complex (P_n 17-23). This finding was related to the higher solubility of the proposed final polyethylene (PE) containing product $(\text{BHT})_2\text{Mg}(\text{PE})_2$, compared to the $\text{Mg}_2(\text{PE})_4$ product, obtained from MgEt_2 activation and which precipitates during the reaction. The Nd complex with one 2-MeO-phenyl substituent showed lower catalytic activity than the other complexes, probably due to Nd-O coordination. The Tb complex allowed the monitoring of the polymerization process using luminescence spectroscopy. It was found that the catalytically active species has close structural proximity compared to the starting complex, however, with a higher degree of symmetry. A loss of the Tb-aryl interaction observed in the initial complex might explain this finding.^[56]

The CH_2 -bridged dimeric dimethylamino tethered half-sandwich lanthanide alkyl complexes $[(\text{C}_5\text{Me}_4\text{-C}_6\text{H}_4\text{-o-CH}_2\text{N}(\text{Me})\text{CH}_2\text{-}\mu)\text{Ln}(\text{CH}_2\text{SiMe}_3)]_2$ (see Scheme 40) were employed in the polymerization of 1-hexene. Moderate catalytic activity was observed after activation with $\text{AlR}_3/\text{co-A}$, MAO or MMAO providing atactic poly(1-hexene)s with moderate molecular weights. Chain-transfer to aluminium was proposed as termination step instead of $\beta\text{-H}$ elimination according to ^1H and ^{13}C NMR spectroscopy.^[52]

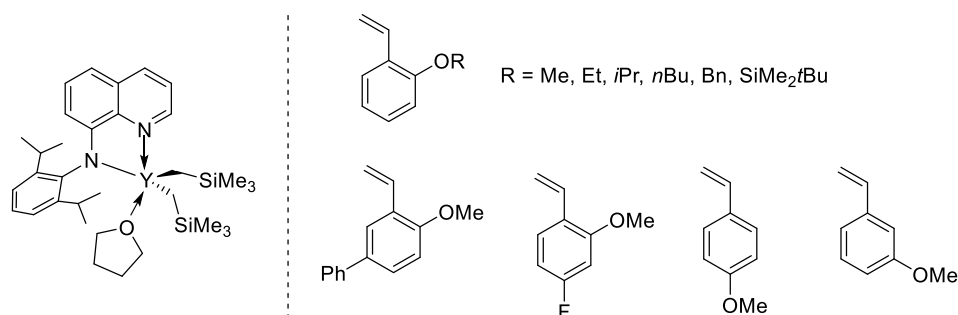
The stereoselective polymerization of polar and/or substituted styrene derivatives, such as alkoxystyrenes, halogenated styrenes or vinylpyridine, has been increasingly studied in recent years.

The isospecific coordination polymerization of ortho-methoxystyrene (oMos) was investigated with a variety of β -diketiminato lanthanide bis(alkyl) complexes shown in Scheme 8. After activation of these complexes with Al^iBu_3 /co-A, the resulting homogeneous catalytic system underwent oMos polymerization with different activity and iso-selectivity depending on the metal size and the ligand (Scheme 83). Cationic catalysts enabling σ - π chelation of the oMos substrate to the metal center provided high activity for high molecular weight polymers, such as the Y or Gd complexes carrying the ligands with four o-methyl groups on the N-aryl substituent. In contrast, smaller metals such as Lu or Sc led to reduced or no catalytic activity. Chelating o-OMe groups on the N-aryl substituent also decreased the catalytic activity by blocking the metal center. The stereoselectivity was influenced by the size and the chelating properties of the N-aryl substituent, with the Tm and Lu pre-catalysts providing perfect isotactic P(oMOS) (mmmm=99%). In addition, the Tm complex afforded isotactic, high molecular weight P(oMOS)s with a broad range of monomer-to-initiator ratios (200–3200) in a pseudo-living and controllable fashion.[18]



Scheme 83. Coordination polymerization of o-methoxystyrene using cationic β -diketiminato lanthanide complexes.[18]

The self-activated polymerization of various ortho-alkoxy styrenes using a cationic quinolyl anilido yttrium alkyl complex (shown in Scheme 84) was studied applying the conditions presented in Scheme 83, leading to highly syndiotactic polymers with narrow molecular weight distributions. The activity and the stereoselectivity depended on the alkoxy group, decreasing while going from methoxy to butoxy groups. With benzyloxystyrene no stereoselectivity was observed and with a bulky trialkylsiloxy group or methoxy groups in the meta or para-position no polymerization occurred at all. Additional phenyl or fluorine groups in the o-methoxy styrene did not alter the reaction outcome compared to oMos. DFT calculations were performed to investigate the polymerization process, indicating that the C_s symmetry of the catalyst plays an important role for the syndioselective polymerization of oMos.[119]



Scheme 84. Quinolyl anilido yttrium bis(alkyl) complex employed in the polymerization of various ortho-alkoxy styrenes.[119]

Several bisphenolate lanthanide alkyl complexes have been studied as catalysts in the isotactic polymerization of 2-vinylpyridine (2-VP). The tetradentate phenol ether derivatives shown in Scheme 19 afforded moderate to high activity in toluene at room temperature, which was influenced by metal size and ligand structure. The holmium complexes gave the best results in terms of activity and isoselectivity, the highest *mm* value of 0.99 was achieved with the ligand having a (CH₂)₄ bridge. The bulkier *t*Bu substituents led to lower selectivity and the use of THF instead of toluene provided atactic polymers.[29]

The dinuclear yttrium biphenolate alkyl complexes shown in Scheme 20 also showed high activity and isotacticity in the 2-VP polymerization in toluene leading to high molecular weight polymers. In contrast, the mononuclear complex gave lower activity and selectivity. The low initiation efficiency was attributed to the slow incorporation of 2-VP into the

yttrium complex due to unfavored THF dissociation. Addition of Et_3Al proved useful for decreasing M_n while still providing high activity and selectivity.[30]

A theoretical study on the origin of the stereoselectivity in the yttrium-catalysed 2-VP polymerization was reported. Based on the previously reported biphenolate yttrium alkyl complex shown in Figure 17, which displayed high isoselectivity in the polymerization process, this study explored the catalytic pathway. Whereas the first insertion is kinetically favored for the Re side – steric repulsion between the metal center and the monomer seem responsible for this – the second molecule of 2-VP is inserted preferentially from the Si side – here the steric repulsion between the ancillary ligand and the polymer chain are responsible. Overall, the stereoselectivity was proposed to be under kinetic control and reverse reactions during chain growth are difficult as each enchainment step is exergonic because of the C-C bond formation. Further studies showed that the steric factors of the two substituents near the metal center govern the stereoselectivity whereas electronic effects have low influence.[120]

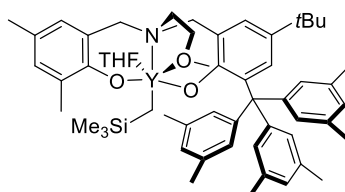


Figure 17. Y-bisphenolate complex employed as catalyst in DFT study of 2-VP polymerisation.[120]

The bulky pyridyl-methylene-fluorenyl and dibenzofluorenyl scandium bis(alkyl) complexes showed high activity in the syndiotactic polymerization of *o*-fluorostyrene (oFS) after activation with co-A (Figure 18). High molecular weight polymers with a narrow MW distribution were obtained in 10 minutes at room temperature in toluene up to a monomer:catalyst ratio of 2000:1. In addition, the copolymerization of oFS and styrene was successful with the dibenzofluorenyl based Sc complex providing random copolymers with various oFS contents ranging from 10-90% depending on the oFS feed. A drop of the T_g value was observed with increasing oFS content.[121]

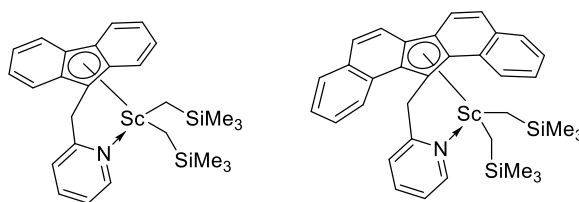


Figure 18: Fluorenyl Sc bis(alkyl) complexes for syndiotactic polymerization of *o*-fluorostyrene.[121]

The influence of coordinated THF to cationic Sc complexes on the stereoselectivity in the polymerization of halogenated styrenes was investigated by DFT studies. A comparison of the cationic $[(C_5Me_4SiMe_3)Sc(CH_2TMS)THF]^+$ complex and the solvent-free $[(C_5Me_4SiMe_3)Sc(o-CH_2C_6H_4NMe_2)]^+$ complex in the polymerization of *para*-Cl-styrene was carried out revealing that the C-H... π interactions between the THF and the aryl ring weaken the interactions between the metal center and the monomer in the first insertion step. This leads to similar energies for the transition states for *Re* or *Si* insertion (26.5 vs 26.9 kcal mol⁻¹) and consequently to atactic polymerization. In contrast, for the THF-free complex a significant difference in energy between the two transition states was observed (28.4 vs 23.7 kcal mol⁻¹), providing highly syndiotactic polymers. Whereas a similar result was observed in the case of *o*-Cl-styrene, with *m*-Cl-styrene only syndiotactic polymers were obtained. Analysis of the NPA charges of the phenyl ring in different chlorinated styrenes (-2.14 for *o,p* and -2.23 for *m*) in the transition states of the first monomer insertion pointed towards more or less strong C-H... π interactions between THF and the aryl ring, hence a varying influence of the presence of THF on the stereoselectivity.[122]

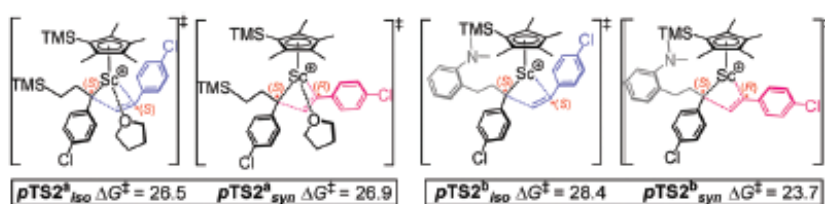


Figure 19. Transition states of first insertion into THF and THF-free complexes. Reprinted with permission from [Ln122]. Copyright 2019@Royal Society of Chemistry.

The production of highly syndiotactic polystyrenes containing Si-H groups in the *para* position was achieved using the catalytic system $(C_5Me_4SiMe_3)Sc(CH_2Ph)_2(THF)/co-A$. Three different styrene monomers with *p*-MeSiH₂, *p*-Me₂SiH and *p*-*i*Pr₂SiH groups were successfully transformed to the corresponding polymers with narrow MW distribution which could be readily further functionalized via hydrosilylation reaction. As the

polymerization proceeded in a quasi-living fashion, the controlled synthesis of diblock and triblock copolymers with styrene was also achieved.[123]

Three different vinylnaphthalene derivatives (1-VN, 2-VN, MVN) were transformed to their corresponding homopolymers with excellent syndiotacticity by using a pyridyl-tethered fluorenyl yttrium bis(alkyl) complex in combination with $\text{Al}(i\text{Bu})_3/\text{co-A}$. The corresponding Sc and Lu complexes provided lower activity, possibly due to their stronger Lewis acidity which could cause side-reactions, such as the nucleophilic addition to the naphthalene ring. Also, the pyridyl arm of the ligand contributed significantly to the activity in the MVN polymerization by increasing the steric bulk and reducing the Lewis acidity of the metal, hence reducing the coordination of the OMe group to the metal.[124]

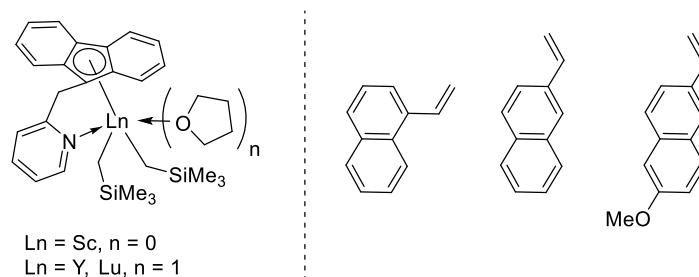
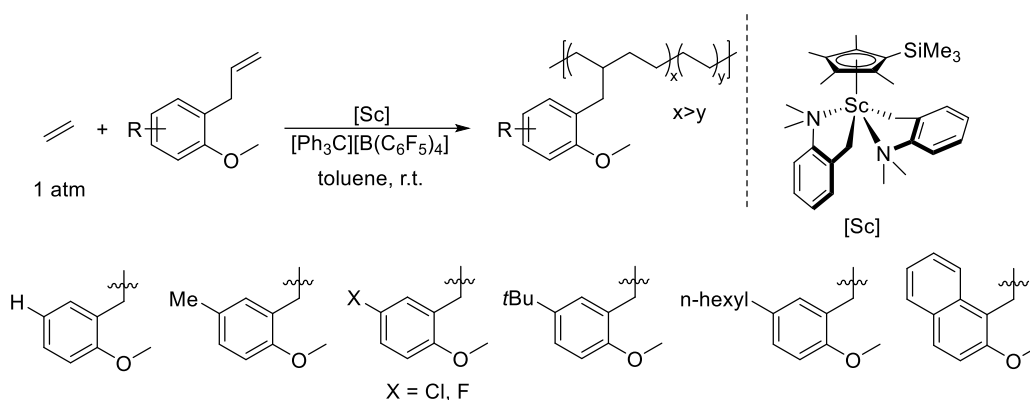


Figure 20. Fluorenyl-based constrained-geometry lanthanide complexes for the syndiotactic polymerization of vinylnaphthalene derivatives.[124]

The controlled co-polymerisation of ethylene (E) and anisyl-substituted propylenes (AP) under $(\text{C}_5\text{Me}_4\text{SiMe}_3)\text{Sc}(o\text{-CH}_2\text{C}_6\text{H}_4\text{NMe}_2)_2/\text{co-A}$ catalysis, provided high molecular weight, multi-block copolymers with varying glass-transition temperatures (T_g) (Scheme 85). The formation of the unique alternating E-alt-AP sequence, which made up to 76% of the copolymer structure, could be explained by the high affinity of Sc for the anisyl group and the steric hindrance of the Cp ligand, which could block further AP monomer insertion and favor instead ethylene coordination/insertion. The mechanical properties of the polymers could be influenced by the substituents on the anisyl group. Several copolymers with T_g lower than room temperature exhibited robust self-healing properties under dry conditions and in water at different pH. On the other hand, when T_g was around or above room temperature, the copolymers revealed excellent shape-memory properties.[125]



Scheme 85. Sc-catalysed synthesis of ethylene and anisyl-substituted propylene copolymers with self-healing and shape-memory properties.[125]

The thiophene-fused Cp scandium complexes **A** and **B** shown in Fig. 21 were applied in the copolymerization of ethylene and styrene to investigate steric and electronic effects on the sequence regulation. Activation of the Sc complex **A** (2,4,5,6-Me₄-4H-cyclopenta[b]thiophenyl)Sc(CH₂SiMe₃)₂ with co-A provided an efficient catalyst system for the copolymerization of ethylene and styrene. The obtained copolymer contained long syndiotactic polystyrene (PS) sequences (58% styrene content), in agreement with its $T_m = 211^\circ\text{C}$. In contrast, much shorter PS sequences were obtained in the copolymer when the THF-adduct of the Sc complex **A** was employed, however, this also drastically reduced the TOF of the copolymerization. With other Lewis base adducts (pyridine or pentafluoropyridine) of the Sc complex **A**, no copolymerization was observed. These results were explained by the reduced ability of the pyridine adduct to promote ethylene polymerization for electronic reasons and inhibition of styrene polymerization by pentafluoropyridine for steric reasons. The use of the thiophene-fused Cp Sc complex **B** (2,5-dimethyl-3-phenyl-4-H-cyclopenta[b]thiophenyl)Sc(CH₂SiMe₃)₂ having a phenyl group perpendicular to the metal showed lower activity than complex **A**, however, in this case, a “random” copolymer was obtained with discrete styrene units. Finally, the constrained-geometry type complex (C₁₃H₈CH₂C₅H₅N)Sc(CH₂TMS)₂ **C** bearing a pyridine-functionalized, less electron-donating fluorenyl ligand, provided alternating ethylene/styrene copolymers in a living manner. Addition of Al*i*Bu₃ to this catalyst system allowed fast and reversible chain transfer reaction to afford Al*i*Bu chain ends.[126]

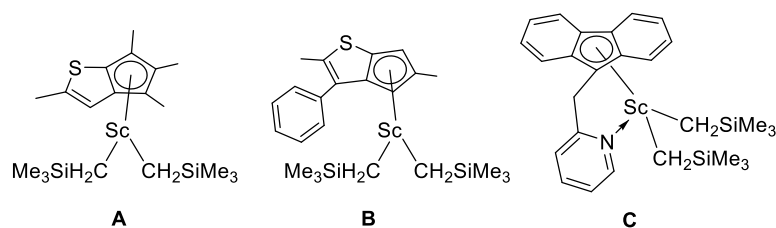
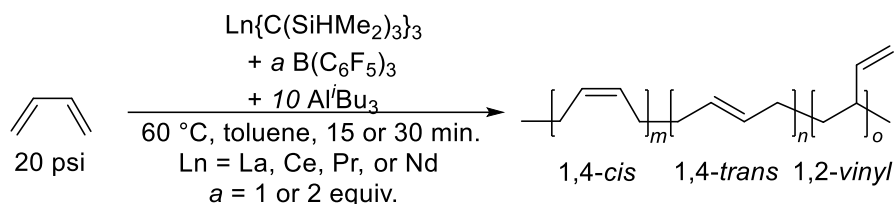


Figure 21. Sc complexes applied in the ethylene/styrene copolymerisation.[126]

The fluorenyl-amide based constrained geometry lanthanide alkyl complexes (see Scheme 61) provided syndiotactic polystyrene in low to moderate yields after activation with a cocatalyst (co-A, co-B or co-C) and $\text{Al}i\text{Bu}_3$ in dichlorobenzene.[70]

b) *Dienes (butadiene, isoprene, myrcene, etc.)*

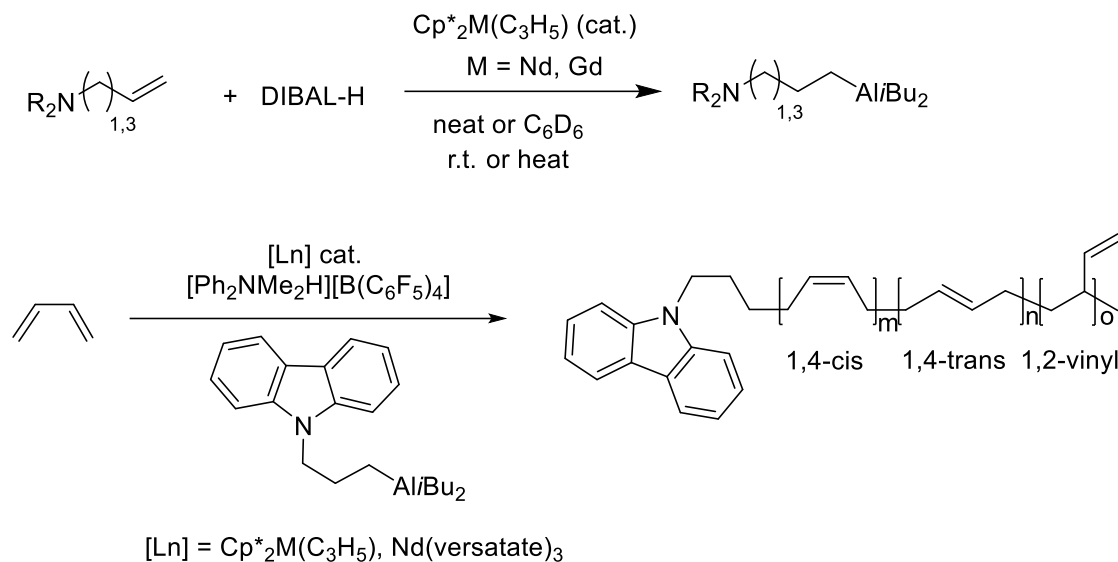
The zwitterionic hydridoborate di(alkyl) or mono(alkyl) complexes, shown in Scheme 6, are precatalysts for polymerization of butadiene in the presence of $\text{Al}i\text{Bu}_3$. Under constant butadiene pressure, the activity of these complexes follows the trend $\text{Nd} > \text{Ce} \gg \text{Pr} > \text{La}$ with the mono(alkyl) species being more reactive than the corresponding bis(alkyl) complexes except for La. The dicationic neodymium alkyl complex has the highest activity of the series, and its performance is consistent with chain-transfer reactions with $\text{Al}i\text{Bu}_3$. The microstructure of the obtained poly(butadienes) has varying amounts of 1,4-*cis* and 1,4-*trans* parts, in contrast 1,2-vinyl sections are below 5%. [16]



Scheme 86. Butadiene polymerization using hydridoborate di(alkyl) or mono(alkyl) complexes as pre-catalysts.[16]

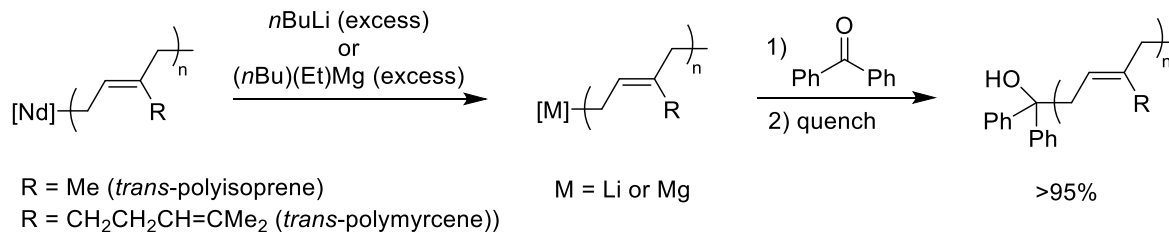
The metallocene lanthanide allyl complexes $\text{Cp}^*_2\text{Ln}(\text{C}_3\text{H}_5)$ ($\text{Ln} = \text{Nd}, \text{Gd}$) were employed in the coordinative chain transfer (CCT) polymerization of butadiene with functionalized aluminum reagents.[127] Initially, various aluminum reagents were obtained from the hydroalumination reactions of α -amino- ω -enes with DIBAL-H using the Ln metallocenes as catalysts (Scheme 87). Activation of the Gd complex with co-B in the presence of butadiene and the UV-vis active carbazole-containing aluminum reagent provided a range of polymers, with different end groups, including the carbazole moiety (only 5%). Closer

analysis showed that the CCTP process was not efficient with these metallocene complexes. In contrast, Nd(versatate)₃ provided an effective CCTP in which 90% of all aluminum-bound carbazole groups initiated polymer chains resulting in butadienes with high 1,4-cis enchainment (>90%).[127]



Scheme 87. Ln-catalysed hydroalumination and CCTP of butadiene.[127]

Nd-capped polydienes (isoprene, myrcene) obtained through living CCT polymerization from Nd(BH₄)₃/MgR₂/diene reactions, were end-functionalized by various strategies.[128] Whereas quenching with benzophenone directly after the polymerization provided low yields of the desired compound, addition of an excess of Grignard reagent or nBuLi followed by reaction with a ketone afforded high to excellent yields of the functionalized polymer (Scheme 88). In addition, the functionalization with benzaldehyde or styrene-oxide was also highly efficient after Nd/Li transfer.[128]



Scheme 88. End-functionalisation of Nd-capped polydienes via Nd/Li or Nd/Mg transfer.[128]

Activation of the trimetallic complexes [(Cp*Ln₃Me₂)₃] (Ln = Y, Lu) with borates co-A or co-B afforded 1,3-butadiene polymerization in low (Y) to very high (Lu) yield at room

temperature. The polymers showed a high cis-1,4 content, up to 95.2 for Y and 85.3 for Lu, with MWD ranging from 1.20 to 1.84. In contrast, with isoprene both metal complexes provided PIPs in high yields but lower cis-selectivity and large amounts of 3,4-PIP and narrow MWD for Y. Lowering the temperature to -10°C for the Y/co-A system afforded 92.2 cis-selectivity without any trans-content in the polymer. Substantial polymer cross-linking was observed under these conditions. Furthermore, addition of AlMe_3 to the Y/co-B system gave high trans-1,4 selectivity (85.5). The isolated complex $[(\text{Cp}^*_3\text{Y})_3\text{Me}_4(\text{CH}_2)(\text{THF})]$ resulting from degradation of $[(\text{Cp}^*\text{Ln}_3\text{Me}_2)_3]$ with THF (see scheme 53) showed lower reactivity after activation with co-A or co-B in isoprene polymerization.[62]

The new $[\text{Sc}(\text{AlMe}_4)_3(\text{Al}_2\text{Me}_6)_{0.5}]$ complex (see Scheme 5) was investigated in isoprene polymerization. No polymerization occurred without activation of this complex, however, upon addition of borates co-A or co-B, polymers with very high cis-1,4-polyisoprene content ($>90\%$) and no trans-1,4 content were obtained in very good yield ($>95\%$). Activation with co-C afforded poor polymer yield and both cis-1,4 and trans-1,4 polyisoprene sequences.[15]

The mono(pentadienyl)lanthanide aluminate complexes shown in Scheme 28 were applied to the polymerization of isoprene after activation with co-A, co-B or co-C. With equimolar amounts of cocatalyst, polymers with equal amounts of 1,4-cis and 1,4-trans contents were obtained, whereas reactions with 2 equiv. of cocatalyst provided higher 1,4-cis contents, with a maximum of 90% for the La/2co-C combination. In contrast, the isolated single-component catalyst provided higher trans-content than the binary La/co-C system. The pentadienyl substitution (iPr vs tBu groups) did not significantly influence the polymerization activity of the complexes, in contrast to the metal size. The smaller Nd complex provided higher cis-contents than the larger La and Ce complexes after activation with co-B or co-C. Surprisingly, the bis(pentadienyl) Lu and Y complexes showed similar activity to the mono(pentadienyl) complexes, which may be related to a possible η^5 to η^1 switch of the 2,4-dimethylpentadienyl ligand. The obtained high molecular weight polymers showed a relatively broad molecular weight distribution. The highest 1,4-cis content was observed for the Y/co-C system (89%). [39]

The Y-aluminabenzene complex shown in Scheme 68 provided polyisoprene after activation with co-A or co-B in 99% yield after 2h with major 1,4-cis content (71-77%) and minor 3,4-polyisoprene content (23-27%), whereas no 1,4-trans content was observed. The isolated cationic complex $(1\text{-Me-}3,5\text{-}t\text{Bu}_2\text{-C}_5\text{H}_3\text{Al})(\mu\text{-Me})\text{Y}(\text{benzene})][\text{B}(\text{C}_6\text{F}_5)_4]$

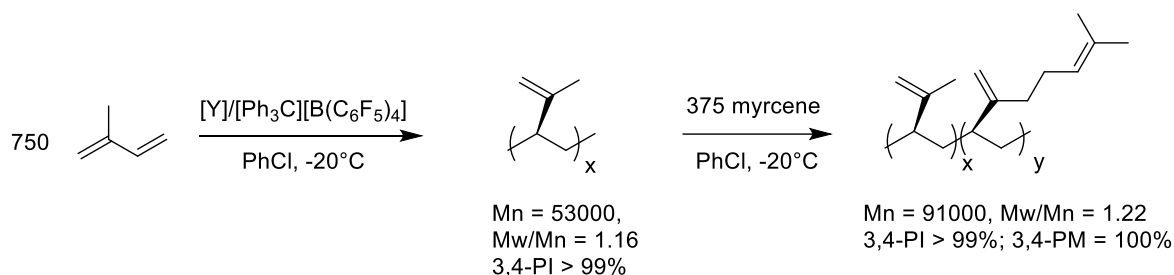
(Scheme 69) was shown to be an efficient single-component catalyst, providing polyisoprenes in different solvents (toluene, benzene, n-hexane) with similar characteristics as the binary systems. No polymerization was observed when the Y-aluminabenzene was activated with dialkylaluminium chlorides.[77]

The indenyl-based half-sandwich lanthanum complexes shown in Scheme 60 were investigated in isoprene polymerization. Upon activation with A or B excellent yields and high 1,4-trans PIP were obtained, the best results with the ethyl-substituted indenyl ligand (85.9/10.4 trans/cis content). Interestingly, upon activation with B(C₆F₅)₃ the silyl-substituted indenyl ligand based complex afforded good cis selectivity (77.0/13.0). The polymerization proceeded in a living manner. NMR studies indicated that activation led to methyl abstraction and the indenyl ligand remained coordinated to the metal.[69]

The anilido-oxazoline-ligated lanthanide dialkyl complexes shown in Scheme 10 afforded high activity and cis-1,4 selectivity after activation with co-A. Among the THF adducts, the Y complexes showed higher activity than the Sc complex, providing PIPs with high molecular weight and narrow molecular weight distribution. The THF-free Sc complex was most active but the produced polymer displayed broader M_w/M_n . The Y complexes showed the best cis-selectivity, especially with bulky substituents (**L**² and **L**³) on the anilido and the oxazolidine ring (>95%), whereas no substituent on the oxazolidine ring (**L**⁴) led to the lowest cis-selectivity (75.7%).[21]

The homopolymerisation of isoprene was investigated with the mono and binuclear bis(aminobenzyl) formamidinato lanthanide complexes shown in Scheme 21, using co-A as activator.[31] In the case of Y, the binuclear complexes showed the highest activity for 3,4-polymerisation of isoprene and lower M_n values than the mononuclear complex at room temperature. The Lu and Sc binuclear complexes showed lower activity. Single-site activity and interesting living polymerization characteristics were observed for the binuclear complexes. Performing the polymerization at -20°C, excellent 3,4 selectivity (up to 99.5%) was obtained. In contrast, at 80°C, this selectivity dropped considerably for the mononuclear complex (41%) whereas the binuclear complex still gave 76%, probably due to steric effects. The living polymerization of myrcene and the copolymerization of myrcene and isoprene were also successfully conducted with the binuclear Y complex. Highly 3,4-regioselective polymyrcene could be obtained with high catalytic activity, as well as di-block copolymers with excellent 3,4-selective PIP-b-PM and narrow PDI (see Scheme 89). Finally, a blend of different polyisoprenes (3,4 and cis-1,4) was obtained with

the binuclear Y system, upon addition of AlMe_3 after polymerization of the first batch of isoprene.[31]



Scheme 89. Living co-polymerisation of myrcene/isoprene using a binuclear Y complex.[31]

The heterobimetallic complexes $[\text{Ln}(\text{Ph}_3\text{CCOO})_3(\text{THF})_3]_2[\text{AlMe}_4]_2$ shown in Scheme 76, are not active catalysts for butadiene or isoprene polymerization without addition of a co-catalyst such as $\text{Al}i\text{Bu}_3$ or AlEt_3 . Upon activation, the Nd complex showed moderate activity providing polymers with high *cis*-1,4 contents. [87]

The CH_2 -bridged dimeric dimethylamino tethered half-sandwich lanthanide alkyl complexes (see Scheme 40) were good precatalysts for the polymerization of isoprene. The activity of the binary system (with co-A) was considerably improved upon further addition of $\text{Al}i\text{Bu}_3$. In all cases, PIPs with high 1,4-*cis* contents (> 90%), no 1,4-*trans* content and broad MWD were obtained.[52]

The two series of differently substituted 2-amidate indolyl lanthanide complexes shown in Scheme 16 were studied in isoprene polymerization reactions.[27] Only the ternary systems complex/co-A/ AlR_3 were successful for polymerization initiation. Complexes with the bulkier substituent on the amidate moiety provided moderate 1,4 selectivity (80%), however, showing good activity only in chlorobenzene and with $\text{Al}i\text{Bu}_3$. The lanthanide metal had a strong influence on the reactivity, with Gd, Dy and Y providing similar results (100% conversion after 12h), whereas Er gave lower conversion and no reaction was observed for the Yb complex. On the other hand, complexes with the smaller substituent on the amidate provided higher 1,4 selectivity (up to 96%) with different alkylaluminiums ($\text{R} = \text{Me}, \text{Et}, t\text{Bu}$) in either toluene or chlorobenzene.[27]

Application of fluorenyl-amide based constrained geometry lanthanide alkyl complexes (see Scheme 61) activated with co-A and AlMe_3 gave moderate activity and high *cis*-1,4 selectivity in isoprene polymerization in dichlorobenzene. In the case of myrcene, high activities and up to 100% *cis*-1,4 selectivity was obtained in the combination of the CG complexes with co-C and $\text{Al}i\text{Bu}_3$ in toluene. In both cases, bimodal MWD were observed.

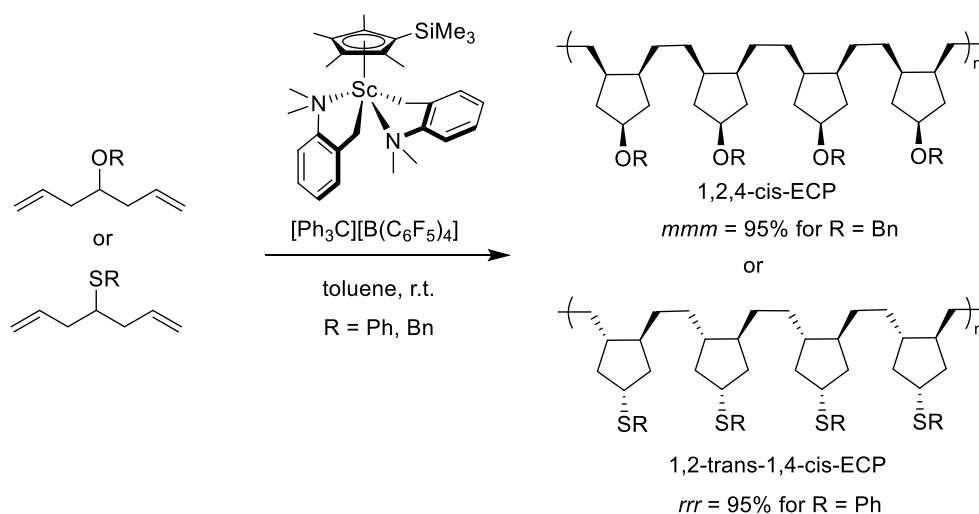
From a mechanistic point of view, the transfer of the chelating indenyl ligand from the lanthanide to the aluminum center was proposed as key step according to in-situ NMR studies.[70]

The copolymerisation of ethylene and butadiene using the ansa-bisfluorenyl complex $\{\text{Me}_2\text{Si}(\text{C}_{13}\text{H}_8)_2\text{Nd}(\text{BH}_4)_2\text{Li}(\text{THF})\}_2/\text{BOMAG}$ system (BOMAG = (nBu)(nOct)Mg) was investigated.[129] Kinetic studies and theoretical investigations provided evidence for the living character of this copolymerisation which operates via a reversible coordinative chain transfer mechanism between the Nd and the Mg centers. Analysis of the copolymer chain ends indicated the presence of a vinylcyclohexane motif, however, this was not detected in the polymer backbone. An explanation was provided based on DFT calculations indicating the reversibility of its formation and its ready transformation to a decalin motif via insertion of another ethylene unit. The presence of the decalin unit was confirmed for the first time by pyrolysis GC-MS analyses of the copolymers. The calculations also showed that the fluorenyl ligand on the Nd center can adopt different binding modes ($\eta^5, \eta^{3:2}, \eta^{3\text{exo}}$) depending on the steric constraints imposed by the polymer during the monomer insertion.[129]

A theoretical study on the mechanism of Sc-catalysed copolymerization of ethylene with amino-olefins (AO) of varying chain lengths was conducted.[130] The cationic Sc complex $[\text{C}_5\text{Me}_4(\text{SiMe}_3)\text{Sc}(\text{CH}_2\text{CH}_2\text{CH}_3)][\text{B}(\text{C}_6\text{F}_5)_4]$ was used as model catalyst in the copolymerization of ethylene with the short chain AO N-(1-butenyl) $n\text{Pr}_2$ or the long chain AO N-(1-octenyl) $n\text{Pr}_2$. Initial studies on the coordination of the AO onto the cationic Sc complex showed that for the short AO the simultaneous π -coordination of olefin and σ -coordination of amine was energetically most favorable, whereas for the long AO the amine σ -coordination was preferred. Concerning the AO insertion pathways, the short AO underwent self-assisted 1,2 insertion, whereas for the long AO 1,2-insertion in the presence of another amine coordinated to the Sc center was most favorable. After this insertion, no backbiting, i.e. coordination of the inserted amine group to the metal, was observed neither for the long or the short AO. The main catalyst inhibition process was proposed to occur via intermolecular coordination of other AOs. Finally, it was shown that the energetic barrier for ethylene insertion increased due to competing AO coordination.[130]

The regio-, diastereoselective and stereoregular cyclopolymerization of different ether and thioether substituted 1,6-heptadienes using cationic Sc half-sandwich complexes as catalysts was reported (Scheme 90).[131] In the ether series, the 4-benzyloxy-1,6-heptadiene substrate provided the best results with the bulky $\text{C}_5\text{Me}_4\text{SiMe}_3$ -ligated

scandium complex in combination with co-A, avoiding the formation of cross-linking products. The obtained polymers contained only the 1,2,4-cis-substituted ethylenecyclopentane (ECP) units, which were oriented with a high isotactic stereoregularity ($mmm = 95\%$). In contrast, under the same conditions, the phenoxy-substituted substrate provided atactic polymers in lower yields, showing the influence of the substituent on the oxygen atom. A significant heteroatom effect was determined by switching to the thioether series. In this case, the 4-phenylthio-1,6-heptadiene provided the best results in terms of activity and stereoselectivity, compared to the 4-benzylthio-derivative. The bulky Sc half-sandwich complex provided isotactic polymers ($rrr = 95\%$) with 1,2-trans, 1,4-cis ECP units in very high yields. DFT calculations were performed to gain understanding on the polymerization course, highlighting the importance of the coordination of the heteroatom to the Sc center on the regio and stereoselective outcome. Finally, the copolymerization of ethylene with the O or S functionalized 1,6-heptadienes was conducted, providing polymers with varying incorporation of the same ECP units observed in the homopolymers.[131]



Scheme 90. Sc-catalyzed cyclopolymerisation of 1,6-dienes.[131]

c) *Cyclic esters and amides (ϵ -caprolactone, lactide etc.), acrylates and vinylphosphonates*

The ring-opening polymerization (ROP) of rac-lactide (rac-LA) was studied using chiral anilido-oxazolidine Sc complexes (shown in Scheme 10).[22] The polymerization initiation occurred at room temperature and nearly full conversion was achieved after 20 min in THF. Higher heteroselectivity of the Sc catalysts was observed for the complexes with phenyl groups on the oxazoline moiety (L^9 , L^{10}) with $P_r = 0.70$ - 0.71 , compared to the

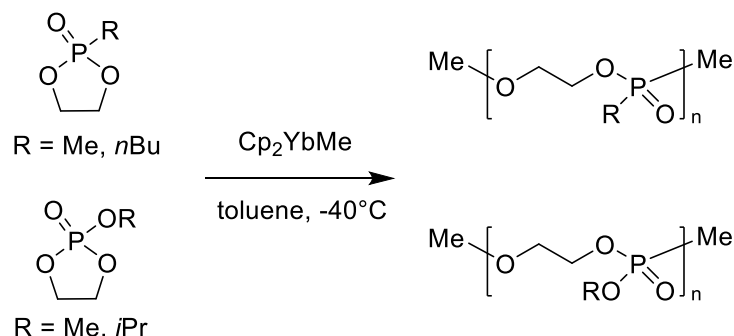
complexes with alkyl groups (\mathbf{L}^{5-8}) with $P_r = 0.62-0.64$. An increase in temperature to 50°C led to lower heterotacticity and higher catalytic activity. Whereas rather low activity was observed in toluene at room temperature, at 60°C complete conversion was obtained after 4 min only. Maldi-TOF spectrometry studies indicated that the alkyl groups on the catalyst were acting as initiating groups in the ROP of rac-LA. Furthermore, both alkyl groups could participate in the initiation and the polymerization was shown to proceed in a controlled manner. The Y complexes showed higher activity but lower control on the molecular weight distribution compared to the Sc complexes.[22]

The lanthanide complexes bearing an ansa-bis(amidinate) ligand with a rigid *o*-phenylene linker (shown in Scheme 66) were shown to be active initiators in the ROP of ϵ -caprolactone and L-lactide. The monomeric complexes showed higher catalytic activity compared to the dimeric La and Nd complexes, which was related to the absence of the active $\text{N}(\text{SiMe}_3)_2$ ligand in these dimeric complexes.[74]

The constrained-geometry permethylindenyl based Sc complexes (shown in scheme 59) bearing aryloxy groups were active initiators for the living ring-opening polymerization of L-lactide and rac-LA yielding pure isotactic PLA or moderately heterotactic PLA ($P_r = 0.68-0.72$), respectively, with narrow M_w/M_n values.[68] With these complexes, an induction period of 5-45 minutes and a first-order dependence in monomer concentration was observed by kinetic studies. A coordination-insertion mechanism was suggested based on the aryloxy polymer end groups observed by ^1H NMR. The Sc complex with the less bulky 2,4-*t*Bu-substituted aryloxy ligand revealed higher activity due to less steric crowding around the metal center, making lactide monomer coordination and polymerization initiation more favorable. In comparison to these aryloxy based complexes, the analogous Sc complex having an active BH_4 group, showed higher activity for the ROP of rac-LA or L-LA, however, with less control of molecular weight and broader polydispersities, which was related to intermolecular transesterifications. Furthermore, in this case a second-order dependence on monomer concentration was established.[68]

The ring-opening polymerization of cyclic phosphoesters (phosphates and phosphonates) was achieved using the simple ytterbium metallocene complex Cp_2YbMe as catalyst (Scheme 91).[132] The two cyclic phosphonate monomers, methyl and *n*-butyl ethylene phosphonate, afforded polymers with narrow molecular weight distribution after reaction at -40°C in toluene, indicating the living manner of the polymerization. Block copolymers of these two monomers were further successfully synthesized. MALDI-TOF analysis showed that the transfer of the methyl group of Cp_2YbMe to a monomer is involved in the

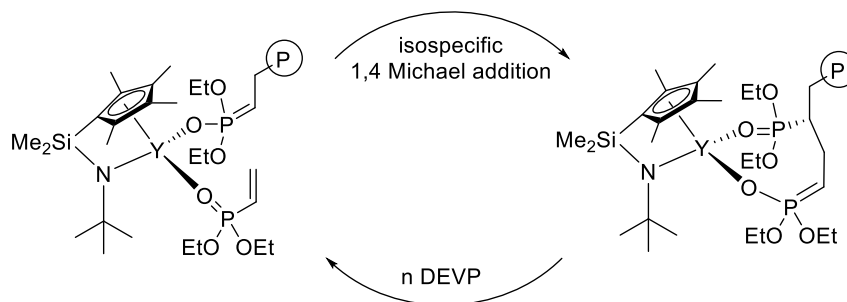
initial step. For the cyclic phosphate monomers, oligomers were obtained for methyl ethylene phosphate, due to its hydrophilicity and precipitation from toluene, whereas polymers were isolated with isopropyl ethylene phosphate.[132]



Scheme 91. Ring-opening polymerization of cyclic phosphoesters using Cp_2YbMe as catalyst.[132]

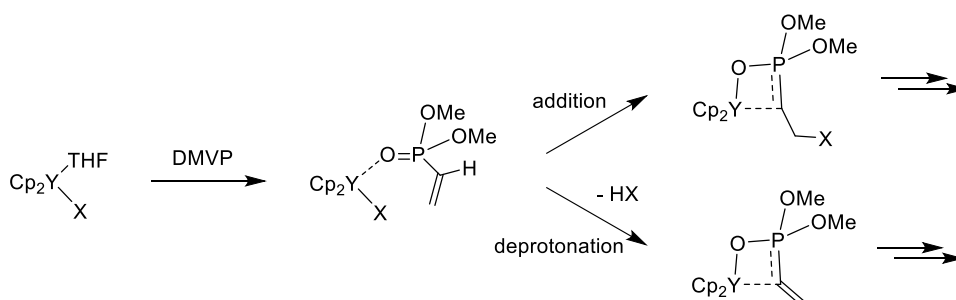
Methylmetacrylate (MMA) polymerization was studied using the dimeric borohydride complexes shown in Scheme 40.[52] The Sm complex provided higher catalytic activity than the Nd complex in neat MMA, leading in both cases to atactic polymer products. In THF, polymers with relatively high rr triad content were obtained with good monomer conversion, whereas in toluene low monomer conversion was observed and polymers with relatively high mm triad content. Attempts to influence the stereoselectivity with alkyl lithium reagents as co-catalysts did not lead to significant improvements.[52]

The influence of the steric bulk and the flexibility of the constrained geometry Y lutidynyl complexes (shown in Scheme 39) was explored in the group transfer polymerization of diethylvinylphosphonate (DEVP).[51] The best results concerning activity, isoselectivity and molecular dispersion were obtained with the dimethylsilane bridged complex $[\text{Me}_2\text{Si}(\text{C}_5\text{Me}_4)\text{N}t\text{Bu}]\text{Y}(\text{lut})$. Very high TOFs were achieved down to -30°C with a very narrow molecular weight distribution of the polymer. At -78°C , isotactic polymers with $\text{mmm} > 98\%$ were obtained in 100% yield after 20 min. The corresponding N-Ph substituted complex provided inferior results with respect to catalyst activity, however, better stereoselective outcomes were observed at room temperature. The indenyl complex only led to oligomerization of DEVP. Compared to the rigid dimethylsilyl-bridged complexes, the more flexible ethylene bridged complex was considerably less efficient. The expected lutidynyl transfer from the Y center to the monomer in the initiation step was confirmed by MS analysis of the polymers. A chain-end control mechanism was proposed to explain the iso-selectivity in the living polymerization of DEVP (Scheme 92).[51]



Scheme 92. Proposed mechanism for stereoselective DEVP polymerization.[51]

A DFT study on the Y catalysed polymerization of dialkylvinylphosphonates was conducted to gain further insights on the polymerization process and especially the two possible initiation steps: addition vs. deprotonation (Scheme 93).[133] It was found that for precision polymerization a reactive initiator group leading to fast resting state formation and rate-limiting the propagation steps was essential. Theoretically, Y-alkyl groups should follow the addition pathway, however, experimentally deprotonation with considerable induction periods was observed. Quantum tunneling of the barrier was suggested for the deprotonation process in these cases. Calculations for other initiators showed that they should follow the addition pathway, with the most promising candidate being the dimethylamido group. π -conjugated initiators such as (4,6-dimethylpyridin-2-yl)methyl or 2-propenyl groups were calculated to proceed via Michael addition.[133]

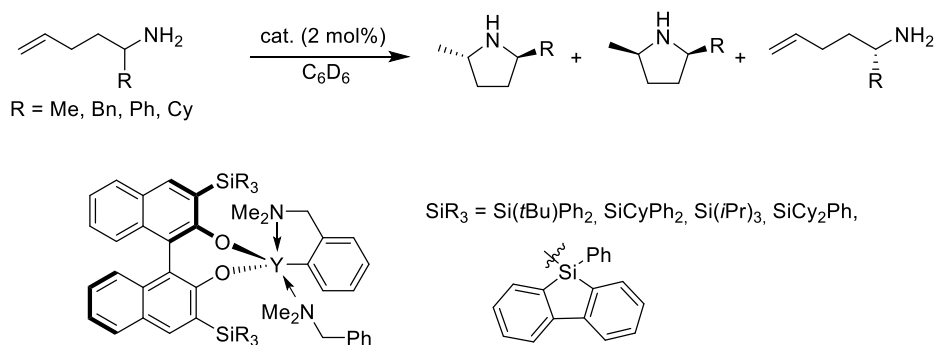


Scheme 93. DFT mechanistic studies on vinylphosphonate polymerization.[133]

2.11.2. Organolanthanide-catalyzed Hydrofunctionalization Reactions

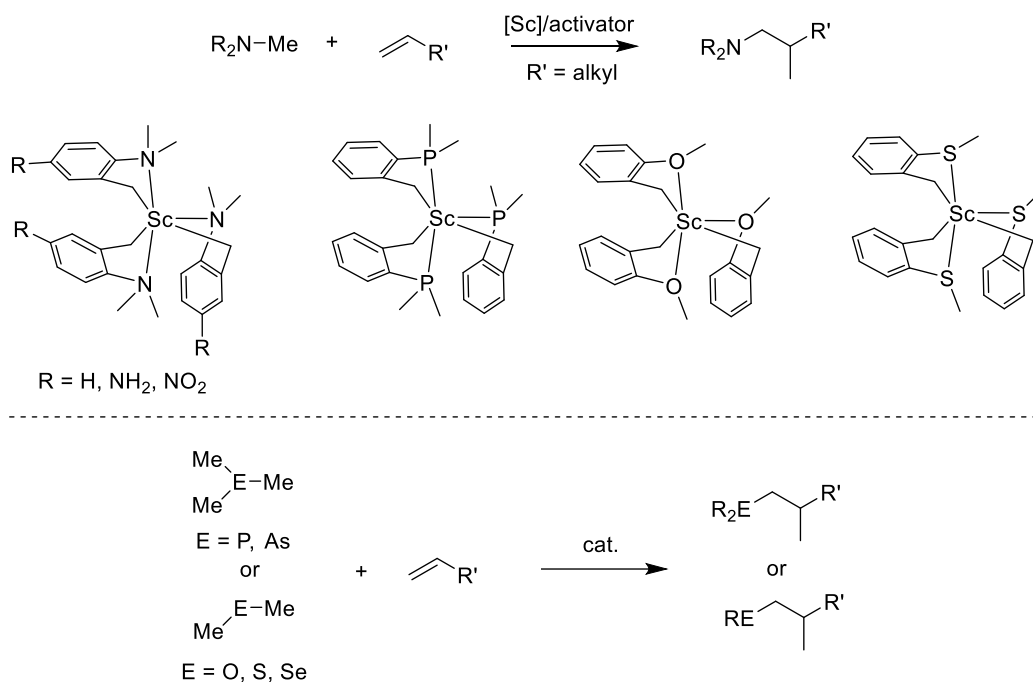
Several chiral 3,3'-silyl-substituted binaphtholate yttrium catalysts with bulky trisaryl, trisalkyl or mixed alkylarylsilyl groups were investigated in the kinetic resolution of α -substituted aminopentenes via intramolecular hydroamination (Scheme 94).[134] This methodology was highly efficient for methyl-, benzyl-, and phenyl-substituted substrates applying the (R)-cyclohexyldiphenylsilyl-substituted catalyst, in contrast, for α -

cyclohexyl-substituted aminopentene low kinetic resolution was obtained. Interestingly, the *trans*:*cis* ratio of the cyclized product depended on the substituent varying from 5:1 for cyclohexyl to >50:1 for phenyl substrate. Studying the hydroamination cyclisation reaction with enantio-enriched substrates having (*S*) configuration showed that for matching (*R*)-catalysts the *trans* product was always largely favored, whereas in the case of the mismatching (*S*)-catalysts poor selectivity was observed, and in certain cases was even in favor of the *cis* product. It was proposed that a Curtin-Hammett pre-equilibrium between the matching or mismatching substrate-catalyst pair should be responsible for this observed selectivity. In the case of the phenyl-substituted substrate a possible interaction between the phenyl ring and the metal center or π - π interactions with the ligands might be at play to account for the excellent *trans* selectivity.[134]



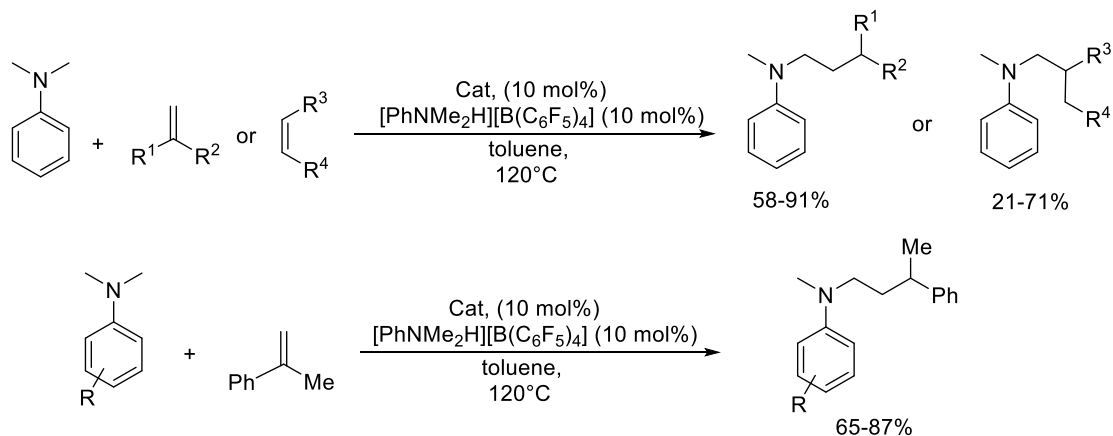
Scheme 94: Kinetic resolution of α -substituted aminopentenes via hydroamination using chiral yttrium binaphtholate complexes.[134]

A theoretical DFT study on the Sc-catalyzed olefin hydroaminoalkylation with tertiary amines was conducted. A series of homoleptic, substituted Sc(benzyl)₃ complexes were investigated as pre-catalysts (Scheme 95), showing that EWGs in the para position of the benzyl ligands improved the catalytic performance of the active cationic Sc species due to an increased Lewis acidity of the metal and a smaller HOMO(amine)-LUMO(metal) gap. Changing the pendant NMe₂ group on the benzyl ligand of the Sc complex to other heteroatoms (OMe, PMe₂, SMe) revealed that the SMe group provided better results by decreasing the steric hindrance around the metal ion. Another point of this study was the addition of the α -C-H bond of different heteroatom-containing substrates, i.e. R₂PMe, R₂AsMe, ROME, RSMc, RSeMe, onto olefins. It was shown that only the alkyl sulfides and selenides were good substrates for α -C-H bond alkylation whereas P, As and O substrates were inert due to steric reasons in the transition state of C-H activation.[135]



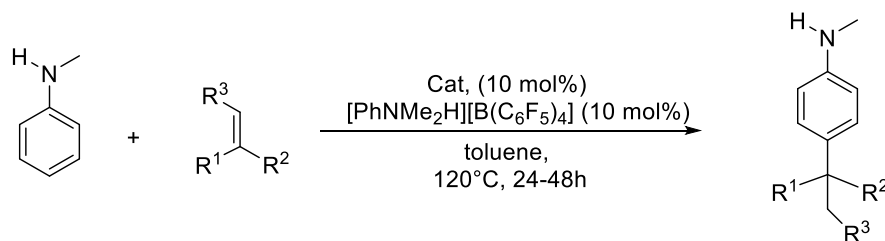
Scheme 95. Various Sc(benzyl)₃ complexes investigated by DFT as pre-catalysts for olefin hydroaminoalkylation reactions and exploration of different heteroatom containing substrates.[135]

The unsymmetrical β-diketoiminato scandium bisalkyl complex (synthesis shown in Scheme 8) was applied as precatalyst in the hydroaminoalkylation of sterically hindered 1,1 and 1,2-disubstituted alkenes, including endocyclic alkenes and α-methylstyrenes, in combination with differently substituted N,N-dimethylanilines (Scheme 96).[19] After activating the scandium complex with [PhNMe₂H][B(C₆F₅)₄], the reaction was conducted in refluxing toluene providing access to a range of alkylated anilines in high yields.[19]



Scheme 96. Cationic Sc catalyzed hydroaminoalkylation of various alkenes using N,N-dimethylanilines.[19]

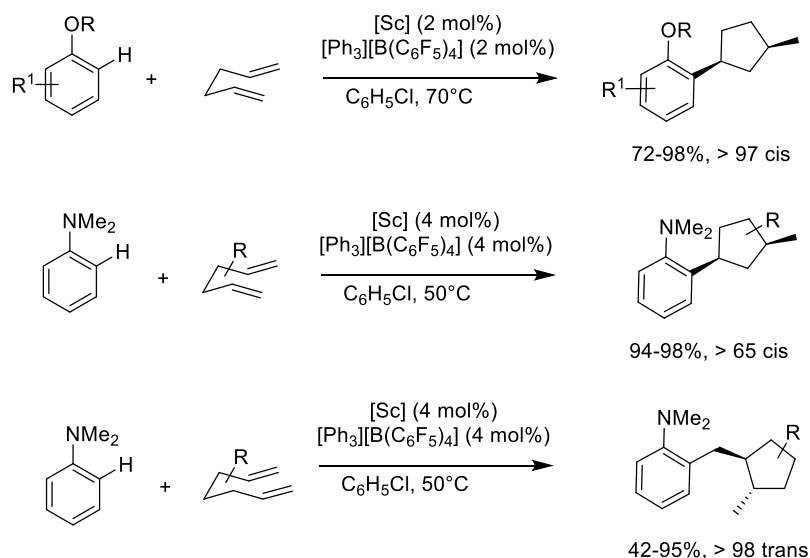
Following this work, N-methylanilines were then studied as substrates using the same cationic Sc catalyst system.[136] However, instead of the expected hydroaminoalkylation products, selective alkylation in the para position of the aromatic ring was observed (Scheme 97). A large variety of styrene derivatives and substituted primary or secondary anilines or bicyclic nitrogen substrates were suitable for this hydroarylation reaction, however, the reaction could not be applied to aliphatic alkenes. When the para-position was blocked, for example with a methyl group, the alkylation occurred in the ortho-position. Various control experiments were conducted to show that this transformation may proceed via a tandem hydroamination/Martius-Hofmann rearrangement and not a classical Lewis acid catalyzed Friedel-Crafts alkylation.



Scheme 97. Para-selective alkylation of primary and secondary anilines using a cationic Sc/borate catalyst system.[136]

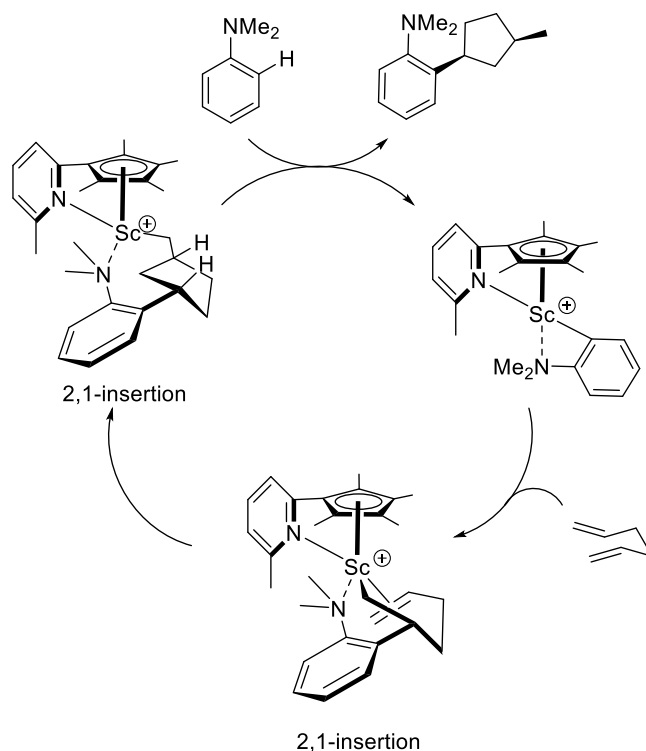
Tandem cyclisation/hydroarylation reactions of α,ω -dienes were investigated using the 2-picoline-tethered Cp scandium bis(alkyl) complex (η^5 : κ -C₅Me₄-C₅H₃NMe-o)Sc(CH₂SiMe₃)₂ (shown in Scheme 41) as precatalyst. After activation with [Ph₃C][B(C₆F₅)₄], the cationic Sc complex showed high catalytic activity with aromatic ethers and 1,5-pentadiene (Scheme 98).[53] High yields and very good cis selectivity of the 1,3-disubstituted arylated methylcyclopentanes were obtained with alkyl/aryl and diarylethers. Double alkylation was observed in the case of 1,4-benzodioxane. Furthermore, the C-H activation occurred selectively next to the OR group in the presence of SR or NR₂ groups in the substrate. Tertiary anilines also reacted with 1,5-pentadiene under Sc catalysis to afford the corresponding cyclopentane products with good yields and high cis-selectivity. A drop in the cis-selectivity was observed with substituted 1,5-pentadienes. Interestingly, the use of 1,6-pentadienes did not provide cyclohexane motifs but 1,2-disubstituted benzylated methylcyclopentanes were obtained in high yields and very good trans selectivity. Finally, the sequential cyclisation of trienes allowed the isolation of spiroalkanes in high yields and stereoselectivity. Deuterium labelling and competition

experiments revealed an intra and intermolecular kinetic isotope effect, pointing towards the implication of the C-H activation in the rate-determining step. [53]



Scheme 98. Tandem cyclisation/hydroarylation reactions of α,ω -dienes catalysed by a cationic Sc complex.[53]

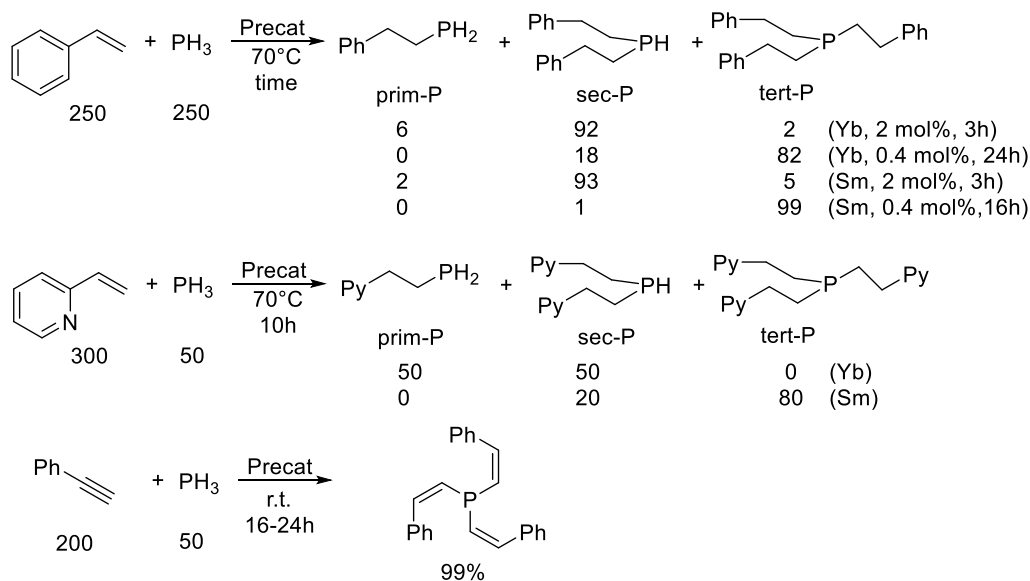
For the mechanism, it was proposed that in a first step, the cationic Sc complex would react with the aromatic substrate via selective ortho-C-H activation due to the coordination of the OR or NR₂ group to the Sc metal. This new complex would then react with 1,5-dienes via a 2,1 insertion into the Sc-aryl bond to afford an intermediate Sc-alkyl complex (Scheme 99). A rapid 2,1 insertion of the remaining C=C double bond into the new Sc-C bond would provide the cyclopentylmethyl scandium complex which would further react with a new substrate molecule via C-H activation to release the final product and regenerate the catalytic species. In the case of 1,6-hexadienes, the first step would be a 1,2 insertion followed by a 2,1-insertion.[53]



Scheme 99. Mechanistic proposal for the tandem cyclisation/hydroarylation reactions of 1,5-dienes catalysed by a cationic Sc complex.[53]

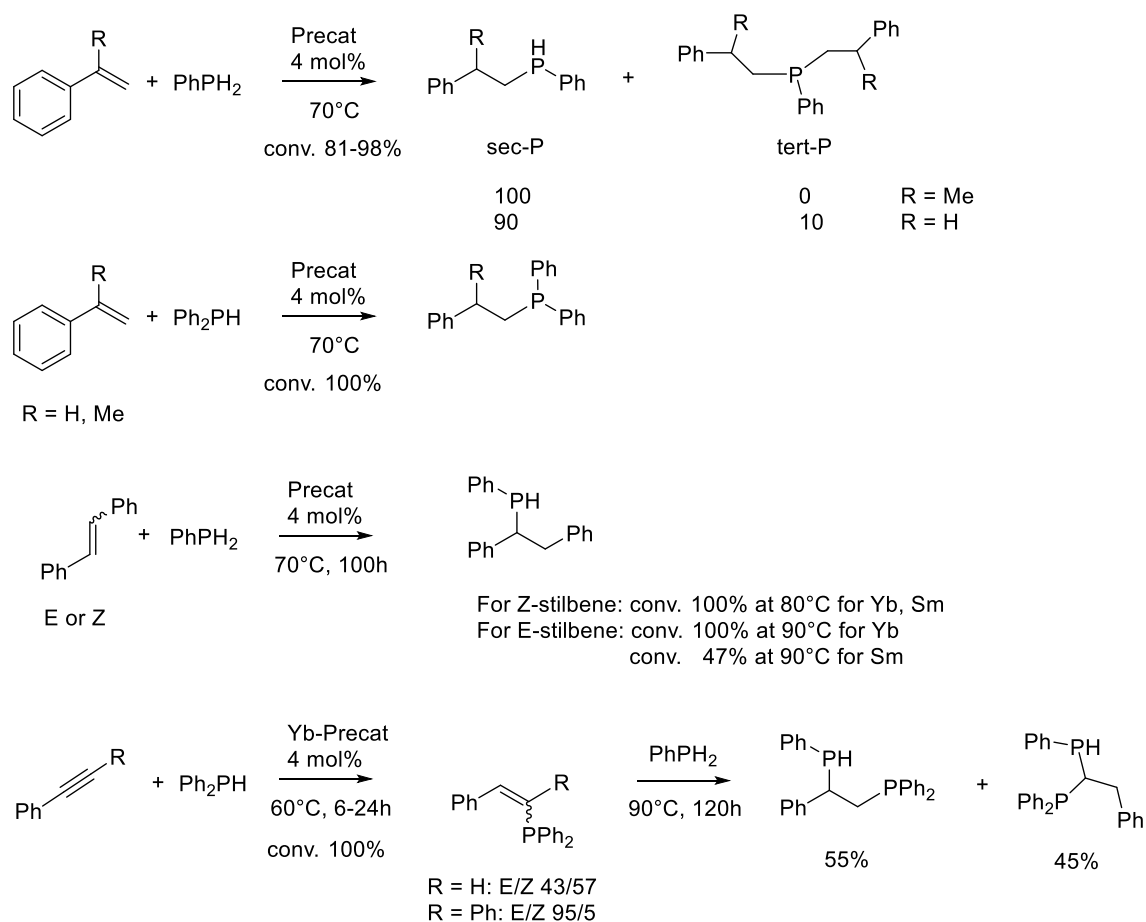
Various organometallic complexes have been studied in the hydrophosphination and hydrophosphinylation of olefins and alkynes.

The divalent Yb and Sm bis(amide) NHC complexes $[(\text{Me}_3\text{Si})_2\text{N}]_2\text{Ln}(\text{NHC})_2$, shown in Scheme 1, were suitable catalysts for the hydrophosphination of styrene with PH_3 under neat conditions at 70°C (Scheme 100). Depending on the catalyst loading, the substrate: PH_3 ratio and the reaction time the secondary or tertiary phosphines were obtained as products in relatively good selectivity. This reaction with styrene was also catalyzed by the NHC ligand alone, however longer reaction times were required and the selectivity for the tertiary phosphine was lower. In the case of 2-vinylpyridine as substrate, the hydrophosphination with PH_3 yielded a mixture of primary and secondary product for the Yb complex, whereas with Sm the tertiary product was the major product. All complexes and NHC ligands catalyzed the transformation of phenylacetylene to the tertiary phosphine as sole product in very high yields, in 16-24 hours for the Sm and Yb catalysts and 48 hours for the NHC ligands.[11]



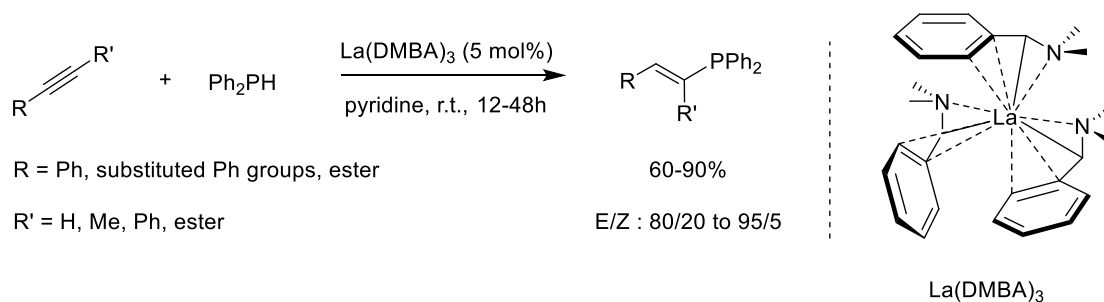
Scheme 100. Hydrophosphination of styrene, 2-vinylpyridine and phenylacetylene using divalent $[(\text{Me}_3\text{Si})_2\text{N}]_2\text{Ln}(\text{NHC})_2$ complexes as precatalysts.[11]

The divalent Yb and Sm bis(benzhydryl) complexes $[(p\text{-}t\text{Bu-C}_6\text{H}_4)_2\text{CH}]_2\text{Ln}(\text{L})_n$ ($\text{Ln} = \text{Sm}$, $\text{L} = \text{DME}$, $n = 2$; $\text{Ln} = \text{Sm}$, Yb , $\text{L} = \text{TMEDA}$, $n = 1$) (see Scheme 4) were shown to catalyze efficiently the hydrophosphination reactions of styrene derivatives with primary or secondary phosphines (Scheme 101).[14] In addition, internal alkenes (E or Z stilbene) reacted in high yields with primary phosphines to the secondary phosphine. Finally, phenylacetylene and 1,2-diphenylacetylene reacted with secondary phosphine to obtain a 1:1 mixture of E/Z alkenes in the case of phenylacetylene and highly selective E olefin for diphenylacetylene with Yb precatalyst. Phenylacetylene underwent double hydrophosphination with Ph_2PH and PhPH_2 to yield a mixture of 1,2 and 1,1-diphosphinoethanes with Yb precatalyst.[14]



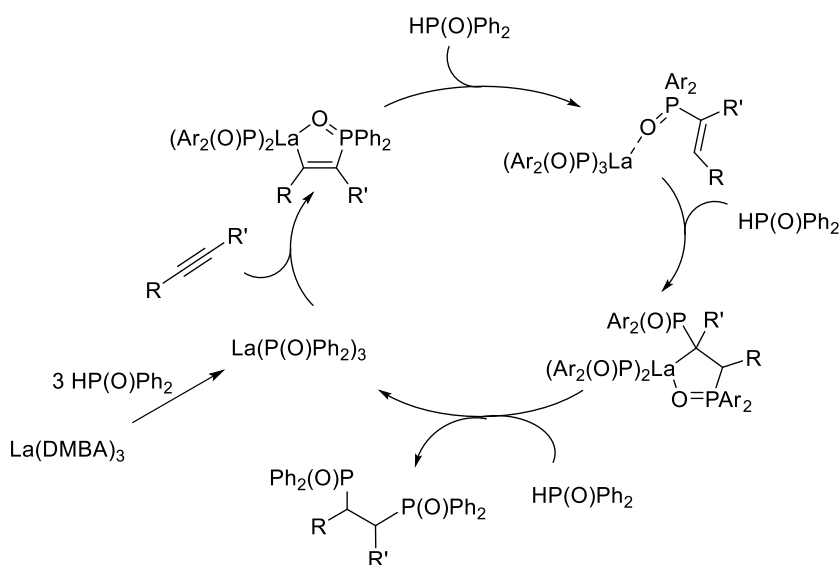
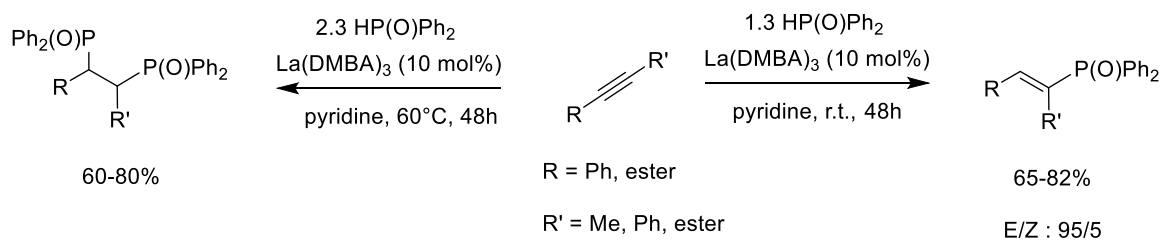
Scheme 101. Hydrophosphination with divalent Yb and Sm bis(benzhydryl) precatalysts $[(p\text{-}t\text{Bu-C}_6\text{H}_4)_2\text{CH}]_2\text{M}(\text{L})_n$. [14]

The hydrophosphination of internal and terminal alkynes using Ph_2PH and the homoleptic lanthanum tris(dimethylbenzylamine) complex, $\text{La}(\text{DMBA})_3$, as precatalyst was studied (Scheme 102). [137] The reaction was carried out in pyridine at r.t. to afford the trisubstituted alkenes with good E:Z selectivity and good to moderate yields. Interestingly, this selectivity could be influenced by the concentration of diphenylphosphine, leading to the Z-isomer with 0.6 eq Ph_2PH and to the E-isomer with 1.6 eq Ph_2PH . For this isomerization, an insertion/deinsertion pathway was proposed. [137]



Scheme 102. Hydrophosphination of alkynes with $\text{La}(\text{dmba})_3$. [137]

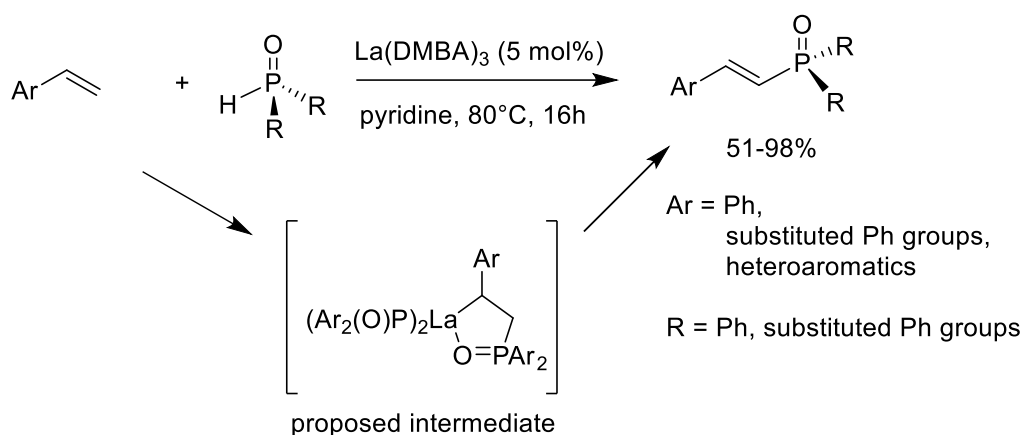
This $\text{La}(\text{DMBA})_3$ complex was further employed in the hydrophosphinylation of styrenes and alkynes. Whereas with terminal alkynes, only selective double hydrophosphinylation was achieved in high yields, with internal alkynes selective mono additions to the E alkene was obtained (Scheme 103). Upon increase of temperature the reaction was further driven to the double addition product. Concerning the proposed mechanism, after activation of the precatalyst with $\text{HP}(\text{O})\text{Ph}_2$, the newly formed $\text{La}(\text{P}(\text{O})\text{Ph}_2)_3$ would react with the alkyne via a [3+2]cycloaddition to afford a lanthanum-heterocyclic intermediate which upon protonolysis would provide the mono-insertion product (Scheme 103). This complex could further react with phosphine oxide via alkene phosphinylation and further protonolysis would yield the double insertion product and regenerate the active catalyst.[137]



Scheme 103. Mono and double hydrophosphinylation of alkynes with $\text{La}(\text{dmba})_3$ as precatalyst: scope and mechanism.[137]

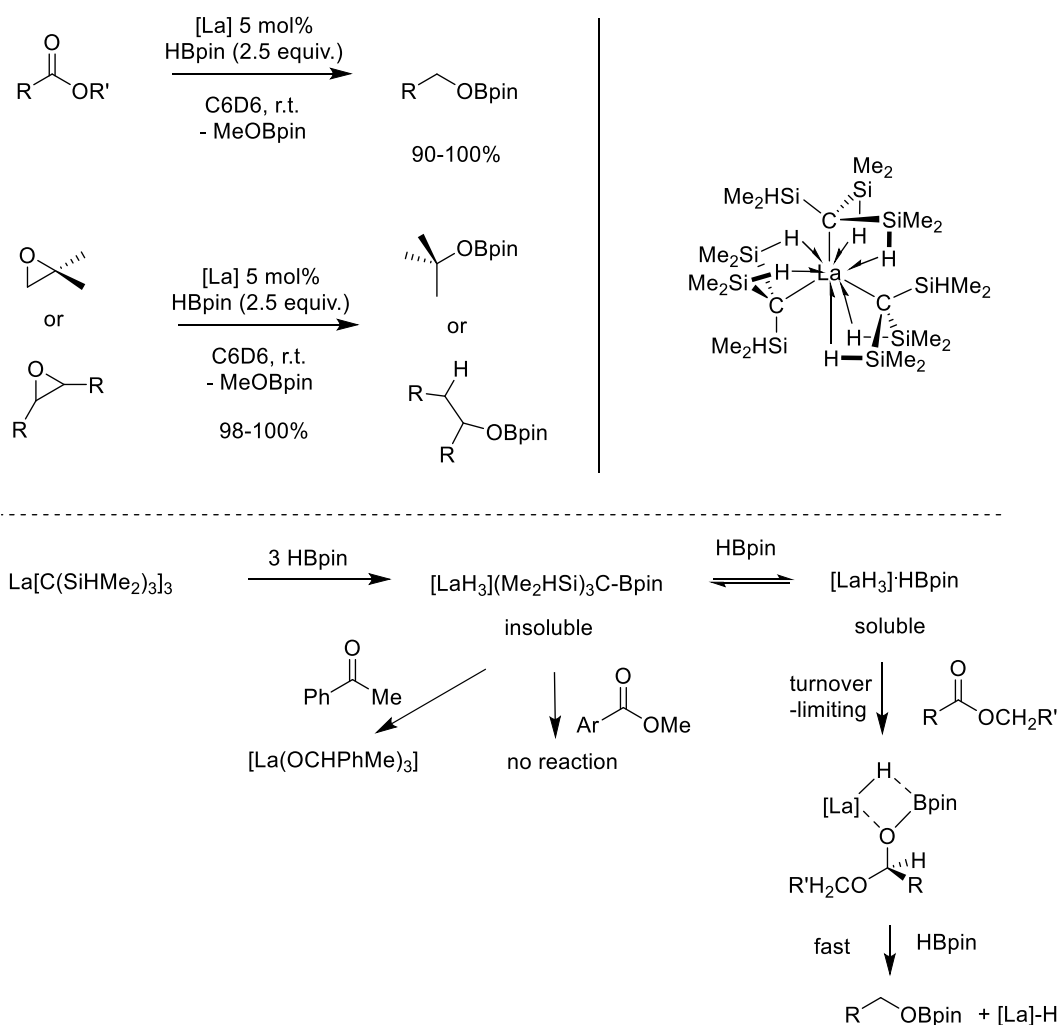
Finally, it was shown that $\text{La}(\text{DMBA})_3$ also acted as precatalyst for the highly regioselective anti-Markovnikov addition of diphenylphosphine oxide onto various styrene derivatives (Scheme 104).[138] Differently substituted phosphine oxides were also suitable for this transformation providing high yields of the final tertiary phosphine oxides. The reaction was proposed to proceed via a five-membered metallacycle obtained from the

insertion of styrene into the La-P bond of $\text{La}(\text{P}(\text{O})\text{Ar}_2)_3$, formed during the activation of $\text{La}(\text{DMBA})_3$ with $\text{HP}(\text{O})\text{Ar}_2$. Protonolysis of this intermediate with $\text{HP}(\text{O})\text{Ar}_2$ would result in the final product and regenerate the active catalytic species.[138]



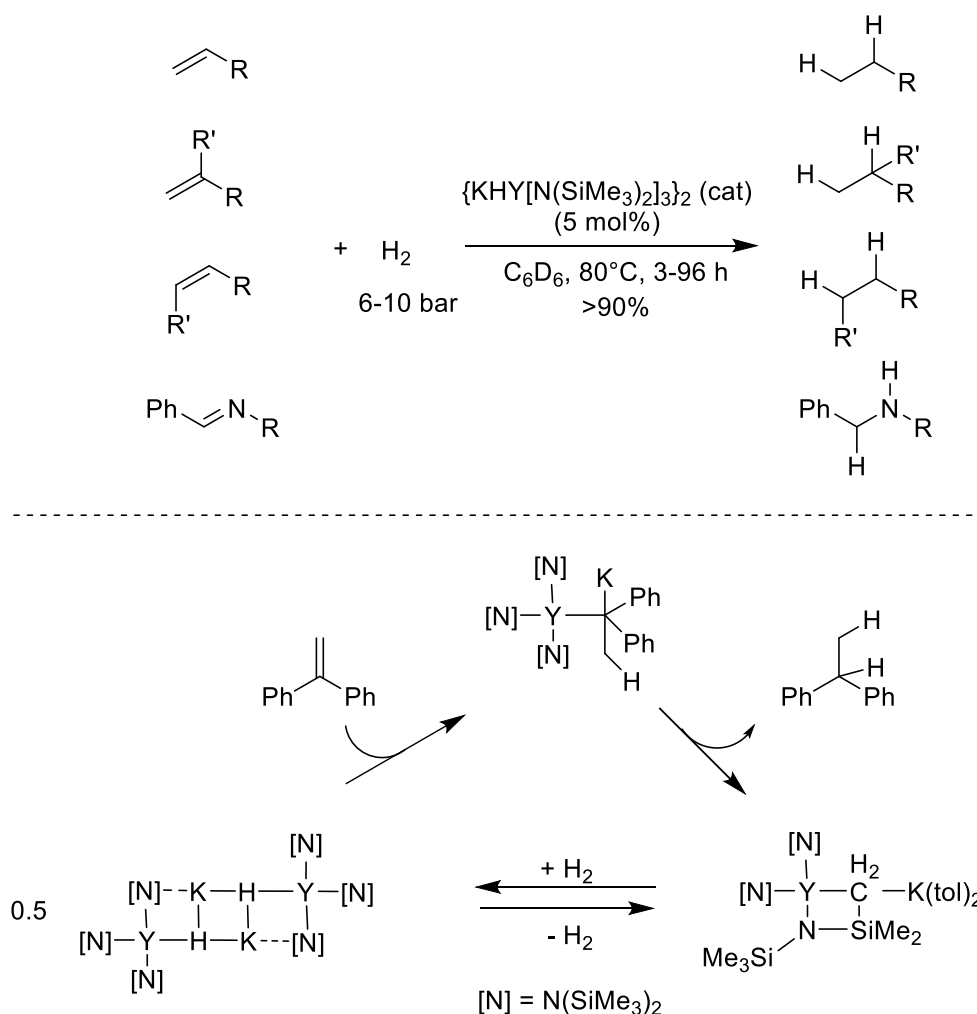
Scheme 104. Hydrophosphinylation of styrene derivatives with $\text{La}(\text{DMBA})_3$ as precatalyst.[138]

The efficient catalytic hydroboration of esters and epoxides using the tris(alkyl)lanthanum complex $\text{La}[\text{C}(\text{SiHMe}_2)_3]_3$ in combination with HBpin was reported (Scheme 105).[139] The reaction operates at room temperature with excellent functional group tolerance on the ester substrates (halides, nitro, alkoxy, CF_3 groups; conjugated esters) and with TONs up to 10000 for aliphatic esters. Different substitution patterns in epoxides were compatible affording primary, secondary or tertiary boryl esters in excellent yields. For mechanistic insights, the reaction of $\text{La}[\text{C}(\text{SiHMe}_2)_3]_3$ with 3 equiv. HBpin was studied, leading to the formation of $(\text{Me}_2\text{HSi})_3\text{C-Bpin}$ according to ^{11}B NMR and insoluble $[\text{LaH}_3]_n$ salt, which did not react with esters but only ketones. Addition of further HBpin afforded a soluble LaH_3 complex which could reduce esters. From kinetic experiments it was deduced that the C-O cleavage should occur after the turnover-limiting step. It was proposed that initially the soluble $[\text{La}]-\text{H}_2\text{Bpin}$ complex reduces the ester and that another HBpin molecule interferes in the C-O cleavage step (Scheme 105).[139]



Scheme 105. Hydroboration of esters and epoxides with $\text{La}\{\text{C}(\text{SiHMe}_2)_3\}_3$. [139]

A wide range of mono and disubstituted alkenes as well as aldimines could be hydrogenated using the dimeric potassium-yttrium ate complex $\{\text{KHY}[\text{N}(\text{SiMe}_3)_2]_3\}_2$ (preparation shown in Scheme 22) as a catalyst under a hydrogen pressure of 6-10 bars at 80°C (Scheme 106). Control experiments showed the reaction with D_2 to be two times slower than with H_2 . The following mechanism was proposed for this transformation. After coordination of the alkene to the complex, insertion into the Y-H bond would occur to afford an alkyl ate complex. The reactive Y-C bond would then deprotonate one of the methyl groups on the amide moiety to form the hydrogenation product and a four-membered metallacycle, which after addition of H_2 would regenerate the catalyst. [32]

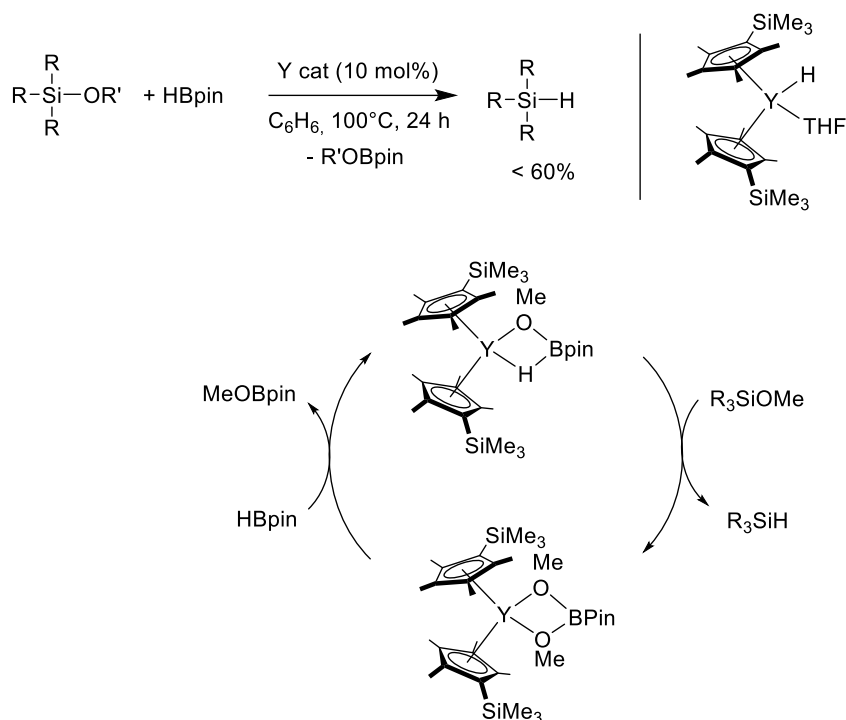


Scheme 106. Hydrogenation of various alkenes and aldimines using dimeric potassium-yttrium ate complex $\{\text{KHY}[\text{N}(\text{SiMe}_3)_2]_3\}_2$ and proposed mechanism.[32]

2.11.3. Other Organolanthanide-catalyzed Reactions

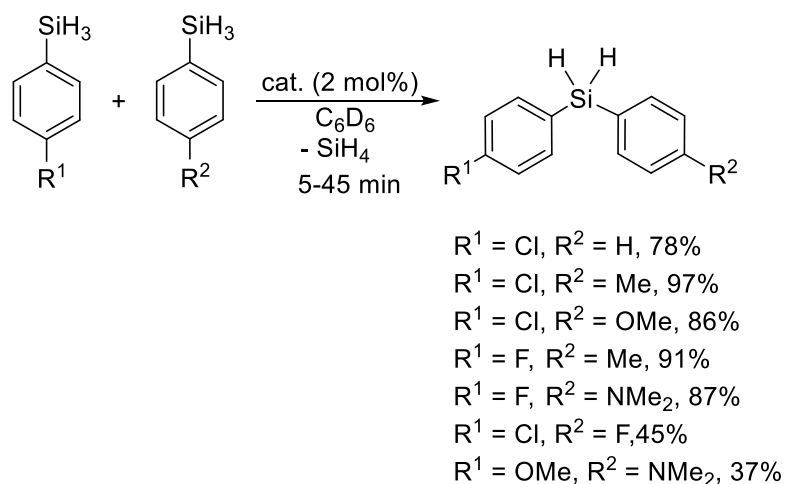
The catalytic reduction of several alkoxy-silanes was reported using the yttrium metallocene hydride $\text{Cp}'_2\text{YH}(\text{THF})$ in combination with HBpin (Scheme 107). [57] The steric bulk on the silyl group and the alkoxy group had a major influence on the reaction outcome, for example, $\text{Me}_2\text{PhSiOMe}$ yielded 57% silane product after 24h at 100°C , whereas the Et_3SiOMe substrate afforded only 22% silane. Similarly, $\text{Me}_2\text{PhSiOEt}$ provided only 11% of product and no reduction was observed for the corresponding OiPr compound. Dialkoxy-silanes R_2SiOMe_2 furnished fully hydrogenated products in moderate yields. Less sterically hindered Y complexes provided lower yields. Stoichiometric reactions between the initial Y hydride complex, alkoxy-silane and HBpin were conducted to gain insights into the mechanism (see Scheme 46). From these results it was proposed that the bridging $\text{Cp}'_2\text{Y}(\mu\text{-H})(\mu\text{-OMe})\text{Bpin}$ complex was the catalytically active species,

yielding the bis(methoxy) bridged complex $\text{Cp}'_2\text{Y}(\mu\text{-OMe})_2\text{Bpin}$ upon reaction with alkoxy silane. Further reaction of this complex with HBpin would lead to the catalyst regeneration.[57]



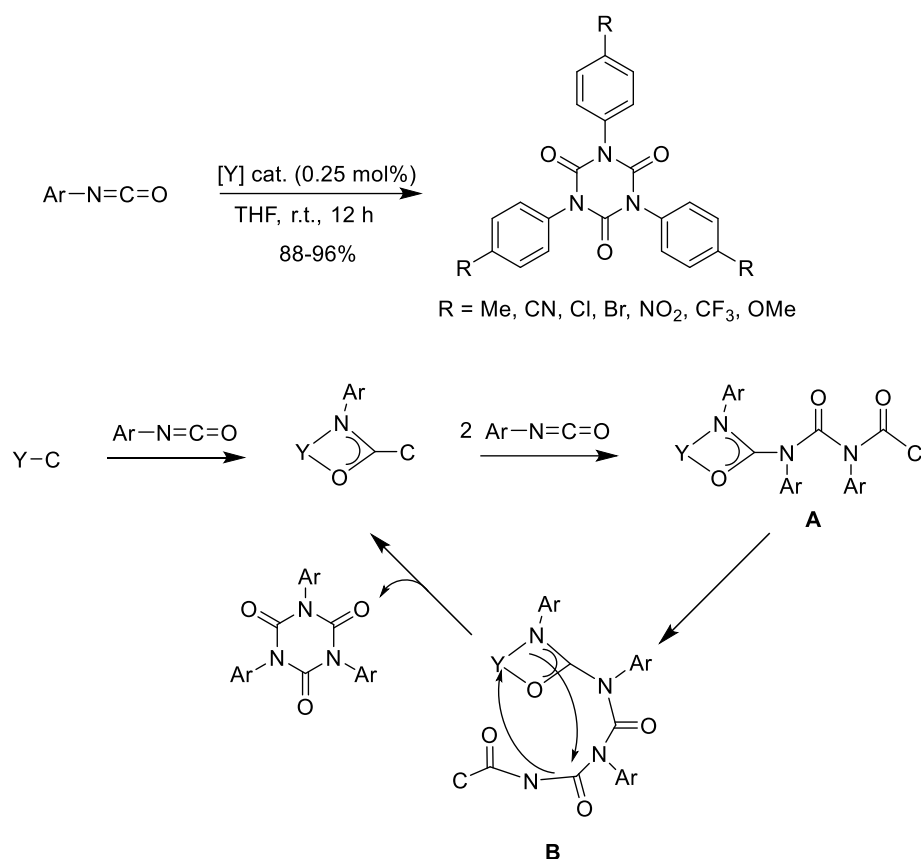
Scheme 107. Y-catalysed reduction of alkoxy silanes.[57]

The homo and cross-coupling of primary arylsilanes was catalyzed by the divalent (β -diketiminato)Yb alkyl and benzyl complexes shown in Scheme 7 at room temperature, with low catalyst loadings and short reaction times (Scheme 108).[17] The redistribution of arylsilanes with electron-withdrawing groups (p-Cl, p-F) was highly efficient, whereas electron-donating groups (p-Me, p-OMe, p-NMe₂) or ortho-substituents slowed down the process. The cross-coupling of arylsilanes bearing p-Cl or p-F substituents with electron-rich arylsilanes having p-Me, p-OMe, p-NMe₂ substituents was efficiently catalyzed by the Yb complexes, affording the diarylsilanes in high yields in only 5 minutes. It should be noted that a trivalent Yb complex could not catalyse the reaction and alkylsilanes were not suitable substrates. Further mechanistic insights were gained from DFT showing that hypervalent silicon intermediates and an Yb-aryl species play a key role. No metal oxidation or radicals were involved.[17]



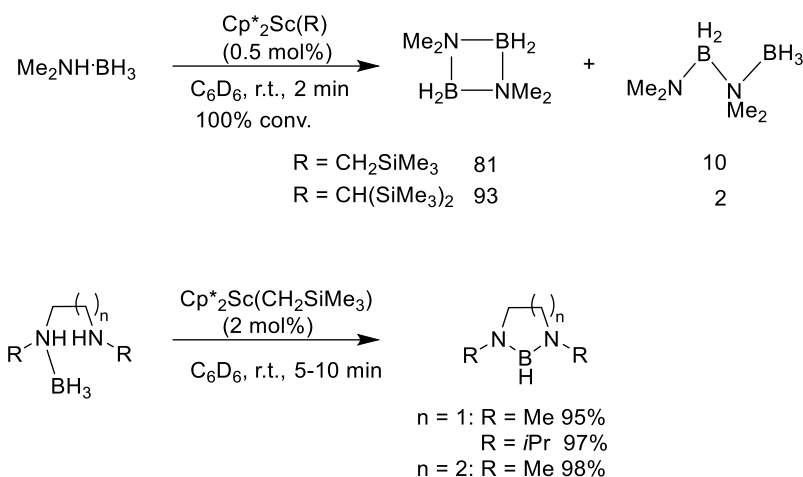
Scheme 108. Coupling of primary to secondary silanes.[17]

The trimerization of a wide range of aryl-isocyanates was catalysed by the silaamidinate Y dialkyl complex shown in Scheme 11.[23] Low catalyst loadings at room temperature provided the products in nearly quantitative yields, even with cyano, chloro, bromo, nitro, CF_3 and OMe groups in the para position (Scheme 109). Ortho-substituents led to a decrease in yield. A benzyl-isocyanate provided 56% yield, whereas alkyl-isocyanates were not suitable substrates. Mechanistically, after an initial insertion of the isocyanate into the Y-C bonds (see Schemes 11 and 109), further insertions should lead to the intermediates A and B which would undergo intramolecular cyclotrimerization to the final product and regeneration of the catalytic species.[23]



Scheme 109. Scope and mechanism of Y-catalysed cyclotrimerization of arylisocyanates.[23]

The dehydrogenation of dimethylaminoborane catalysed by scandium metallocene alkyl complexes Cp^*_2ScR ($\text{R} = \text{CH}_2\text{SiMe}_3$ or $\text{CH}(\text{SiMe}_3)_2$) afforded selectively the cyclic borazane compound $[\text{Me}_2\text{N-BH}_2]_2$ with TOF up to 100 min^{-1} (Scheme 110).[64] Variation of the catalyst using the corresponding Y or Lu complexes or the unsubstituted Cp_2ScR analogue led to lower reactivity and selectivity. For the even more challenging diamminoborane substrates, the $\text{Cp}^*_2\text{Sc}(\text{CH}_2\text{SiMe}_3)$ complex turned out to be the most efficient catalyst to access the cyclic NBN products in high yields. A β -H elimination of a β -agostic B-Sc complex might be involved in the mechanism as deduced from stoichiometric reactions between the Sc complex and dimethylaminoborane as shown in Scheme 58.[64]

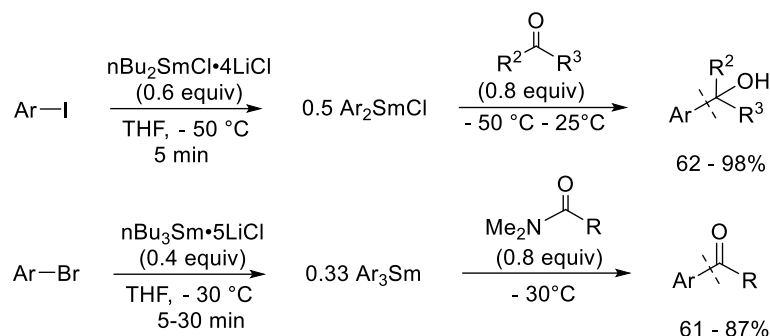


Scheme 110. Dehydrogenation of dimethylaminoborane and diaminoboranes using scandocene alkyl complexes.[Ln64]

2.12. ORGANOLANTHANIDES IN ORGANIC SYNTHESIS

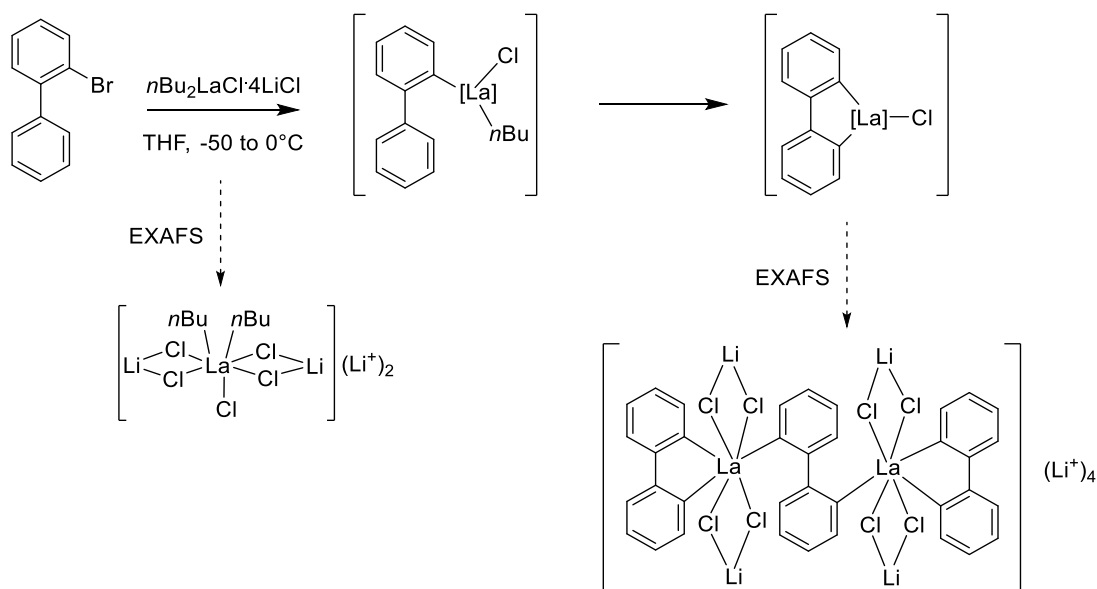
The reactivity of in-situ generated alkyl or aryllanthanide reagents has been found to be situated between the corresponding lithium and magnesium reagents, which is mainly due to the differences in electronegativity (Li 0.98, La 1.10, Ce 1.12, Sm 1.17, Mg 1.31). Various bis and trisalkyllanthanide reagents have been prepared and applied to halogen/metal exchange reactions, providing access to several transformations under mild conditions with good chemoselectivity and functional group tolerance.

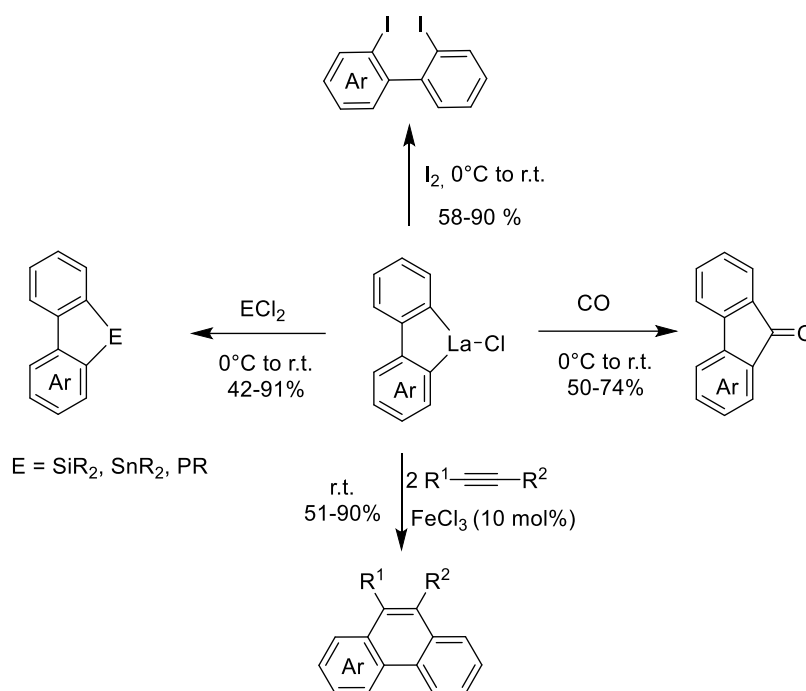
The formation of a $\text{Ce}(n\text{Bu})_3$ equivalent was obtained from the reaction of CeCl_3 with $n\text{BuLi}$ in THF at -30°C , as supported by low-temperature Raman spectroscopy. This intermediate reacted with three equivalents of different aryl and heteroaryl halides (Br, I) at -50°C to form in-situ $\text{Ce}(\text{aryl})_3$ complexes (Scheme 111). These reagents were successfully applied in the Zweifel olefination reaction, involving various cyclic and acyclic alkenyl boronic esters via a vinylborinate intermediate. High yields and E/Z ratios of up to 1:99 were obtained with stereodefined alkenyl boronate esters. Furthermore, halogen/metal exchange was also successful for vinyl and styryl halides providing $\text{Ce}(\text{vinyl})_3$ species which provided the Zweifel olefination in good yields and excellent stereospecificity when stereodefined organoboronic esters were employed. Finally, the in-situ prepared $\text{Ce}(\text{aryl})_3$ also underwent 1,2 addition to different bulky ketones affording the tertiary alcohols in high yields.[140]



Scheme 112. Use of alkylsamarium reagents for halogen/metal exchange leading to the 1,2-addition onto ketones and the acylation reaction with *N,N*-dimethylamides.[141]

Reaction of $\text{LaCl}_3 \cdot 2\text{LiCl}$ with two equivalents of $n\text{BuLi}$ in THF at -50°C gave access to the $n\text{Bu}_2\text{LaCl} \cdot 4\text{LiCl}$ reagent which reacted smoothly with different 2-bromobiaryl substrates to generate a cyclometalated lanthanum species via Br/La exchange and C-H activation.[142] In the case of 2-bromobiphenyl, the organometallic intermediate was studied by EXAFS and a proposed structure is shown in Scheme 113. This complex could be readily transformed with a range of electrophiles: reaction with iodine provided access to polyfunctional 2,2'-diiodobiaryls, whereas reaction with R_2SiCl_2 , R_2PCl or R_2SnCl_2 yielded the corresponding heterofluorenes. Exposure of the lanthanum complex to CO_2 afforded a series of fluoren-9-ones and, finally, reaction with alkynes under FeCl_3 catalysis gave access to phenanthrenes.[142]





Scheme 113. Synthesis and proposed structure by EXAFS of cyclometalated lanthanum species and further transformations.[142]

2.13. ORGANOLANTHANIDES IN MATERIALS SCIENCE

Tris(tetramethylcyclopentadienyl)samarium, $\text{Sm}(\text{C}_5\text{Me}_4\text{H})_3$, was used in an advanced chemical vapor synthesis method to obtain direct encapsulation of samarium single crystals within carbon-nano-onions (CNO) as shown by HRTEM and XRD analysis as well as Raman spectroscopy.[143] These structures were obtained by pyrolysis of the organometallic samarium complex in a quartz boat at 990°C for 15 min under a flow of argon in an electric furnace. It was proposed that the nucleation of CNO layers on the surface of crystalline Sm metal was favored by the high concentrations of carbon species created within the pyrolyzed hydrocarbon vapor of $\text{Sm}(\text{C}_5\text{Me}_4\text{H})_3$. The electrochemical performances of glassy carbon electrodes (GCE) modified by Sm-CNOs were studied by cyclic voltammetry and impedance spectroscopy, showing no significant difference with respect to a Fe_5C_2 -CNO-modified GCE. However, improved electron transfer kinetics were observed when compared to an unmodified GCE.

In the quest for improving low-temperature solid oxide fuel cells (LT-SOFCs), Pt-electrodes with an ultrathin (<10 nm) CeO_2 overlayer were fabricated via atomic layer deposition (ALD).[144] In this procedure, $\text{Ce}(\text{C}_5\text{H}_4\text{iPr})_3$ was evaporated at 150°C in a traveling mode type ALD system and the deposition process took place at 200°C in the reaction chamber. Water was used as the oxidant at room temperature. The best electrochemical results, including better thermal stability and improved performance, were

obtained with Pt-electrodes having CeO₂ overcoating resulting from at least five ALD cycles. Interestingly, the formed CeO₂ was O-deficient with an approximate ratio of Ce:O of 1:1.7 (Ce³⁺ : 67%; Ce⁴⁺ 33%), which turned out to be beneficial for the cathode reaction. Upon combination of such a cathode with an anodized aluminum oxide (AAO) substrate in a thin-film SOFC a high peak power density of 800 mW cm⁻² at 500 °C was obtained, which is among the best performances to-date for such devices.

The growth of nanoscale PrAlO₃ thin films on different substrates (SiO₂, SrTiO₃) using ALD processes was investigated.[145] The complex Pr(C₅H₄iPr)₃ (m.p. 53°C, decomposition temperature 353°C) was found to be a suitable precursor in combination with AlMe₃ and water to form amorphous PrAlO₃ films with smooth surfaces and little carbon impurities. These aluminum-rich films (Pr:Al atomic ratio of 1:1.2-1.4) were obtained by applying a 1:1 ratio of Pr(C₅H₄iPr)₃ to AlMe₃ pulses in an ALD window of 275-325°C and leading to a growth rate of around 1.7 Å/cycle. Interestingly, layers that were grown on (001)-oriented SrTiO₃ substrate afforded fully crystalline (001)-oriented PrAlO₃ films after annealing at 800°C for 3h. In contrast, in the case of native SiO₂ as substrate, the PrAlO₃ films remained amorphous even after annealing at 1000°C for 8h. These results show the importance of the atomic configuration at the interface of film and substrate for solid-phase epitaxy to occur.

A mechanistic study on the formation of scandium oxide thin films on hydroxyl-terminated oxidised Si(111) substrates was performed using the mixed ligand bis(methylcyclopentadienyl)(3,5-dimethylpyrazolate)scandium complex, Sc(C₅H₄Me)₂(Me₂pz), in combination with ozone in an ALD process. Following the reaction at 275°C by infrared spectroscopy provided evidence that the Sc precursor reacted not only with the surface hydroxyl groups but also with the SiO₂ layer to form a ScSi_xO_y interface layer. In the next step, oxidation with ozone afforded the formation of surface carbonates by combustion of the Cp groups of the chemisorbed O-ScCp₂ species, while some of the underlying silicon was also oxidised. During the next pulse of Sc precursor, the pyrazolate reacted with the surface carbonates affording the Sc-O-Sc bonds (Sc₂O₃ deposition), hence providing again a O-ScCp₂ surface. It was shown that the overall process was temperature dependant as the film growth was inferior at 225°C (2.18nm) than at 275°C (3.88nm) 20 cycles. It should be noted the deposition of some additional Sc₂O₃ and surface carbonates also resulted from gas phase reaction between the Sc precursor and residual water.[146]

A new synthetic method for EuCOT nanowires was developed for the investigation of the electronic and magnetic properties of this material.[147] Exposing simultaneously a pressure of 5×10^{-7} mbar of COT molecules with a flux of 1.9×10^{16} s⁻¹m⁻² Eu atoms for 105s, afforded a 60% coverage of a graphene/Ir(111) surface with EuCOT nanowire islands. In each wire, an alternating sequence of Eu²⁺ cations and COT²⁻ anions was observed, with each Eu²⁺ displaying η^8 -coordination to the neighbouring COT²⁻. XAS analysis confirmed the presence of divalent europium. The spin magnetic moment was determined to be $\mu_s = (7.0 \pm 0.6)\mu_B$ in agreement with a half-filled $4f^7$ configuration. X-ray magnetic circular dichroism (XMCD) measurements at various fields showed an open hysteresis loop at 5K, providing evidence for ferromagnetic coupling in EuCOT nanowires. In addition, STS measurements showed the insulating properties of EuCOT with a minor band gap of 2.3 eV. DFT calculations were in agreement with the experimental findings.

3 ACTINIDES

3.1. ACTINIDE CARBONYLS

The octacarbonyl ion complexes $[\text{An}(\text{CO})_8]^{+/-}$ (An = U, Th) have been prepared in the gas phase using a colinear tandem time-of-flight mass spectrometer, using pulsed laser ablation of metal target and 5-10% CO in He.[148] The mass data are shown in Figure 22. The octacarbonyl complexes were also characterised by mass-selected photodissociation spectroscopy. Assignments of the CO stretching frequencies were confirmed by isotopic labelling studies. The experimental CO stretching frequencies all occur at significantly longer wavelengths than free CO, the anionic species $[\text{Th}(\text{CO})_8]^-$ at 1865 and 1919 cm⁻¹, $[\text{U}(\text{CO})_8]^-$ at 1885 cm⁻¹ and the cationic $[\text{An}(\text{CO})_8]^+$ at An = Th 2074 cm⁻¹, An = U 2087 cm⁻¹. Quantum chemical calculations revealed that the thorium octacarbonyls had distorted octahedral D_{4h} equilibrium geometry with a $^2A_{1g}$ ground state for $[\text{Th}(\text{CO})_8]^+$ and a $^2B_{1u}$ ground state for $[\text{Th}(\text{CO})_8]^-$. The uranium octacarbonyls had cubic O_h equilibrium geometry with a $^6A_{1g}$ ground state for $[\text{U}(\text{CO})_8]^+$ and $^4A_{1g}$ ground state for $[\text{U}(\text{CO})_8]^-$. The neutral actinide octacarbonyl species were also calculated $[\text{An}(\text{CO})_8]$ (An = U, D_{4h} , $^5B_{1u}$; Th O_h , $^1A_{1g}$). The calculated C-O distances were found to be longer than free CO. The bond dissociation energies were rather high in all cases. Good agreement was observed between experimental and calculated CO stretching frequencies (although not all calculated bands were observed experimentally). The authors conclude that the bonding

picture in these octacarbonyl species is consistent with dominant 6d character, but with significant 5f participation, in both of the synergic bonding interactions with CO.[148]

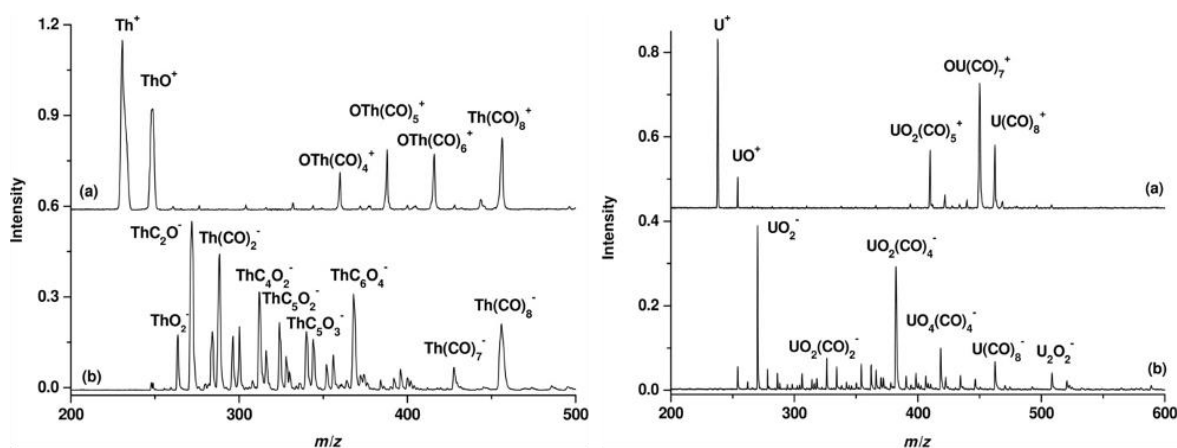
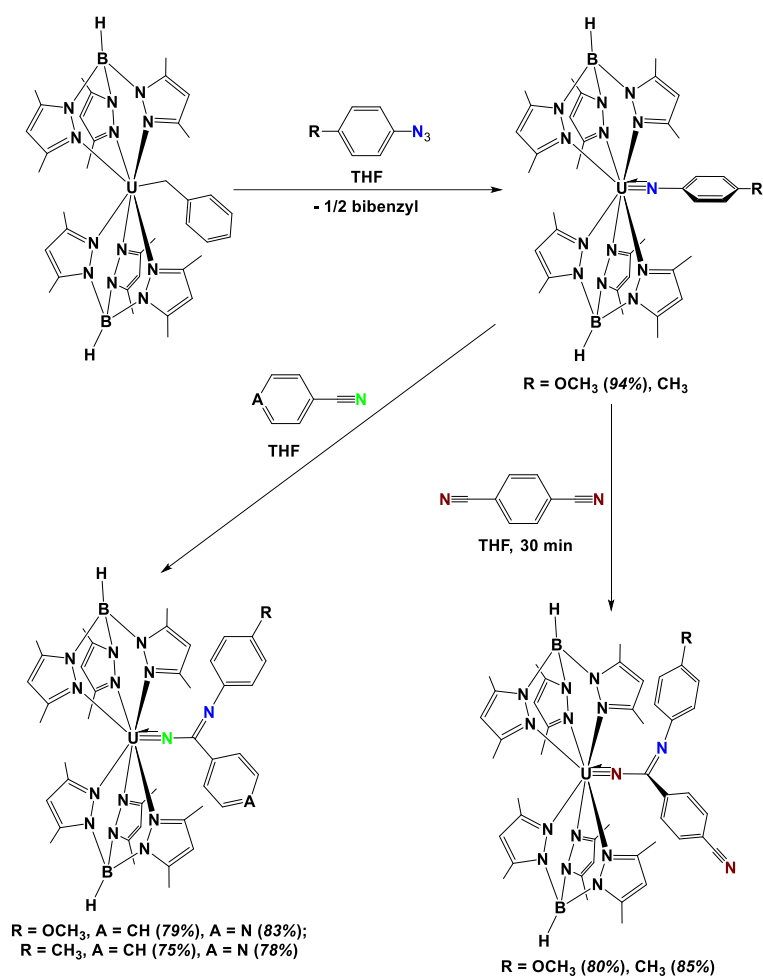


Figure 22. Mass spectra of thorium and uranium a) carbonyl cations and b) carbonyl anion complexes. Reproduced with permission from [148]. Copyright 2019 Wiley VCH.

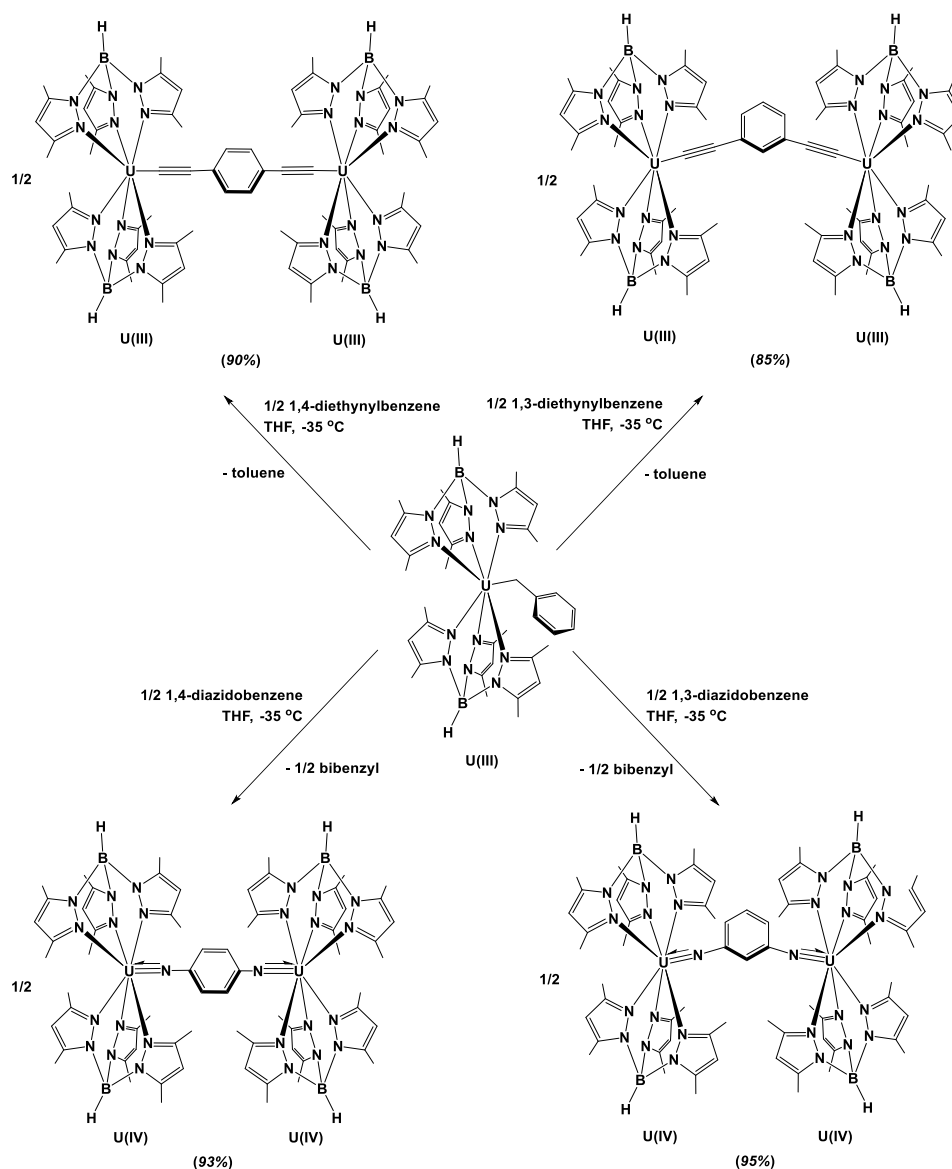
3.2 ACTINIDE HYDROCARBYLS

The U(IV) imido complexes $\text{Tp}^*_2\text{U}(=\text{N}-p\text{-RPh})$ ($\text{R} = \text{Me}$ or OMe) have been synthesised by reaction of $\text{Tp}^*_2\text{U}(\text{CH}_2\text{Ph})$ with the corresponding p -substituted phenyl azides, in THF solution in a 1:1 ratio. An analogous synthesis using azides with electron withdrawing groups on the aryl ring was unsuccessful. The reaction of these imido complexes with benzonitriles Ar-CN ($\text{Ar} = \text{Ph}$, py) in THF solution in a 1:1 ratio resulted in unusual κ^1 -coordinated uranium amidinate compounds $\text{Tp}^*_2\text{U}(=\text{N}-\text{C}\{=\text{N}-p\text{-RPh}\}\{\text{Ar}\})$ in excellent yields ($\text{R} = \text{OMe}$; $\text{Ar} = \text{Ph}$ 79%, py 83% and $\text{R} = \text{Me}$; $\text{Ar} = \text{Ph}$ 75%, py 78%). The reaction of the imido complexes with $\frac{1}{2}$ eq. terephthalonitrile in THF solution resulted in the isolation of the U(IV) amidinates $\text{Tp}^*_2\text{U}(=\text{N}-\text{C}(=\text{N}-p\text{-RPh})-p\text{-cyanobenzene})$, again in excellent yields ($\text{R} = \text{Me}$ 85% or OMe 80%) (Scheme 114). The unusual κ^1 -amidinate coordination was confirmed by single-crystal X-ray diffraction (XRD) data, and the $\text{U}=\text{N}$ bond distances in the amidinate complexes were consistent with other U(IV) imido complexes. The formation of the new κ^1 -amidinate complexes was proposed to proceed *via* a $[2\pi+2\pi]$ cycloaddition of the nitrile to the imido moiety, followed by a $[2\pi+2\pi]$ cycloreversion of the metallacycle to yield the amidinate complexes. The multiple bond metathesis reactivity of the U(IV) imido complexes with nitriles observed here diverges from that previously reported for uranium complexes.[149]



Scheme 114. The synthesis of bis-Tp*U(IV) imido complexes and bis-Tp*U(IV) κ^1 -amidinate complexes *via* nitrile metathesis. [149]

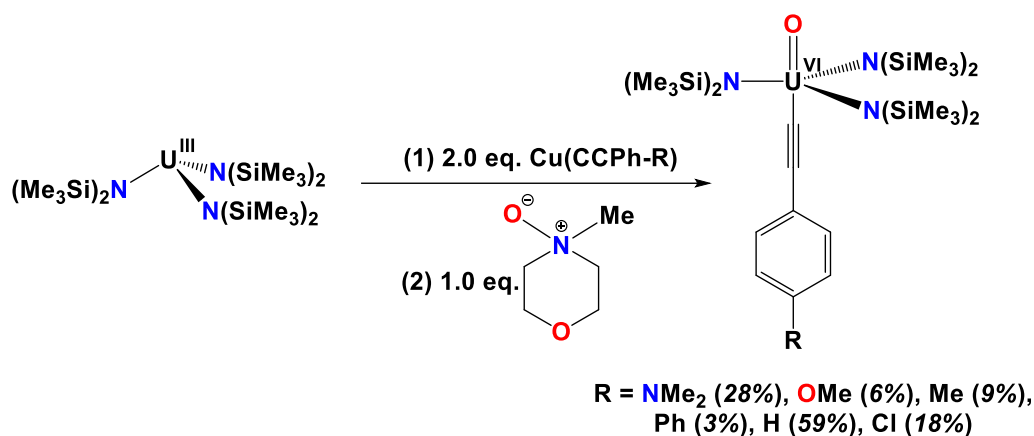
A series of bimetallic alkynyl and imido uranium complexes were synthesised to investigate communication between uranium centres. The uranium(III) benzyl compound $\text{Tp}^*_2\text{U}(\text{CH}_2\text{Ph})$ ($\text{Tp}^* = \text{hydro-tris}(1,3\text{-dimethylpyrazolyl})\text{borate}$) was reacted with 0.5 eq. 1,3-diethynylbenzene, 1,4-diethynylbenzene, 1,3-diazidobenzene or 1,4-diazidobenzene in THF at -35°C , to obtain the bridged uranium(III) dimers $\text{Tp}^*_2\text{UCC}(1,3\text{-C}_6\text{H}_4)\text{CCUTp}^*_2$ (85%), $\text{Tp}^*_2\text{UCC}(1,4\text{-C}_6\text{H}_4)\text{CCUTp}^*_2$ (90%) as green solids, and the uranium(IV) dimers $\text{Tp}^*_2\text{UN}(1,3\text{-C}_6\text{H}_4)\text{NUTp}^*_2$ (95%) and $\text{Tp}^*_2\text{UN}(1,3\text{-C}_6\text{H}_4)\text{NUTp}^*_2$ (93%) as bright red solids (Scheme 115). Spectroscopic data were consistent with U(III) and U(IV). An attempt to synthesise a similar datively bridged dimer by reaction of $[\text{Tp}^*_2\text{U}][\text{BPh}_4]$ with 1,4-dicyanobenzene resulted in isolation of coordination polymer $[\text{Tp}^*_2\text{U}(\text{NCPHCN})]_n[\text{BPh}_4]_n$. Spectroscopic, structural, computational, magnetic and electrochemical data established that there is no significant electronic communication between uranium ions.[150]



Scheme 115. Synthesis of dinuclear U(III) alkynyl and U(IV) imido aryl-bridged complexes. [150]

An experimental and computational study has probed covalency of the U–C bond in a series of uranium(VI) (aryl)acetylides, as a function of the electron donating or withdrawing groups on the acetylide. The degree of covalency was demonstrated to correlate well with ^{13}C NMR. The uranium(VI) acetylides $\text{UO}(\text{N}(\text{SiMe}_3)_2)_3(\text{CC}\{1,4\text{-C}_6\text{H}_4\}\text{R})$ ($\text{R} = \text{NMe}_2$ (28%), OMe (6%), Me (9%), Ph (3%), Cl (18%)) were synthesised by the reaction of $\text{U}(\text{N}(\text{SiMe}_3)_2)_3$ with 2 eq. $\text{Cu}(\text{CC}(1,4\text{-C}_6\text{H}_4)\text{R})$ ($\text{R} = \text{NMe}_2$, OMe , Me , Ph , Cl) in diethyl ether, followed by reaction with 1 eq. *N*-ethylmorpholine *N*-oxide (Scheme 116). The ^{13}C NMR spectra of the complexes showed that the C bound to uranium in the acetylide was significantly downfield shifted to between 390–410 ppm (*ca* 325 ppm difference from the parent alkynes). The magnitude of the downfield shift correlated well

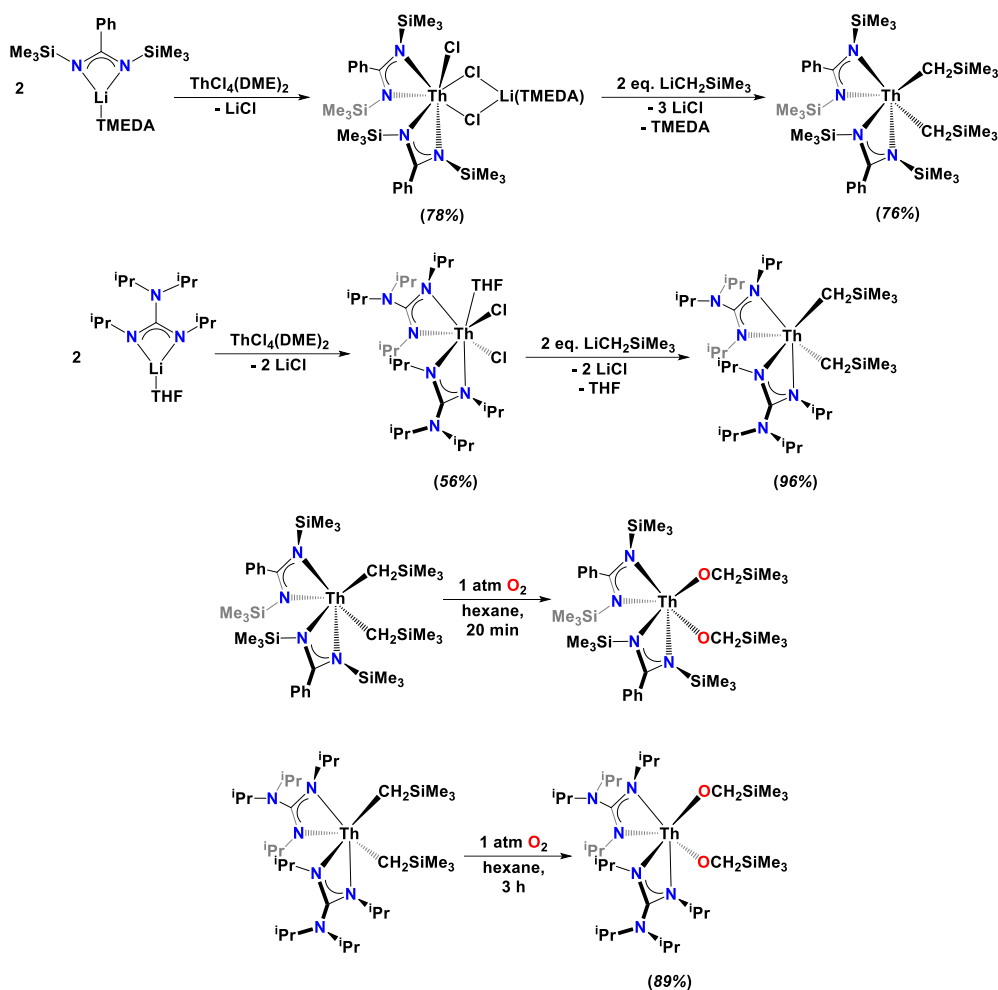
with the electron-donating ability of the *para* substituent of the aryl group ($\text{NMe}_2 > \text{OMe} > \text{Me} > \text{Ph} > \text{H} > \text{Cl}$). DFT computational analysis was applied to the system, including aryl groups with electron-withdrawing groups CN and NO_2 , which could not be synthesised. It was found that both the bond length and covalency of the U–C bond had a strong correlation with the experimentally determined and calculated ^{13}C NMR shift of the terminal carbon of the acetylide, and the electron donating or withdrawing ability of the *para* substituent. Magnetic susceptibility measurements of the complexes showed magnetic-field induced mixing of the singlet ground state of U(VI) with thermally inaccessible paramagnetic excited states. Therefore, the deshielding of the ^{13}C nucleus was proposed to derive from a combination of paramagnetic shift (driven by proximity to the metal centre) and spin-orbit effects (due to a Fermi-contact-type mechanism), enabling the ^{13}C NMR shift to serve as a simple and direct probe of the actinide-carbon bond covalency in the acetylides.[151]



Scheme 116. Synthesis of U(VI) (phenyl)acetylide complexes. [151]

The incorporation of dioxygen into thorium amidinate and guanidinate dialkyl complexes has been investigated. Thorium amidinate and guanidinate chloride complexes were synthesised by the reaction of $\text{ThCl}_4(\text{DME})_2$ with 2 eq. of the lithium amidinate salt $\text{Li}(\text{BTBA})(\text{TMEDA})$ (BTBA = *N,N'*-bis(trimethylsilyl)benzamidinate, TMEDA = tetramethylethylenediamine) or guanidinate salt $\text{Li}(\text{TIG})(\text{THF})$ (TIG = *N,N,N',N''*-tetraisopropylguanidinate) yielding $\text{ThCl}_3(\text{BTBA})_2\text{Li}(\text{TMEDA})$ (78%) and $\text{ThCl}_2(\text{TIG})_2(\text{THF})$ (56%) respectively. These were each reacted with 2 eq. of the lithium alkyl compound $\text{LiCH}_2\text{SiMe}_3$ to access $\text{Th}(\text{BTBA})_2(\text{CH}_2\text{SiMe}_3)_2$ (76%) and $\text{Th}(\text{TIG})_2(\text{CH}_2\text{SiMe}_3)_2$ (96%), as (Scheme 117). The reaction of $\text{Th}(\text{DTBA})_2(\text{CH}_2\text{SiMe}_3)_2$ with dry O_2 rapidly afforded the alkoxide $\text{Th}(\text{DTBA})_2(\text{OCH}_2\text{SiMe}_3)_2$ within 5 minutes, high solubility prevented bulk isolation but XRD data confirmed product formulation. The

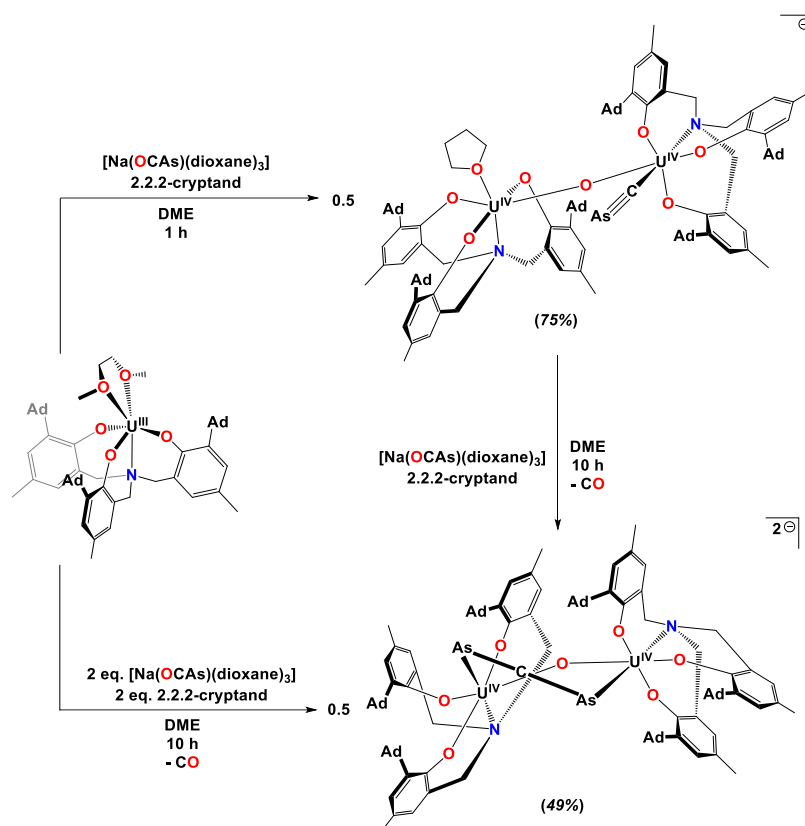
reaction of $\text{Th}(\text{TIG})_2(\text{CH}_2\text{SiMe}_3)_2$ with O_2 produced the less soluble $\text{Th}(\text{TIG})_2(\text{OCH}_2\text{SiMe}_2)_2$ in 89% yield. Preliminary mechanistic studies were undertaken and provided some evidence for a radical mechanism of O_2 incorporation.[Ac-11]



Scheme 117. Synthesis of thorium bis-amidinate and bis-guanidinate complexes and dioxygen incorporation to give thorium bis(alkoxides).[152]

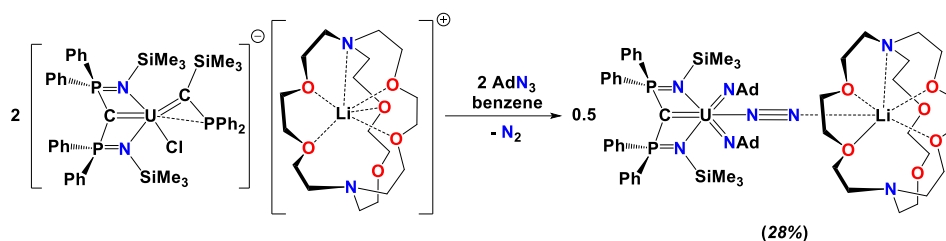
The synthesis and full characterisation of the first actinide complexes with terminal η^1 -coordinated cyarside ligands ($\text{C}\equiv\text{As}^-$) or bridging diarsallene ($\text{As}=\text{C}=\text{As}$)²⁻ have been reported. The addition of 2.2.2-cryptand (crypt) to a DME solution of $(\{\text{Ad,MeArO}\}_3\text{N})\text{U}^{\text{III}}(\text{DME})$ ($\{\text{Ad,MeArO}\}_3\text{N}^{3-}$ = tris(2-oxy-3-(1-adamantyl)-5-methylbenzyl)amine), followed by the addition of 1 eq. sodium arsaethynolate $\text{Na}(\text{OCAs})(\text{dioxane})_3$ resulted in the isolation of $[\text{Na}(\text{crypt})][(\{\text{Ad,MeArO}\}_3\text{N})(\text{THF})\text{U}^{\text{IV}}(\mu\text{-O})(\{\text{Ad,MeArO}\}_3\text{N})\text{U}^{\text{IV}}(\text{CAs})]$ (75%). Addition of 2 equivalents of sodium arsaethynolate to $(\{\text{Ad,MeArO}\}_3\text{N})\text{U}^{\text{III}}(\text{DME})$ resulted in the formation of $[\text{Na}(\text{crypt})]_2\{(\{\text{Ad,MeArO}\}_3\text{N})\text{U}^{\text{IV}}\}_2(\mu\text{-O})(\mu\text{-}\eta^1:\eta^1\text{-AsCAs})$ (49%), containing the bridging ligand 1,3-diarsallendiide (AsCAs^{2-}). It was also demonstrated that η^1 -cyarside complex

could be converted to the bridging diarsallene complex (Scheme 118). The spectroscopic data were consistent with other examples of $(C\equiv As)^-$ and $(AsCAs^{2-})$. [153]



Scheme 118. Synthesis of $[Na(crypt)][\{({}^{Ad,Me}ArO)_3N\}(THF)U^{IV}(\mu-O)\{({}^{Ad,Me}ArO)_3N\}U^{IV}(CAs)]$ and $[Na(crypt)]_2[\{({}^{Ad,Me}ArO)_3N\}U^{IV}]_2(\mu-O)(\mu-\eta^1:\eta^1-AsCAs)]$, and the synthetic interconversion route. [153]

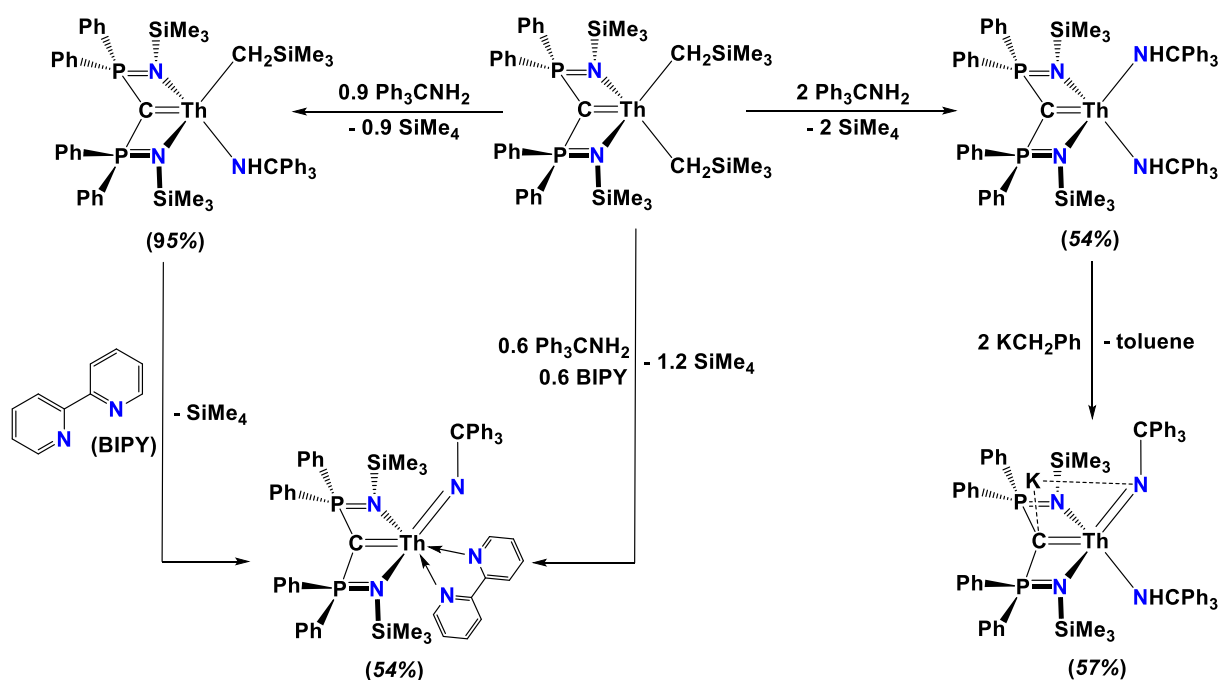
A remarkable uranium(V) carbene complex coordinated end-on to dinitrogen, has been synthesised and fully characterised. Reaction of the U(IV) carbene complex $[U(=C(PPh_2NSiMe_3)_2)(=C(SiMe_3)\{PPh_2\})(Cl)][Li(crypt)]$ (crypt = 2,2,2-cryptand) with 1-adamantylazide (AdN_3) in a 1:1 ratio, resulted in effervescence of N_2 and a blackish-red crystalline solid $U(=C(PPh_2NSiMe_3)_2)(=NAd)_2(\mu-\eta^1:\eta^1-N_2)Li(crypt)$ (28% by uranium content) (Scheme 119). Spectroscopic data and computational analysis are consistent with a U(V) $5f^1$ ion and with π -backbonding to the dinitrogen ligand. This highly unusual bonding situation was proposed to result from a combination of, the lithium coordination to dinitrogen and the unusually electron-rich U(V) ion resulting from complexation with three multiply-bonded π -donor ancillary ligands. [154]



Scheme 119. Synthesis of $U\{=C(PPh_2NSiMe_3)_2\}(=NAd)_2(\mu-\eta^1:\eta^1-N_2)(Li-2,2,2\text{-cryptand})$. [154]

An experimental and computational study has concluded that f-orbitals can have a structure-directing role in overlap-driven covalency in carbene-stabilised metalla-allene complexes. The reaction of $Th(=C(PPh_2NSiMe_3)_2)(CH_2SiMe_3)_2$ with 2 equivalents of Ph_3CNH_2 in toluene yielded first $Th(C(PPh_2NSiMe_3)_2)(NHCPH_3)_2$ (54%), then on reaction with 2 equivalents of KCH_2Ph in benzene, the novel thorium carbene-imido compound $[K][Th(C(PPh_2NSiMe_3)_2)(=NCPH_3)(NHCPH_3)]$ (57%). The reaction of 2,2'-bipyridine and $Th(=C(PPh_2NSiMe_3)_2)(CH_2SiMe_3)_2$ with Ph_3CNH_2 in a 1:1:1.6 ratio in toluene resulted in isolation of the thorium carbene-imido complex $Th(=C(PPh_2NSiMe_3)_2)(=NCPH_3)(\kappa^2\text{-}2,2'\text{-bipyridine})$ (54%). The reaction of $Th\{=C(PPh_2NSiMe_3)_2\}(CH_2SiMe_3)_2$ with Ph_3CNH_2 resulted in isolation of the thermally unstable intermediate $Th(=C(PPh_2NSiMe_3)_2)(CH_2SiMe_3)(NHCPH_3)$ (95%), the addition of 2,2'-bipyridine to this intermediate also yielded $Th(=C(PPh_2NSiMe_3)_2)(=NCPH_3)(\kappa^2\text{-}2,2'\text{-bipyridine})$ (Scheme 120). As was the case in the previously reported uranium analogues, these thorium carbene-imido complexes exhibited geometries where the imido ligand is *cis* to the carbene ligand. The nine model compounds $[C]=M=E$ ($[C] = C(PH_2NSiH_3)_2$; $M = Ce(IV), Th(IV), U(IV)$; $E = CMe_2, NMe, O$) were used in the computational analysis. The geometry optimisation used Gaussian-09 and two different density functional approximations and the total self-consistent field (SCF) energy surface was investigated by variation of the $[C]=M=E$ angle. In the cases, where $E = CMe_2$ or NMe , for all metals a *cis* geometry was preferred, and Th had the greatest preference for this geometry, followed by Ce and U. In the case where $E = O$, where $M = Ce$ or U a *trans* geometry was preferred, whereas for $M = Th$, a *cis* geometry was preferred. For all M, the energy barrier to *cis-trans* isomerisation was calculated to be lowest when $E = O$. Electrostatic potential (ESP) calculations performed on $([C]=Th)^{2+}$ agree with previously reported calculations on $([C]=U)^{2+}$, producing an anisotropic ESP field around Th which is *cis*-directing to a negatively charged incoming ligand. The origin of the *cis*-directing ESP was identified by natural localised molecular orbital (NLMO) analysis, which revealed that significant repulsion

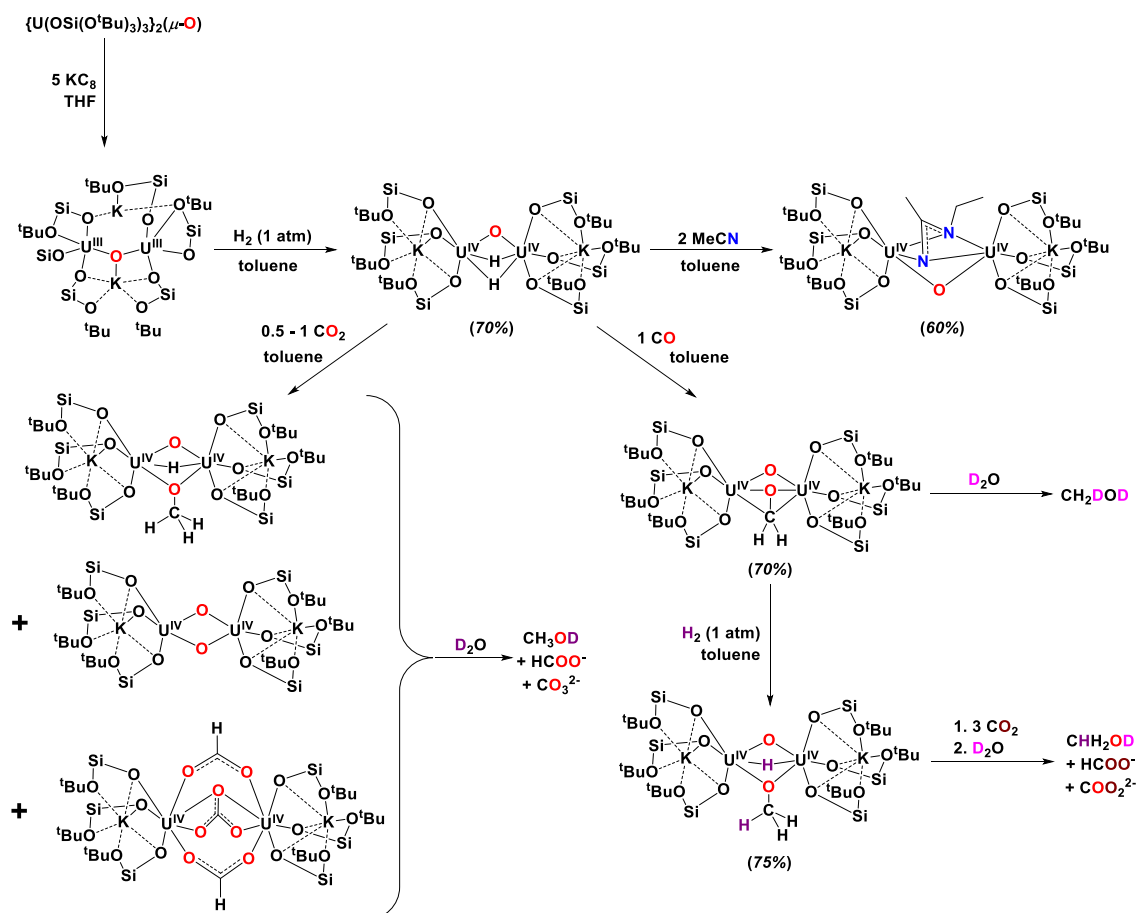
would occur between a negatively charged ligand approaching from the *trans* position and the electron occupying the NLMO. These ESP and NLMO data are consistent with the *cis* geometries adopted by most of the complexes studied, with the exception of the *trans* geometries preferred by Ce and U carbene-oxo compounds. Application of NLMO analysis to all [C]=M=E revealed significant variation in M-E σ -bonding. The metal contribution to the σ -bonding varied in the order Ce \approx U>Th and was predominantly of *d*-character, except in the cases where M = Ce, U and E = O, when the dominant contribution was of *f*-character. While NLMO assesses specific orbitals, the quantum theory of atoms in molecules (QTAIM) was used to form an overall picture of covalency. The electron density, total energy density and the delocalisation index all increase at the bond critical point for E = CMe₂ < NMe < O, and for any E, the order of increase in metals was Th < U < Ce. Thus, the bonding is most covalent in the uranium and cerium carbene-oxos. In conclusion, ESP effects were found to be dominant in the absence of other factors, for example, in all the thorium complexes where bonding is ionic the *cis*-directing effect of the build-up of charge at Th can be readily rationalised. The authors also make the important point that the *cis* geometry does not result from d-orbital participation in bonding, rather that the adoption of a *cis* geometry may result in d-orbital participation in bonding. This is clearly not the case for the uranium and cerium carbene-oxos, which have a *trans* geometry. The authors conclude that in these cases the orbital-driven overlap resulting from the very short covalent M=O bonds, overcomes the ionic ESP effect, resulting in *trans* geometry. Therefore, in these cases ionic and covalent effects are working against one another and the f-orbitals do have a structure-directing role, contrary to the long established bonding model FEUDAL (f's essentially unaffected, d's accommodate ligands).[155]



Scheme 120. Synthesis of Th(IV) carbene-imido complexes from $\text{Th}\{\text{=C}(\text{PPh}_2\text{NSiMe}_3)_2\}(\text{CH}_2\text{SiMe}_3)_2$. [155]

A remarkable stable dinuclear U(IV) dihydride complex has been isolated and its reactivity with CO_2 and CO/H_2 to form methoxide, and by hydrolysis methanol, has been demonstrated. Treatment of $\text{K}_2[(\text{U}(\text{OSi}(\text{O}^t\text{Bu})_3)_3)_2(\mu\text{-O})]$ with H_2 (at 1 atm) in toluene yielded the dihydride complex $\text{K}_2[(\text{U}(\text{OSi}(\text{O}^t\text{Bu})_3)_3)_2(\mu\text{-O})(\mu\text{-H})_2]$ (70%). Reaction of this dihydride complex with acetonitrile in toluene in a 1:2 ratio resulted in the reductive coupling of two acetonitrile molecules to form $\text{K}_2[(\text{U}(\text{OSi}(\text{O}^t\text{Bu})_3)_3)_2(\mu\text{-O})(\mu\text{-}\kappa^2\text{-NC}(\text{CH}_3)\text{-NCH}_2\text{CH}_3)]$ (60%). The reaction of the hydride complex with CO in toluene in a 1:1 ratio was carried out, resulting in the bridging oxomethylene complex $\text{K}_2[(\text{U}(\text{OSi}(\text{O}^t\text{Bu})_3)_3)_2(\mu\text{-O})(\mu\text{-CH}_2\text{O})]$ (70%). The subsequent hydrolysis of this complex with D_2O afforded methanol. Alternatively, the addition of H_2 at 1 atm in toluene yielded the methoxide complex $\text{K}_2[(\text{U}(\text{OSi}(\text{O}^t\text{Bu})_3)_3)_2(\mu\text{-O})(\mu\text{-H})(\mu\text{-OCH}_3)]$ (75%). The reaction of the methoxide complex with CO_2 and subsequent hydrolysis with D_2O produced a mixture of formate, carbonate and methanol, unambiguously verifying the mixed bridging hydride-methoxide formulation. The dihydride complex $\text{K}_2[(\text{U}(\text{OSi}(\text{O}^t\text{Bu})_3)_3)_2(\mu\text{-O})(\mu\text{-H})_2]$ was also reacted with 0.5-1 eq. CO_2 , giving a mixture of three uranium species, the methoxide $\text{K}_2[(\text{U}(\text{OSi}(\text{O}^t\text{Bu})_3)_3)_2(\mu\text{-O})(\mu\text{-H})(\mu\text{-OCH}_3)]$, the *bis*-oxo bridged $\text{K}_2[(\text{U}(\text{OSi}(\text{O}^t\text{Bu})_3)_3)_2(\mu\text{-O})_2]$ and the mixed formate-carbonate compound $\text{K}_2[(\text{U}(\text{OSi}(\text{O}^t\text{Bu})_3)_3)_2(\mu\text{-CO}_3)(\mu\text{-HCOO})_2]$. Hydrolysis of the reaction mixture resulted in isolation of methanol, formate and

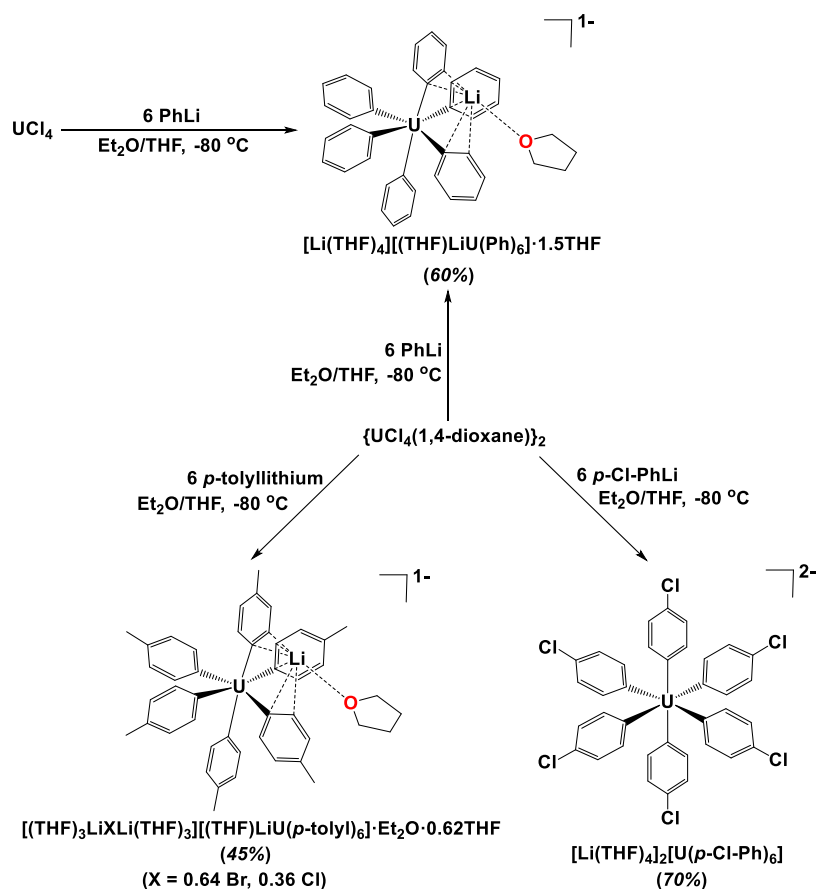
carbonate products. The reactions are shown in Scheme 121. The combination of the supporting siloxide ligand environment and the oxo-bridged uranium centres uniquely enable this exciting small molecule reduction and functionalisation chemistry, which is significantly different to that seen for uranium(III) and (IV) in other ligand environments.[156]



Scheme 121. Synthesis of $K_2\{U(OSi(O^tBu)_3)_2(\mu-O)(\mu-H)_2\}$ and subsequent reactions with CO/H_2 and CO_2 . Only the $-O^tBu$ groups bound to the metals are shown. [156]

The first examples of structurally-characterised uranium homoleptic aryl complexes in the U(IV) oxidation state have been reported. The reaction of UCl_4 with 6 eq. $ArLi$ ($Ar = Ph$, p -tolyl, p -Cl-Ph) in a cold Et_2O/THF solution enabled the isolation of $[Li(THF)_4][[(THF)LiU(Ph)_6] \cdot 1.5(THF)$ (60%), $[(THF)_3LiXLi(THF)_3][[(THF)LiU(p\text{-tolyl})_6] \cdot Et_2O \cdot 0.62(THF)$ ($X = 0.64 \text{ Br}, 0.36 \text{ Cl}$) (45%) and $[Li(THF)_4]_2[U(p\text{-Cl-Ph})_6]$ (70%), (Scheme 122). The complexes were fully characterised, including determination of their solid-state molecular structures by single-crystal XRD. The electronic structure of the complexes was investigated by magnetic circular dichromism and computational analysis.

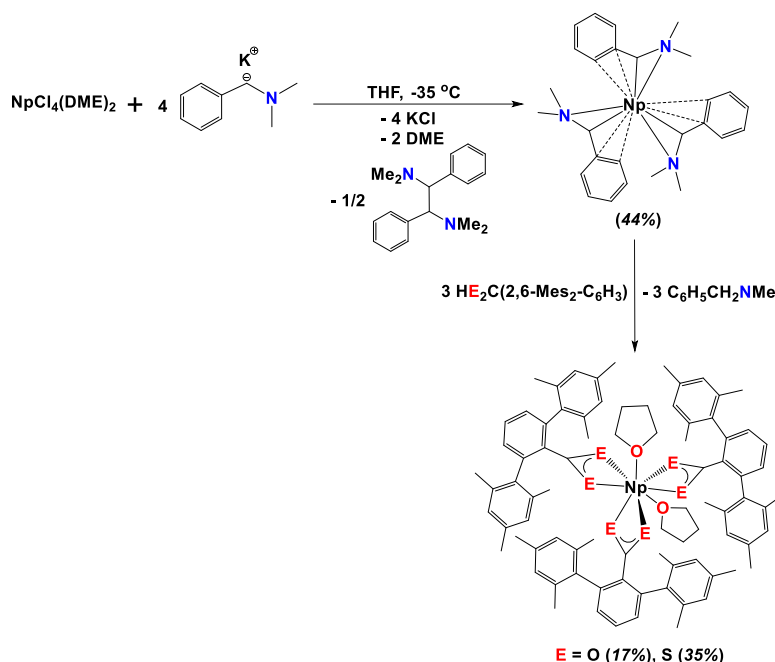
The covalency of the U-C bonding in $[\text{U}(\text{Ar})_6]^{2-}$ was found to be more covalent than the previously studied $[\text{Th}(\text{Ph})_6]^{2-}$. [157]



Scheme 122. Synthesis of U(IV) homoleptic aryl complexes with phenyl, *p*-tolyl and *p*-Cl-phenyl ligands. The independent cations of the complexes have been omitted for clarity. [157]

The synthesis, full characterisation and reactivity of the first transuranic hydrocarbyl Np(III) complex has been reported. The reaction of Np(IV) precursor $\text{NpCl}_4(\text{DME})_2$ (DME = dimethoxyethane) with 4 eq. $\text{K}[\text{Me}_2\text{NC}(\text{H})\text{C}_6\text{H}_5]$ in a cold THF solution resulted in the isolation of the Np(III) complex $\text{Np}(\eta^4\text{-Me}_2\text{NC}(\text{H})\text{C}_6\text{H}_5)_3$ (44%), with concomitant elimination of reductively coupled ligand (Scheme 123). The solid-state-molecular structure of $\text{Np}(\eta^4\text{-Me}_2\text{NC}(\text{H})\text{C}_6\text{H}_5)_3$ was determined by single-crystal XRD and shown to be analogous to the previously reported U(III) analogue. The utility of $\text{Np}(\eta^4\text{-Me}_2\text{NC}(\text{H})\text{C}_6\text{H}_5)_3$ as a precursor to other Np(III) complexes was demonstrated by reaction with 3 eq. $\text{HE}_2\text{C}(2,6\text{-Mes}_2\text{-C}_6\text{H}_3)$ (E = O, S; Mes = 1,3,5-trimethylbenzyl) in a 1:3 ratio, which yielded Np(III) carboxylate and thiocarboxylate products ($\{2,6\text{-Mes}_2\text{-C}_6\text{H}_3\}\text{CE}_2)_3\text{Np}(\text{THF})_2$ (E = O, 17%; S, 35%) (Scheme 123). This reactivity is divergent from the U(III) analogue, which oxidises under analogous conditions. The magnetism of

$(\{2,6\text{-Mes}_2\text{-C}_6\text{H}_3\}\text{CE}_2)_3\text{Np}(\text{THF})_2$ was investigated and the larger magnetic moment found for the complex where $\text{E} = \text{O}$, was attributed to the larger crystal field splitting expected for $\text{E} = \text{O}$, in comparison to $\text{E} = \text{S}$. [158]



Scheme 123. Synthesis of $\text{Np}[\eta^4\text{-Me}_2\text{NC}(\text{H})\text{C}_6\text{H}_5]_3$ and $(\{2,6\text{-Mes}_2\text{-C}_6\text{H}_3\}\text{CE}_2)_3\text{Np}(\text{THF})_2$ ($\text{E} = \text{O}, \text{S}$). [158]

The bonding and electronic structure in the ThCO and OThC molecules has been investigated *via* multireference computational calculations. The authors find that in the linear ThCO it was shown that the carbonyl ligand partakes in classical π -backbonding (Figure 23). In the bent OThC molecule, the bonding was calculated to be more traditionally ionic, with either one or no electrons residing in the valence orbitals of Th. The interconversion between the two isomers was also investigated, particularly as a function of the O-X-C angle, where X is the midway point of the Th-C bond. It was found that a relatively low energy barrier was required for the interconversion. The authors compared these data to data for TiCO and OTiC , where Ti is considered as isoelectronic with Th, finding that the energy barrier was lower in the case of Th, and the reaction was significantly less exothermic. [159]

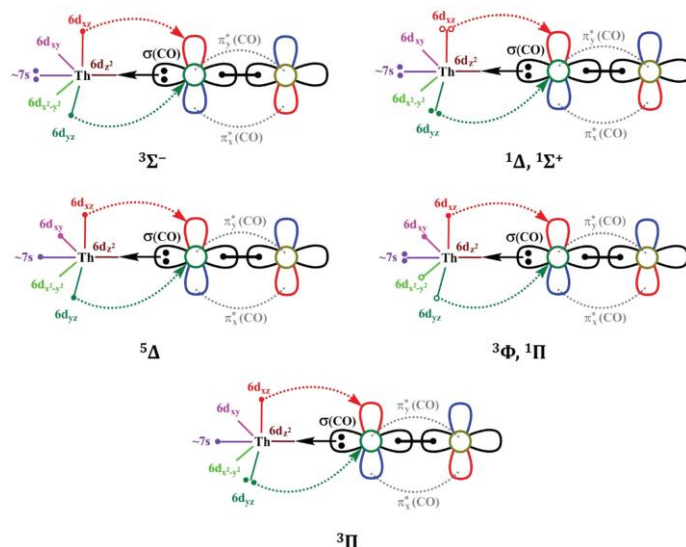
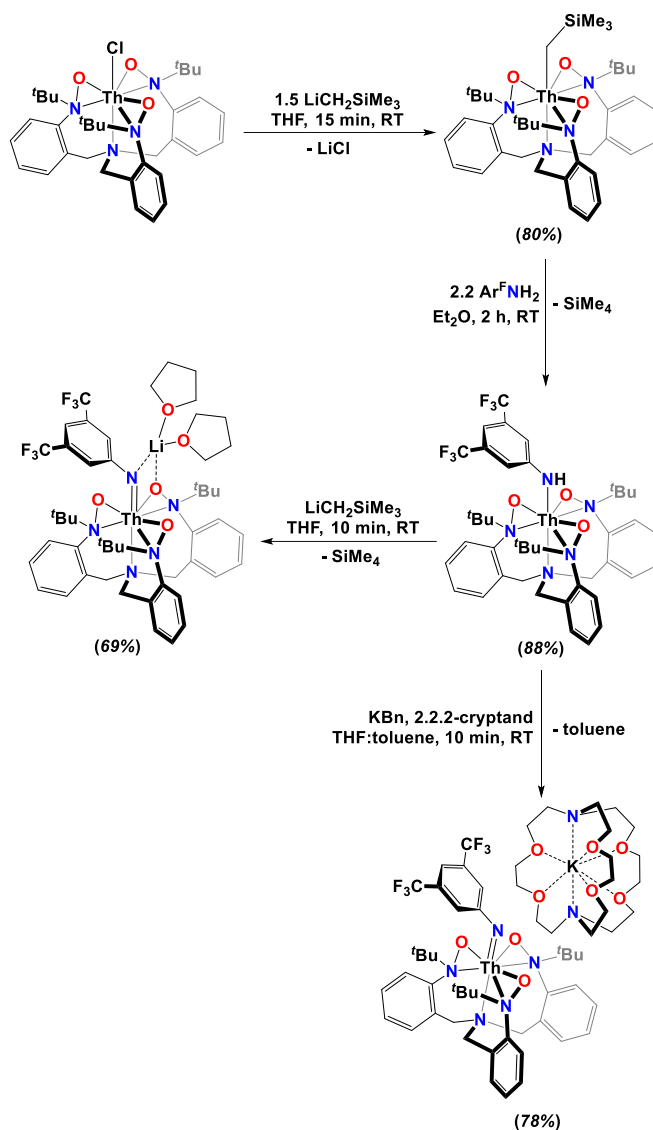


Figure 23. Proposed valence-bond-Lewis diagrams for the seven lowest states of ThCO, highlighting the interactions between Th and CO. Reprinted with permission [159]. Copyright 2019 the Owner Societies.

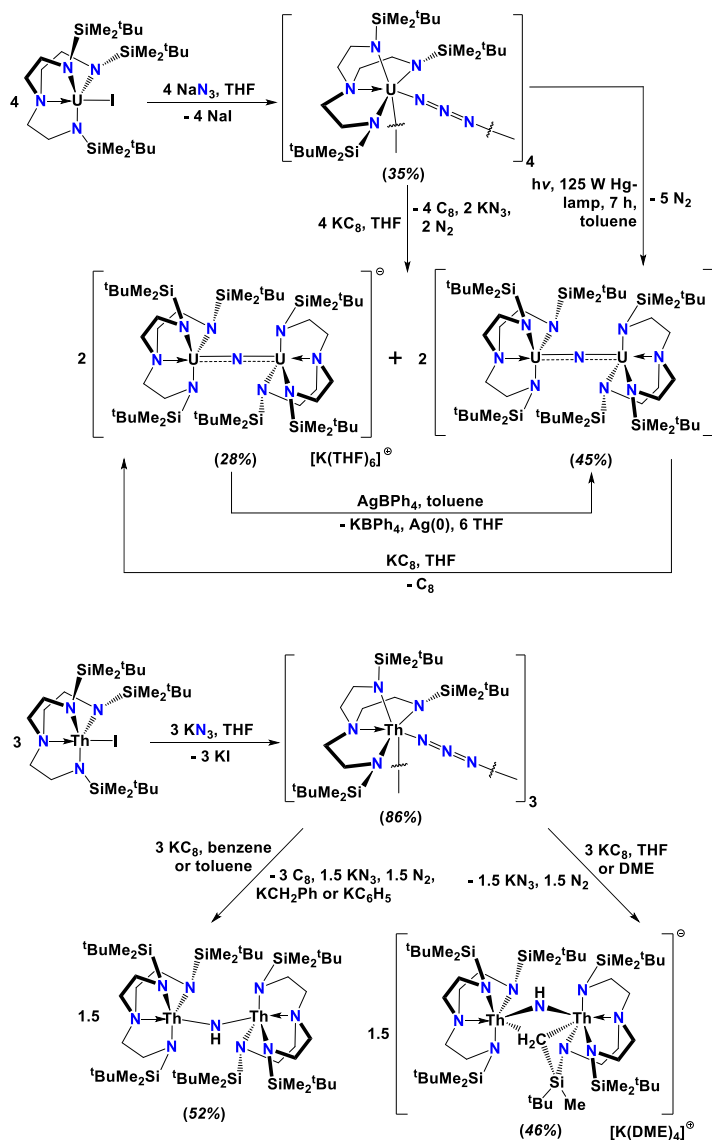
The differences in the bonding and reactivity of Th(IV) and Ce(IV) imido complexes has been investigated, with quantification of the relative differences in covalency and basicity. The reaction of ThCl(TriNOx) (TriNOx³⁻ = tris(2-tertbutylhydroxylamino)benzylamine) with 1.5 eq. LiCH₂SiMe₃ in THF formed the hydrocarbyl complex Th(TriNOx)(CH₂SiMe₃) (80%). This was reacted with 2.05 eq. 3,5-bis(trifluoromethyl)aniline (Ar^FNH₂) to form the anilide Th(TriNOx)(Ar^FNH) (88%). Deprotonation of the anilide by LiCH₂SiMe₂ accessed the bent terminal imido complex Th(=NAr^F)(TriNOx)Li(THF)₂ (69%). Alternatively, the reaction of Th(TriNOx)(Ar^FNH) with KBn in the presence of 2,2,2-cryptand (crypt) yielded the same terminal imido complex but as an ion pair [K(crypt)][Th(=NAr^F)(TriNOx)] (78%). These reactions are shown in Scheme 124. A combination of crystallography and computational analysis, in comparison to analogous Ce(IV) complexes, indicated that the Th=N bond had significantly less covalent character than that of the Ce=N bond, in contrast to generally accepted lanthanide and actinide trends. The pK_a of the thorium imido complexes was determined to be 28.6(3) by ¹H NMR titrations, while the less basic cerium imido complexes had a pK_a of 25.2(2). This large difference was supported by experimental observations. The imido-transfer reaction of [K(crypt)][Th(=NAr^F)(TriNOx)] with [Ce(THF)(TriNOx)][BAR^F] resulted in the reduction of Ce(IV) to Ce(III) as [Ce(THF)(TriNOx)], elimination of [K(crypt)][BAR^F], and H-atom abstraction resulting in reprotonation of the thorium imido complex to the anilide Th(TriNOx)(Ar^FNH). [160]



Scheme 124. Synthesis of TriNOx bound Th(IV) imido complexes. [160]

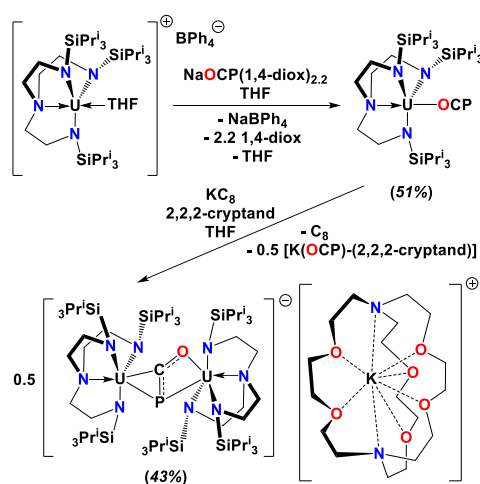
The synthesis of uranium and thorium azides and their subsequent reduction chemistry have been reported, specifically the formation of robust diuranium nitrides and some evidence for transient dithorium nitride species. The reaction of $\text{M}(\text{Tren}^{\text{DMBS}})(\text{I})$ ($\text{M} = \text{U}$, Th; $\text{Tren}^{\text{DMBS}} = \{\text{N}(\text{CH}_2\text{CH}_2\text{NSiMe}_2\text{tBu})_3\}^{3-}$) with NaN_3 or KN_3 respectively in a 1:1 ratio in THF to yielded rare actinide molecular square and triangle complexes $\{\text{M}(\text{Tren}^{\text{DMBS}})(\mu\text{-N}_3)\}_n$ ($\text{M} = \text{U}$ 35%, $n = 4$; Th 86%, $n = 3$). Reduction of $\{\text{U}(\text{Tren}^{\text{DMBS}})(\mu\text{-N}_3)\}_4$ with KC_8 in THF in a 1:1 ratio resulted $[\{\text{U}(\text{Tren}^{\text{DMBS}})\}_2(\mu\text{-N})][\text{K}(\text{THF})_6]$ and $\{\text{U}(\text{Tren}^{\text{DMBS}})\}_2(\mu\text{-N})$ in poor yields of 28% and 14%, respectively. The nitride complex $\{\text{U}(\text{Tren}^{\text{DMBS}})\}_2(\mu\text{-N})$ was isolated separately in good yields (45%) by photolysis of $\{\text{U}(\text{Tren}^{\text{DMBS}})(\mu\text{-N}_3)\}_4$ in toluene. The nitride complexes $[\{\text{U}(\text{Tren}^{\text{DMBS}})\}_2(\mu\text{-N})][\text{K}(\text{THF})_6]$ and $\{\text{U}(\text{Tren}^{\text{DMBS}})\}_2(\mu\text{-N})$ can be reversibly inter-converted by oxidation with AgBPh_4 in toluene and reduction with KC_8 in THF, respectively. The UNU cores showed no evidence of C–H bond

activation as a result of redox chemistry. The assignment of the oxidation states as U(IV)/U(IV) and U(IV)/U(V) in $[\{U(\text{Tren}^{\text{DMBS}})\}_2(\mu\text{-N})][\text{K}(\text{THF})_6]$ and $\{U(\text{Tren}^{\text{DMBS}})\}_2(\mu\text{-N})$ were verified by magnetic measurements and EPR. In contrast, the reduction of $\{\text{Th}(\text{Tren}^{\text{DMBS}})(\mu\text{-N}_3)\}_3$ with KC_8 in benzene/toluene or THF in a 1:1 ratio yielded C-H activation products $\{\text{Th}(\text{Tren}^{\text{DMBS}})\}_2(\mu\text{-NH})$ or $[\{\text{Th}(\text{Tren}^{\text{DMBS}})\}\{\text{Th}(\text{N}(\text{CH}_2\text{CH}_2\text{NSiMe}_2^t\text{Bu})_2\text{CH}_2\text{CH}_2\text{NSi}(\mu\text{-CH}_2)\text{Me}^t\text{Bu})\}(\mu\text{-NH})][\text{K}(\text{DME})_4]$ in moderate yields 52% and 46% respectively and alkyl byproducts (Scheme 125). Computational studies revealed a more polar, reactive and basic nitride in the transient ThNTh fragments $\{\text{Th}(\text{Tren}^{\text{DMBS}})\}_2(\mu\text{-N})^-$ than $\{U(\text{Tren}^{\text{DMBS}})\}_2(\mu\text{-N})^-$, and $\sigma > \pi$ energies for all the bridging nitride bonds consistent with terminal uranium nitrides and uranyl containing very short U–N or U–O distances.[161]



Scheme 125. Synthesis of actinide azide and nitride complexes. [161]

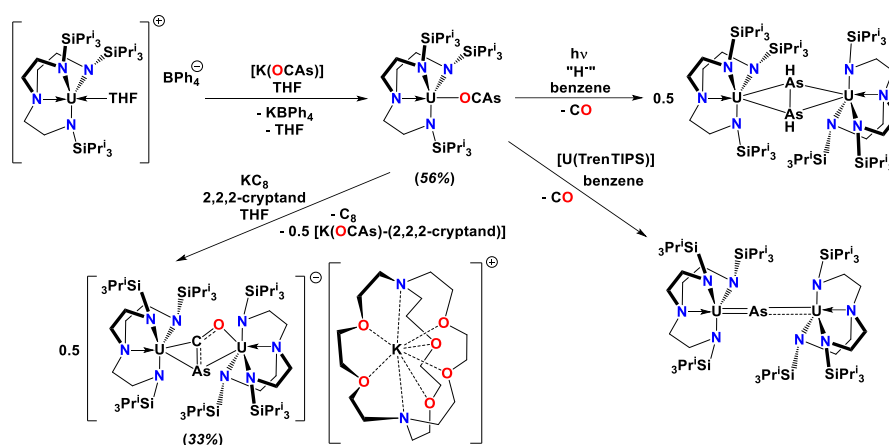
A bimetallic uranium complex containing an unprecedented trapped radical dianion of the phosphoethynolate ($\text{OCP}^{2-\bullet}$) ligand has been reported. The reaction of $[\text{U}(\text{Tren}^{\text{TIPS}})(\text{THF})][\text{BPh}_4]$ ($\text{Tren}^{\text{TIPS}} = \text{N}(\text{CH}_2\text{CH}_2\text{NSi}^i\text{Pr}_3)_3$) with $\text{NaOCP}(\text{1,4-dioxane})_{2,2}$ in THF in a 1:1 ratio yielded $\text{U}(\text{Tren}^{\text{TIPS}})(\text{OCP})$ (51%). The subsequent reaction of $\text{U}(\text{Tren}^{\text{TIPS}})(\text{OCP})$ with KC_8 and 2,2,2-cryptand in THF in a 1:1:1 ratio resulted in the isolation of $[(\text{U}(\text{Tren}^{\text{TIPS}}))_2(\mu\text{-}\eta^2(\text{OP})\text{:}\eta^2(\text{CP})\text{-OCP})][\text{K}(\text{2,2,2-cryptand})]$ (43%) (Scheme 126). The molecular structure of $[(\text{U}(\text{Tren}^{\text{TIPS}}))_2(\mu\text{-}\eta^2(\text{OP})\text{:}\eta^2(\text{CP})\text{-OCP})][\text{K}(\text{2,2,2-cryptand})]$ displayed a bridging highly reduced phosphoethynolate ligand, with a very acute O-C-P angle of 127° with a short C–O bond compared and a lengthened C–P bond consistent with reduction. The spectroscopic data, particularly SQUID magnetometry and EPR, and quantum chemical calculations were consistent with a mixed-valence U(III)/U(IV) oxidation state and ($\text{OCP}^{2-\bullet}$). Computational analysis of the molecule showed reduced ligand bond orders consistent with significant charge transfer to $\text{OCP}^{2-\bullet}$ and even some carbene character to the donor-acceptor interaction between uranium and the $\text{OCP}^{2-\bullet}$ ligand.[162]



Scheme 126. Synthesis of a bimetallic uranium complex for the trapping of highly reduced form of the phosphoethynolate species. [162]

The synthesis of the first ever isolable actinide complex of the 2-arsa-ethynolate anion, has also been reported, and its reactivity investigated. The synthesis of $\text{U}(\text{Tren}^{\text{TIPS}})(\text{OCAs})$ (56%) ($\text{Tren}^{\text{TIPS}} = \text{N}(\text{CH}_2\text{CH}_2\text{NSi}^i\text{Pr}_3)_3$) was achieved by reaction of $[\text{U}(\text{Tren}^{\text{TIPS}})(\text{THF})][\text{BPh}_4]$ with $[\text{K}(\text{OCAs})]$ in THF in a 1:1 ratio. The crystal structure of $\text{U}(\text{Tren}^{\text{TIPS}})(\text{OCAs})$ was consistent with the previously synthesised $\text{U}(\text{Tren}^{\text{TIPS}})(\text{OCP})$ and other uranium-Tren complexes. Photolysis of $\text{U}(\text{Tren}^{\text{TIPS}})(\text{OCAs})$ in a benzene solution, resulted in loss of CO and abstraction of a proton from solvent to form the diuranium

complex $(U(\text{Tren}^{\text{TIPS}}))_2(\mu\text{-}\eta^2\text{:}\eta^2\text{-As}_2\text{H}_2)$. It is of note that this reactivity was not observed for the isoelectronic $U(\text{Tren}^{\text{TIPS}})(\text{OCP})$. Whereas, the reduction of $U(\text{Tren}^{\text{TIPS}})(\text{OCAs})$ by the U(III) species $U(\text{Tren}^{\text{TIPS}})$ in benzene in a 1:1 ratio also resulted in decarbonylation, affording an unstable mixed-valence U(IV)/U(V) complex $\{U(\text{Tren}^{\text{TIPS}})\}_2(\mu\text{-As})$. Neither of these products was isolable in significant quantities. In a similar manner to the isoelectronic OCP⁻ ligand, the reaction of $U(\text{Tren}^{\text{TIPS}})(\text{OCAs})$ with KC_8 in the presence of 2,2,2-cryptand in THF in a 1:1:1 ratio, resulted in the trapping of a highly bent and reduced OCAs²⁻ ligand in the compound $[(U(\text{Tren}^{\text{TIPS}}))_2(\mu\text{-}\eta^2(\text{OAs})\text{:}\eta^2(\text{CAs})\text{-OCAs})][\text{K}(2,2,2\text{-cryptand})]$ (33%), without fragmentation of the O-C-As unit (Scheme 127). X-ray crystallography revealed that the arsaethynolate ligand was bent, with the most acute O-C-As angle ever observed of 128°. EPR spectroscopy and SQUID magnetometry confirmed that the compound had diuranium(IV) character, in contrast to $[(U(\text{Tren}^{\text{TIPS}}))_2(\mu\text{-}\eta^2(\text{OP})\text{:}\eta^2(\text{CP})\text{-OCP})][\text{K}(2,2,2\text{-cryptand})]$, which had some U(III) character. The authors attribute this to the greater electron accepting ability of the OCAs unit in comparison to the OCP unit. Quantum chemical calculations of the bonding revealed that the highly-reduced arsaethynolate compound also exhibited some carbene-like character, with weak π -backbonding.[163]

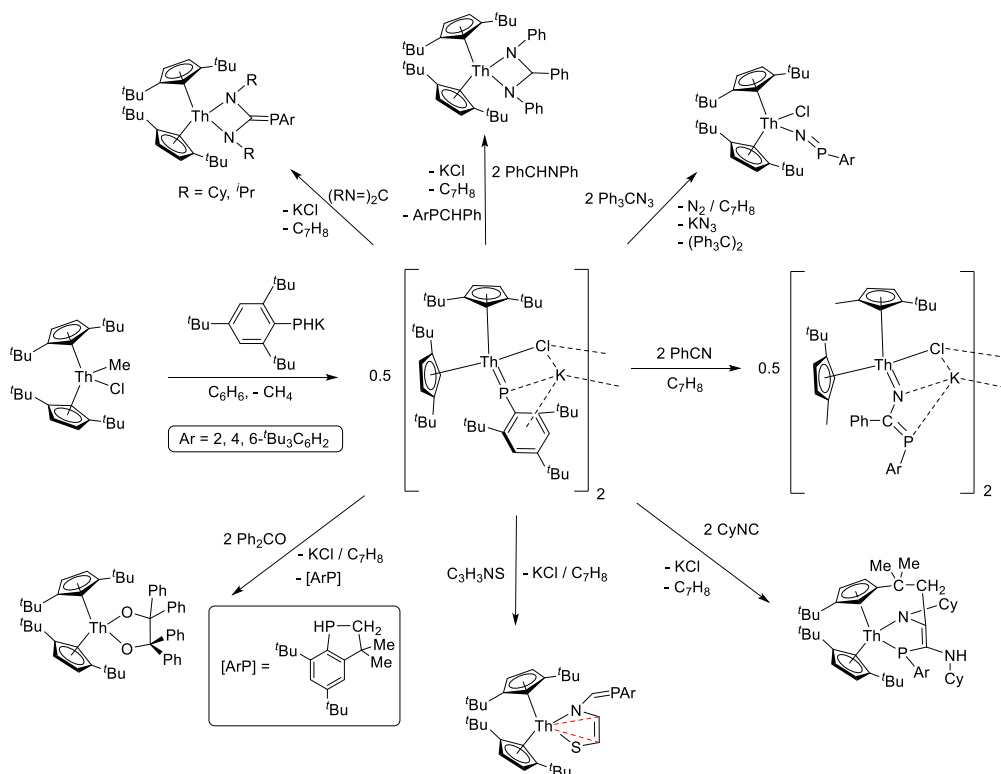


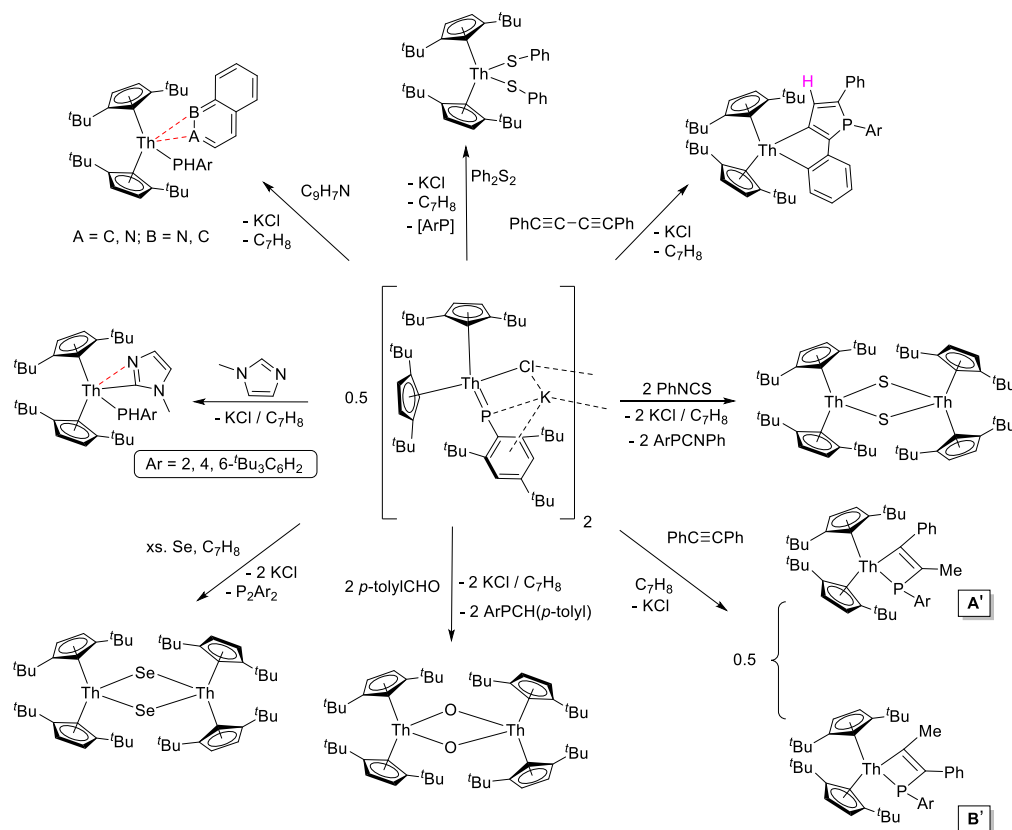
Scheme 127. Photolytic and reductive activation of 2-arsaethynolate in uranium-triamidoamine complexes and trapping of a highly bent and reduced form of 2-arsaethynolate. [163]

3.3. ACTINIDE CYCLOPENTADIENYL COMPOUNDS

3.3.1 Cp_3An , $CpAnX_3$, Cp_2AnX_2 and Cp_3AnX Compounds

The alkali-metal halide-bridged phosphinidene metallocene $\{(\text{Cp}^{\text{tBu}_2})_2\text{Th}(\text{PAr})(\text{ClK})\}_2$ ($\text{Cp}^{\text{tBu}_2} = \text{C}_5^{\text{tBu}_2}\text{H}_3$; $\text{Ar} = 2,4,6\text{-tBu}_3\text{C}_6\text{H}_2$) was synthesised *via* the salt metathesis reaction of the thorium methyl chloride compound $(\text{Cp}^{\text{tBu}_2})_2\text{Th}(\text{Cl})\text{Me}$ with KPHAr in benzene (78% yield). DFT studies indicate significant contributions of the 5f orbitals to covalent bonding within the $\text{Th}=\text{P}(2,4,6\text{-tBu}_3\text{C}_6\text{H}_2)$ moiety. The complex $\{(\text{Cp}^{\text{tBu}_2})_2\text{Th}(\text{PAr})(\text{ClK})\}_2$ was shown to react with alkynes and an array of heterounsaturated small molecules such as nitriles, isonitriles, carbodiimides, imines, isothiocyanates, aldehydes, ketones, thiazoles, quinolines, pyridines, imidazoles and organic azides. In addition, $\{(\text{Cp}^{\text{tBu}_2})_2\text{Th}(\text{PAr})(\text{ClK})\}_2$ reacted with elemental selenium and Ph_2S_2 , to form thorium selenido and sulfido compounds, respectively. Scheme 128 summarizes these reactions with mechanistic information derived from DFT studies.[164]

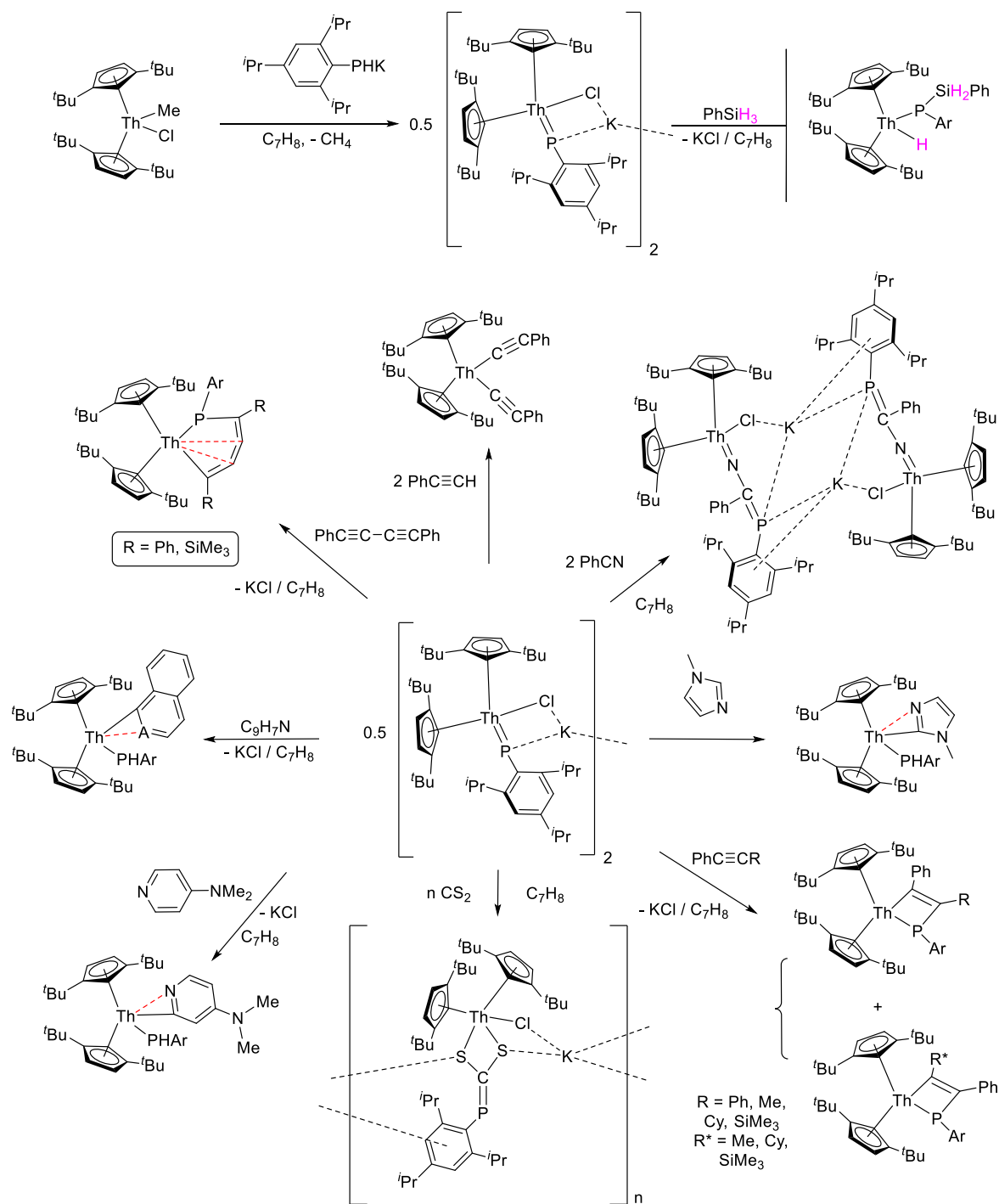




Scheme 128. Synthesis of $\{(\text{Cp}^{t\text{Bu}2})_2\text{Th}(\text{PAr})(\text{ClK})\}_2$ and reactivity with various heterounsaturated substrates. [164]

The Alkali-metal halide-bridged phosphinidene metallocene $\{(\text{Cp}^{t\text{Bu}2})_2\text{Th}(\text{PAr}')(\text{ClK})\}_2$ ($\text{Cp}^{t\text{Bu}2} = \text{C}_5^t\text{Bu}_2\text{H}_3$; $\text{Ar}' = 2,4,6\text{-}^t\text{Pr}_3\text{C}_6\text{H}_2$) was synthesised *via* the salt metathesis reaction of the thorium methyl chloride compound $(\text{Cp}^{t\text{Bu}2})_2\text{Th}(\text{Cl})\text{Me}$ with KPHAr' in toluene (82% yield). Both $\{(\text{Cp}^{t\text{Bu}2})_2\text{Th}(\text{PAr}')(\text{ClK})\}_2$ and $\{(\text{Cp}^{t\text{Bu}2})_2\text{Th}(\text{PAr})(\text{ClK})\}_2$ ($\text{Ar} = 2,4,6\text{-}^t\text{Bu}_3\text{C}_6\text{H}_2$) undergo a [2+2] addition with alkynes, while $(\text{Cp}^{t\text{Bu}3})_2\text{Th}(\text{PAr})$ did not show any reactivity towards alkynes. Reactions of $\{(\text{Cp}^{t\text{Bu}2})_2\text{Th}(\text{PAr}')(\text{ClK})\}_2$ and $\{(\text{Cp}^{t\text{Bu}2})_2\text{Th}(\text{PAr})(\text{ClK})\}_2$ with 1-methylimidazole yielded 1-methylimidazole phosphido imidazolyl complexes, while $(\text{Cp}^{t\text{Bu}3})_2\text{Th}(\text{PAr})$ formed a bis-imidazolyl compound (irrespective of the amount of 1-methylimidazole) (Scheme 129). Differences in reactivity also were observed between $\{(\text{Cp}^{t\text{Bu}2})_2\text{Th}(\text{PAr}')(\text{ClK})\}_2$ and $\{(\text{Cp}^{t\text{Bu}2})_2\text{Th}(\text{PAr})(\text{ClK})\}_2$. For example, the reaction with $\text{PhC}\equiv\text{CMe}$ yielded one single isomer and a mixture of isomers, respectively, whereas, the reaction with $\text{PhC}\equiv\text{C}-\text{C}\equiv\text{CPh}$ yielded a 6-membered metalloheterocycle and a phospholyl complex, respectively. This difference in reactivity was concluded to be due to differences in ligand sterics and electronics of the different phosphinidene ligands. Reactions of $\{(\text{Cp}^{t\text{Bu}2})_2\text{Th}(\text{PAr}')(\text{ClK})\}_2$ with various small organic

molecules (alkynes, nitriles, CS₂, quinolones, silanes, pyridine and imidazoles) are summarised in Scheme 129. [165]

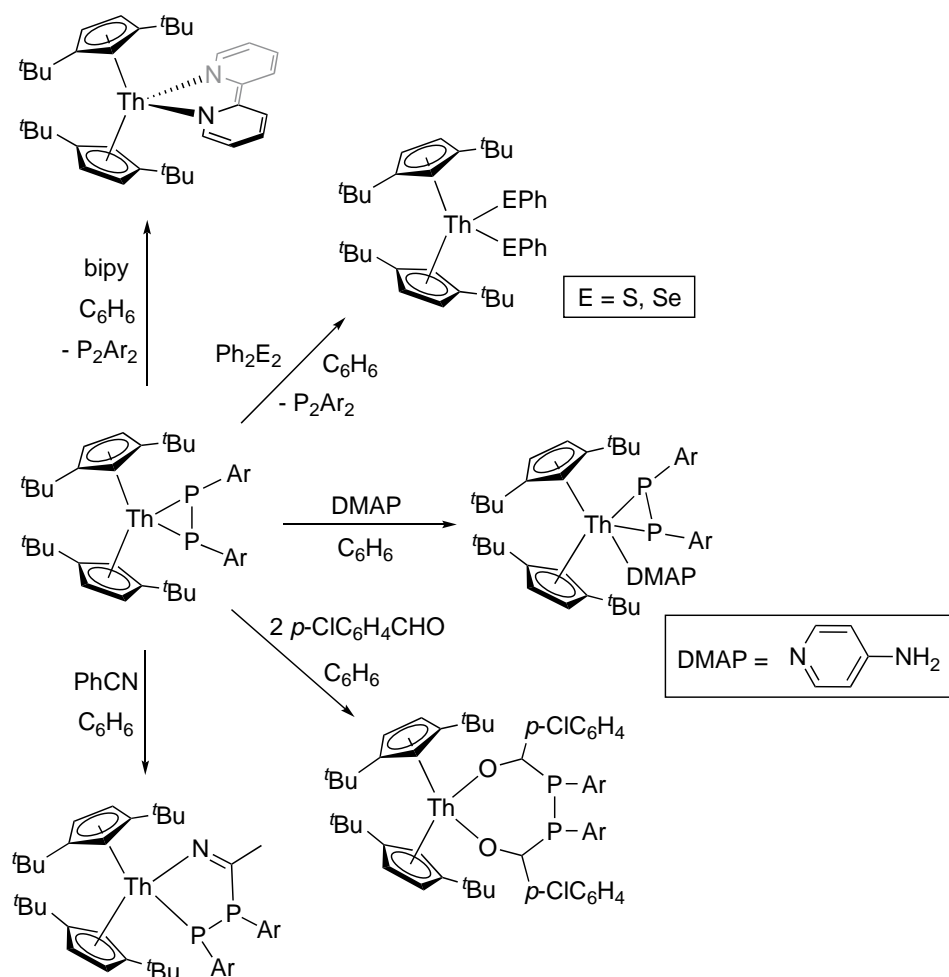
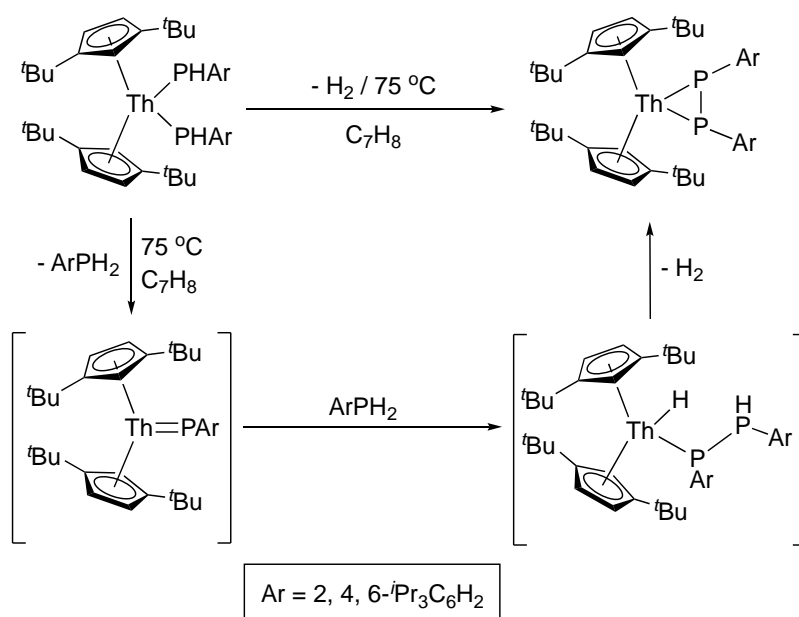


Scheme 129. Synthesis of $\{(Cp^{tBu2})_2Th(P-2,4,6-iPr_3C_6H_2)(Cl)K\}_2$ and reactivity with alkynes, quinolines, pyridines, imidazoles, silanes and CS₂. [165]

The stable base-free terminal phosphinidene thorium metallocene $(Cp^{tBu3})_2Th(PAr)$ ($Cp^{tBu3} = C_5^tBu_3H_2$; $Ar = 2,4,6-tBu_3C_6H_2$) was synthesised *via* the reaction of thorium dichloride

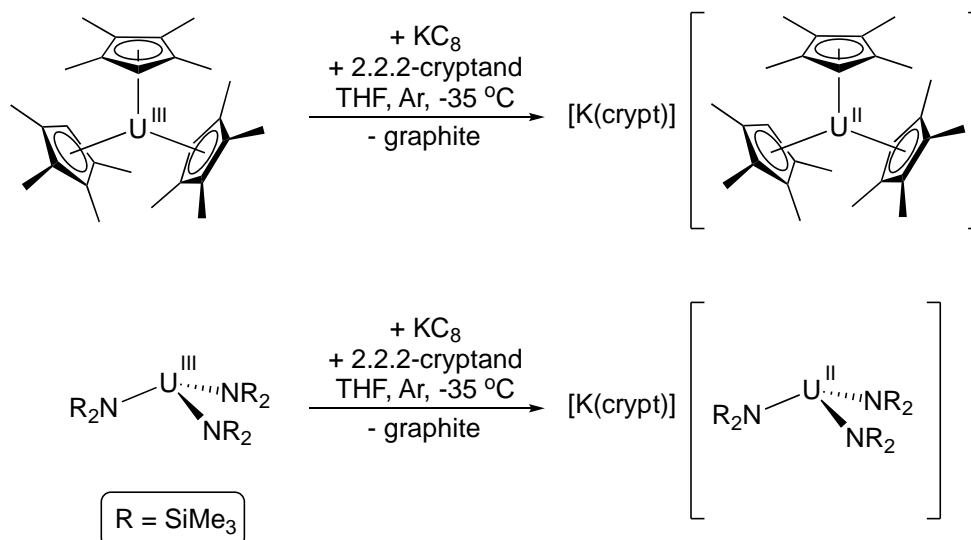
complex $(\text{Cp}^{\text{tBu}_3})_2\text{ThCl}_2$ with two equivalents of KPHAr in THF (85% yield) (Scheme 130). Treatment of $(\text{Cp}^{\text{tBu}_3})_2\text{Th}(\text{PAr})$ with diselenide Ph_2Se_2 resulted in the displacement of the phosphinidene ligand and formation of a diselenido compound $(\text{Cp}^{\text{tBu}_3})_2\text{Th}(\text{SePh})_2$. Furthermore, $(\text{Cp}^{\text{tBu}_3})_2\text{Th}(\text{PAr})$ was shown to activate E–H (E = P, N, C) bonds in phosphines, imines, ketones, phosphine oxides, thiazole, imidazole derivatives and amines (Scheme 130). The labile nature of the phosphinidene ligand in $(\text{Cp}^{\text{tBu}_3})_2\text{Th}(\text{P-2,4,6-}^t\text{Bu}_3\text{C}_6\text{H}_2)$ contrasts with that of thorium imido metallocene complexes, which are inert to ligand exchange.[166]

A three-membered thorium metallaheterocycle (Cp^{tBu_2})₂Th($\eta^2\text{-P}_2\text{Ar}'_2$) ($\text{Cp}^{t\text{Bu}_2} = \text{C}_5^t\text{Bu}_2\text{H}_3$; $\text{Ar}' = 2,4,6\text{-}i\text{Pr}_3\text{C}_6\text{H}_2$) was synthesised by the dehydrogenation of (Cp^{tBu_2})₂Th(PHAr')₂ in heated toluene, as shown in Scheme 131. DFT studies reveal significant covalent bonding between the fragments, with both 5f and 6d orbital contributions to bonding. The complex (Cp^{tBu_2})₂Th($\eta^2\text{-P}_2\text{Ar}'_2$) exhibited varied reactivity. It formed a Lewis base adduct with DMAP, and underwent ligand exchange with bipy, Ph₂S₂ and Ph₂Se₂ (Scheme 131). However, (Cp^{tBu_2})₂Th($\eta^2\text{-P}_2\text{Ar}'_2$) showed no reactivity towards alkynes, but behaved as a nucleophile towards hetero-unsaturated molecules (such as nitriles and aldehydes, see Scheme 131) forming five- or seven-membered metallaheterocycles. [167]

Scheme 131. Synthesis of $(\text{Cp}^{\text{tBu}_2})_2\text{Th}(\eta^2\text{-P}_2\text{Ar}'_2)$ and reactivity with various substrates.

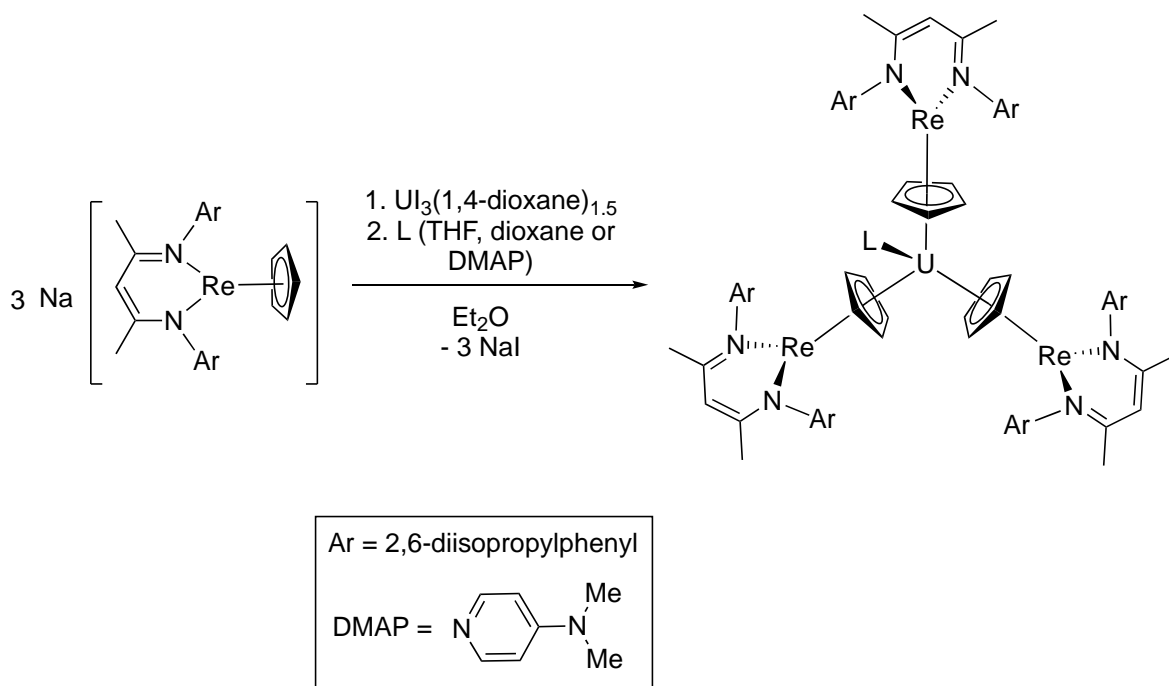
[167]

U(II) complexes featuring electron donating ligands have been synthesised *via* the reduction of $(\text{Cp}^{\text{tet}})_3\text{U}$ ($\text{Cp}^{\text{tet}} = \text{C}_5\text{Me}_4\text{H}$) and $\text{U}(\text{NR}_2)_3$ ($\text{R} = \text{SiMe}_3$), with KC_8 in the presence of 2.2.2-cryptand (crypt), yielding $[\text{K}(\text{crypt})][(\text{Cp}^{\text{tet}})_3\text{U}]$ and $[\text{K}(\text{crypt})][\text{U}(\text{NR}_2)_3]$, respectively (Scheme 132). The solid-state molecular structures of both U(II) complexes were determined by single-crystal X-ray diffraction and spectroscopic data were consistent with a $5f^3 6d^1$ electronic configuration. [168]



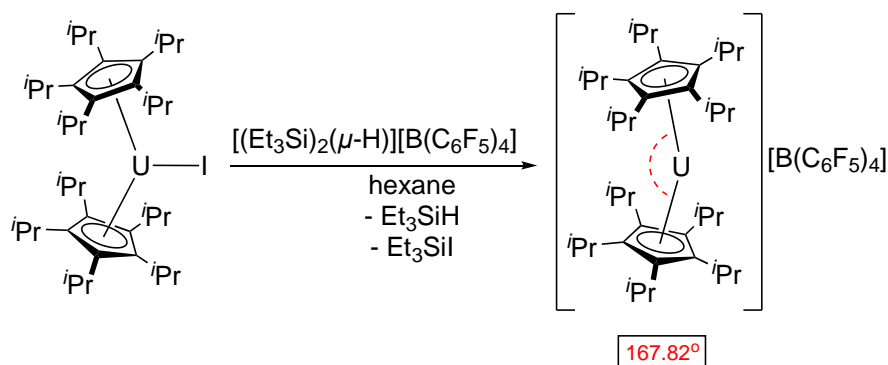
Scheme 132. Synthesis of U(II) complexes featuring the electron donating ligands Cp^{tet} and $\text{N}(\text{SiMe}_3)_2$. [168]

The triple inverse sandwich complex $(\text{L})\text{U}[(\mu\text{-}\eta^5\text{:}\eta^5\text{-Cp})\text{Re}(\text{BDI})]_3$ ($\text{L} = \text{THF}$, 1,4-dioxane, DMAP; $\text{BDI} = N,N'$ -bis(2,6-diisopropylphenyl)-3,5-dimethyl- β -diketiminate) was synthesised *via* salt metathesis between anionic Re(I) compound $\text{Na}[\text{Re}(\eta^5\text{-Cp})(\text{BDI})]$ and $\text{U}(\text{I}_3(1,4\text{-dioxane})_{1.5})$ (62 – 83% yield), as shown in Scheme 133. The complex $\text{U}[(\mu\text{-}\eta^5\text{:}\eta^5\text{-Cp})\text{Re}(\text{BDI})]_3$ was characterised by X-ray crystallography, NMR and EPR spectroscopies, which confirmed the assignment of one U(III) and three Re(I) centres. DFT studies were consistent with experimental data and revealed atypical inverse sandwich bonding in the bridging Cp ligands, where electron density is redistributed from Re(I) to U(III). [169]



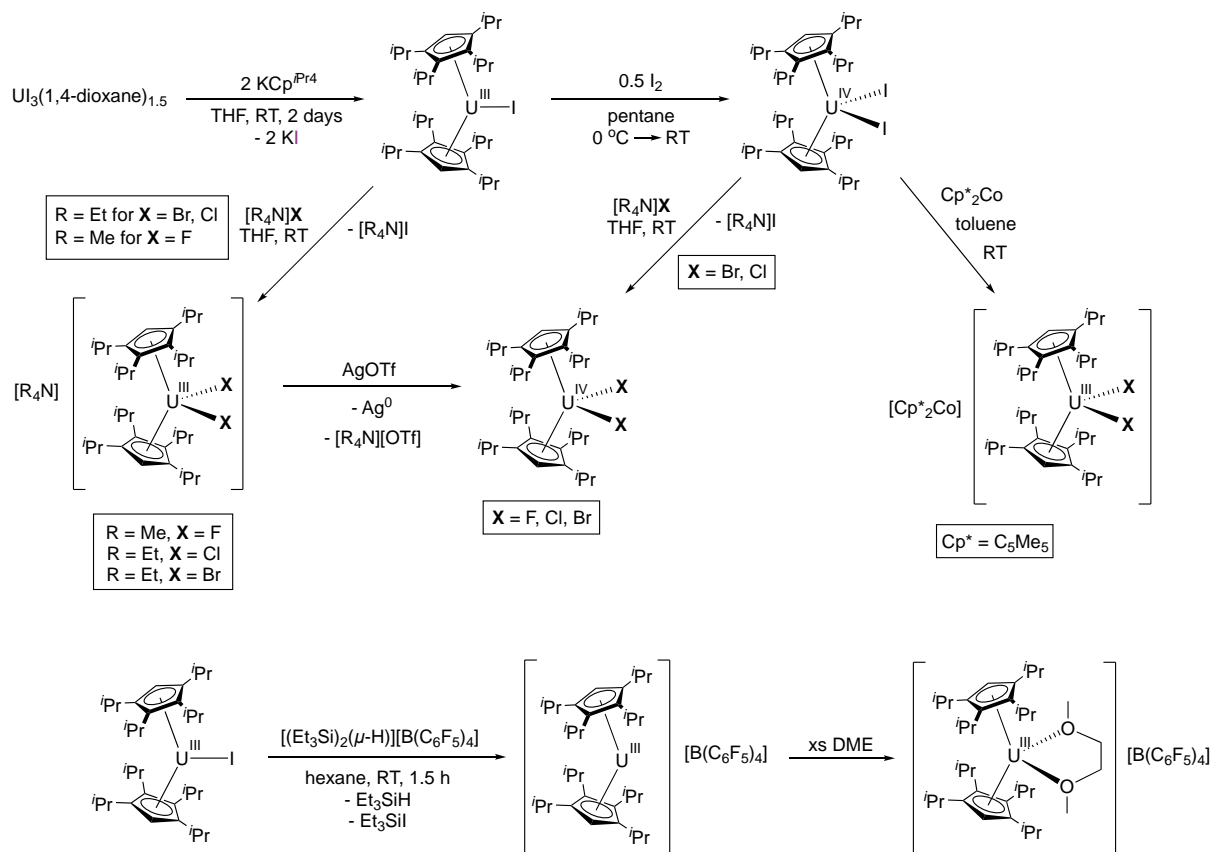
Scheme 133. Synthesis of the triple inverse sandwich complex $(L)U[(\mu\text{-}\eta^5:\eta^5\text{-Cp})\text{Re}(\text{BDI})]_3$. [169]

The cationic U(III) metallocene $[(\text{Cp}^{i\text{Pr}5})_2\text{U}]^+[\text{B}(\text{C}_6\text{F}_5)_4]^-$ ($\text{Cp}^{i\text{Pr}5} = \text{C}_5^i\text{Pr}_5$) was synthesised as a *via* the iodide abstraction of $(\text{Cp}^{i\text{Pr}5})_2\text{UI}$ using the super-electrophile $[(\text{Et}_3\text{Si})_2(\mu\text{-H})][\text{B}(\text{C}_6\text{F}_5)_4]$, as shown in Scheme 134. The crystal structure of $[(\text{Cp}^{i\text{Pr}5})_2\text{U}]^+$ showed a metallocene geometry with a Cp-U-Cp angle of 167.82° . DFT calculations revealed that there is non-negligible covalent character to the bonding in $[(\text{Cp}^{i\text{Pr}5})_2\text{U}]^+$. In fact, the U(III) 5f orbitals experience strong splitting as a result of mixing with ligand orbitals. The metal-ligand covalency also resulted in a partial quenching of orbital angular momentum and an absence of slow magnetic relaxation at zero field due to efficient quantum tunnelling. [170]



Scheme 134. Synthesis of the cationic U(III) metallocene $[(\text{Cp}^{i\text{Pr}5})_2\text{U}]^+$. [170]

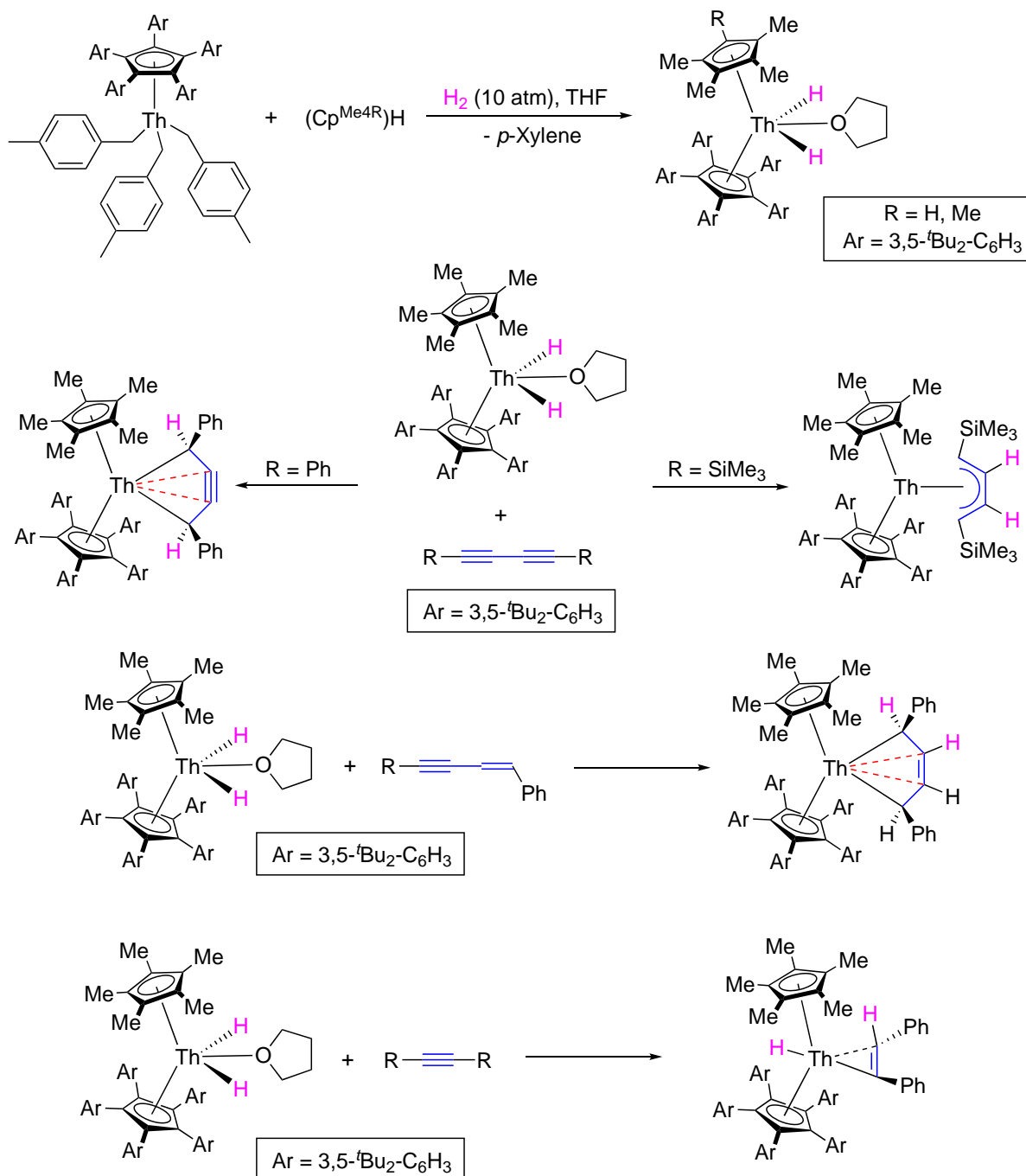
The U(III) metallocene iodide $(\text{Cp}^{i\text{Pr}_4})_2\text{UI}$ ($\text{Cp}^{i\text{Pr}_4} = \text{C}_5^i\text{Pr}_4\text{H}$) was synthesised *via* the salt metathesis reaction of $\text{UI}_3(\text{dioxane})_{1.5}$ and $\text{KCp}^{i\text{Pr}_4}$ in THF (Scheme 135). The complex $(\text{Cp}^{i\text{Pr}_4})_2\text{UI}$ can be converted to U(IV) metallocene dihalides $(\text{Cp}^{i\text{Pr}_4})_2\text{UX}_2$ ($\text{X} = \text{F}, \text{Cl}, \text{Br}$) and anionic U(III) metallocene dihalides $[(\text{Cp}^{i\text{Pr}_4})_2\text{UX}_2]^-$ ($\text{X} = \text{F}, \text{Cl}, \text{Br}, \text{I}$) *via* different redox pathways, summarised in Scheme 135. The iodide abstraction from $(\text{Cp}^{i\text{Pr}_4})_2\text{UI}$, with super electrophile $[(\text{Et}_3\text{Si})_2(\mu\text{-H})][\text{B}(\text{C}_6\text{F}_5)_4]$, formed a ‘base-free’ U(III) metallocenium cation salt and its more stable DME adduct (Scheme 135). Magnetic susceptibility studies of $(\text{Cp}^{i\text{Pr}_4})_2\text{UI}$ and $[(\text{Cp}^{i\text{Pr}_4})_2\text{U}][\text{B}(\text{C}_6\text{F}_5)_4]$ revealed similar magnetic relaxation behaviour under applied fields; the relaxation is slower than that of other reported mononuclear actinide single molecule magnets, including recently reported $[(\text{Cp}^{i\text{Pr}_5})_2\text{U}]^+$ cation. [170][171]



Scheme 135. The synthesis of U(III) and U(IV) metallocenes with Cp^{iPr_4} ligands. [171]

The first example of a monomeric thorium terminal dihyrido compound $(\text{Cp}^{\text{Ar}_5})(\text{Cp}^*)\text{ThH}_2(\text{THF})$ (where $\text{Cp}^{\text{Ar}_5} = \text{C}_5\text{Ar}_5$; $\text{Ar} = 3,5\text{-}^t\text{Bu}_2\text{-C}_6\text{H}_3$; $\text{Cp}^* = \text{C}_5\text{Me}_5$) has been synthesised by the hydrogenolysis of thorium tribenzyl compound $(\text{Cp}^{\text{Ar}})\text{Th}(p\text{-CH}_2\text{-C}_6\text{H}_4\text{-Me})_3$, as shown in Scheme 136. The complex $(\text{Cp}^{\text{Ar}_5})(\text{Cp}^*)\text{ThH}_2(\text{THF})$ was shown to undergo Th–H addition with various unsaturated compounds (Scheme 136) to produce the

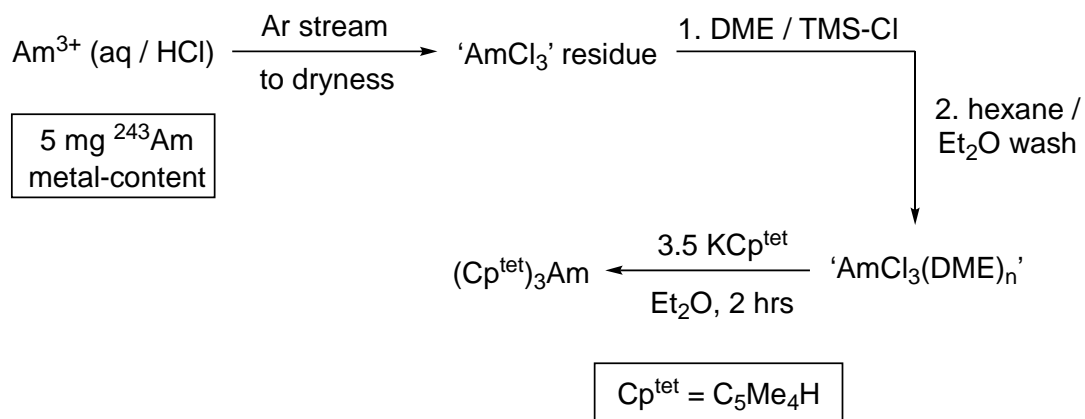
corresponding five-membered metallacycles, including the metallacyclopentyne $(Cp^{Ar5})(Cp^*)Th(PhCH-C\equiv C-CHPh)$. [172]



Scheme 136. Synthesis of a thorium terminal dihyrido compound $(Cp^{Ar})(Cp^*)ThH_2(THF)$ ($Ar = 3,5\text{-}^tBu_2\text{-}C_6H_3$; $Cp^* = C_5Me_5$) and reactivity with unsaturated substrates. [172]

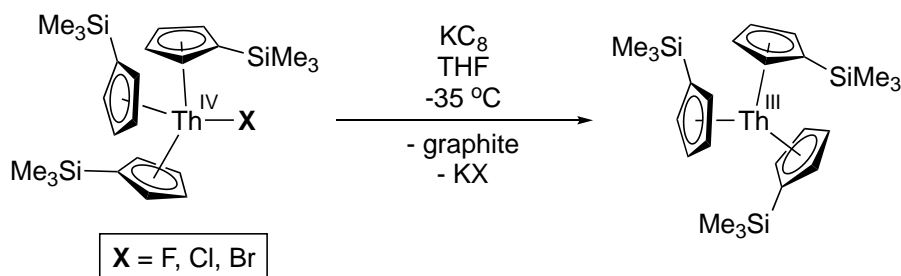
The organoamericium(III) compound $(Cp^{tet})_3Am$ ($Cp^{tet} = C_5Me_4H$) has been isolated and characterised by X-ray crystallography, 1H NMR and UV-vis-NIR spectroscopy, as well as analysed by computational studies (Scheme 137). These quantitative data are the first example of Am-C bonding and structural examination in a molecular complex.

Experimental data and computational modelling of the electronic structure of $(\text{Cp}^{\text{tet}})_3\text{Am}$ provided evidence of an increase in band gap between the 5f and 6d orbitals across the 'Cp₃An' series from Np to Am. [173]



Scheme 137. Synthesis of $(\text{Cp}^{\text{tet}})_3\text{Am}$. [173]

The reduction of $(\text{Cp}')_3\text{ThCl}$, $(\text{Cp}')_3\text{ThBr}$ and $(\text{Cp}')_3\text{ThI}$ ($\text{Cp}' = \text{C}_5\text{H}_4\text{SiMe}_3$) with potassium graphite (Scheme 138) has been reported to produce a blue solution with reactivity and spectroscopic properties (EPR and UV-vis spectroscopy) consistent with that of $\text{Cp}'_3\text{Th}$. The isolation of $\text{Cp}'_3\text{Th}$ as a molecular species was not achieved, in contrast to $\text{Cp}''_3\text{Th}$ ($\text{Cp}'' = \text{C}_5\text{H}_3(\text{SiMe}_3)_2$), suggesting that the smaller Cp' ligand is unable to stabilise the Th(III) centre well enough to allow isolation. The blue solution reacted with Me_3SiCl , I_2 and $\text{HC}\equiv\text{CPh}$ to yield the expected products from $\text{Cp}'_3\text{Th}$, $\text{Cp}'_3\text{ThCl}$, $\text{Cp}'_3\text{ThI}$ and $\text{Cp}'_3\text{Th}(\text{C}\equiv\text{CPh})$, respectively. Experimental data and DFT analysis are consistent with $\text{Cp}'_3\text{Th}$ and not $[\text{Cp}'_3\text{ThBr}]^-$. [174]



Scheme 138. Synthesis of $\text{Cp}'_3\text{Th}$ by the reduction of $\text{Cp}'_3\text{ThX}$. [174]

The structure and electronic properties of theoretical divalent actinocene compounds $(\text{Cp}^{i\text{Pr}5})_2\text{An}$ ($\text{Cp}^{i\text{Pr}5} = \text{C}_5^i\text{Pr}_5$; An = Th, U, Pu, Am, Bk, No, Lr) have been investigated computationally. DFT calculations predict Th, U and Lr to have ground states with

significant 6d occupation, while Am, Bk and No showed 5f occupation, as depicted in Figure 24. Pu is shown to be a borderline case with both 5f and 6d occupation in a mixed ground state configuration (Figure 24). The complexes $(\text{Cp}^{i\text{Pr}5})_2\text{An}$ are shown to exhibit linear coordination geometry and high S_{10} symmetry, except for $(\text{Cp}^{i\text{Pr}5})_2\text{Pu}$ and $(\text{Cp}^{i\text{Pr}5})_2\text{Am}$, which are calculated to be bent by 11 and 12°, respectively. Time-dependent DFT was used to simulate UV-vis absorption spectra and good agreement was obtained with experimental data. The complexes $(\text{Cp}^{i\text{Pr}5})_2\text{An}$ exhibit strong MLCT bands for An = Th, U in the UV region, which are also observed for $(\text{Cp}^{i\text{Pr}5})_2\text{Dy}$, $(\text{Cp}^{i\text{Pr}5})_2\text{Tb}$ and tris Cp'/Cp'' actinide species (Cp' = $\text{C}_5\text{H}_4\text{SiMe}_3$; Cp'' = $\text{C}_5\text{H}_3(\text{SiMe}_3)_2$). Low intensity broad absorption envelopes in the region of 600 to 1000 nm were observed for $(\text{Cp}^{i\text{Pr}5})_2\text{An}$, and also observed for $(\text{Cp}^{i\text{Pr}5})_2\text{Dy}$ and $(\text{Cp}^{i\text{Pr}5})_2\text{Tb}$. The thermodynamic stability of $(\text{Cp}^{i\text{Pr}5})_2\text{An}$ were assessed by calculating adiabatic reduction potentials of the trivalent precursors $[(\text{Cp}^{i\text{Pr}5})_2\text{An}]^+$, as well as investigations into accessible Ac(I) oxidation states *via* ligand modification. [175]

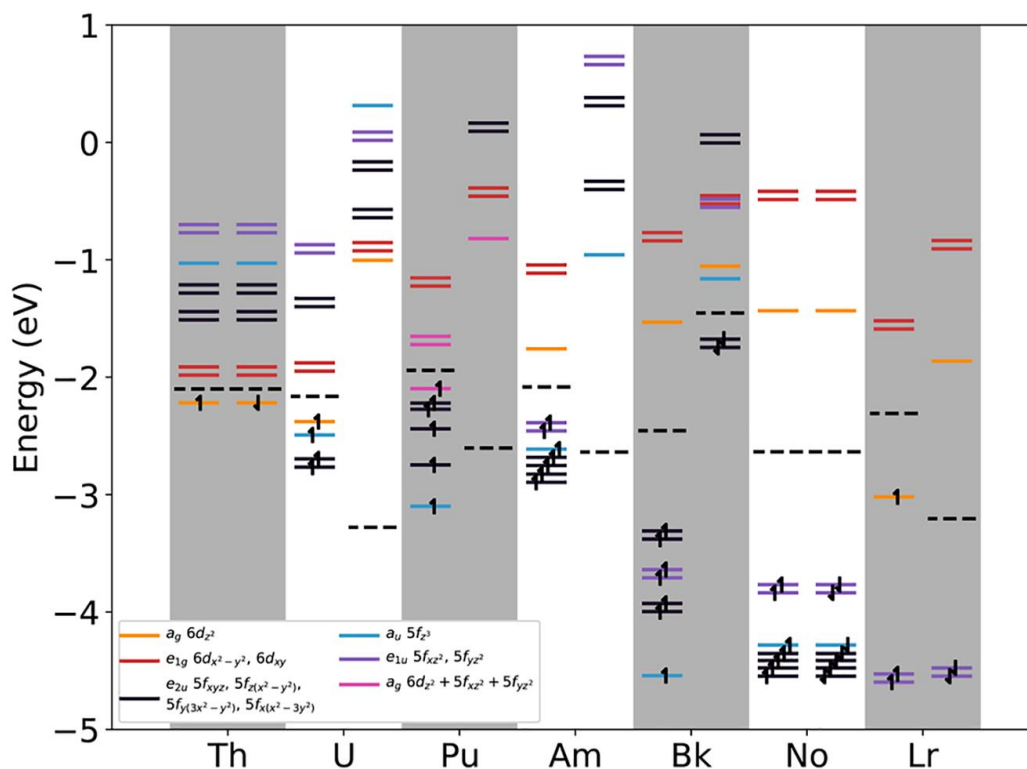


Figure 24. Frontier molecular orbital diagram for $(\text{Cp}^{i\text{Pr}5})_2\text{An}$. Fermi levels denoted with a dashed line. Reprinted with permission from [175] Copyright 2019 American Chemical Society

The mixed-metal complexes $(\text{Cp}^{\text{tt}})_2\text{ThH}_3\text{Al}(\text{CTMS})_3$ ($\text{Cp}^{\text{tt}} = 1,3\text{-}^i\text{Bu}_2\text{C}_5\text{H}_3$; TMS = SiMe_3) have been synthesised and characterised by electron paramagnetic resonance (EPR) and

electron-nuclear double resonance (ENDOR) spectroscopy (Figure 25). These data were used to calculate the spin-density distribution. The hyperfine interactions between the paramagnetic trivalent metal centres Th(III) and Ti(III), and surrounding magnetic nuclei ^1H and ^{27}Al were analysed. The bridging hydrides show similar hyperfine couplings to both Th and Ti. The Al hyperfine interactions were dramatically different, with 5-fold larger spin density Al in $(\text{Cp}^{\text{t}})_2\text{ThH}_3\text{Al}(\text{CTMS})_3$. These data are consistent with direct orbital overlap and significant covalent bonding between Th and Al. [176]

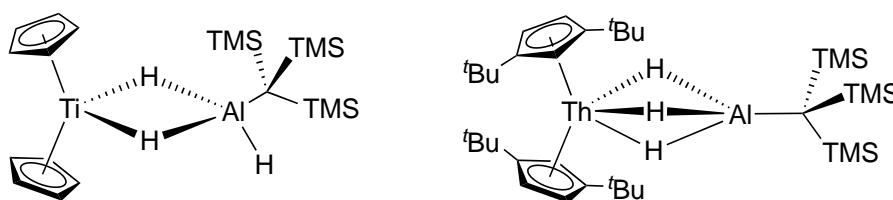
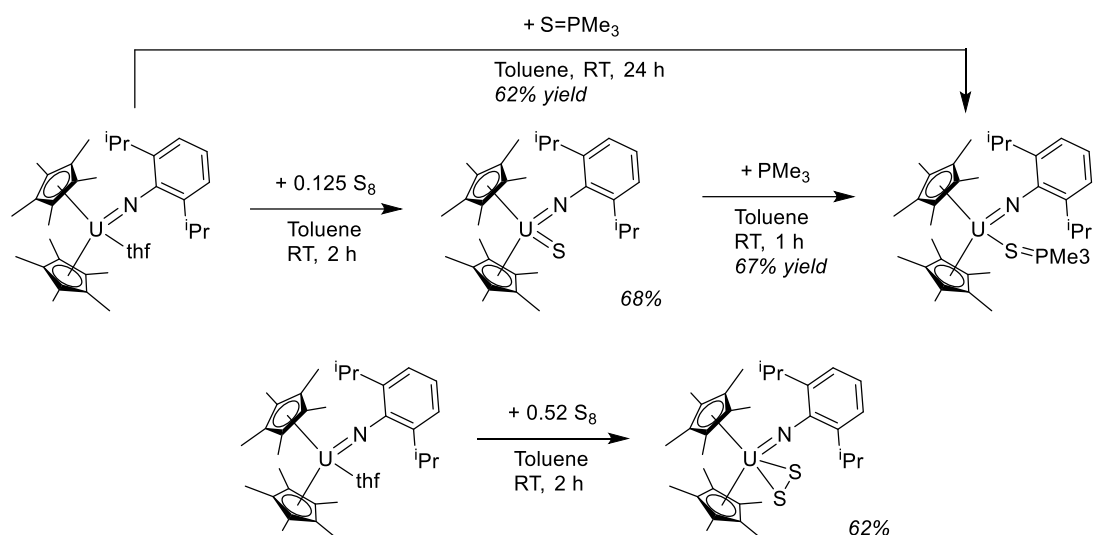


Figure 25. Complexes $\text{Cp}_2\text{TiH}_3\text{Al}(\text{CTMS})_3$ and $(\text{Cp}^{\text{t}})_2\text{ThH}_3\text{Al}(\text{CTMS})_3$ were characterised by advance EPR spectroscopies. [176]

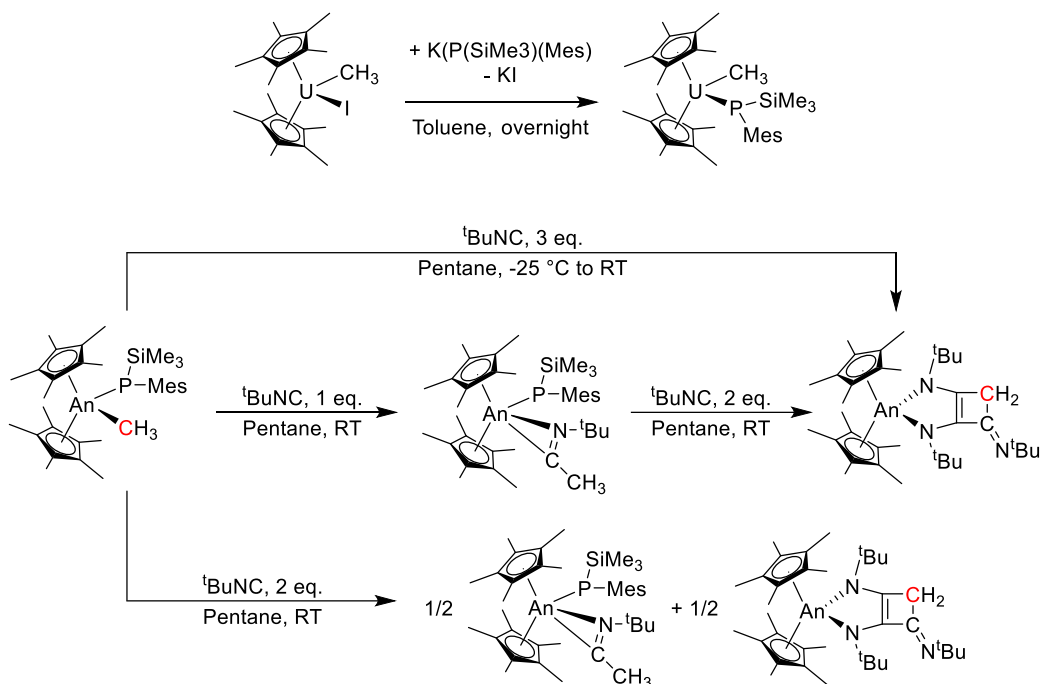
3.3.2. Pentamethylcyclopentadienyl Compounds

A rare example of a uranium(VI) terminal sulfido complex, and the first uranium phosphine sulfide complex have been reported. Reaction of the *bis*-cyclopentadienyl uranium imido complex $(\text{Cp}^*)_2\text{U}(=\text{NAr})(\text{thf})$ ($\text{Ar} = 2,6\text{-}^i\text{Pr}_2\text{C}_6\text{H}_3$) with either 0.125 or 0.52 eq. S_8 afforded either the sulphido complex $(\text{Cp}^*)_2\text{U}(=\text{NAr})(=\text{S})$ or the bisulfide $(\text{Cp}^*)_2\text{U}(=\text{NAr})(\eta_2\text{-S}_2)$, respectively. The reaction of $(\text{Cp}^*)_2\text{U}(=\text{NAr})(=\text{S})$ with trimethyl phosphine was used to access $(\text{Cp}^*)_2\text{U}(=\text{NAr})(\text{S}=\text{PMe}_3)$, the first uranium phosphine sulfide complex (Scheme 139). This complex was also synthesized directly from $(\text{Cp}^*)_2\text{U}(=\text{NAr})(\text{thf})$ by reaction with trimethyl phosphine sulfide. [177]



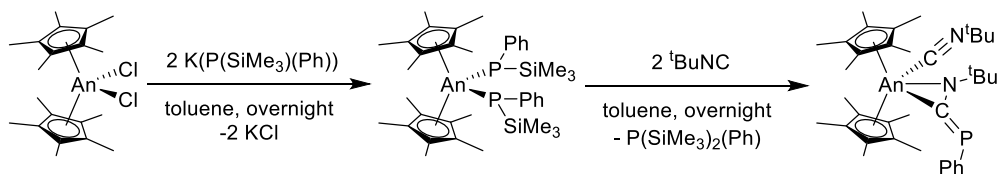
Scheme 139. Formation of $(\text{Cp}^*)_2\text{U}(=\text{N}(\text{Ph}(\text{iPr})_2))(\text{=S})$, $(\text{Cp}^*)_2\text{U}(=\text{N}(\text{Ph}(\text{iPr})_2))(\text{S}=\text{PMe}_3)$ and $(\text{Cp}^*)_2\text{U}(=\text{N}(\text{Ph}(\text{iPr})_2))(\eta^2\text{-S}_2)$ from $(\text{Cp}^*)_2\text{U}(=\text{N}(\text{Ph}(\text{iPr})_2))(\text{thf})$. [177]

By reaction of $(\text{Cp}^*)_2\text{U}\text{MeI}$ with $\text{K}(\text{P}\{\text{SiMe}_3\}\{\text{Mes}\})$ ($\text{Mes} = 2,4,6\text{-Me}_3\text{C}_6\text{H}_2$), a new uranium phosphido complex $(\text{Cp}^*)_2\text{U}\text{Me}(\text{P}\{\text{SiMe}_3\}\{\text{Mes}\})$ has been synthesised in an analogous manner to the previously synthesised $(\text{Cp}^*)_2\text{Th}(\text{CH}_3)(\text{P}\{\text{SiMe}_3\}\{\text{Mes}\})$ (Scheme 140). The reactions of these mixed alkyl-phosphido complexes with various equivalents of *tert*-butyl cyanide were investigated, shown in Scheme 140. The reaction with one equivalent of *tert*-butyl cyanide was performed, and it was found that the cyanide inserted into the actinide-methyl bond, forming the iminoacyl complexes $(\text{Cp}^*)_2\text{An}(\eta^2\text{-}^t\text{BuN}=\text{CCH}_3)(\text{P}\{\text{SiMe}_3\}\{\text{Mes}\})$ ($\text{An} = \text{Th}, \text{U}$). Reaction with three equivalents of *tert*-butyl cyanide resulted in initial formation of the iminoacyl complexes, followed by coupling of the iminoacyl to two further equivalents of *tert*-butyl cyanide and methyl deprotonation, and yielded heterocyclic α -diimine N,N' actinide complexes $(\text{Cp}^*)_2\text{An}(\kappa^2\text{-N,N}'\text{-N}(\text{tBu})\text{C}=\text{CN}(\text{tBu})\text{C}=\text{N}(\text{tBu})\text{CH}_2)$. This pathway was also investigated by DFT. These complexes could also be accessed by reaction of the iminoacyl product with two further equivalents of *tert*-butyl cyanide, and reaction with two equivalents resulted in a mixture of the iminoacyl and α -diimine products. [178]



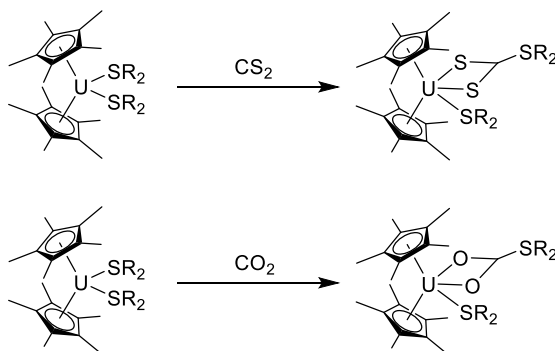
Scheme 140. Formation of uranium alkyl phosphide (Cp*)₂U(CH₃)(P(SiMe₃)(Mes)), and the reactions of (Cp*)₂An(CH₃)(P(SiMe₃)(Mes)) (An = Th, U) with various equivalents of tBuNC to form iminoacyl (Cp*)₂An(η²-tBuN=CCH₃)(P(SiMe₃)(Mes)) and α-diimine (Cp*)₂An(κ²-N,N'-N(tBu)C=CN(tBu)C=N(tBu)CH₂). [178]

The first uranium phosphazaallene has been synthesised by reaction of a *bis*-phosphido complex with *tert*-butyl cyanide. Actinide *bis*-phosphido complexes (Cp*)₂An(P{SiMe₃}{Ph}) (An = Th, U) were synthesised by the reaction of (Cp*)₂AnCl₂ with 2 eq. K(P{SiMe₃}{Ph}) as shown in Scheme 141. These compounds were then reacted with 2 eq. *tert*-butyl cyanide, resulting in migration of the silyl group of one phosphido ligand to the other, elimination of one equivalent of the phosphine P(SiMe₃)₂(Ph) and the formation of the phosphazaallene ligand N(tBu)C=P(Ph). The coordination of a second equivalent of *tert*-butyl cyanide completes the coordination sphere of the actinide phosphazaallene complexes (Cp*)₂An(CN^tBu)(η²-N(tBu)C=P(Ph)) (An = Th, U) as shown in Scheme 141. [179]



Scheme 141. Synthesis of (Cp*)₂An(P(SiMe₃)(Ph)) (An = Th, U) and subsequent reaction with *tert*-butyl cyanide to form phosphazaallenes (Cp*)₂An(CN^tBu)(η²-N(tBu)C=P(Ph)) (An = Th, U). [179]

A theoretical investigation of the reaction of various uranium *bis*-pentamethyl cyclopentadienyl thiolate compounds with small molecules CO₂ and CS₂ has been carried out. The uranium complexes (Cp*)₂U(SR)₂ (R = Me, ^tBu, ⁱPr, Ph) were first geometry-optimised by DFT, and the bond distances and angles thus obtained gave good agreement to X-ray crystal data. Their reaction pathways with CO₂ and CS₂ were investigated, and it was found that the small molecules inserted directly into the U-S bond, forming a C-S bond in the insertion products (Cp*)₂U(SR)(S₂CSR) and (Cp*)₂U(SR)(O₂CSR) as shown in Scheme 142. A significantly higher energy barrier was calculated with more bulky R groups such as ^tBu, in agreement with reactivity studies which found a slower reaction in the reaction with more sterically hindered thiolates. Additionally, the reaction with CO₂ had a lower activation energy than that with CS₂, due to the more polar C=O bonds, again in agreement with the previous experimental work. [180]



Scheme 142. Computational reactivity study of uranium bis thiolates (R = R = Me, ^tBu, ⁱPr, Ph) with small molecules CS₂ and CO₂. [180]

The Th(IV)/Th(III) redox couple is exceedingly difficult to study experimentally. However, using the electrolyte [ⁿBu₄N][BPh₄] has enabled the determination of the Th(IV)/Th(III) redox couple for a range of thorium organometallic complexes. The redox couples of the Th(IV) complexes (Cp'')₃ThCl, (Cp*)Th(COT^{TIPS2})Cl, Th(COT^{TBDMS2})₂ (Cp'' = 1,3-*bis*-trimethylsilyl cyclopentadienyl, COT^{TIPS2} = 1,4-*bis*-triisopropylsilyl cyclooctatetraenyl, COT^{TBDMS2} = 1,4-*bis-tert*-butyldimethylsilyl cyclooctatetraenyl) and the Th(III) complex Th(Cp'')₃ (Figure 26), were determined to be in the range -2.96 to -3.32 V vs FeCp₂⁺⁰, consistent with extremely reducing metal centres. [181]

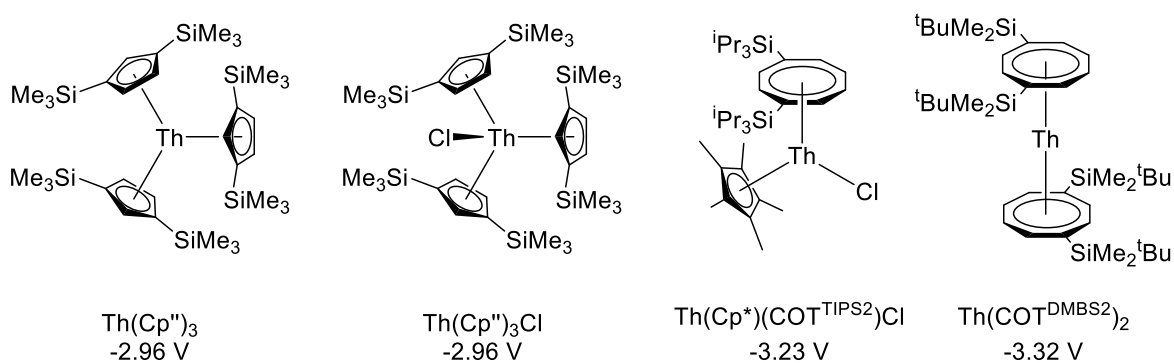


Figure 26. Structures of some thorium organometallic compounds with their Th(IV)/Th(III) redox couple (vs $\text{FeCp}_2^{+/0}$) as determined by cyclic voltammetry in 0.05 M $[\text{tBu}_4\text{N}][\text{BPh}_4]$ in tetrahydrofuran.[181]

3.4. ACTINIDE ARENE COMPLEXES

A computational study of uranium complexes has been undertaken to assess which ligand environment is most likely to support a putative U(I) complex. The ligands used in this study were *trans*-calix[2]pyrrolide[2]benzene, tris(alkyloxy) arenes and substituted cyclopentadienyl (Figure 27) and the oxidation state of uranium was varied *in silico* from +3 to +1. Relativistic DFT and QTAIM methods were used and the authors concluded that of the three ligand sets, U(I) is mostly likely to be stabilised by *trans*-calix[2]pyrrolide[2]benzene. [182]

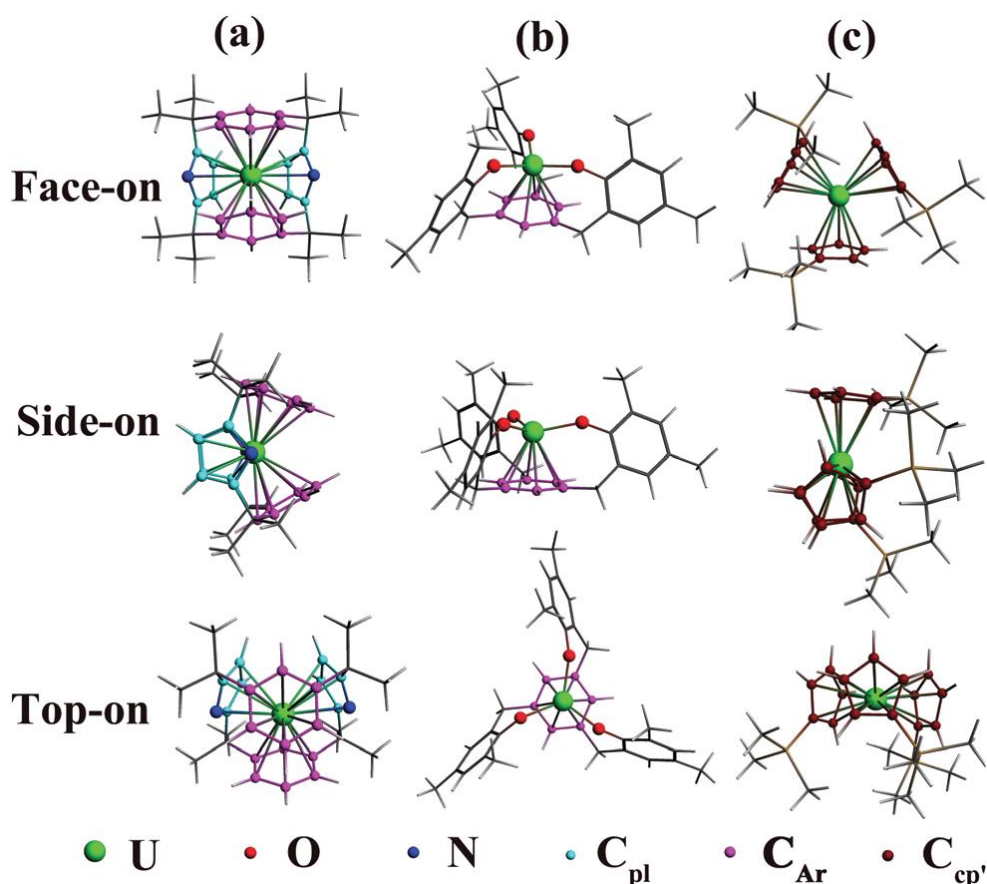


Figure 27. Structures of low-valent uranium complexes supported by (a) *trans*-calix[2]pyrrolide[2]benzene, (b) tris(alkyloxy) arenes and (c) substituted cyclopentadienyl were used in the computational study. Reprinted with permission from [182] Copyright 2019 The Royal Society of Chemistry and the Centre National de la Recherche Scientifique.

3.5. ACTINIDE METALLOFULLERENES

The small monometallic endohedral metallofullerenes (EMFs) $U@C_{2n}$ ($2n = 28, 60, 66, 68, 70$), in particular $U@C_{28}$, were synthesised for the first time by arc-discharge methodology. This was accomplished by optimisation of experimental conditions to achieve higher current and plasma temperatures, during the arc-discharge of U_3O_8 /graphite on carbon rods, in the absence of reactive gases. Extraction of the raw soot with polar solvents such as orthodichlorobenzene and Fourier Transform Ion Cyclotron Resonance (FT-ICR) Mass Spectrometry, enabled the first unambiguous characterisation of these smallest $U@C_{2n}$. The encapsulated U^{4+} ions stabilise the T_d -symmetric C_{28} cage, making this isomer an exception to the isolated pentagon rule (IPR) because it contains three fused pentagons. Computational studies and spin-density distribution calculations on $U@C_{2n}$ ($2n = 60, 66, 68, 70$) were also performed and are shown in Figure 28. The EMF $U@C_{74}$, was

predicted to be stable over the largest temperature range and also the most abundantly detected EMF. A mechanism for the formation of $U@C_{74}$ from $U@C_{70}$ was also proposed. [183]

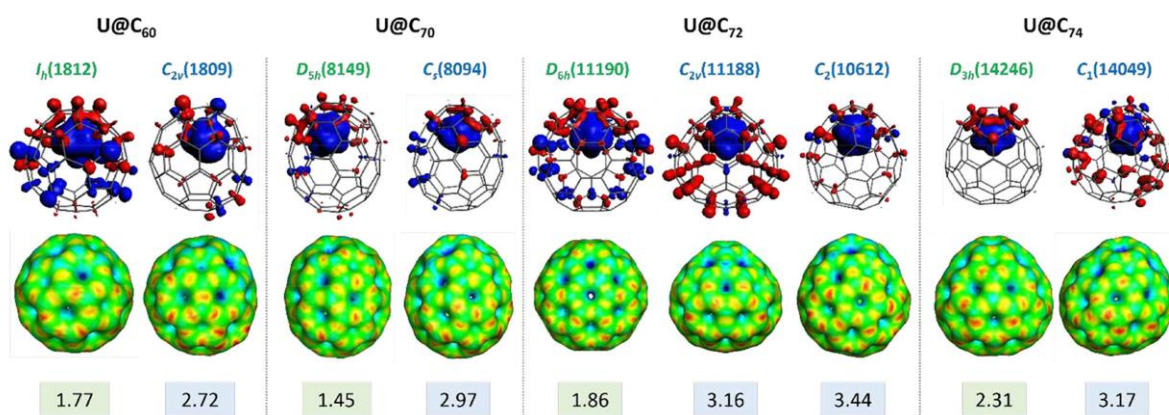


Figure 28. Spin density distributions, molecular electrostatic potential maps and dipole moments (in Debye) for $U@C_{2n}$ ($2n = 60, 70, 72, 74$). IPR cages are labelled in green and non-IPR cages in blue. Reprinted with permission from [183] Copyright 2019 Wiley-VHCA AG, Zurich, Switzerland.

The endohedral clusterfullerenes, $Sc_2UX@C_{80}$ ($X = C, N$) (Figure 29), were investigated by DFT and statistical thermodynamic analysis. The triplet $Sc_2UC@I_h(31924)-C_{80}$ and quartet $Sc_2UN@I_h(31924)-C_{80}$ structures were calculated to be aromatic and thermodynamically stable. The formal electronic structures were calculated as $[(Sc^{3+})_2U^{4+}C^4]^{6+}$ and $[(Sc^{3+})_2U^{3+}N^3]^{6+}$ respectively $@C_{80}^{6-}$, with unpaired electron density in the 5f orbitals on uranium. Quantum theory of atoms in molecules (QTAIM) theory, bond critical point (BCP) analysis and electronic localised function (ELF) maps demonstrated that there are significant covalent interactions between the cluster and cage. The data were consistent with $U=C$ double bonds and $U-N$ single bonds in the Sc_2UX ($X = C, N$) clusters. [184]

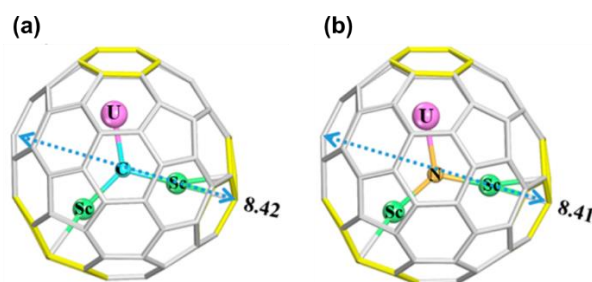


Figure 29. Geometrical structures of (a) $Sc_2UC@I_h(31924)-C_{80}$ and (b) $Sc_2UN@I_h(31924)-C_{80}$. Reprinted with permission.[184] Copyright 2019 American Chemical Society.

Non-chromatographic supramolecular purification of U-based EMFs, namely $U_2@D_{3h}-C_{78}$ and $U_2C@D_{3h}-C_{78}$ has been reported. A tetragonal prismatic nanocapsule was shown to encapsulate U-containing EMFs selectively (Figure 30) from complex soot mixtures containing empty fullerenes and EMFs (ranging from C_{60} to C_{96}). For EMF purifications, a toluene solution of the nanocapsule crystals were added to a soot mixture with diuranium-containing EMFs. Stepwise purifications of the same carbon cage containing different clusters, $U_2@C_{78}$ and $U_2C@C_{78}$ were achieved using this method. DFT studies revealed that the binding energies of U_2C and U_2 were invariant despite the change in uranium oxidation states from +3 to +5 in the linear $U=C=U$ cluster. The electron density of the fullerene surface did not change between $U_2C@D_{3h}-C_{78}$ and $U_2@D_{3h}-C_{78}$. Computational analysis concluded that the selectivity of the nanocapsule is based on both shape and electronic structure.[185]

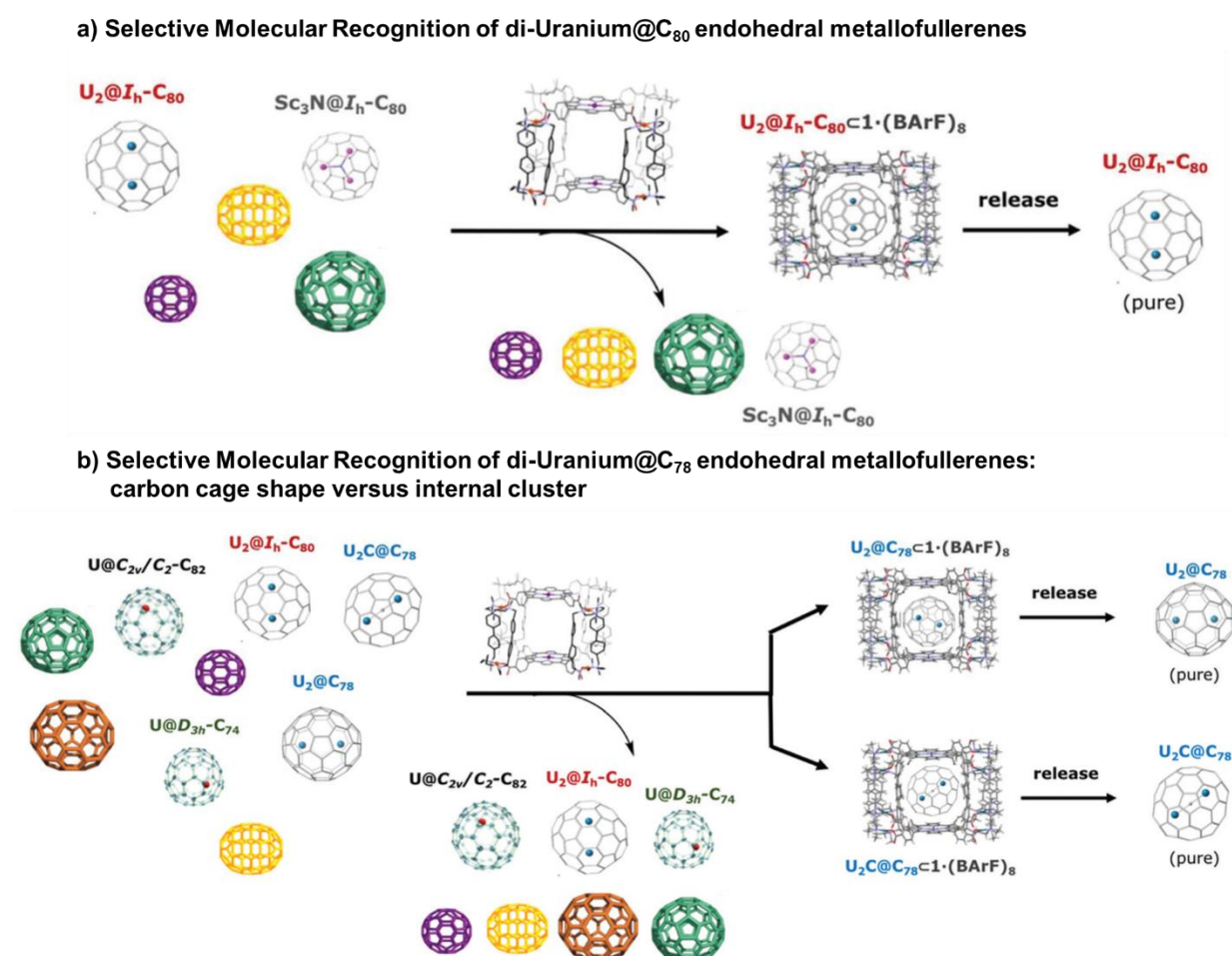


Figure 30. (a) Non-chromatographic purification of U-based@ C_{80} EMF by selective encapsulation in supramolecular nanocage (based on previous work). (b) Highly selective encapsulation and purification of U-based@ C_{78} EMFs (reported in this work). Reprinted with permission.[185] Copyright 2019 The Royal Society of Chemistry.

The triplet $U@D_3(31921)-C_{80}$ EMF has been verified to be thermodynamically stable by DFT and statistical thermodynamic analysis (Figure 31). This new stable isomer of $U@C_{80}$ is a thermodynamically optical isomer of the previously experimentally observed triplet $U@C_1(28324)-C_{80}$. Frontier molecular orbital (FMO) theory was used to deduce the formal four-electron transfer from U to C_{80} resulting in $U^{4+}@D_3(31921)-C_{80}^{4-}$ and $U^{4+}@C_1(28324)-C_{80}^{4-}$. Bond critical point (BCP) and Mayer bond order (MBO) analysis showed that the covalent interactions between U and C_{80} in $U@D_3(31921)-C_{80}$ were stronger than those in $U@C_1(28324)-C_{80}$. Calculations also showed that $U@D_3(31921)-C_{80}$ was more reactive than $U@C_1(28324)-C_{80}$ towards electrophiles and nucleophiles, and that both isomers were more reactive towards electrophiles over nucleophiles in polar solvents. Electronic circular dichroism (ECD) and UV–vis–NIR spectra were simulated to aid future experimental distinction of the two enantiomers of $U@C_{80}$. [186]

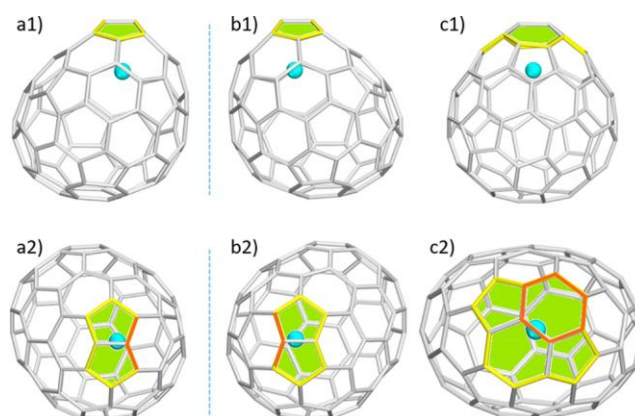


Figure 31. Optimized geometries of thermodynamically stable isomers: (a) one enantiomer of $U@C_1(28324)-C_{80}$, (b) the other enantiomer of $U@C_1(28324)-C_{80}$, and (c) $U@D_3(31921)-C_{80}$: (1) side view (on the top); (2) top view (on the bottom). Reprinted with permission.[186] Copyright 2019 American Chemical Society.

Two novel actinide EMFs, $U_2C_2@I_h(7)-C_{80}$ and $U_2C_2@D_{3h}(5)-C_{78}$ have been synthesized using arc-discharge methodology and comprehensively characterized, both spectroscopically and theoretically. The solid-state molecular structures were determined by single-crystal X-ray diffraction. The diuranium carbide cluster adopted a flexible butterfly-like geometry, with U-C single bonds and a carbon-carbon triple bond (Figure 32). Both uranium ions are in the 4+ oxidation state and the bonding in the U_2C_2 was found to be predominantly ionic, in contrast to previous reports of strong covalent character to bonding in similar actinide EMFs. Electronic structure analyses indicate that U_2C_2 , in contrast to Ln EMFs, stabilises the fullerene by transferring 6 electrons to the cage, thus enabling the isolation of the first example of $M_2C_2@I_h(7)-C_{80}$. [187]

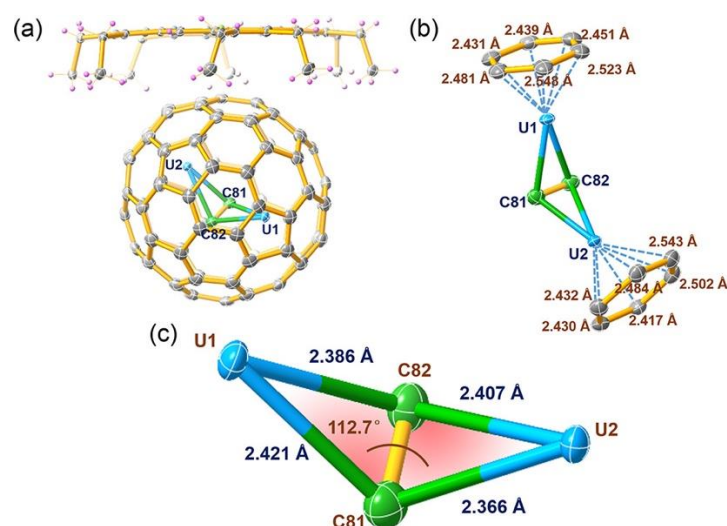


Figure 32: (a) ORTEP drawing of $U_2C_2@I_h(7)-C_{80} \cdot [Ni^{II}(OEP)]$ with 20% thermal ellipsoids. Only the major U sites (U1 and U2 with occupancies of 0.849(5) and 0.630(7)) are shown. For clarity, the solvent molecules and minor metal sites are omitted. (b) View showing the relationship of the major U_2C_2 cluster with the closest cage portions. (c) Configuration of the endohedral $U_1-C_2-U_2$ fragment. Reprinted with permission. [187] Copyright 2019 American Chemical Society.

A novel mono-metallic actinide EMF $Th@C_{I(11)}-C_{86}$ has been synthesized using arc-discharge methodology and comprehensively characterized, both spectroscopically and computationally. This chiral cage $C_{I(11)}-C_{86}$ had not been previously isolated either as an empty fullerene or an EMF. The solid-state molecular structure was determined by single-crystal X-ray diffraction (Figure 33). Electrochemical measurements and electronic structure calculations, determined that $Th@C_{I(11)}-C_{86}$ is stabilized by the 4 electrons donated to the fullerene cage from Th(IV). As in other actinide EMFs, strong interactions

were observed between Th(IV) and the cage, that cannot be explained by an ionic interaction model. [188]

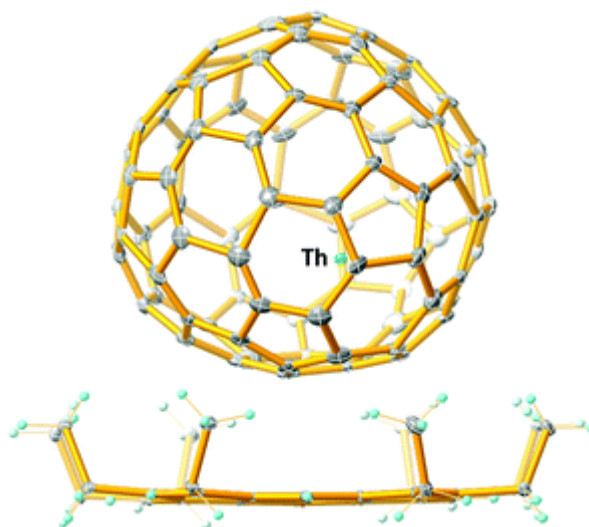


Figure 33: The solid-state structure of Th@C₈₆, with co-crystallised Ni(OEP) (OEP = octaethyl porphyrin). Thermal ellipsoids are shown at 25% probability. Only the major thorium site (Th1 with 0.31 occupancy) is shown. Solvent molecules and minor metal sites are omitted for clarity. Reprinted with permission.[188] Copyright 2019 The Royal Society of Chemistry.

A monometallic thorium EMF Th@C₇₆ has been synthesised, by arc-discharge methodology and characterized by a range of spectroscopic techniques. The molecular structure was determined by single-crystal X-ray diffraction, this is the first example of thorium in the high-symmetry $T_d(19151)$ -C₇₆ cage (Figure 34). This cage has been previously stabilised by 4-electron transfer from Sc₂ and Lu₂, indicating that Th has also transferred 4 electrons to the cage. This assessment is supported by previous computational predictions and electrochemical measurements on Th@C₇₆. [189]

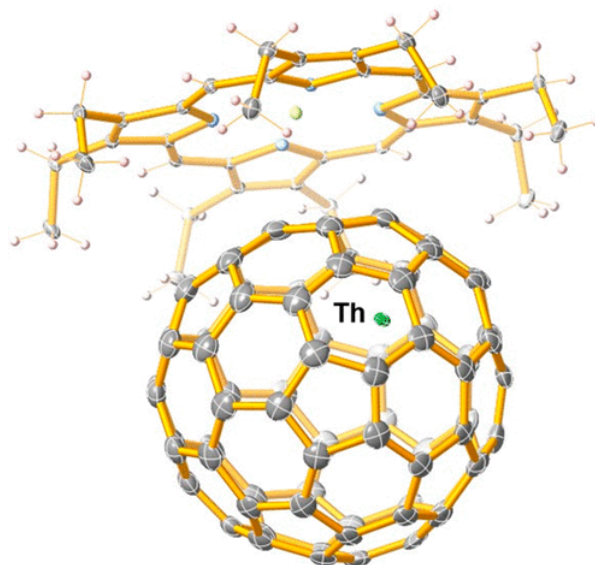
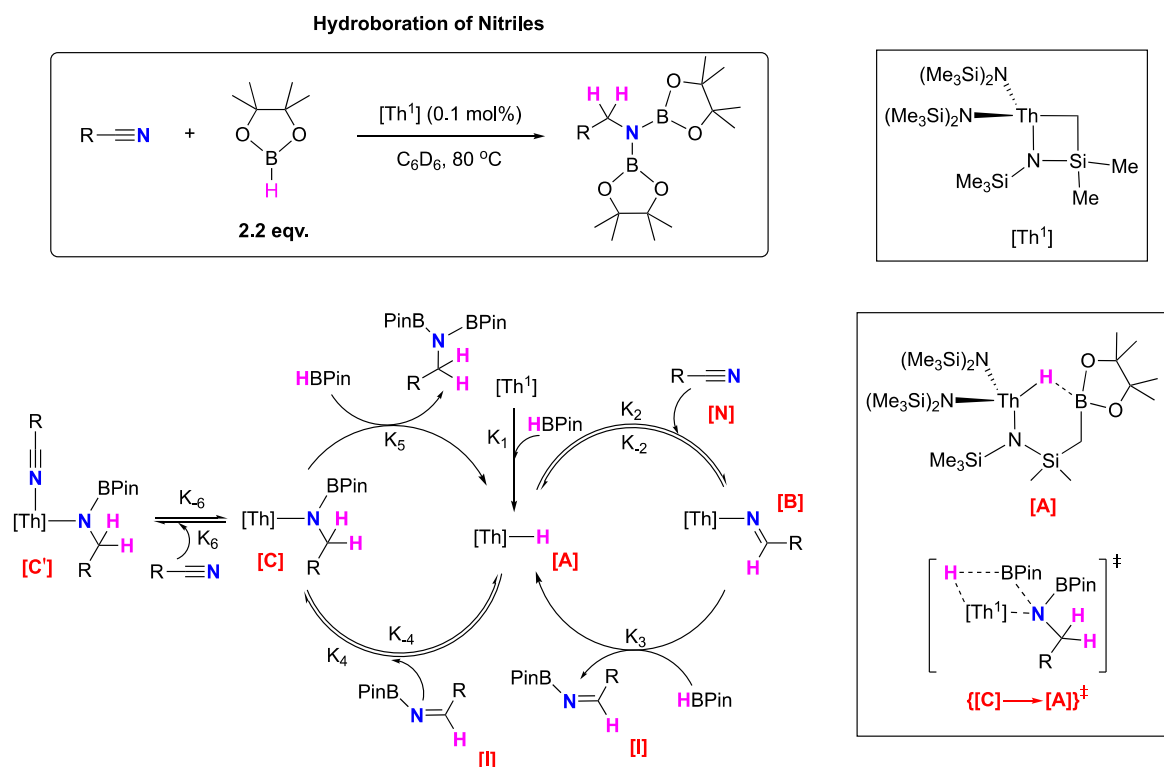


Figure 34: The solid-state structure of Th@C₇₆, with co-crystallised [Ni(OEP)] (OEP = octaethyl porphyrin). Thermal ellipsoids are shown at 25% probability. Only the major thorium site (Th1 with 0.308 occupancy) is shown. Solvent molecules and minor metal sites are omitted for clarity. Reprinted with permission.[189] Copyright 2019 American Chemical Society.

3.6. ORGANOACTINIDES IN CATALYSIS

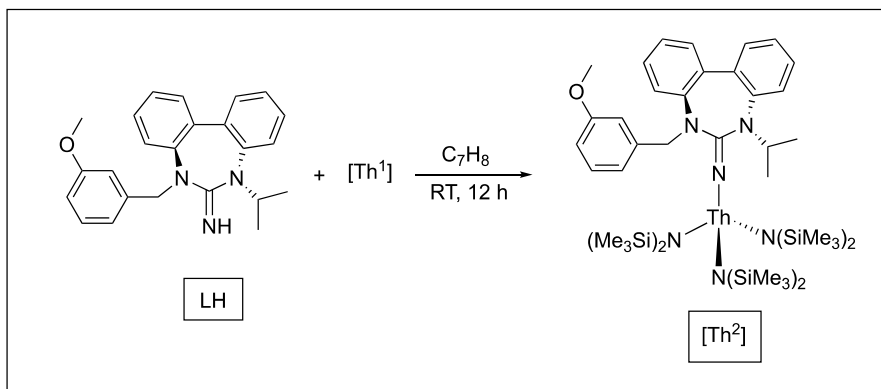
The catalytic performance of metallacycle thorium amide [(Me₂Si)₂N]₂Th[κ²-(N,C)-CH₂SiMe₂N(SiMe₃)] towards the selective dihydroboration of nitriles with pinacolborane (HBPin) has been reported. High turnover frequency was observed with low catalyst loading (0.1 mol%) and a variety of nitrile backbone groups, including aromatic, aliphatic and heteroatom. Based on a combination of stoichiometric, kinetic and temperature dependence studies the authors derived a plausible mechanism; consisting of two catalytic cycles (Scheme 143). The first step proposed is the activation of [Th¹] to thorium hydride complex [A] *via* the insertion of HBPin. The activated thorium hydride complex [A] undergoes an addition reaction across the nitrile, forming intermediate complex [B]. Complex [B] subsequently undergoes a σ-bond metathesis (Th – N/H – B) with a second molecule of HBpin to regenerate complex [A] and intermediate imine [I]. Activation of the second catalytic cycle is accomplished by the instant addition of complex [A] across intermediate imine [I], yielding intermediate [C] which undergoes a σ-bond metathesis (Th – N/H – B) reaction (rate determining step) to yield the target dihydroborated amine product and regenerate complex [A]; completing the catalytic cycle. Due to the final hydroboration step being the turn-over limiting step the authors could not

eliminate an alternative rapid nitrile coordination equilibrium yielding intermediate [C']. [190]

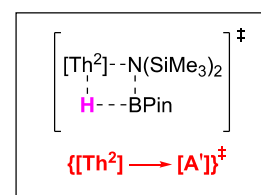
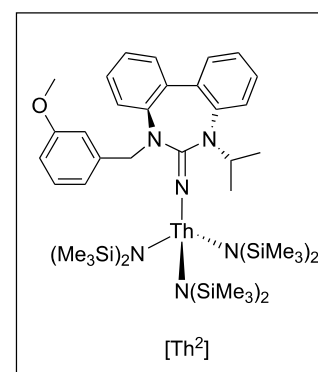
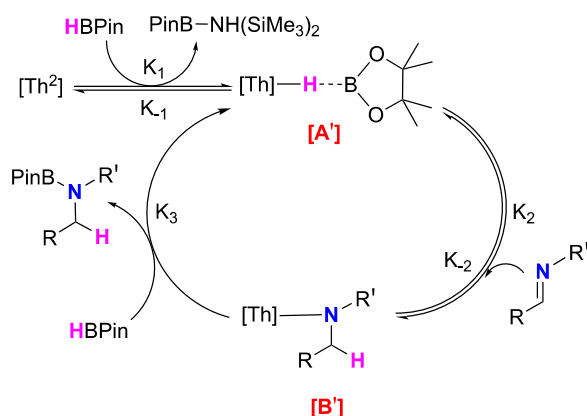
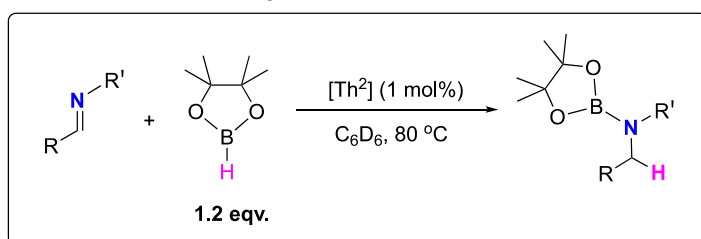


Scheme 143. Proposed catalytic cycle for the thorium catalysed dihydroboration of nitriles. [190]

The complex $[(\text{Me}_2\text{Si})_2\text{N}]_2\text{Th}[\kappa^2-(\text{N},\text{C})-\text{CH}_2\text{SiMe}_2\text{N}(\text{SiMe}_3)] = [\text{Th}^1]$ was reported to undergo a protonolysis reaction with the seven-membered N-heterocyclic iminato ligand (LH) to yield $[\text{Th}^2]$ (Scheme 144). The complex $[\text{Th}^2]$ was characterised by X-ray crystallography and exhibited catalytic activity towards the hydroboration of imines with HBPIn to yield hydroborated secondary amines. Stoichiometric, kinetic and temperature dependence studies were employed by the authors to investigate plausible catalytic mechanisms (Scheme 144). The initiation reaction for the catalytic cycle is proposed to begin with a σ -bond metathesis ($\text{Th} - \text{N}/\text{H} - \text{B}$) between $[\text{Th}^2]$ and HBPIn, passing through transition state $\{[\text{Th}^2] - [\text{A}']\}^\ddagger$ and forming intermediate $[\text{A}']$. Addition reaction of $[\text{A}']$ across the imine $\text{C}=\text{N}$ exists at rapid equilibrium to afford intermediate $[\text{B}']$, which reacts with an additional molecule of HBPIn via σ -bond metathesis ($\text{Th} - \text{N}/\text{H} - \text{B}$) producing the target hydroborated secondary amine and simultaneously regenerating the active species $[\text{A}']$. [190]



Hydroboration of Imines



Scheme 144. Synthesis of $[\text{Th}^2]$ pre-catalyst and proposed catalytic cycle for the hydroboration of imines. [191]

A series of mono-anionic ligands have been reported to stabilise corresponding Th(IV) trialkyl complexes. These include bidentate benzamidinate $[\text{PhC}(\text{NDipp})_2]$ (Dipp = 2,6- $i\text{Pr}_2\text{C}_6\text{H}_3$), iminophosphinamide $[\text{Ph}_2\text{P}(\text{NDipp})_2]$, phosphinoamide $[\text{Ph}_2\text{PNDipp}]$ and tridentate hydrotris(3,5-dimethyl-1-pyrazolyl)borate (Tp^{Me_2}) (Figure 35). All four thorium compounds exhibited catalytic activity towards the polymerisation of isoprene when combined with $i\text{Bu}_3\text{Al}$ and $[\text{Ph}_3\text{C}][\text{B}(\text{C}_6\text{F}_5)]$. The selectivities were dependent on the ligand environment. Complexes $[\text{PhC}(\text{NDipp})_2]\text{Th}(\text{CH}_2\text{SiMe}_3)_3$, $[\text{PhC}(\text{NDipp})_2]\text{Th}(\text{CH}_2\text{-4-MeC}_6\text{H}_4)_3$ and $(\text{Tp}^{\text{Me}_2})\text{Th}(\text{CH}_2\text{SiMe}_3)_3$ showed moderate-to-high selectivity towards cis-polyisoprene, while $[\text{Ph}_2\text{P}(\text{NDipp})_2]\text{Th}(\text{CH}_2\text{SiMe}_3)_3$ exhibited high selectivity towards

trans-polyisoprene. The authors proposed that the steric hindrance around the Th centre was a key driving force for cis-/trans-selectivity. [191]

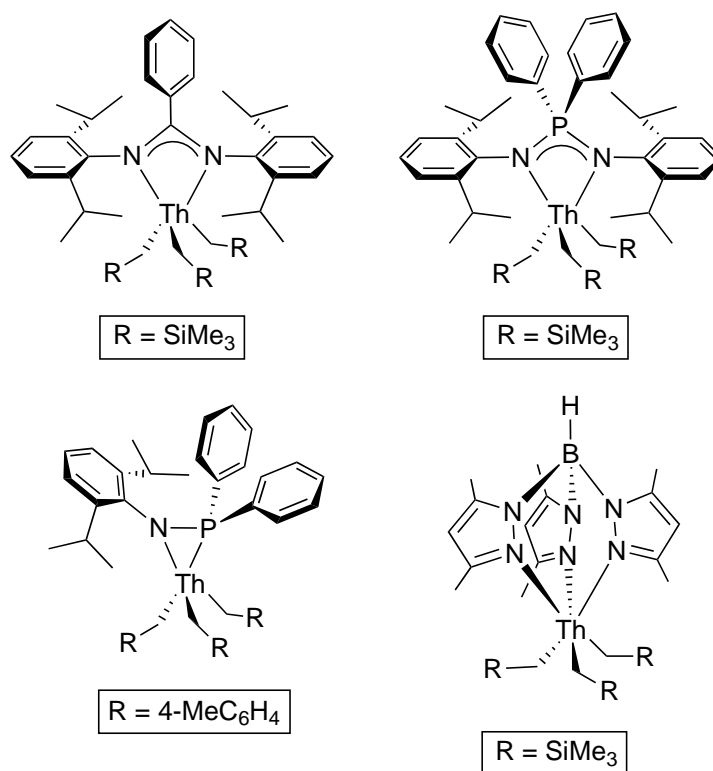


Figure 35. Th(IV) trialkyl compounds reported to exhibit catalytic polymerisation of isoprene.[191]

ACKNOWLEDGEMENTS

Special thanks are due to Ms. Désirée Schneider for preparing some ChemDraw Schemes for this review article. FJ acknowledges financial support from the CNRS.

REFERENCES

- [1] O. Walter, Chem. Eur. J. 25 (2019) 2927-2934.
- [2] D. Liu, B. Liu, Z. Pan, J. Li, C. Cui, Sci. China Chem. 62 (2019) 571-582.
- [3] D.M. Lyubov, A.O. Tolpygin, A.A. Trifonov, Coord. Chem. Rev. 392 (2019) 83-145.
- [4] F.-S. Guo, A. K. Bar, R. A. Layfield, Chem. Rev. 119 (2019) 8479–8505.
- [5] F. Liu, L. Spree, D.S. Krylov, G. Velkos, S.M. Avdoshenko, A.A. Popov, Acc. Chem. Res. 52 (2019) 2981–2993.
- [6] L. Spree A.A. Popov, Dalton Trans. 48 (2019) 2861–2871.

- [7] J. Li, L. Chen, L. Yan, Z. Gu, Z. Chen, A. Zhang, F. Zhao, *Molecules* 24 (2019) 2387.
- [8] W. Cai, C.-H. Chen, N. Chen, L. Echegoyen, *Acc. Chem. Res.* 52 (2019) 1824-1833.
- [9] J. Jin, S. Pan, X. Jin, S. Lei, L. Zhao, G. Frenking, M. Zhou, *Chem. Eur. J.* 25 (2019) 3229-3234.
- [10] Y. Chen, K. Xin, J. Jin, W. Li, Q. Wang, X. Wang, G. Wang *Phys. Chem. Chem. Phys.* 21 (2019) 6743-6749.
- [11] I.V. Lapshin, I.V. Basalov, K.A. Lyssenko, A.V. Cherkasov, A.A. Trifonov, *Chem. Eur. J.* 25 (2019) 459 – 463.
- [12] T. Simler, T.J. Feuerstein, R. Yadav, M.T. Gamer, P.W. Roesky, *Chem. Commun.* 55 (2019) 222-225.
- [13] W. Su, S. Pan, X. Sun, L. Zhao, G. Frenking, C. Zhu, *Dalton Trans.* 48 (2019) 16108–16114.
- [14] A.N. Selikhov, G.S. Plankin, A.V. Cherkasov, A.S. Shavyrin, E. Louyriac, L. Maron, A.A. Trifonov, *Inorg. Chem.* 58 (2019) 5325-5334.
- [15] D. Barisic, D. Diether, C. Maichle-Mössmer, R. Anwander, *J. Am. Chem. Soc.* 141 (2019) 13931–13940.
- [16] B.M. Schmidt, A. Pindwal, A. Venkatesh, A. Ellern, A.J. Rossini, A.D. Sadow, *ACS Catal.* 9 (2019) 827–838.
- [17] X. Liu, L. Xiang, E. Louyriac, L. Maron, X. Leng, Y. Chen, *J. Am. Chem. Soc.* 141 (2019) 138-142.
- [18] Y. Chai, L. Wang, D. Liu, Z. Wang, M. Run, D. Cui, *Chem. Eur. J.* 25 (2019) 2043-2050.
- [19] J. Su, Y. Zhou, X. Xu, *Org. Biomol. Chem.* 17 (2019) 2013–2019.
- [20] T. Yao, P. Xu, X. Xu, *Dalton Trans.* 48 (2019) 7743–7754.
- [21] Y. Pan, W. Li, N.-N. Wei, Y.-M. So, Y. Li, K. Jiang, G. He, *Dalton Trans.* 48 (2019) 3583-3592.
- [22] Y. Pan, W. Li, N.-N. Wei, Y.-M. So, X. Lai, Y. Li, K. Jiang, G. He, *Dalton Trans.* 48 (2019) 9079-9088.
- [23] D. Liu, D. Zhou, H. Yang, J. Li, C. Cui, *Chem. Commun.* 55 (2019) 12324-12327.
- [24] A.P. de Lima Batista, A.G.S. de Oliveira-Filho, A.A.C. Braga, *New J. Chem.* 43 (2019) 12257-12263.

- [25] V.M. Birkelbach, C. Stuhl, C. Maichle-Mössmer, R. Anwander, *Organometallics* 38 (2019) 4485–4496.
- [26] V.M. Birkelbach, R. Thim, C. Stuhl, C. Maichle-Mössmer, R. Anwander, *Chem. Eur. J.* 25 (2019) 14711 – 14720.
- [27] D. Hong, X. Zhu, S. Wang, Y. Wei, S. Zhou, Z. Huang, S. Zhu, R. Wang, W. Yue, X. Mu, *Dalton Trans.* 48 (2019) 5230–5242.
- [28] A. Vasanthakumar, D.J.H. Emslie, J.F. Britten, *J. Organomet. Chem.* 903 (2019) 120980.
- [29] T.-Q. Xu, Z.-Q. Yu, C.-H. Li, *Polyhedron* 165 (2019) 68–72.
- [30] M. Oishi, R. Yoshimura, N. Nomura, *Inorg. Chem.* 58 (2019) 13755–13760.
- [31] X. Yu, Meng Li, J. Hong, X. Zhou, L. Zhang, *Chem. Eur. J.* 25 (2019) 2569-2576.
- [32] D.-D. Zhai, H.-Z. Du, X.-Y. Zhang, Y.-F. Liu, B.-T. Guan, *ACS Catal.* 9 (2019) 8766–8771.
- [33] F. Zhang, J. Zhang, Z. Chen, L. Weng, X. Zhou, *Inorg. Chem.* 58 (2019) 8451–8459.
- [34] Z. Guo, J. Luu, V. Blair, G.B. Deacon, P.C. Junk, *Eur. J. Inorg. Chem.* (2019) 1018–1029.
- [35] W. Mao, Y. Wang, L. Xiang, Q. Peng, X. Leng, Y. Chen, *Chem. Eur. J.* 25 (2019) 10304 – 10308.
- [36] F. Yan, S. Li, L. Li, W. Zhang, D. Cui, M. Wang, Y. Dou, *Eur. J. Inorg. Chem.* (2019) 2277–2283.
- [37] J. Li, J. Zhao, G. Ma, R. McDonald, R.G. Cavell, *J. Organomet. Chem.* 895 (2019) 7-14.
- [38] W. Cao, Y. Zhang, D.-S. Yang, *J. Organomet. Chem.* 880 (2019) 187-195.
- [39] D. Barisic, D.A. Buschmann, D. Schneider, C. Maichle-Mössmer, R. Anwander, *Chem. Eur. J.* 25 (2019) 4821-4832.
- [40] A.C. Fecker, M. Freytag, P.G. Jones, M.D. Walter, *Dalton Trans.* 48 (2019) 8297–8302.
- [41] Z. Feng, Z. Huang, S. Wang, Y. Wei, S. Zhoua, X. Zhua, *Dalton Trans.* 48 (2019) 11094–11102.
- [42] L.-J. Ma, J. Wang, M. Han, J. Jia, H.-S. Wu, X. Zhang, *Int. J. Hydrogen Energ.* 44 (2019) 18145-18152.
- [43] D. Werner, G.B. Deacon, P.C. Junk, *Inorg. Chem.* 58 (2019) 1912-1918.

- [44] D. Toniolo, A.R. Willauer, J. Andrez, Y. Yang, R. Scopelliti, L. Maron, M. Mazzanti, *Chem. Eur. J.* 25 (2019) 7831 – 7834.
- [45] C.A. Gould, K.R. McClain, J.M. Yu, T.J. Groshens, F. Furche, B.G. Harvey, J.R. Long, *J. Am. Chem. Soc.* 141 (2019) 12967–12973.
- [46] M.A. Angadol, D.H. Woen, C.J. Windorff, J.W. Ziller, W. J. Evans, *Organometallics* 38 (2019) 1151-1158.
- [47] M.T. Dumas, J.W. Ziller, W.J. Evans, *ACS Omega* 4 (2019) 398–402.
- [48] V.E. Fleischauer, G. Ganguly, D.H. Woen, N.J. Wolford, W.J. Evans, J. Autschbach, M.L. Neidig, *Organometallics* 38 (2019) 3124–3131.
- [49] A.-M. Ariciu, D.H. Woen, D.N. Huh, L.E. Nodaraki, A.K. Kostopoulos, C.A.P. Goodwin, N.F. Chilton, E.J.L. McInnes, R.E.P. Winpenny, W.J. Evans, F. Tuna, *Nat. Commun.* 10 (2019) 3330.
- [50] F. Zhang, W. Yi, J. Zhang, Q. You, L. Weng, X. Zhou, *Dalton Trans* 48 (2019) 10596–10603.
- [51] M. Weger, P. Pahl, F. Schmidt, B.S. Soller, P.J. Altmann, A. Pöthig, G. Gemmecker, W. Eisenreich, B. Rieger, *Macromolecules* 52 (2019) 7073–7080.
- [52] T. Song, N.Liu, X. Tong, F. Li, X. Mu, Y. Mu *Dalton Trans.* 48 (2019) 17840–17851.
- [53] B. Tang, X. Hu, C. Liu, T. Jiang, F. Alam, Y. Chen, *ACS Catal.* 9 (2019) 599–604.
- [54] J. Liu, D. Reta, J.A. Cleghorn, Y.X. Yeoh, F. Ortu, C.A.P. Goodwin, N.F. Chilton, D.P. Mills, *Chem. Eur. J.* 25 (2019) 7749 – 7758.
- [55] D. Gu, C. Yi, W. Ren, *Inorg. Chem.* 58 (2019) 9260–9269.
- [56] M.E. Minyaev, P.D. Komarov, D.M. Roitershtein, K.A. Lyssenko, I.E. Nifant'ev, L.N. Puntus, E.A. Varaksina, R.S. Borisov, V.P. Dyadchenko, P.V. Ivchenko, *Organometallics* 38 (2019) 2892–2901.
- [57] K. Aoyagi, K. Matsumoto, S. Shimada, K. Sato, Y. Nakajima, *Organometallics* 38 (2019) 210-212.
- [58] R. Zitz, J. Hlina, H. Arp, D. Kinschel, C. Marschner, J. Baumgartner, *Inorg. Chem.* 2019, 58, 7107–7117.
- [59] R.L. Halbach, G. Nocton, J.I. Amaro-Estrada, L. Maron, C.H. Booth, R.A. Andersen, *Inorg. Chem.* 58 (2019) 12083–12098.
- [60] Z.-J. Lv, Z. Huang, W.-X. Zhang, Z. Xi, *J. Am. Chem. Soc.* 141 (2019) 8773-8777.
- [61] Z.-J. Lv, Z. Huang, J. Shen, W.-X. Zhang, Z. Xi, *J. Am. Chem. Soc.* 141 (2019) 20547–20555.

- [62] C.O. Hollfelder, L.N. Jende, H.-M. Dietrich, K. Eichele, C. Maichle-Mössmer, R. Anwander, *Chem. Eur. J.* 2019, 25, 7298 – 7302.
- [63] J. Long, A.O. Tolpygin, A.V. Cherkasov, K.A. Lyssenko, Y. Guari, J. Larionova, A.A. Trifonov, *Organometallics* 38 (2019) 748-752.
- [64] P. Xu, X. Xu, *Organometallics* 38 (2019) 3212–3217.
- [65] D.H. Woen, J.R.K. White, J.W. Ziller, W.J. Evans, *J. Organomet. Chem.* 899 (2019) 120885.
- [66] C.P. Gordon, D.B. Culver, M.P. Conley, O. Eisenstein, R.A. Andersen, C. Copéret, *J. Am. Chem. Soc.* 141 (2019) 648-656.
- [67] A.N. Selikhov, A.S. Shavyrin, A.V. Cherkasov, G.K. Fukin, A.A. Trifonov, *Organometallics* 38 (2019) 4615-4624.
- [68] N. Diteepeng, J.-C. Buffet, Z.R. Turner, D. O'Hare, *Dalton Trans.* 48 (2019) 16099–16107.
- [69] D. Diether, C. Maichle-Mössmer, R. Anwander, *Organometallics* 38 (2019) 3007–3017.
- [70] G. Guo, X. Wu, X. Yan, L. Yan, X. Li, S. Zhang, N. Qiu, *Polymers* 11 (2019) 836.
- [71] P. Evans, D. Reta, G.F.S. Whitehead, N.F. Chilton, D.P. Mills, *J. Am. Chem. Soc.* 141 (2019) 19935-19940.
- [72] H. Ying, M. Gong, C. Pi, *Dalton Trans.* 48 (2019) 2722–2729.
- [73] A.O. Tolpygin, A.S. Shavyrin, A.V. Cherkasov, G.K. Fukin, I. del Rosal, L. Maron, A.A. Trifonov, *Dalton Trans.* 48 (2019) 8317–8326.
- [74] F. Wang, X. Zhao, X. Meng, S. Wang, *Dalton Trans.* 48 (2019) 12193-12198.
- [75] S.S. Galley, S.A. Pattenaude, R.F. Higgins, C.J. Tatebe, D.A. Stanley, P.E. Fanwick, M. Zeller, E.J. Schelter, S.C. Bart, *Dalton Trans.* 48 (2019) 8021–8025.
- [76] D. Barisic, D. Schneider, C. Maichle-Mössmer, R. Anwander, *Angew. Chem. Int. Ed.* 58 (2019) 1515-1518.
- [77] D. Barisic, J. Lebon, C. Maichle-Mössmer, R. Anwander, *Chem. Commun.* 55 (2019) 7089-7092.
- [78] A.J. Martínez-Martínez, A.R. Kennedy, V. Paprocki, F. Fantuzzi, R.D. Dewhurst, C.T. O'Hara, H. Braunschweig, R.E. Mulvey, *Chem. Commun.* 55 (2019) 9677-9680.
- [79] J. Greenough, Z. Zhou, Z. Wei, M.A. Petrukhina, *Dalton Trans.* 48 (2019) 5614–5620.
- [80] P. Shao, L.P. Ding, D.-B. Luo, C. Lu, *J. Mol. Graph. Model.* 90 (2019) 226-234.

- [81] F. Gendron, J. Autschbach, J.-P. Malrieu, H. Bolvin, *Inorg. Chem.* 58 (2019) 581-593.
- [82] Ravi Yadav, T. Simler, M.T. Gamer, R. Köppe, P.W. Roesky, *Chem. Commun.* 55 (2019) 5765-5768.
- [83] C. Schoo, S. Bestgen, A. Egeberg, J. Seibert, S.N. Konchenko, C. Feldmann, P.W. Roesky, *Angew. Chem. Int. Ed.* 58 (2019) 4386–4389.
- [84] J. Caballo, M. Mena, A. Pérez-Redondo, C. Yélamos, *J. Organomet. Chem.* 896 (2019) 139-145.
- [85] M. Bonath, C. Maichle-Mössmer, P. Sirsch, R. Anwander, *Angew. Chem. Int. Ed.* 58 (2019) 8206–8210.
- [86] R. Thim, D. Schädle, C. Maichle-Mössmer, R. Anwander, *Chem. Eur. J.* 25 (2019) 507 – 511.
- [87] D.M. Roitershteina, A.A. Vinogradova, K.A. Lyssenkod, I.V. Ananyevd, V.A. Yakovleva, N.N. Kostitsynaa, I.E. Nifant'ev *Inorg. Chim. Acta* 487 (2019) 153-161.
- [88] A. Jaoul, M. Tricoire, J. Moutet, M. Cordier, C. Clavaguéra, G. Nocton, *Chem Sq.* 3 (2019) 1.
- [89] D. Wang, J. Moutet, M. Tricoire, M. Cordier, G. Nocton, *Inorganics* 7 (2019) 58.
- [90] S. Hu, T. Liu, W. Shen, Z. Slanina, T. Akasaka, Y. Xie, F. Uhlik, W. Huang, X. Lu, *Inorg. Chem.* 58 (2019) 2177–2182.
- [91] S. Hu, W. Shen, L. Yang, G. Duan, P. Jin, Y. Xie, T. Akasaka, X. Lu, *Chem. Eur. J.* 25 (2019) 11538 – 11544.
- [92] F. Liu, G. Velkos, D.S. Krylov, L. Spree, M. Zalibera, R. Ray, N.A. Samoylova, C.-H. Chen, M. Rosenkranz, S. Schiemenz, F. Ziegls, K. Nenkov, A. Kostanyan, T. Greber, A.U.B. Wolter, M. Richter, B. Büchner, S.M. Avdoshenko, A.A. Popov, *Nat. Commun.* 10 (2019) 571.
- [93] G. Velkos, D.S. Krylov, K. Kirkpatrick, L. Spree, V. Dubrovin, B. Büchner, S.M. Avdoshenko, V. Bezmelnitsyn, S. Davis, P. Faust, J. Duchamp, H.C. Dorn, A.A. Popov, *Angew. Chem. Int. Ed.* 58 (2019) 5891 –5896.
- [94] C. Pan, W. Shen, L. Yang, L. Bao, Z. Wei, P. Jin, H. Fang, Y. Xie, T. Akasaka X. Lu, *Chem. Sci.* 10 (2019) 4707–4713.
- [95] W. Shen, L. Bao, S. Hu, L. Yang, P. Jin, Y. Xie, T. Akasaka X. Lu, *Chem. Sci.* 10 (2019) 829–836.
- [96] S. Hu, W. Shen, P. Zhao, T. Xu, Z. Slanina, M. Ehara, X. Zhao, Y. Xie, T. Akasaka X. Lu, *Nanoscale* 11 (2019) 17319–17326.

- [97] H. Cong, A. Liu, Y. Hao, L. Feng, Z. Slanina, F. Uhlik, *Inorg. Chem.* 58 (2019) 10905–10911.
- [98] W. Yang, G. Velkos, F. Liu, S.M. Sudarkova, Y. Wang, J. Zhuang, H. Zhang, X. Li, X. Zhang, B. Büchner, S.M. Avdoshenko, A.A. Popov, N. Chen, *Adv. Sci.* 6 (2019) 1901352.
- [99] S. Stevenson, A.J. Rothgeb, K.R. Tepper, J. Duchamp, H.C. Dorn, X.B. Powers, M. Roy, M.M. Olmstead, A.L. Balch, *Chem. Eur. J.* 25 (2019) 12545 – 12551.
- [100] S. Hu, P. Zhao, W. Shen, P. Yu, W. Huang, M. Ehara, Y. Xie, T. Akasaka, X. Lu, *Nanoscale* 11 (2019) 13415–13422.
- [101] T. Greber, A.P. Seitsonen, A. Hemmi, J. Dreiser, R. Stania, F. Matsui, M. Muntwiler, A.A. Popov, R. Westerström, *Phys. Rev. Mater.* 3 (2019) 014409.
- [102] C. Schlesier, F. Liu, V. Dubrovin, L. Spree, B. Büchner, S.M. Avdoshenko, A.A. Popov, *Nanoscale* 11 (2019) 13139–13153.
- [103] W. Shen, L. Yang, Y. Wu, L. Bao, Y. Li, P. Jin, H. Fang, Y. Xie, X. Lu *J. Org. Chem.* 84 (2019) 606–612.
- [104] M. Kako, Y. Arikawa, S. Kanzawa, M. Yamada, Y. Maeda, M. Furukawa, T. Akasaka, *Helv. Chim. Acta* 102 (2019) e1900064.
- [105] Y.-P. Xie, C. Pan, L. Bao, Z. Slanina, T. Akasaka, X. Lu, *Organometallics* 38 (2019) 2259–2263.
- [106] P. Zhao, S. Hu, X. Lu, X. Zhao, *J. Org. Chem.* 84 (2019) 14571–14578.
- [107] O. Semivrazhskaya, A. Romero-Rivera, S. Aroua, S.I. Troyanov, M. Garcia-Borràs, S. Stevenson, S. Osuna, Y. Yamakoshi, *J. Am. Chem. Soc.* 141 (2019) 10988–10993.
- [108] M. Izquierdo, B. Platzer, A.J. Stasyuk, O.A. Stasyuk, A.A. Voityuk, S. Cuesta, M. Solà, D.M. Guldi, N. Martín, *Angew. Chem. Int. Ed.* 58 (2019) 6932 –6937.
- [109] T. Wei, O. Martin, M. Chen, S. Yang, F. Hauke, A. Hirsch, *Angew. Chem. Int. Ed.* 58 (2019) 8058 –8062.
- [110] D. Xu, Y. Jiang, Y. Wang, T. Zhou, Z. Shi, H. Omachi, H. Shinohara, B. Sun, Z. Wang, *Inorg. Chem.* 58 (2019) 14325–14330.
- [111] Z.N. Cisneros-García, J.G. Rodríguez-Zavala, *Chem. Phys.* 523 (2019) 114–123.
- [112] D.V. Konarev, A.A. Popov, L.V. Zorina, S.S. Khasanov, R.N. Lyubovskaya, *Chem. Eur. J.* 25 (2019) 14858 – 14869.
- [113] H. Meng, C. Zhao, M. Nie, C. Wang, T. Wang *J. Phys. Chem. C* 123 (2019) 6265–6269.

- [114] V.A. Basiuk, D.E. Tahuilan-Anguiano, *Chem. Phys. Lett.* 722 (2019) 146–152.
- [115] L. Bao, B. Wang, P. Yu, C. Huang, C. Pan, H. Fang, T. Akasaka, D.M. Guldi, X. Lu, *Chem. Commun.* 55 (2019) 6018–6021.
- [116] C. Zhao, H. Meng, M. Nie, Q. Huang, P. Du, C. Wang, T. Wang, *Chem. Commun.*, 55 (2019) 11511–11514.
- [117] C. Zhao, H. Meng, M. Nie, X. Wang, Z. Cai, T. Chen, D. Wang, C. Wang, T. Wang, *J. Phys. Chem. C* 123 (2019) 12514–12520.
- [118] E.S. Tabatabaie, S. Dehghanpour, E. Mosaddegh, R. Babaahmadi, A. Chipman, B.F. Yates, A. Ariafard, *Dalton Trans.* 48 (2019) 6997–7005.
- [119] D. Liu, M. Wang, Y. Chai, X. Wan, D. Cui, *ACS Catal.* 9 (2019) 2618–2625.
- [120] Y. Zhao, H. Lu, G. Luo, X. Kang, Z. Hou, Y. Luo, *Catal. Sci. Technol.* 9 (2019) 6227–6233.
- [121] T. Wang, D. Liu, D. Cui, *Macromolecules* 52 (2019) 9555–9560.
- [122] Y. Zhao, G. Luo, X. Kang, F. Guo, X. Zhu, R. Zheng, Z. Hou, Y. Luo, *Chem. Commun.* 55 (2019) 6689–6692.
- [123] H. Yu, K. Yang, H. Niu, J. Yu, J. Dong, J. Wang, Y. Li, *Macromol. Rapid Commun.* 40 (2019) 1900048.
- [124] S. Li, F. Yan, Z. Zhang, Y. Dou, W. Zhang, D. Cui, *Macromol. Rapid Commun.* 40 (2019) 1900061.
- [125] H. Wang, Y. Yang, M. Nishiura, Y. Higaki, A. Takahara, Z. Hou, *J. Am. Chem. Soc.* 141 (2019) 3249–3257.
- [126] B. Liu, L. Wang, C. Wua, D. Cui, *Polym. Chem.* 10 (2019) 235–243.
- [127] I. Göttker-Schnetmann, P. Kenyon, S. Mecking, *Angew. Chem. Int. Ed.* 58 (2019) 17777 – 17781.
- [128] S. Georges, O. H. Hashmi, M. Bria, P. Zinck, Y. Champouret, M. Visseaux, *Macromolecules* 52 (2019) 1210–1219.
- [129] I. Belaid, B. Macqueron, M.-N. Poradowski, S. Bouaouli, J. Thuilliez, F. Da Cruz-Boisson, V. Monteil, F. D’Agosto, L. Perrin, C. Boisson, *ACS Catal.* 9 (2019) 9298–9309.
- [130] J. Chen, A. Motta, J. Zhang, Y. Gao, T.J. Marks, *ACS Catal.* 9 (2019) 8810–8818.
- [131] H. Wang, Y. Zhao, M. Nishiura, Y. Yang, G. Luo, Y. Luo, Z. Hou, *J. Am. Chem. Soc.* 141 (2019) 12624–12633.
- [132] Q. Wang, S. Chen, B. Deng, Y. Wang, D. Dong, N. Zhang, *Polym. Chem.* 10 (2019) 2101–2105.

- [133] B. Pudasaini, *Organometallics* 38 (2019) 1091–1098.
- [134] H.N. Nguyen, K.C. Hultsch, *Eur. J. Org. Chem.* (2019) 2592–2601.
- [135] G. Luo, F. Liu, Y. Luo, G. Zhou, X. Kang, Z. Hou, L. Luo, *Organometallics* 38 (2019) 1887–1896.
- [136] J. Su, Y. Cai, X. Xu, *Org. Lett.* 21 (2019) 9055–9059.
- [137] M.M.I. Basiouny, D.A. Dollard, J.A.R. Schmidt, *ACS Catal.* 9 (2019) 7143–7153
- [138] Y.A. Rina, J.A.R. Schmidt, *Organometallics* 38 (2019) 4261–4270
- [139] S. Patnaik, A.D. Sadow, *Angew. Chem. Int. Ed.* 58 (2019) 2505–2509.
- [140] A. Music, C. Hoarau, N. Hilgert, F. Zischka, D. Didier, *Angew. Chem. Int. Ed.* 58 (2019) 1188–1192.
- [141] L. Anthore-Dalio, A.D. Benischke, B. Wei, G. Berionni, P. Knochel, *Angew. Chem. Int. Ed.* 58 (2019) 4046–4050.
- [142] B. Wei, D. Zhang, Y.-H. Chen, A. Lei, P. Knochel, *Angew. Chem. Int. Ed.* 58 (2019) 15631–15635.
- [143] F.S. Boi, X. Zhang, J. Borowiec, D. Medranda, S. Wang, K. Yan, J. Zhang, J. Wen, *Mater. Today Chem.* 12 (2019) 173–177.
- [144] J.W. Shin, S. Oh, S. Lee, J.-G. Yu, J. Park, D. Go, B.C. Yang, H.J. Kim, J. An, *ACS Appl. Mater. Interfaces* 11 (2019) 46651–46657.
- [145] W.L.I. Waduge, Y. Chen, P. Zuo, N. Jayakodiarachchi, T.F. Kuech, S.E. Babcock, P.G. Evans, C.H. Winter, *ACS Appl. Nano Mater.* 2 (2019) 7449–7458.
- [146] R. Rahman, J.P. Klesko, A. Dangerfield, M. Fang, J.-S.M. Lehn, C.L. Dezelah, R.K. Kanjolia, Y.J. Chabal, *J. Vac. Sci. Technol. A* 37 (2019) 011504.
- [147] F. Huttmann, N. Rothenbach, S. Kraus, K. Ollefs, L.M. Arruda, M. Bernien, D. Thonig, A. Delin, J. Fransson, K. Kummer, N.B. Brookes, O. Eriksson, W. Kuch, T. Michely, H. Wende, *J. Phys. Chem. Lett.* 10 (2019) 911–917.
- [148] C. Chaoxian, S. Pan, J. Jin, L. Meng, M. Lao, L. Zhao, M. Zhou, G. Frenking, *Chem. Eur. J.* 25 (2019) 11722–11784.
- [149] C.J. Tatebe, T.S. Collins, G. R. Barnett, M. Zeller, S. C. Bart, *Polyhedron* 158 (2019) 1–7.
- [150] C.J. Tatebe, J.J. Kiernicki, R.F. Higgins, R.J. Ward, S.N. Natoli, J.C. Langford, C.L. Clark, M. Zeller, P. Wenthold, M.P. Shores, J.R. Walensky, S.C. Bart, *Organometallics* 38 (2019) 1031–1040.
- [151] K.C. Mullane, P. Hrobárik, T. Cheisson, B.C. Manor, P.J. Carroll, E.J. Schelter, *Inorg. Chem.* 58 (2019) 4152–4163.

- [152] N. S. Settineri, A.A. Shiau, J. Arnold, Dalton Trans. 48 (2019) 5569–5573.
- [153] C.J. Hoerger, F.W. Heinemann, E. Louyriac, M. Rigo, L. Maron, H. Grützmacher, M. Driess, K. Meyer, Angew. Chem. Int. Ed. 58 (2019) 1679–1683.
- [154] E. Lu, B. E. Atkinson, A.J. Wooles, J.T. Boronski, L.R. Doyle, F. Tuna, J.D. Cryer, P.J. Cobb, I.J.V. Yrezabal, G.F.S. Whitehead, N. Kaltsoyannis, S.T. Liddle, Nature Chem. 11 (2019) 806–811.
- [155] E. Lu, S. Sajjad, V.E.J. Berryman, A.J. Wooles, N. Kaltsoyannis, S.T. Liddle, Nature Commun. 10 (2019) 634.
- [156] M. Falcone, R. Scopelliti, M. Mazzanti, J. Am. Chem. Soc. 141 (2019) 9570–9577.
- [157] N. J. Wolford, D.C. Sergentu, W.W. Brennessel, J. Autschbach, M.L. Neidig, Angew. Chem. Int. Ed. 58 (2019) 10266–10270.
- [158] A.J. Myers, M.L. Tarlton, S.P. Kelley, W.W. Lukens, J.R. Walensky, Angew. Chem. Int. Ed. 58 (2019) 14891–14895.
- [159] I. R. Ariyaratna, E. Miliordos, Phys.Chem.Chem.Phys. 21 (2019) 24469.
- [160] T. Cheisson, K.D. Kersey, N. Mahieu, A. McSkimming, M.R. Gau, P.J. Carroll and E.J. Schelter, J. Am. Chem. Soc. 141 (2019) 9185–9190.
- [161] J. Du, D.M. King, L. Chatelain, E. Lu, F. Tuna, E.J.L. McInnes, A.J. Wooles, L. Maron and S.T. Liddle, Chem. Sci. 10 (2019) 3738–3745.
- [162] R. Magnall, G. Balázs, E. Lu, F. Tuna, A.J. Wooles, M. Scheer, S.T. Liddle, Angew. Chem. Int. Ed. 58 (2019) 10215–10219.
- [163] R. Magnall, G. Balázs, E. Lu, M. Kern, J.v. Slageren, F. Tuna, A.J. Wooles, M. Scheer, S.T. Liddle, Chem. Eur. J. 25 (2019) 14246–14252.
- [164] C. Zhang, G. Hou, G. Zi, W. Ding, M. D. Walter, Inorg. Chem. 58 (2019) 1571–1590.
- [165] Y. Wang, C. Zhang, G. Zi, W. Ding, M. D. Walter, New. J. Chem. 43 (2019) 9527–9539.
- [166] C. Zhang, G. Hou, G. Zi, M. D. Walter, Dalton Trans. 48 (2019) 2377–2387.
- [167] C. Zhang, Y. Wang, G. Hou, W. Ding, G. Zi, M. D. Walter, Dalton Trans. 48 (2019) 6921–6930.
- [168] A. J. Ryan, M. A. Angadol, J. W. Ziller, W. J. Evans, Chem. Commun. 55 (2019) 2325–2327.
- [169] M. A. Boreen, T. D. Lohrey, G. Rao, R. D. Britt, L. Maron, J. Arnold, J. Am. Chem. Soc. 141 (2019) 5144–5148.

- [170] F-S. Guo, Y-C. Chen, M-L. Tong, A. Mansikkamäki, R. A. Layfield, *Angew. Chem. Int. Ed.* 58 (2019) 10163-10167.
- [171] M. A. Boreen, D. J. Lussier, B. A. Skeel, T. D. Lohrey, F. A. Watt, D. K. Shuh, J. R. Long, S. Hohloch, J. Arnold, *Inorg. Chem.* 58 (2019) 16629-16641.
- [172] G. Qin, Y. Qang, X. Shi, I. del Rosal, L. Maron, J. Cheng, *Chem. Commun.* 55 (2019) 8560-8563.
- [173] C. A. P. Goodwin, J. Su, T. E. Albrecht-Schmitt, A. V. Blake, E. R. Batista, S. R. Daly, S. Dehnen, W. J. Evans, A. J. Gaunt, S. A. Kozimor, N. Lichtenberger, B. L. Scott, P. Yang, *Angew. Chem. Int. Ed.* 58 (2019) 11695-11699.
- [174] J. C. Wedal, S. Bekoe, J. W. Ziller, F. Furche, W. J. Evans, *Dalton Trans.* 48 (2019) 16633-16640.
- [175] J. M. Yu, F. Furche, *Inorg. Chem.* 58 (2019) 16004-16010.
- [176] G. Rao, A. B. Altman, A. C. Brown, L. Tao, T. A. Stich, J. Arnold, R. D. Britt, *Inorg. Chem.* 58 (2019) 7978-7988.
- [177] J. K. Pagano, D. A. S. Arney, B. L. Scott, D. E. Morris, J. L. Kiplinger, C. J. Burns, *Dalton Trans.* 48 (2019) 50-57.
- [178] P. Rungthanaphatsophon, I. del Rosal, R. J. Ward, S. P. Vilanova, S. P. Kelley, L. Maron, J. R. Walensky, *Organometallics* 38 (2019) 1733-1740.
- [179] P. Rungthanaphatsophon, O. J. Fajen, S. P. Kelley, J. R. Walensky, *Inorganics* 7 (2019) 105.
- [180] F. Talbi, L. Castro, F. Kias, A. Elkechai, A. Boucekkine, M. Ephritikhine, J. *Organomet. Chem.* 901 (2019) 120947.
- [181] C.J. Inman, F.G.N. Cloke, *Dalton Trans.* 48 (2019) 10782-10784.
- [182] J. N. Tian, M. Zheng, L. Li, G. Schreckenbach, Y. R. Guo, Q. J. Pan, *New J. Chem.* 43 (2019) 1469-1477.
- [183] A.G. Torres, R. Esper, P. W. Dunk, R. M. Martínez, A. R. Fortea, L. Echegoyen, J.M. Poblet, *Helv. Chim. Acta* 102 (2019) e1900046.
- [184] Y. X. Zhao, K. Yuan, M. Y. Li, M. Ehara, X. Zhao, *Inorg. Chem.* 58 (2019) 10769–10777.
- [185] C.F. Espinosa, J. Murillo, M.E. Soto, M.R. Ceron, R.M. Martínez, A.R. Fortea, J.M. Poblet, L. Echegoyen, X. Ribas, *Nanoscale* 11 (2019) 23035–23041.
- [186] Y.X. Zhao, M.Y. Li, P. Zhao, M. Ehara, X. Zhao, *Inorg. Chem.* 58 (2019) 14159–14166.

- [187] J. Zhuang, L. Abella, D-C. Sergentu, Y-R. Yao, M. Jin, W. Ye, X. Zhang, X. Li, D. Zhang, Y. Zhao, X. Li, S. Wang, L. Echegoyen, J. Autschbach, N. Cheng, *J. Am. Chem. Soc.* 141 (2019) 20249-20260.
- [188] Y. Wang, R. M. Martinez, W. Cai, J. Zhuang, W. Yang, L. Echegoyen, J. M. Poblet, A. R. Fortea, N. Chen, *Chem. Commun.* 55 (2019) 9271-9274.
- [189] M. Jin, J. Zhuang, Y. Wang, W. Yang, X. Liu, N. Chen, *Inorg. Chem.* 58 (2019) 16722-16726.
- [190] S. Saha, M. S. Eisen, *ACS Catal.* 9 (2019) 5947-5956.
- [191] G. Qin, J. Cheng, *Dalton Trans.* 48 (2019) 11706-11714.